universität wien

DISSERTATION / DOCTORAL THESIS

Titel der Dissertation /Title of the Doctoral Thesis

„Nonlinear wave-current interactions in water flows“

verfasst von / submitted by

Biswajit Basu

angestrebter akademischer Grad / in partial fulfilment of the requirements for the degree of

Doktor der Naturwissenschaften (Dr. rer. Nat.)

Wien, 2019 / Vienna 2019

Studienkennzahl lt. Studienblatt / degree programme code as it appears on the student record sheet:	A 796 605 405
Dissertationsgebiet lt. Studienblatt / field of study as it appears on the student record sheet:	Mathematik
Betreut von / Supervisor:	Univ.-Prof /Dr. Adrian Constantin

Acknowledgements

At the outset, I wish to express my deep gratitude to my advisor Prof. Adrian Constantin for the generous support, valuable suggestions and constant encouragement he has provided throughout the period of the doctoral research. His positive outlook and enthusiastic approach has had a profound influence on me and my work. I am also indebted to Prof. Robin S. Johnson for the valuable discussions and useful interactions I had with him. I am also fortunate to have the opportunity to attend his lectures on 'Oceanic Fluid Dynamics' in Erwin Schrödinger Institute (ESI), Vienna. The summer/winter schools I have attended in ESI and the programme I attended in Newton Institute in Cambridge have exposed me to several interesting ideas and added value to my thesis. During the course of my doctoral studies, I came across several mathematicians and scientists - I cherish the interactions I had with them. I would like to thank my colleagues in Trinity College Dublin for their inspiring support and the enthusiasm they have shown. Two names worth mention are my former Head of School, Brian Foley and my former Head of Discipline, Brian Broderick. Among others, Liam Dowling and Bruce Misstear were my inspirations too. Thanks to Dermot O'Dwyer for lending his patient listening ears, to Breiffni Fitzgerald for assisting and covering for me whenever required and to Aonghus McNabola for showing enthusiasm in my doctoral research work. Thanks are also due to Mary Curley for helping me with the logistics to make my hectic travel schedule as smooth as possible. I sincerely thank all my colleagues and friends who had taken keen interest in my work but are not named individually. Thanks to Prof Sumit Chakraborty, Ruhr-Universität Bochum not only for helping in translating the abstract in German but also having intellectually stimulating discussions from time to time. I would also like to thank my students Dr Lin Chen, Dr Himanshu Nagpal, Hoa Nguyen, Saptarshi Sarkar and Giacomo Poiliti for their patience in waiting for my advise during periods I have been busy, and also for their assistance in editing and typing when necessary. I also take this opportunity to acknowledge the enjoyable company I had with my colleagues and fellow researchers, Dr Anna Geyer, Dr Arindam Biswas, Dr Calin Martin, Dr Gaurav Bhatnagar, Dr Katerya Marynets, Dr Miles Wheeler, Dr Vikas Krishnamurthy, Susanna Haziot, Diksha Tiwari and Manjil Saikia during my stay in Vienna. The seed of enthusiasm to undertake this doctoral study in mathematics was probably already sown when my aunt Mrs Santwana Palit, an economist and computer scientist, exposed me to the idea of mass, energy and 'relativity' when I was a child; and my uncle Dr Susanta Basu (who himself is a mathematician) introduced me to the topics of topology and linear algebra, at an early age of nine. I feel this to be an appropriate time to acknowledge their contributions. Finally, I would like to mention the love, support and encouragement I have received from my mother Ratna, wife Malabika and daughter Atmaja during the past few years. They had willingly made sacrifices to allow me to fulfill my dream. My daughter's interest in 'funny maths' has been my constant source of encouragement. This thesis would not have been written without their active support.

Contents

Introduction

0.1 Overview and motivation

Most of the current analysis related to estimating forces on maritime and offshore structures, estimating power generated by wave energy devices and design of possible means of flood control at coastal regions are based on linear irrotational potential theory of wave propagation. However, it is well known from field data and experimental evidence that linear theory is not valid in reality and small perturbations from linearity is at best an approximation. Recent failures of several wave energy converters and problems associated with offshore wind turbines is a testimony to this fact. Moreover, in most cases waves are associated with vorticity and hence potential theory miserably fails to account for wave-current interactions.

0.2 Background and literature review

The nonlinear interaction between current and wave in flows over finite depth influencing the ocean dynamics and sediment transportation is not unknown [71]. Several regions around the world witness the effect of surface waves and internal current. The Bay of Biscay is one of the world's strongest generation sites for internal currents where current amplitudes of 25 cm/s have been observed [67]. A maximum value of 12 cm/s of current speed has been observed at a station over the French continental slope down to a water depth of 2300 m [99]. This also validates the influence of internal currents on the flow field as measurements confirm that the barotropic tidal current speed due to the surface tide is only 3 cm/s. Measurements at a point further offshore located at the south edge of the Merriadzeck Terrace revealed an increase in the velocity of the current near the deepest level at 2400 m reaching a value more than 20 cm/s [99]. Scottish coasts are mainly influenced by North Atlantic currents. In addition, a jet-like current along the edge of the continental slope with speeds in the range of 15 to 30 cm/s exists centred approximately over a 400-500 m depth contour [14]. Tidal currents are intensified in localised areas, usually when the topography constrains the flow such as between Orkney and Shetland, where tidal currents can be as high as 3.5-4.5 m/s [14]. Speed of current is observed to be relatively slower in Galway bay test site in the west of Ireland on a typical summer day. Real time observations are provided by Marine Institute at the Spiddal wave buoy site (available from www.oceanenergyireland.com) and the mean current speed on a typical day of June 2016 has been observed to be 0.26 m/s at a location 1.5 km offshore with a shallow water depth less than 25 m.

The topic of Stokes waves of large amplitude is an interesting hydrodynamic problem which has drawn attention of researchers in the recent years. Contributions to analytical theories and studies related to deepwater waves mainly have been due to the work carried out by Toland and his co-workers (e.g., [2, 3, 18, 106, 107]). An irrotational two-dimensional periodic wave solution of the governing fluid equations of motion with a free surface flowing over a flat bed, and possessing (i) a symmetric profile, (ii) a crest and a trough per wavelength and (iii) a constant speed at the surface, leads to a Stokes wave. The only driving force of action in this case is the gravity. Such a problem can be mathematically formulated as a nonlinear wave propagation problem with free boundary for harmonic functions over a planar domain and exhibits rich mathematical structures. This allows the study of the Stokes wave problem of large amplitude following mathematical approaches like the maximum principles, nonlinear operator theory and topological methods for global bifurcation. Strong qualitative conclusions can be derived from maximum principles for harmonic functions in combination with exploiting some of the physical structures of the problem itself. Significant amount of research has been carried out by Constantin and his colleagues on investigating the structures and behavior of Stokes wave, pressure and flow beneath the surface and trajectories of particles [25, 26, 32, 36, 43, 46, 49]. Some other noteworthy work has been carried out in this area of nonlinear water waves (see [23, 27, 34, 74, 75, 81, 110]). However, large amplitude steady travelling waves in flows over a finite depth with an underlying current have received little attention so far.

In contrast to steady periodic waves, solitary waves demonstrate a localized presence having a symmetrical profile and propagating on the water surface as a single hump decaying rapidly on either side to almost flat level far ahead and far away from the crest. Since its first discovery by Scott Russell from experiments carried out in canals, solitary waves have been observed in nature and also have been simulated in laboratory. Solitary waves have attracted the attention of the researchers and a large volume of research has been carried out including some recent revelations about these waves [37, 50]. Solitary waves are gravity waves as the only restoring force acting on the water in this case is gravity (and surface tension can be ignored if amplitudes are not very small). These waves have a one-dimensional structure as no localized steady gravity waves with a two-dimensional profile (i.e., 3D solitary waves) can exist [54].

The rigorous theory of solitary waves was developed by Fredrich and Hyers [66] and was further addressed by Beale [15]. A significant contribution to the analytical theory for solitary waves has been made by Toland and collaborators ([1, 2, 3]) which has provided information about the structure of these waves. Even though a large amount of investigation has been carried out on the solitary waves, properties of the underlying flow only has been the attention of research in the recent past, with only a few papers concentrating on this aspect. A good survey of the literature is available in [27]. Constantin and Escher [37] studied the particle trajectories in solitary waves while Constantin et al. [50] developed the mathematical theory for the pressure beneath a solitary wave including experimental verification of the same. The rigorous analysis of the pressure field in its own right for water waves was initiated in [46], and some interesting further recent developments can be found in the papers [33, 75, 91, 92]. Some studies have focussed on linearized theories for small amplitudes [61, 108] and on numerical investigations [62]. Focus on large amplitude waves has been recent and has been concentrated on by researchers such as Chen et al. [22], Constantin [26], Constantin and Strauss [46] and Hsu et al. [79]. Wheeler [117, 118] constructed large amplitude solutions for solitary waves with vorticity and provided some bounds on Froude number. Henry [76] has developed the pressure transfer function for solitary water waves in the presence of vorticity. Existing literature on solitary waves indicates that inspite of the large volume of research activities in the area, investigations focussing on the flow and pressure fields beneath the water surface for solitary waves of large amplitude over a fixed mean depth (including underlying current) are still incomplete.

Since the systematic investigation by Constantin and Strauss [43], the classical hydrodynamic problem concerning two-dimensional travelling water waves with vorticity has generated considerable interest among researchers. The existence of global continua of smooth solutions for waves with vorticity was proved by Constantin and Strauss [43] for the finite depth problem and Hur [80] considered the related problem of periodic waves over infinite depth. The solutions in [43] and in [80] have exactly one crest and one trough per period, and are monotone between successive crests and troughs, having a vertical axis of symmetry. Symmetry of steady periodic surface waves with vorticity both for deep water and for water waves over finite depth have been investigated by Constantin and Escher [35, 36]. Variational approach for water waves with vorticity was formulated by Constantin et al. [52] and stability properties of steady water waves with vorticity were studied by Constantin and Strauss [44]. Further, Constantin and Escher [38] proved that periodic travelling free surface waves are analytic in the absence of stagnation points. Constantin and Strauss [45] investigated the location of the point of maximal horizontal velocity for steady periodic water waves with vorticity to provide an insight to water waves near stagnation and a similar investigation was carried out by Varvaruca [113] for a large class of vorticity functions. In both the cases, it was assumed that the horizontal velocity of the fluid, u is less than the travelling wave speed, c. Existence of extreme waves with vorticity and the Stokes conjecture was proved by Varvaruca [114, 115]. Constantin and Strauss [47] investigated the periodic travelling gravity waves in the case of discontinuous vorticity. Regularity and local bifurcation results were proved by Constantin and Varvaruca [48] for constant vorticity. Further, global bifurcation results of steady gravity water waves with critical layers in a flow of constant vorticity were proved by Constantin et al. [53] and some conjectures were put forward based on results available from numerical computations ([57, 112]).

Even though there has been development on water waves with vorticity in the last few years, still very little is known about velocity field in the fluid domain. Numerical evidence ([57, 86]) in the case of constant vorticity suggests that stagnation points exist for negative and small positive vorticity. Also, for large positive vorticity, the solutions can bifurcate from trivial solutions to waves with overhanging profile, without approaching extreme waves. Constantin and Strauss [43] proved that for an arbitrary vorticity distribution and for any given wave speed $c > 0$ with a given relative mass flux, there exists a global continuum of steady periodic water waves travelling at a speed c, such that $u < c$ throughout the fluid. The continuum contains waves with u arbitrarily close to c. In [45], it was shown that the points of maximal horizontal velocity is necessarily the crest for a certain class of waves (with small negative vorticty). This result was further extended by Varvaruca [113] for a larger class of vorticity but with a further condition on the derivative of vorticity function. However, knowledge about the precise location of the points of maximum/minimum horizontal velocity or the properties of the velocity field in the fluid domain for more general classes of vorticity with less restrictions is still lacking. Ehrnström [60] established some results on streamlines, velocity field and particle paths within the fluid domain for rotational flows relying on strong maximum principles. Existing literature suggest that results and knowledge on the behaviour of the flow field within the fluid domain for large amplitude rotational water waves are still far from complete. For example, it was noted in [60] that there are no results available on how the horizontal velocity varied within the domain or on the general control of horizontal velocity in the interior of the fluid; or for that matter even on how the slope of the streamlines varied vertically along the depth of the fluid medium.

Typically, in previous studies related to the existence of water waves, an essential approach is to formulate an equivalent problem in a fixed domain. Bifurcation theory is then used as the most successful tool to prove the existence results. For example, in the case of irrotational flows, hodograph transform is used to map the unknown domain occupied by the fluid to a fixed horizontal strip in a complex plane, where the variable is the complex potential of the fluid flow. In these transformed coordinates, a nonlinear integral equation is formulated for a function of one variable, which is the angle of inclination between the tangent to the free surface and the horizontal [2, 87, 106]. Another approach which also works for water waves with vorticity, under the assumption that the streamfunction ψ is monotone in the vertical direction, is a streamfunction formulation where a transform $(X, Y) \mapsto (X, -\psi)$ can be used [43] to convert the problem into a nonlinear boundary value problem with quasilinear elliptic equation on a strip. The studies by [16, 88] have mentioned in their papers about a quantity called flow force, related to flow of fluid with free surface over a flat bed. The quantity, flow force, has the property that it is zero on the flow bed and is invariant on the free surface. This opens up a possibility to transform the unknown free boundary problem to a fixed domain with a suitable transformation involving the flow force.

Wave heights play also an important role in estimating forces on maritime and offshore structures, estimating power generated by wave energy devices and designing possible means of flood control at costal regions. Observations of sea waves can be either done remotely by satellite measurements or by in situ measurements. Remote-sensing techniques being an indirect way of measurement require ground-truth verification. Recovery of wave heights from pressure data at the bed is a practical means to estimate wave heights from in-situ measurements which can be also used for such verifications. Use of pressure sensors among other types of sensors are widespread in practice due to their low costs, ease of installation and relatively less liability in the event of damage [82]. Pressure sensors are usually deployed underwater at fixed loactions on the rigid bed. These sensors provide accurate measurement of the pressure at the bed, but recovery of wave heights from these pressure measurements requires some additional considerations to unfold the pressure-wave height relationship. Researchers in the past have developed expressions for recovering the wave height from the pressure at the bed, e.g. [97] used the hydrostatic formula for tsunami detection and [61] developed explicit expressions for pressure and surface waves in the setting of linear wave theory. However, these studies either did not consider the wave effects or are valid for waves of small amplitude. In fact, linear theory may overestimate wave heights by over 10% even for waves of moderate amplitude when compared with observed data [108]. Since most waves relevant in ocean engineering do not fall into the category of small amplitude theory, it is necessary to consider the governing equations without approximations. Researchers such as [97], [58], [28], [25], [24], [31] and [33] have pursued further investigations in this direction. Considering the presence of vorticity, Henry [76] showed that pressure function on the flat bed prescribes a unique surface profile for the resulting solitary waves. The conclusion derived from these investigations was that an exact recovery of the wave profile from the pressure at the flat bed is indeed possible. However, in this context the only explicit results for the recovery of surface profile is due to [28] for solitary waves while others such as [25] and [24] require either the solution of either a non-linear differential equation or an implicit functional equation for periodic travelling waves. Constantin [32] recently developed another approach to provide simple, explicit but accurate estimates of wave heights for the fully nonlinear large amplitude 2D travelling gravity waves which differed from some of the previously proposed approaches and results. Inspite of several results available on the wave height recovery problem, simple and accurate expressions for the recovery of wave heights from the pressure data at the bed for the case of large amplitude surface waves with underlying currents, are not available in the literature currently.

Currents also play a major role in influencing the ocean dynamics. Understanding of undercurrents and their effect in general and specifically for Pacific Equatorial Undercurrent is important because of the contribution made to various sources has profound influence on temperature, salinity, and the nutrient enrichment of equatorial thermocline and will impact the biological productivity, atmospheric carbon exchange and El-Niño Southern Oscillation (ENSO). Presence of Pacific equatorial undercurrents were first observed in the 1950s by Cromwell [56] and subsequently measured [85]. Several further investigations have been carried out in the past few decades [93]. The equatorial undercurrent (EUC) has been mapped over the years, a study worthy of mention is the Tahiliti-Hawaii Shuttel Experiment [119] as a part of the World Ocean Circulation Experiment (WOCE). Investigations using global observation models have also shown that Pacific EUC will strengthen in future [59], which then is expected to impact the equatorial ocean dynamics.

The EUC is the major source of water upwelled to the eastern Pacific equatorial region of cold tongue [119] and is also the primary supplier of the limiting nutrient iron brought from the sedimentary sources of Papua New Guinea shelves [101]. The role of this supply of iron nutrient is vital in production of CO_2 fluxes in the equatorial Pacific and further controls the export of carbon into the deep ocean [59, 64, 84].

The EUC has also been associated with the cause of long-term (decadal) climate variability. Extratropical sea surface temperature anomalies are transmitted to the Tropics by way of intergyre exchange; reappearing along the equator after several years of incorporation into the EUC and then resufacing again. Existence of a subsurface ocean 'bridge' is a possible connection between the warm sea surface temperature (SST) anomaly in the North Pacific during the early 1970s and the subsequent warm SST anomaly along the equator in the 1980s. However, the possible contribution of low latitude wind stresses to equatorial warming cannot be ignored [103, 73].

Equatorial ocean dynamics has some striking features. Close to the Equator the meridional component of the Coriolis force is negligible (vanishing at the Equator). This leads to the breakdown of geostrophy. The flow in this region is essentially wind-driven: by the easterly trade winds in the Pacific and Atlantic, and by the seasonally reversing monsoonal winds in the Indian Ocean [105]. Equatorial ocean regions also present a pronounced stratification, greater than anywhere else in the ocean [63]. Several aspects of undercurrents such as termination, source, divergence and upwelling have been the focus of research in the past decades [90, 109, 83]. Measurements and observations have been the basis of modelling the nature of undercurrents [93, 111]. The simplest model of the EUC is based on a homogeneous fluid subject to uniform westward stress at the surface. This local model is unstratified. More realistic models considering effects of stratification lead to layered models of undercurrents. Other non-local and physical models include a pressure head and has an extra-equatorial origin. Observations indicate that some of the water in the EUC flows from sub-tropical gyres. A two layer inertial model of undercurrents can account for equatorial and extra-equatorial dynamics.

Initially proposed local theories of undercurrent [55] were developed further [104, 116, 102] including the development of linear non-dissipative models [68, 69, 96]. Subsequently, linear models [94] have been significantly extended to include effects of continuous stratification [94]. Some nonlinear models have also been developed [19, 20, 21, 96]. and inertial theories [65] also have been further advanced [98]. The inertial approach was integrated with the local perspective by McCreary and Lu [95] who considered the EUC as a part of a larger and more complex subtropical current system, with both local and inertial effects. A complete model to capture the effect of integrated dynamics, however, requires recourse to numerical computations.

The basic variation with depth of the main azimuthal flow of the EUC can be modelled in the spherical geometry of a rotating Earth [41], to capture the fine structure. However, there are advantages in using the standard β-plane approximation. It permits one to capture variations in the meridional direction (in particular, following the Earth's curvature) that are not available within the framework of the f-plane approximation; see [40], for an overview of ocean dynamics in the equatorial Pacific in the f-plane setting. Without further approximations, explicit solutions to the nonlinear governing equations in the equatorial β-plane, were recently obtained in the Lagrangian framework [29, 39, 30, 77, 78]. These solutions represent realistic flow only for the region near the surface or in the neighbourhood of the thermocline. The performance is not so satisfactory within the entire vertical extent of the equatorial flow and this is due to the limitations on the permissible underlying currents.

A model based on fundamentals of fluid mechanics has been recently proposed by Constantin and Johnson [42]. The model is developed following a systematic approach which is mathematically consistent capturing the essential properties of the nature of flow observed in the Pacific equatorial undercurrent (EUC). The model is nonlinear and three-dimensional in nature. This analytical model avoids any oversimplification and, for example, accounts for the Coriolis effects due to the rotation of the Earth and retains non-traditional terms arising in the formulation. The model is based on the assumption of slow evolution of a two-layer flow in the equatorial direction and successfully provides asymptotic solutions.

Past studies have used trajectory analysis to look at various aspects of Pacific EUC. A 3 $\frac{1}{2}$ layer model was used to study the tropical cells and quantitative estimation of source of the EUC water [89]. A relatively coarse resolution Oceanic General Circulation Model (OGCM) simulation was carried out to quantify local exchanges as EUC flows from Indonesia to Peru [17]. Other studies examined the mean-time composition of EUC waters [70, 72] and variability in pathways of Pacific EUC [100]. While increasing computing resources and parametrizing subgrid-scale phenomena have resulted in more realistic simulations, analytically tractable and mathematically consistent models such as the one proposed by Constantin and Johnson, which arise out of and inherently satisfies the fluid dynamics equations and principles, are valuable to provide insight to complex nonlinear phenomena. It also has the potential to be integrated with other OGCM for computational efficiency. This motivates a numerical and parametric study of the flow paths /trajectories in the ocean based on the Constantin-Johnson model with a view to identify the nonlinear three-dimensional nature of the flow, correlate with known observations and explore the unknowns.

0.3 General setting of the problem

We consider the governing equations of fluid dynamics for 2D free surface gravity waves represented by the Euler equations of fluid flow. It is assumed that

(i) the flow velocities u and v along the horizontal axis X and the vertical axis Y respectively have one crest and one trough for period L ,

(ii) free surface η is strictly monotonic between successive crests and troughs,

(iii) η, u, and the pressure P are symmetric about crest line X = 0, and

(iv) v is anti-symmetric about crest line.

We assume all these functions to be smooth: in absence of stagnation points they must be real-analytic (see the discussion in [38]). Further, a profile that is monotone between successive crests and troughs has to be symmetric (see [51]). Under these assumptions, various specific sub-problems addressed in this thesis involve seeking and hence dealing with smooth solution(s) for which there exist(s) a period $L > 0$, a wave speed c for some current profiles considered, such that the free surface profile η, the flow field $(u; v)$ and the pressure P have period L in X variable, η depends on $X - cT$ while $(u; v)$, and P are dependent on $x = X - cT$ and $y = Y$, where T is the time variable.

In the moving frame, the flow is steady occupying a fixed region in the (x, y) plane, lying between the horizontal axis $B = \{(x; -d) : x \in \mathbb{R}\}$ which is the flat bed for some $d > 0$ and some apriori unknown free surface $S = \{(x; \eta(x)) : x \in \mathbb{R}\}$, with η a periodic function. Hence, the governing equations are considered in the moving frame of reference with $x = X - cT$; $y = Y$.

0.4 Proposed objectives

Based on the review of the existing literature some research questions have been identified. To address these questions the following objectives have been proposed:

(i) To investigate the 2D free boundary non-linear problem for large amplitude smooth Stokes waves over finite depth with uniform currents by proving the nature of flow and pressure fields and also by proving the existence of such waves.

(ii) To investigate the propagation of 2D solitary waves over finite depth with uniform underlying currents and examine the flow and pressure fields.

(iii) To prove the velocity and pressure profiles for large amplitude water waves with a general vorticity including carrying out investigations on the possible locations of the global/local maxima/minima of the velocity field.

(iv) To obtain bounds on estimates of wave heights (without limitation on amplitudes) for flows with uniform currents.

(v) To develop a novel reformulation of the classical water wave problem with flowforce functions by converting the free boundary problem to a fixed domain problem.

(vi) To prove the existence of wave solutions for the flowforce based reformulated problem and investigate the local bifurcation behaviour.

(vii) To apply Euler equations in a rotating frame of reference for modelling geophysical flows in ocean and to investigate both analytically (by deriving some exact results based on asymptotics) and numerically the influence of undercurrents on ocean dynamics.

0.5 Structure and contribution of the thesis

The proposed objectives have been met in this thesis by carrying out various mathematical analysis to address the related research questions. The results have been published or accepted for publication as articles in journals, and one article is currently under review in a journal for consideration of publication. This doctoral thesis is composed of these publications and articles which I have written during my PhD studies at the Faculty of Mathematics at the University of Vienna, and may be divided into three parts.

In the first part, presented in the six research articles, [4], [5], [8], [6], [7] and [11], the results on the qualitative behaviour of the flow field inside the fluid domain for large amplitude waves (both steady and solitary) propagating over finite depth in the presence of underlying currents (both pure uniform and possessing the characteristics of a more general vortcity) governed by Euler equations are discussed. More precisely, exploiting the maximum principles, mathematical approaches have been developed in [4] and [11] to analyze the velocity and the pressure field, including investigating the precise location of the global/local maxima/minima, generalizing some of the existing results (meeting objectives (i) and (iii)). Two possible situations, one with current speed $k >$ wave speed c, and the other with $k < c$, have been identified and analyzed. Amongst other results, the possibility of co-existence of propagating steady surface waves and an underlying uniform current at the wave speed is settled - this can only happen if the surface is flat. The existence result for steady waves with uniform current (for the case of current speed $k >$ the wave speed c) has also been proved in [5] based on a bifurcation approach using nonlinear operator theory for integral equations. This leads to a new branch of bifurcation not reported previously in the literature. Also derived in [8] are results on the existence and some properties of the solitary waves in the presence of underlying uniform currents in terms of Froude number (objective (ii)). In [11], the properties of the velocity field for steady periodic water waves over a flat bed for a generalized class of C^1 vorticity functions γ are investigated. Results are proved based on the maximum principles and on the hodograph transformation of Dubreil-Jacotin of the fluid domain. For $u < c$ and a monotonically varying positive vorticity ($= u_y - v_x \geq 0$), the location of the maximal horizontal velocity has been proven to be the crest, generalizing some of the recently proven results available in the literature (objective (iii)). Using the results derived in [4], the recovery problem of obtaining the wave heights from the flow field (pressure/velocity) measurements is addressed in [6] and [7] (achieving objective (iv)). Several lower and upper bounds on wave height estimates have been obtained for waves with underlying uniform current, from the measured pressure at the bed and also from the measurements (of pressure and velocity) at intermediate depth.

In the second part of the thesis, laid out in the paper [13], the focus is on a novel reformulation of the irrotational steady water wave problem (also applicable to waves with underlying uniform current satisfying $k < c$), as proposed in objective (v). Exploiting the monotonicity property of the flowforce lines with depth, the unknown boundary problem is transformed into a problem with fixed domain. A flowforce function formulation of the irrotational water wave problem is developed. Variational approach is used to prove the existence of small amplitude irrotational travelling wave solutions. Local bifurcation results have been proved relying on the Crandall-Rabinowitz bifurcation theorem. These fulfill objective (vi).

The final part of the thesis consists of application of the Euler equation for water waves in a rotating frame of reference to Geophysical Fluid Dynamics (GFD) for studying the influence of the undercurrents on ocean dynamics, and results have been reported in the publications [9, 10, 12]; attaining objective (vii). For the purpose of analysis in this part of the thesis, the recently developed model by Constantin and Johnson which is a nonlinear, three-dimensional Pacific equatorial undercurrent model has been considered. Numerical investigations carried out verify some of the results related to single and multiple cellular flow structures obtained from the theoretical results and further explores additional features that may be present. In addition to streamlines, to examine the flow behavior, velocity amplitude maps have also been obtained. These maps assess the relative strength of the flow in the individual cells. Numerical results indicate that the flow configuration evolves along the line of the equator as evidenced from streamlines and velocity maps. The sensitivity of the flow field and the flow paths to the Pacific equatorial undercurrent is also examined. Analysis of the flow paths indicate the presence of several known and unknown features which are essentially non-linear and three dimensional, such as upwelling/downwelling, cellular flow structures, divergence of flow from the equator and extra-equatorial flows, subsurface ocean 'bridge' in the equatorial direction and sharp change in gradient of the flow path; and these can be simulated by the model. Finally, the model has been further developed to consider linear variation of density with depth, while retaining the Coriolis effect and consistency with β - plane approximation. Exact results of the asymptotic system of equations have been derived in a region close to the equator in the presence of an undercurrent and a thermocline.

References

[1] C J Amick and J F Toland. On solitary water-waves of finite amplitude. *Arch. Ration. Mech. Anal.*, 76(1):9–95, 1981.

[2] C J Amick and J F Toland. On periodic water-waves and their convergence to solitary waves in the long-wave limit. *Phil. Trans. Roy. Soc. London A*, 303:633–669, 1981.

[3] C J Amick, L E Fraenkel and J F Toland. On the Stokes conjecture for the wave of extreme form. *Acta Mathematica*, 148:193–214, 1982.

[4] B Basu. Irrotational two-dimensional free-surface steady water flows over a flat bed with underlying currents. *Nonlinear Anal. TMA*, 147:110–124, 2016.

[5] B Basu. On the existence of two-dimensional irrotational water waves over finite depth with uniform current. *Applicable Anal.*, 97(14):2523–2532, 2017.

[6] B Basu. Estimation of wave heights from pressure data at the bed in the presence of uniform underlying currents. *Nonlinear Anal.*, 156:82–89, 2017.

[7] B Basu. Wave height estimates from pressure and velocity data at an intermediate depth in the presence of uniform currents. *Phil. Trans. Roy. Soc. London A*, 376:2017.0087, pp1-12, 2017.

[8] B Basu. Solitary water waves propagating on an underlying uniform current over a finite depth. *Nonlinear Anal.*, 172:25–35, 2018.

[9] B Basu. One a three-dimensional nonlinear model of Pacific equatorial ocean dynamics: Velocities and flow paths. *Oceanography*, 31(3): 51–58, 2018.

[10] B Basu. Some numerical investigations into a nonlinear three-dimensional model of Pacific equatorial ocean dynamics. *Deep-Sea Res. Part II*, 160:7-15, 2019, https://doi.org/10.1016/j.dsr2.2018.11.013.

[11] B Basu. On some properties of velocity field for two dimensional rotational steady water waves. *Nonlinear Anal.*, 184:17–34, 2019.

[12] B Basu. On an exact solution of a nonlinear three-dimensional model in ocean flows with Equatorial Undercurrent. *Discr. Cont. Dyn. Sys.*, accepted, 2019.

[13] B Basu. A flowforce reformulation of steady irrotational water waves: Existence, regularity and local bifurcation *submitted*, 2019.

[14] J M Baxter, I L Boyd, M Cox, A E Donald, S J Malcolm, H Miles, B Miller and C F Moffat. *Scotland's Marine Atlas: Information for the national marine plan.* Marine Scotland, Edinburgh(UK), 2011.

[15] J T Beale. The existence of solitary water waves. *Comm. Pure Appl. Math.*, 30(4):373–389, 1977.

[16] T B Benjamin and M J Lighthill. On cnoidal waves and bores. *Proc. Roy. Soc. London A*, 224:448–4601954.

[17] B Blanke and S Raynaud. Kinematics of the Pacific equatorial undercurrent: An Eulerian and Lagrangian approach from GCM results. *J. Phys. Oceanogr.*, 27:1038–1053, 1997.

[18] B Buffoni, É Séré and J F Toland. Minimization methods for quasi-linear problems with an application to periodic water waves. *SIAM J. Math. Anal.*, 36:1080–1094, 2005.

[19] M A Cane. The response of an equatorial ocean to simple wind stress patterns: I. model formulation and analytical results. *J. Mar. Res.*, 37:232–252, 1979.

[20] M A Cane. The response of an equatorial ocean to simple wind stress patterns: II. numerical results. *J. Mar. Res.*, 6:355–398, 1979.

[21] J G Charney. Non-linear theory of a wind-driven homogeneous layer near the equator. *Deep Sea Res.*, 6:303–310, 1960.

[22] Y-Y Chen and H-C Hsu. A modified Euler–Lagrange transformation for particle orbits in nonlinear progressive waves. *Ocean Eng.*, 36(9):747–753, 2009.

[23] D Clamond. Note on the velocity and related fields of steady irrotational two–dimensional surface gravity waves. *Phil. Trans. Roy. Soc. London A*, 370:1572–1586, 2012.

[24] D Clamond. New exact relations for easy recovery of steady wave profiles from bottom pressure measurements. *J. Fluid Mech.*, 726:547–558, 2013.

[25] D Clamond and A Constantin. Recovery of steady periodic wave profiles from pressure measurements at the bed, *J. Fluid Mech.*, 714:463–475, 2013.

[26] A Constantin. The trajectories of particles in Stokes waves. *Invent. Math.*, 166(3):523–535, 2006.

[27] A Constantin. *Nonlinear Water Waves with Applications to Wave-Current Interactions and Tsunamis.* CBMS-NSF Conf. Series in Appl. Math., Vol. 81, SIAM, Philadelphia, 2011.

[28] A Constantin. On the recovery of solitary wave profiles from pressure measurements. *J. Fluid Mech.*, 699:376–384, 2012.

[29] A Constantin. An exact solution for equatorially trapped waves. *J. Geophys. Res.: Oceans*, 117:C05029, 2012.

[30] A Constantin. Some nonlinear, equatorially trapped, nonhydrostatic internal geophysical waves. *J. Phys. Oceanogr.*, 44:781–789, 2014.

[31] A Constantin. Stokes waves in water with a non-flat bed. *J. Fluid Mech.*, 740:17–27, 2014.

[32] A Constantin. Estimating wave heights from pressure data at the bed. *J. Fluid Mech.*, 743:R2, 2014.

[33] A Constantin. Extrema of the dynamic pressure in an irrotational regular wave train. *Phy. Fluids*, 28:113604, 2016.

[34] A Constantin. *Exact travelling periodic water waves for two-dimensional irrotational flows in "Nonlinear Water Waves, Cetaro, Italy 2013", pp 1–82.* Editor Adrian Constantin, Springer Lecture Notes in Mathematics, Vol. 2158, 2016.

[35] A Constantin and J Escher. Symmetry of steady deep-water waves with vorticity. *Eur. J. Appl. Math.*, 06:755–768, 2004.

[36] A Constantin and J Escher. Symmetry of steady periodic surface water waves with vorticity. *J. Fluid Mech.*, 498:171–181, 2004.

[37] A Constantin and J Escher. Particle trajectories in solitary water waves. *Bull. Amer. Math. Soc.*, 44(3):423 – 431, 2007.

[38] A Constantin and J Escher. Analyticity of periodic travelling free surface waves with vorticty. *Annals of Mathematics*, 173:559–568, 2011.

[39] A Constantin and P Germain. Instability of some equatorially trapped waves. *J. Geophys. Res.: Oceans*, 118(6): 2802 – 2810, 2013.

[40] A Constantin and R S Johnson. The dynamics of waves interacting with the Equatorial Undercurrent. *Geophys. Astrophys. Fluid Dyn.*, 109: 311–358, 2015.

[41] A Constantin and R S Johnson. An exact, steady, purely azimuthal equatorial flow with a free surface. *J. Phys. Oceanogr.*, 46:1935–1945, 2016.

[42] A Constantin and R S Johnson. A nonlinear, three-dimensional model for ocean flows, motivated by some observations of the Pacific equatorial undercurrent and thermocline. *Phys. Fluids*, 29:056604, 2017.

[43] A Constantin and W Strauss. Exact steady periodic water waves with vorticity. *Comm. Pure Appl. Math.*, 57:481–527, 2004.

[44] A Constantin and W Strauss. Stability properties of steady water waves with vorticity. *Comm. Pure Appl. Math.*, 60:911–950, 2007.

[45] A Constantin and W Strauss. Rotational steady water waves near stagnation. *Phil. Trans. Roy. Soc. London A*, 365(1858):2227–2239, 2007.

[46] A Constantin and W Strauss. Pressure beneath a Stokes wave. *Comm. Pure Appl. Math.*, 63:533–557, 2010.

[47] A Constantin and W Strauss. Periodic travelling gravity water waves with discontinuous vorticity. *Arch. Ration. Mech. Anal.*, 202: 133–175, 2011.

[48] A Constantin and E Varvaruca. Steady periodic water waves with constant vorticity: regularity and local bifurcation. *Arch. Ration. Mech. Anal.*, 199: 33–67, 2011.

[49] A Constantin and G Villari. Particle Trajectories in Linear Water Waves. *J. Math. Fluid Mech.*, 10:1–18, 2008.

[50] A Constantin, J Escher and H-C Hsu. Pressure beneath a solitary water wave: Mathematical theory and experiments. *Arch. Ration. Mech. Anal.*, 201:251 – 269, 2011.

[51] A Constantin, M Ehrnström and E Wahlén. Symmetry of steady periodic gravity water waves with vorticity. *Duke Math. J.*, 140:591–603, 2007.

[52] A Constantin, D Sattinger and W Strauss. Variational formulations for steady water waves with vorticity. *J. Fluid Mech.*, 548:151–163, 2006.

[53] A Constantin, W Strauss and E Varvaruca. Global bifurcation of steady gravity water waves with critical layers. *Acta Mathematica*, 217: 195–262, 2016.

[54] W Craig. Non–existence of solitary water waves in three dimensions. *Phil. Trans. Roy. Soc. London A*, 360(1799):2127–2135, 2002.

[55] T Cromwell. Circulation in a meridional plane in the central equatorial Pacific. *J. Mar. Res.*, 12:196–213, 1953.

[56] T Cromwell, R B Montgomery and E D Stroup. Equatorial undercurrent in Pacific ocean revealed by new methods. *Science*, 119:648– 649, 1954.

[57] A F T da Silva and D H Peregrine. Steep, steady surface waves on water of finite depth with constant vorticity. *J. Fluid Mech.*, 195:281–302, 1988.

[58] B Deconinck, K L Oliveras and V Vasan. Relating the bottom pressure and the surface elevation in the water wave problem. *J. Nonlin. Math. Phys.*, 19:179–189, 2012.

[59] E J Drenkard and K B Karnaukas. Strengtheing of Pacific equatorial undercurrent in the SODA reanalysis: Mechanics, ocean dynamics, and implications. *J. Amer. Meteorol. Soc.*, 27:2405–2415, 2014.

[60] M Ehrnström. Deep-water waves with vorticity: symmetry and rotational behaviour. *Discr. Cont. Dyn. Sys.*, 21:1141–1154, 2008.

[61] J Escher and T Schlurmann. On the recovery of the free surface from the pressure within periodic traveling water waves. *J. Nonlinear Math. Phys.*, 15:50 – 57, 2008.

[62] W A B Evans and M J Ford. An exact integral equation for solitary waves (with new numerical results for some 'internal' properties). *Proc. Roy. Soc. London A*, 452:373–390, 1996.

[63] A V Fedorov and J N Brown. *Equatorial waves, in "Enclycopedia of Ocean Sciences"*, edited by J. Steele, pp. 3679–3695. Academic Press, New York, 2009.

[64] R A Feely, T Takahashi, R Wanninkhof, M J McFadden, C E Cosca, S C Sutherland and M E Carr. Decadal variability of the air-sea CO_2 fluxes in the equatorial Pacific ocean. *J. Geophys. Res.: Oceans*, 111:C08S90, 2006.

[65] N P Fofonoff and R B Montgomery. The equatorial undercurrent in the light of the vorticity equation. *Tellus*, 7:518–521, 1955.

[66] K O Friedrichs and D H Hyers. The existence of solitary waves. *Comm. Pure Appl. Math.*, 7(3):517–550, 1954.

[67] T Gerkema, F-P A Lam and L R M Maas. Internal tides in the Bay of Biscay: Conversion rates and seasonal effects. *Deep Sea Res. Part II*, 51:2995–3008, 2004.

[68] A. E. Gill. The equatorial current in a homogeneous ocean. *Deep Sea Res.*, 18:421–431, 1971.

[69] A E Gill. Models of equatorial currents. *Proc. Numerical Models of Ocean Circulation*, pp. 181– 203, 1975.

[70] P J Goodman, W Hazeleger, P de Vries and M Cane. Pathways into the Pacific equatorial undercurrent: A trajectory analysis. *J. Phys. Oceanogr.*, 35:2134–2151, 2005.

[71] W D Grant and O S Madsen. Combined wave and current interaction with a rough bottom. *J. Geophys. Res.: Oceans*, 84:1797–1808, 1979.

[72] M Grenier, S Cravatte, B Blanke, C Menkes, A Koch-Larrouy, F Durand, A Melet and C Jeandel. From the western boundary currents to the Pacific equatorial undercurrent: Modelled pathways and water mass evolutions. *J. Geophys. Res.: Oceans*, 116:C12044, 2011.

[73] W Hazeleger, M Visbeck, M Cane, A Karspeck and N Naik. Decadal upper ocean temperature variability in the tropical Pacific. *J. Geophys. Res.: Oceans*, 106:8971–8988, 2001.

[74] D Henry. The trajectories of particles in deep-water Stokes waves. *Int. Math. Res. Not.*, 2006:23405,2006.

[75] D Henry. Pressure in a deep-water Stokes wave. *J. Math. Fluid Mech.*, 13:251–257, 2011.

[76] D Henry. On the pressure transfer function for solitary water waves with vorticity. *Math. Ann.*, 357:23–30, 2013.

[77] D Henry. An exact solution for equatorial geophysical water waves with an underlying current. *Eur. J. Mech.-B/Fluids*, 38:18–21, 2013.

[78] D Henry. Equatorially trapped nonlinear water waves in a beta-plane approximation with centripetal forces. *J. Fluid Mech.*, 804: R1,2016.

[79] H-C Hsu, Y-Y Chen, J R C Hsu and W-J Tseng. Nonlinear water waves on uniform current in Lagrangian coordinates. *J. Nonlin. Math. Phys.*, 16:47–61, 2009.

[80] V M Hur. Global bifurcation theory of deep-water waves with vorticity. *SIAM J. Math. Anal.*, 37(5):1482–1521, 2006.

[81] R S Johnson. *A modern introduction to the mathematical theory of water waves.* Cambridge University Press, 1997.

[82] N L Jones and S G Monismith. Measuring short-period wind waves in a tidally forced environment with a subsurface pressure gauge. *Limnol. Oceanogr. Methods*, 5:317–327, 2007.

[83] G C Johnson, M J McPhaden and E Firing. Equatorial Pacific ocean horizontal velocity, divergence, and upwelling. *J. Phys. Oceanogr.*, 31(3):839–849, 2001.

[84] K B Karnauskas and A L Cohen. Equatorial refuge and amid tropical warming. *Nat. Clim. Change*, 2(7):530–534, 2012.

[85] J A Knauss and J E King. Observations of the Pacific equatorial undercurrent. *Nature*, 158:601–602, 1958.

[86] J Ko and W Strauss. Large-amplitude steady rotational water waves. *Eur. J. Mech.-B/Fluids*, 27:96–109, 2008.

[87] G Keady and J Norbury. On the existence theory for irrotational water waves. *Math. Proc. Cambridge Phil. Soc.*, 83:137–157, 1978.

[88] G Keady and J Norbury. Waves and conjugate streams with vorticity. *Mathematika*, 25:129–150, 1978.

[89] P Lu, J P McCreary Jr and B A Klinger. Meridional circulation cells and the source waters of the Pacific equatorial undercurrent. *J. Phys. Oceanogr.*, 28:62–84, 1998.

[90] R Lukas. The termination of the equatorial undercurrent in the eastern Pacific. *Prog. Oceanogr.*, 16:63–90, 1986.

[91] T Lyons. The pressure distribution in extreme Stokes waves. *Nonlinear Anal. Real World Appl.*, 31:77 – 87, 2016.

[92] T Lyons. The pressure in a deep-water Stokes wave of greatest height. *J. Math. Fluid Mech.*, 18:209 – 218, 2016.

[93] J P McCreary Jr. Modeling equatorial ocean circulation. *Annual Rev. Fluid Mech.*, 17(1):359–409, 1985.

[94] J P McCreary. A linear stratified ocean model of the equatorial undercurrent. *Phil. Trans. Roy. Soc. London A*, 298:603– 635, 1981.

[95] J P McCreary Jr and P Lu. Interaction between the subtropical and equatorial ocean circulations: the subtropical cell. *J. Phys. Oceanogr.*, 24:466– 497, 1994.

[96] W D McKee. The wind-driven equatorial circulation in a homogeneous ocean. *Deep Sea Res.*, 20:889–899, 1973.

[97] K L Oliveras, V Vasan, B Deconinck and D Henderson. Recovering the water-wave profile from pressure measurements, *SIAM J. Appl. Math.*, 72: 897–918, 2007.

[98] J Pedlosky. Thermocline theories. In *General Circulation of the Ocean*, pp. 55–101. Springer, 1987.

[99] A Pichon and S Correard. Internal tides modelling in the Bay of Biscay. Comparisons with observations. *Scientia Marina*, 70:65–88, 2006.

[100] X Qin, A Sengupta and E van Sebille. Variability in the origins and pathways of Pacific equatorial undercurrent water. *J. Geophys. Res.:Oceans*, 120:3113–3128, 2015.

[101] J P Ryan, I Ueki, Y Chao, H Zhang, P S Polito and F P Chavez. Western Pacific modulation of large phytoplankton blooms in the central and eastern equatorial Pacific. *J. Geophys. Res.:Biogeosci.*, 111:G02013, 2006.

[102] A R Robinson. An investigation into the wind as the cause of the equatorial undercurrent. *J. Mar. Res.*, 24:179 – 204, 1966.

[103] N Schneider, S Venzke, A J Miller, D W Pierce, T Barnett, C Deser and M Latif. Pacific thermocline bridge revisited. *Geophys. Res. Lett.*, 26:1329–1332, 1999.

[104] H Stommel. Wind-drift near the equator. *Deep Sea Res.*, 6:298 – 302, 1960.

[105] L D Talley, G L. Pickard, W J Emery and J H Swift. *Descriptive physical oceanography: An introduction.* Elsevier, London, 2011.

[106] J F Toland. Stokes waves. *Topol. Methods Nonlinear Anal*, 7(1):1–48, 1996.

[107] J F Toland. Stokes waves in Hardy spaces and as distributions. *J. Math. Pures Appl.*, 79:901–917, 2000.

[108] C-H Tsai, M-C Huang, F-J Young, Y-C Lin and H W Li. On the recovery of surface wave by pressure transfer function. *Ocean Eng.*, 32:1247–1259, 2005.

[109] M Tsuchiya, R Lukas and F A Fine. Source waters of the Pacific equatorial undercurrent. *Prog. Oceanogr.*, 23:101–147, 1989.

[110] M Umeyama. Eulerian–Langrangian analysis for particle velocities and tracjectories in a pure wave motion using particle image velocimetry. *Phil. Trans. Roy. Soc. London A*, 370:1687–1702, 2012.

[111] G K Vallis. *Atmospheric and Oceanic Fluid Dynamics.* Cambridge University Press, 2006.

[112] J-M Vanden-Broeck. Some new gravity waves in water of finite depth. *Phys. Fluids*, 26:2385–2387, 1983.

[113] E Varvaruca. On some properties of travelling water waves with vorticity. *SIAM J. Math Anal.*, 39(5):1686–1692, 2008.

[114] E Varvaruca. On the existence of extreme waves and the Stokes conjecture with vorticity. *J. Differential Equations*, 246:4043–4076, 2009.

[115] E Varvaruca. The Stokes conjecture for waves with vorticity. *Ann. Inst. H. Poincaré Anal. Non Linéaire*, 29:861–885, 2012.

[116] G Veronis. An approximate theoretical analysis of the equatorial undercurrent. *Deep Sea Res.*, 6:318–327, 1960.

[117] M H Wheeler. Large-amplitude solitary water waves with vorticity. *SIAM J. Math. Anal.*, 45(5):2937–2994, 2013.

[118] M H Wheeler. The Froude number for solitary water waves with vorticity. *J. Fluid Mech.*, 768:91–112, 2015.

[119] K Wyrtki and B Kilonsky. Mean water and current structure during the hawaii-totahiti shuttle experiment. *J. Phys. Oceanogr.*, 14:242–254, 1984.

Irrotational two-dimensional free-surface steady water flows over a flat bed with underlying currents

Biswajit Basu

Nonlinear Anal. TMA 147, 110-124, 2016

Abstract

We investigate the free boundary non-linear problem for large amplitude smooth Stokes waves in flows of finite depth with underlying currents. The qualitative nature of the flow and pressure fields is investigated using maximum principles. Bounds on the surface profile have been derived. Influence of the relative magnitude of wave and current speed on the flow and pressure fields has been shown. The possible co-existence of propagating surface waves and an underlying uniform current at the wave speed is settled-this can only happen if the surface is flat.

1 Introduction

The topic of Stokes waves of large amplitude is an interesting hydrodynamic problem which has drawn attention of researchers in the recent years. Contributions to analytical theories and studies related to deep-water waves mainly have been due to the work carried out by Toland and his co-workers (e.g., [2, 1, 23, 24, 4]). An irrotational two-dimensional periodic wave solution of the governing fluid equations of motion with a free surface flowing over a flat bed, and possessing (i) a symmetric profile, (ii) a crest and a trough per wavelength and (iii) a constant speed at the surface, lead to a Stokes wave over a flat bed. The only driving force of action in this case is the gravity. Such a problem can be mathematically formulated as a nonlinear wave propagation problem with free boundary for harmonic functions over a planar domain and exhibits rich mathematical structures. This allows the study of the Stokes wave problem of large amplitude following mathematical approaches like the maximum principles. Strong qualitative conclusions can be derived from maximum principles for harmonic functions in combination with exploiting some of the physical structures of the problem itself. Significant amount of research has been carried out by Constantin and his colleagues on investigating the structures and behavior of Stokes wave, pressure and flow beneath the surface and trajectories of particles [12, 14, 16, 9, 7, 15, 6]. Some other noteworthy work has been carried out in this area of nonlinear water waves (see [20, 19, 21, 5, 25, 8]). However, large amplitude Stokes waves in flows of finite depth with an underlying current have received little attention so far.

The nonlinear interaction between current and wave in flows over finite depth influencing the ocean dynamics and sediment transportation is not unknown [18]. Several regions around the world witness the effect of surface waves and internal current. The Bay of Biscay is one of the world's strongest generation sites for internal current where current amplitudes of 25 cm/s have been observed [17]. A maximum value of 12 cm/s of current has been observed at a station over the French continental slope down to a water depth of 2300 m [22]. This also validates the influence of internal current propagating on the flow field as measurements confirm that the barotropic tidal current due to the surface tide is only 3 cm/s. Measurements at a point further offshore located at the south edge of the Merriadzeck Terrace revealed an increase in the velocity of the current near the deepest level at 2400 m reaching a value more than 20 cm/s [22]. Scottish coasts are mainly influenced by North Atlantic currents. In addition, a jet-like current along the edge of the continental slope with speeds in the range of 15 to 30 cm/s exist centred approximately over a 400-500 m depth contour [3]. Tidal currents are intensified in localised areas, usually when the topography constrains the flow such as between Orkney and Shetland, where tidal currents can be as high as 3.5-4.5 m/s [3]. Speed of current is observed to be relatively slower in Galway bay test site in the west of Ireland on a typical summer day. Real time observations are provided by Marine Institute at the Spiddal wave buoy site (available from www.oceanenergyireland.com) and the mean current speed on a typical day of June 2016 has been observed to be 0.26 m/s at a location 1.5 km offshore with a shallow water depth less than 25 m.

This paper aims to study the qualitative behavior of large amplitude smooth Stokes waves in flows of finite depth with uniform current. Velocity fields, pressure fields and surface profiles for flow under the joint influence of surface waves and an underlying uniform current are investigated and results on their qualitative nature have been proved. Since the explicit functional form of the surface profile is unknown, the current state-of-art on flow patterns and underneath pressure for large amplitude Stokes waves with underlying current is still not fully solved. Only recently some information and solutions are available from studies on nonlinear large amplitude Stokes wave over a finite depth [7, 15]. In this paper, maximum principles for harmonic functions on elliptic equations in combination with some structural properties of physical boundary conditions provide a way to unveil some of the structures of the flow and pressure fields as well as surface profile of the free boundary. Three specific situations arise depending on the relative speed of the surface waves and the average strength (speed) of the underlying current. It is shown that when the speed of the current is greater than the wave speed, the nature of the flow fields is different from what is expected where no underlying current was considered [7, 10]. The pressure field however is unaffected due to the presence of underlying currents. Further, we prove that a Stokes surface wave and an underlying uniform current of same speed cannot coexist in an irrotational two dimensional flow field.

This paper is organized as follows. In Section 2 we present the governing equations of motion. Section 3 establishes the framework for flow with currents. Section 4 analyses the case when the speed of the current exceeds the speed of surface waves. Qualitative nature of flow and pressure fields are obtained and proved. Bounds on surface profiles have also been presented. Section 5 and 6 analyze the cases when the speed of the current is equal to and less than the surface wave velocity respectively followed by some comments in Section 7.

1.1 Problem Definition

We seek an irrotational smooth solution to the governing equations of fluid dynamics represented by the Euler equations for which there exists a period $L > 0$, a wave speed c, and a current strength k such that the free surface profile η, the flow field (u, v) and the pressure P have period L in X variable, η depends on $X - cT$ while u, v, and P are dependent on $X - cT$ and Y. Also, it is assumed that

(i) u and v have one crest and one trough for period L

(ii) η is strictly monotonic between successive crests and troughs

(iii) η, u, and P are symmetric about crest line

(iv) v is anti-symmetric about crest line

We assume all these functions to be smooth: in absence of stagnation points they must be real-analytic (see the discussion in [13]). Further, in an irrotational two-dimensional free-surface flow over a flat bed with no stagnation points the free surface has to be a graph (see [26]) and a profile that is monotone between successive crest and troughs has to be symmetric (see [11]).

2 Governing equations in moving frame

In moving frame

$$x = X \ - cT \ , \quad y = Y \ , \tag{2.1}$$

the governing equations are

$$\begin{aligned}
(u-c)u_x + vu_y &= -\frac{1}{\rho}P_x, \quad \text{for} \quad -d \le y \le \eta(x)\\
(u-c)v_x + vv_y &= -\frac{1}{\rho}P_y - g, \quad \text{for} \quad -d \le y \le \eta(x)\\
u_x + v_y &= 0, \quad \text{for} \quad -d \le y \le \eta(x)\\
u_y &= v_x, \quad \text{for} \quad -d \le y \le \eta(x)\\
v &= 0, \quad \text{on} \quad Y = -d\\
v &= (u-c)\eta_x, \quad \text{on} \quad y = \eta(x)\\
P &= P_{atm}, \quad \text{on} \quad y = \eta(x) \ .
\end{aligned} \tag{2.2}$$

The flow invariants in the setting of (2.2) are expressed as follows:

(i) Mass flux (flow rate per unit width), relative to uniform flow at constant speed c

$$M = \rho \int_{-d}^{\eta(x)} \left[u(x,y) - c\right] dy \tag{2.3}$$

is invariant with x. This follows from the third, fifth and sixth relations in (2.2) and by differentiation with respect to x.

(ii) Conservation of energy or head follows from the first, second and fourth relations in (2.2) and by differentiation. The expression of energy

$$\varepsilon = \rho \frac{(u-c)^2 + v^2}{2} + P + \rho g(y+d) \tag{2.4}$$

is constant throughout the fluid (this is Bernoulli's law). This allows us to express the last relation in (2.2) as a constraint in terms of a physical constant, H called head.

(iii) The flow force as a sum of pressure force per unit width and the momentum flux per unit width is expressed as

$$S = \rho \int_{-d}^{\eta(x)} \left[u(x,y) - c\right]^2 dy + \int_{-d}^{\eta(x)} \left[P(x,y) - P_{atm}\right] dy \tag{2.5}$$

is an invariant with respect to x following from the first, third and sixth relation in (2.2) and by differentiation.

Note that if u is constant, v is also constant and hence $P_x = P_y - g = 0$. Thus, differentiation of last relation in (2.2) forces the solution to be a flat surface with uniform underlying flow. For uniform flow with flat surface $\eta(x) = \eta_0 > -d$, the flow field is $(u_0, 0)$ (constant velocity) and the hydrostatic pressure is

$$P = P_{atm} - \rho g(y - \eta_0) \tag{2.6}$$

Also, we have

$$\begin{aligned} M &= \rho(u_0 - c)(\eta_0 + d) \\ H &= \frac{(c - u_0)^2}{2g} + \eta_0 + d \\ S &= \rho(c - u_0)^2(\eta_0 + d) + \frac{1}{2}\rho g(\eta_0 + d)^2 \end{aligned} \tag{2.7}$$

leading to

$$2gH = \left(\frac{M/\rho}{\eta_0 + d}\right)^2 + 2g(\eta_0 + d)\ . \tag{2.8}$$

If $\xi = (\eta_0 + d) > 0$, then $(2gH)^* = 3[gM/\rho]^{2/3}$ is a minimum at the critical value $\xi^* = [(M/\rho)^2/g]^{1/3}$. The value of ξ increases strictly monotonically on either side of ξ^* without any upper bound unless we invoke some physical mechanism. Consequently, for a given $2gH > (2gH)^*$ there are two positive solutions for ξ such that

$$\xi_- < \xi^* < \xi_+\ . \tag{2.9}$$

To reduce the number of variables in (2.2), a stream function $\Psi(x, y)$ can be defined as

$$\Psi_x = -v, \Psi_y = u - c\ . \tag{2.10}$$

The first relation in (2.10) and the fifth and sixth relations in (2.2) ensure that $\Psi_x = 0$ on the flat bed $y = -d$ and $\Psi_x + \Psi_y \eta_x = 0$ on the free surface $y = \eta(x)$. This implies that Ψ must be constant on $y = -d$ and on $y = \eta(x)$. Also, using the second relation in (2.10) leads to

$$\frac{M}{\rho} = \Psi(x, \eta(x)) - \Psi(x, -d)\ . \tag{2.11}$$

Hence, without any loss of generality we can assign $\Psi = 0$ on the free surface and $\Psi = -M/\rho$ on the bed. The transformed governing equations are

$$\begin{aligned} &\Psi_{xx} + \Psi_{yy} = 0, \quad \text{for} \quad -d \le y \le \eta(x) \\ &\Psi = 0, \quad \text{on} \quad y = \eta(x) \\ &\Psi = -M/\rho, \quad \text{on} \quad y = -d \\ &\Psi_x^2 + \Psi_y^2 + 2g(y + d) = 2gH, \quad \text{on} \quad y = \eta(x)\ . \end{aligned} \tag{2.12}$$

The two functions to be determined are $\eta(x)$ and $\Psi(x, y)$ which are both L-periodic and symmetric in the x-variable.

The pressure can be recovered from

$$P = P_{atm} + \rho gH - \rho g(y + d) - \rho\frac{\Psi_x^2 + \Psi_y^2}{2} \tag{2.13}$$

using the last relation of (2.2) and the invariance equation (2.4).

3 Flow with current

It is known that in absence of an underlying current, the horizontal fluid velocity u in the flow beneath a smooth Stokes wave propagating at a speed $c > 0$ can never attain a value of c (see [10]), i.e.

$$u(x, y) \neq c \quad \text{for} \quad -d \leq y \leq \eta(x) \; . \tag{3.14}$$

In the setting of periodic waves traveling at a constant speed at the surface of water in an irrotational flow over flat bed, for a given $y_0 \in [-d, \min_{x \in [0,L]} \{\eta(x)\}]$ we have

$$\int_0^L \int_- d^{y_0} \Psi_{yy}(x, y) dy dx = - \int_- d^{y_0} \int_0^L \Psi_{xx}(x, y) dx dy = 0 \tag{3.15}$$

from (2.12) and the periodicity of Ψ in the x-variable.

Hence,

$$\int_0^L u(x, -d) dx = \int_0^L u(x, y_0) dx \tag{3.16}$$

for any level $y = y_0$ below the trough level $y = \eta(L/2)$; we assume that the crest is located at $x = 0$. Thus, the strength of the uniform underlying current can be characterized by

$$k = \frac{1}{L} \int_0^L u(x, -d) dx \tag{3.17}$$

which is invariant with y as observed from Eq. (3.16).

Using the second relation in (2.10) we get

$$k = c + \frac{1}{L} \int_0^L \Psi_y(x, -d) dx \; . \tag{3.18}$$

Consequently, three cases arise

Case A $k > c$: strength (average speed) of the current greater that the wave speed

Case B $k = c$: strength (average speed) of the current equal to the wave speed

Case C $k < c$: strength (average speed) of the current less than the wave speed

4 Analysis of Case A: $k > c$

By denoting $k - c = \bar{c} > 0$, we get

$$\bar{c} = \frac{1}{L} \int_0^L \Psi_y(x, -d) dx \; . \tag{4.19}$$

To non-dimensionalize the system (2.12), for given M and H, we use the length scale ξ_+ (the depth of uniform supercritical flow corresponding to the invariants). The set of non-dimensional variables is given by

$$\bar{x} = \frac{x}{\xi_+}, \bar{y} = \frac{y + d}{\xi_+}, \zeta(\bar{x}) = \frac{\eta(x) + d}{\xi_+} - 1, \psi(\bar{x}, \bar{y}) = \frac{\rho \Psi(x, y)}{M} \; . \tag{4.20}$$

We assume $M \neq 0$ since we are seeking a nontrivial solution. Indeed, $M = 0$ means that the harmonic function Ψ vanishes on $y = \eta(x)$ and on $y = -d$, so the x-periodicity and maximum principles have $\Psi \equiv 0$ and therefore this corresponds to a trivial flow.

From (2.8),

$$2gH = \left(\frac{M/\rho}{\xi_+}\right)^2 + 2g\xi_+ \; . \tag{4.21}$$

The non-dimensional system of equations is

$$\begin{aligned}
&\Delta\psi = 0, \text{in} \quad 0 < \bar{y} < 1 + \zeta(\bar{x}) \\
&\psi = 0, \quad \text{on} \quad \bar{y} = 1 + \zeta(\bar{x}) \\
&\psi = -1, \quad \text{on} \quad \bar{y} = 0 \\
&|\nabla\psi|^2 + 2\mu\zeta = 1, \quad \text{on} \quad \bar{y} = 1 + \zeta(\bar{x})
\end{aligned} \tag{4.22}$$

where

$$\mu = \frac{g\rho^2\xi_+^3}{M^2} \geq 0 \tag{4.23}$$

is a non-dimensional parameter.

From (4.20) we conclude that $\zeta(\bar{x})$ and $\psi(\bar{x}, \bar{y})$ are periodic in $\bar{x}$-variable, with period

$$l = \frac{L}{\xi_+} \; . \tag{4.24}$$

We assume that wave crest and trough are located at $\bar{x} = jl$ and $\bar{x} = (2j+1)l/2$ with $j \in \mathbb{Z}$.

Using the non dimensional parameters (4.19) can be written as

$$\bar{c} = \frac{M}{\rho\xi_+}\frac{1}{l}\int_0^l \psi_{\bar{y}}(\bar{x}, 0)\, d\bar{x} \tag{4.25}$$

defining the propagation speed associated to a solution of (4.22).

4.1 Velocity field

A solution Ψ of (4.22) is a harmonic function throughout the closure $\bar{D}$ of the dimensionless fluid domain

$$D = \{(\bar{x}, \bar{y}) : 0 < \bar{y} < 1 + \zeta(\bar{x})\} \; .$$

Due to the periodicity in x variable and weak maximum principle, the maximum and minimum of the harmonic function ψ throughout $\bar{\Omega}$, where $\bar{\Omega}$ is the periodic domain

$$\bar{\Omega} = \{(\bar{x}, \bar{y}) : \bar{x} \in (-l/2, l/2), 0 < \bar{y} < 1 + \zeta(\bar{x})\}$$

occur only at the upper or lower boundary, since we are seeking a non-constant solution. The second and third relation in (4.22) thus ensure that the maximum and minimum of ψ are attained only on $\bar{y} = 0$ and $\bar{y} = 1 + \zeta(\bar{x})$ respectively. Further, Hopf's maximum principle yields $\psi_{\bar{y}} > 0$ at these boundaries. Since $\psi_{\bar{y}}(\bar{x}, \bar{y})$ is also harmonic and periodic in $\bar{x}$-variable in $\bar{D}$, we conclude that $\psi_{\bar{y}} > 0$ throughout $\bar{D}$ by maximum principle. Since $\bar{c} > 0$, (4.25) leads to

$$M > 0 \; . \tag{4.26}$$

This and (4.20) together with the fact that $\psi_{\bar{y}} > 0$ in $\bar{D}$, results in $\Psi_Y > 0$ for $-d \leq y \leq \eta(x)$ which in turn implies

$$u(x, y) > c \quad \text{for} \quad -d \leq y \leq \eta(x) \; . \tag{4.27}$$

Due to periodicity and antisymmetry of v, we see that any solution of (4.22) should be such that

$$\begin{aligned} \psi_{\bar{x}}(0,\bar{y}) &= 0 \quad \text{for} \quad \bar{y} \in [0, 1+\zeta(0)] \\ \psi_{\bar{x}}(l/2,\bar{y}) &= 0 \quad \text{for} \quad \bar{y} \in [0, 1+\zeta(l/2)] \\ \psi_{\bar{x}}(\bar{x},0) &= 0 \quad \text{for} \quad \bar{x} \in [0, l/2] \ . \end{aligned} \tag{4.28}$$

By differentiating the second relation in (4.22) with respect to $\bar{x}$-variable

$$\psi_{\bar{x}}(\bar{x}, 1+\zeta(\bar{x})) + \zeta'(\bar{x})\psi_{\bar{y}}(\bar{x}, 1+\zeta(\bar{x})) = 0 \ . \tag{4.29}$$

Since $\zeta'(\bar{x}) < 0$ for $\bar{x} \in (0, l/2)$ and $\psi_{\bar{y}} > 0$ throughout $\bar{D}$ we have

$$\psi_{\bar{x}}(\bar{x}, 1+\zeta(\bar{x})) > 0 \quad \text{for} \quad \bar{x} \in (0, l/2) \ . \tag{4.30}$$

Since $\psi_{\bar{x}}$ is harmonic, using the maximum principle along with (4.28) and (4.30) we conclude that the strict minimum of $\psi_{\bar{x}}$ is obtained on all along $\{(0,\bar{y}) : 0 < \bar{y} < 1+\zeta(0)\}$ for the domain $\{(\bar{x},\bar{y}) : \bar{x} \in (0,l/2), 0 < \bar{y} < 1+\zeta(\bar{x})\}$. Hopf's maximum principle gives $\psi_{\bar{x}\bar{x}}(0,\bar{y}) > 0$, for $\bar{y} \in (0, 1+\zeta(0))$ and thus $\psi_{\bar{y}\bar{y}}(0,\bar{y}) < 0$ (since ψ is harmonic) for $\bar{y} \in (0, 1+\zeta(0))$. Consequently, (4.20) and (4.26) lead to $\psi_{yy}(0,y) < 0$ for $y \in (0, 1+\zeta(0))$ which shows that

$$u(0,y) \ \text{ decreases strictly as } y \text{ raises from } \ -d \ \text{ to } \ \eta(0) \ . \tag{4.31}$$

We also observe that the strict minimum of $\psi_{\bar{x}}$ is obtained on all along $\{(l/2,\bar{y}) : 0 < \bar{y} < 1+\zeta(l/2)\}$ for the domain $\{(\bar{x},\bar{y}) : \bar{x} \in (0,l/2), 0 < \bar{y} < 1+\zeta(\bar{x})\}$. Hopf's maximum principle yields $\psi_{\bar{x}\bar{x}}(l/2,\bar{y}) < 0$ for $\bar{y} \in (0, 1+\zeta(l/2))$ leading to the result that

$$u(L/2,y) \ \text{ increases strictly as } y \text{ raises from } \ -d \ \text{ to } \ \eta(L/2). \tag{4.32}$$

Let us now consider the vertical velocity v. From the sixth relation of (2.2) we know that $v = (u-c)\eta_x$ on $y = \eta(x)$. Using (4.27) and that $\eta(x) \leq 0$ for $x \in [0, L/2]$ ensures $v(x,\eta(x)) \leq 0$ for $x \in [0, L/2]$. Also, $v(x,-d) = 0$ for $x \in [0, L/2]$ from the fifth relation of (2.2). Further, $v = 0$ on $x = 0$ and $x = L/2$ since v is odd and periodic in x-variable throughout Ω. Since $v \leq 0$ on the whole boundary of $\Omega_+ = \{(\bar{x},\bar{y}) : \bar{x} \in (0,l/2), 0 < \bar{y} < 1+\zeta(\bar{x})\}$, from maximum principle we have

$$v < 0 \quad \text{in} \quad \bar{\Omega}_+ \ . \tag{4.33}$$

Similar argument yields that for $\bar{\Omega}_- = \{(\bar{x},\bar{y}) : \bar{x} \in (-l/2,0), 0 < \bar{y} < 1+\zeta(\bar{x})\}$

$$v > 0 \quad \text{in} \quad \bar{\Omega}_- \tag{4.34}$$

which we expected since v is odd in x-variable.

Further u decreases strictly as we go from crest to trough along the lower three sides of Ω_+ resulting in the following strict inequalities

$$\begin{aligned} u_y(0,y) &< 0 \quad \text{for} \quad y \in [-d, \eta(0)] \\ u_x(x,-d) &> 0 \quad \text{for} \quad y \in [0, L/2] \\ u_y(L/2,y) &> 0 \quad \text{for} \quad y \in [-d, \eta(L/2)] \end{aligned} \tag{4.35}$$

on the three sides. Along these three sides, $v = 0$ and we get the middle relationship in (4.35) from Hopf's principle on using the third relation in (2.2), and (4.33) and (4.34).

4.2 Pressure field

The pressure is subharmonic in Ω since we can deduce from (2.2) that

$$\Delta P = -\Psi_{xx}^2 - 2\Psi_{xy}^2 - \Psi_{yy}^2 \leq 0 \tag{4.36}$$

by using the first two relations in (2.2). We have $P_y = -g < 0$ on $y = -d$. Hopf's maximum principle yields that the minimum value of P in $\bar{\Omega}$ is achieved all along the free surface $y = \eta(x)$, where $P = P_{atm}$ from (2.2). Further, Hopf's principle also states $P_y < 0$ on the free surface $y = \eta(x)$. Differentiating P with respect to the x-variable along the free surface along $(x, \eta(x))$ and using the monotonicity of the wave profile on the top free surface of Ω_+ i.e. along S_+ results in

$$P_x(x, \eta(x)) = -\eta'(x) P_y \leq 0 \tag{4.37}$$

for $x \in (0, L/2)$ with $P_x(x, \eta(x)) < 0$ wherever $\eta_x(x) < 0$. When $\eta_x(x) = 0$, for some $x_0 \in (0, L/2)$, then $v(x_0, \eta(x_0)) = 0$ and $P_x(x_0, \eta(x_0)) = 0$. If the maximum of v is attained within the closure of Ω_+ at $(x_0, \eta(x_0))$, then Hopf's principle implies $v_y(x_0, \eta(x_0)) > 0$. But a contradiction arises using the first and third relation of (2.2), which leads to $P_x = -(c-u)v_y > 0$ at $(x_0, \eta(x_0))$. Thus, we conclude that $\eta_x < 0, v < 0, P_x < 0$ at all points on $S_+ = \{(x, \eta(x)) : 0 < x < L/2\}$.

From the first and sixth relation in (2.2) we can deduce

$$\begin{aligned} P_x(x, \eta(x)) &= [c - u(x, \eta(x))] \cdot [u_x(x, \eta_x(x)) + \eta'(x) u_y(x, \eta(x))] \\ &= [c - u(x, \eta(x))] \partial_x u(x, \eta(x)) \ . \end{aligned} \tag{4.38}$$

Thus, we also conclude that on S_+

$$\partial_y(u(x, \eta(x))) > 0 \quad \text{for} \quad x \in (0, L/2) \ . \tag{4.39}$$

4.3 Surface Profile

Let us consider the crest of the surface profile i.e.

$$\max_{x \in [-L/2, L/2]} \{\eta(x) + d\} = \eta(0) + d \ . \tag{4.40}$$

We claim that $\eta(0) + d > \xi_+$. Indeed let us assume $\xi_+ \geq \eta(0) + d$. The fact that the expression $\left(\frac{M/\rho}{\xi}\right)^2 + 2g\xi$ is increasing for $\xi^* \leq \xi \leq \xi_+$ (where ξ^* is the critical depth) yields

$$\left(\frac{M/\rho}{\eta(0) + d}\right)^2 + 2g[\eta(0) + d] \leq \left(\frac{M/\rho}{\xi_+}\right)^2 + 2g\xi_+ = 2gH \tag{4.41}$$

using (4.21). Also, $v(0,0) = 0$ by anti-symmetry, so evaluating the head at the wave crest $y = \eta(0)$ we obtain

$$\Psi_y^2(0, \eta(0)) + 2g[\eta(0) + d] = 2gH \tag{4.42}$$

Hence, from (4.41) and (4.42) we get

$$[M/\rho]^2 \leq (\eta(0) + d)^2 \cdot \Psi_y^2(0, \eta(0)) \ . \tag{4.43}$$

Since $\Psi_y(0, y)$ is strictly decreasing as y varies from $-d$ to $\eta(0)$, this leads to

$$0 < M/\rho = \int_{-d}^{\eta(0)} \Psi_y(0, y) dy > (\eta(0) + d) \cdot \Psi_y(0, \eta(0)) \tag{4.44}$$

contradicting (4.43). Thus, we infer

$$\eta(0) + d > \xi_+ \ . \tag{4.45}$$

Let us now consider the trough of the surface profile, i.e.

$$\min_{x \in [-L/2, L/2]} \{\eta(x) + d\} = \eta(L/2) + d \ . \tag{4.46}$$

We claim that $\xi_- < \eta(L/2) + d < \xi_+$. Indeed, let us assume $\xi_+ \leq \eta(L/2) + d$. The fact that the expression $\left(\frac{M/\rho}{\xi}\right)^2 + 2g\xi$ is increasing for $\xi > \xi_+$ yields

$$\left(\frac{M/\rho}{\eta(L/2) + d}\right)^2 + 2g[\eta(L/2) + d] \geq \left(\frac{M/\rho}{\xi_+}\right)^2 + 2g\xi_+ = 2gH \tag{4.47}$$

using (2.8). Also we have

$$\Psi_y^2(L/2, \eta(L/2)) + 2g[\eta(L/2) + d] = 2gH \ . \tag{4.48}$$

Hence (4.47) and (4.48) give

$$[M/\rho]^2 \geq (\eta(L/2) + d)^2 \cdot \Psi_y^2(L/2, \eta(L/2)) \tag{4.49}$$

contradicting

$$0 < M/\rho = \int_{-d}^{\eta(L/2)} \Psi_y(L/2, y)dy < (\eta(L/2) + d) \cdot \Psi_y(L/2, \eta(L/2)) \tag{4.50}$$

since $\Psi_y(L/2, y)$ is strictly increasing as y varies from $-d$ to $\eta(L/2)$. Thus

$$\eta(L/2)) + d < \xi_+ \ . \tag{4.51}$$

Let us now assume $\eta(L/2) + d < \xi_-$. The fact that the expression $\left(\frac{M/\rho}{\xi}\right)^2 + 2g\xi$ is decreasing for $\xi < \xi_-$ gives

$$\left(\frac{M/\rho}{\eta(L/2) + d}\right)^2 + 2g[\eta(L/2) + d] \geq \left(\frac{M/\rho}{\xi_-}\right)^2 + 2g\xi_- = 2gH. \tag{4.52}$$

Also

$$\Psi_y^2(L/2, \eta(L/2)) + 2g[\eta(L/2) + d] = 2gH \tag{4.53}$$

leading to

$$[M/\rho]^2 \geq (\eta(L/2) + d)^2 \cdot \Psi_y^2(L/2, \eta(L/2)). \tag{4.54}$$

Since $\Psi_y(L/2, y)$ is strictly increasing in y from $-d$ to $\eta(L/2)$, we get

$$0 < M/\rho = \int_{-d}^{\eta(L/2)} \Psi_y(L/2, y)dy < (\eta(L/2) + d) \cdot \Psi_y(L/2, \eta(L/2)) \tag{4.55}$$

which contradicts (4.54) and therefore

$$\eta(L/2) + d \geq \xi_- \ . \tag{4.56}$$

Thus, we conclude that for the trough

$$\xi_- < \eta(L/2) + d < \xi_+ \ . \tag{4.57}$$

4.4 Some Qualitative Properties of the Velocity and Pressure Fields

We now proceed to prove some claims related to the velocity and pressure field. It may be noted that even though an underlying current exists, the flow is irrotational by virtue of the fact that the current is uniform. Recalling (4.27) and exploiting the irrotationality in the flow and defining velocity potential $\Phi(x,y)$ by

$$\Phi_x = u - c, \Phi_y = v \tag{4.58}$$

we transform the fluid domain with unknown surface boundary at the top to a rectangular domain by a conformal hodograph mapping with

$$\begin{aligned} q &= -\Phi(x,y) \\ p &= -\Psi(x,y) \ . \end{aligned} \tag{4.59}$$

The free boundary problem is transformed into a nonlinear boundary value problem for the harmonic function

$$h(q,p) = y + d \tag{4.60}$$

leading to

$$\begin{aligned} &\Delta_{q,p} h = 0 \quad \text{for} \quad -cL/2 < q < cL/2, -M/\rho < p < 0 \\ &h = 0 \quad \text{on} \quad p = -M/\rho \\ &2(\alpha - gh)(h_q^2 + h_p^2) = 1 \quad \text{on} \quad p = -0 \end{aligned} \tag{4.61}$$

with h-even and with periodicity cL in q, and α is a physical scalar constant related to the hydraulic head.

The images of Ω_+, S_+, B_+ under the transformation become

$$\begin{aligned} \hat{\Omega}_+ &= (0, cL/2) \times (-M/\rho, 0) \\ \hat{S}_+ &= (0, cL/2) \times \{0\} \\ \hat{B}_+ &= (0, cL/2) \times \{-M/\rho\} \end{aligned} \tag{4.62}$$

respectively.

If $(x, y(x))$ is the parametric equation of some streamline, then $\partial_x[\psi(x, y(x))] = 0$ by definition leads to

$$\partial_x[u(x,y(x))] = u_x + y' u_y = u_x + \frac{h_q}{h_p} \cdot u_y = \frac{1}{h_p} \cdot u_q \tag{4.63}$$

since

$$h_p = \frac{c-u}{(c-u)^2 + v^2} \ , h_q = \frac{-v}{(c-u)^2+v^2} . \tag{4.64}$$

Claim 1: The horizontal fluid velocity u, even in x, is a strictly increasing function of x along any streamline in $\bar{\Omega}_+$.

Proof: Since u and v are harmonic in (x,y), they are also harmonic in (q,p). So u_q is harmonic too. Considering the restriction of u_i to $\hat{\Omega}_+$ we have

$$u_q = \frac{1}{(c-u)^2 + v^2} \left[(c-u)u_x - v u_y\right] \ . \tag{4.65}$$

From (4.65), we deduce that only the lateral sides of $\hat{\Omega}_+$ (images of crest and trough lines), we have

$$u_q = \frac{1}{c-u} u_x = -\frac{v_y}{c-u} = 0, \quad \text{for} \quad q = 0 \ . \tag{4.66}$$

Similarly,

$$u_q = 0 \quad \text{for} \quad q = cL/2 \tag{4.67}$$

as $v = v_y = 0$ along these sides. On the boundary B^+, $v = 0$, so

$$u_q = \frac{1}{c-u} u_x < 0 \quad \text{if} \quad q \in (0, cL/2) \tag{4.68}$$

using (4.27) and (4.34). On the top boundary, S^+, we have $p = 0$ as

$$u_q = \frac{c-u}{(c-u)+v^2} \partial_x [u(x, \eta(x))] < 0 \tag{4.69}$$

for $p = 0$, $q \in (0, cL/2)$, using the sixth relation in (2.2), (4.27), and (4.39).

From (4.66)-(4.69) and applying the strong maximum principle applied to the harmonic function u_q, we find that $u_q < 0$ in the open rectangle $\hat{\Omega}_+$. But (4.63) together with $h_p < 0$ ensures that u is a strictly increasing function of x along any streamline in $\bar{\Omega}_+$. Since u is even in x, the function u is a strictly decreasing function of x along any streamline in $\bar{\Omega}_-$.

Claim 2: Along any fixed vertical line in the moving frame the absolute value of the slope of a streamline decreases with depth.

Proof: The slope of a streamline $y = y(x)$ is given by $y' = \frac{v}{u-c}$. The derivative of the slope is

$$\partial_y \frac{v}{u-c} = u_q \left(1 + \frac{v^2}{(c-u)^2}\right) < 0 \quad \text{in} \quad \Omega_+ \tag{4.70}$$

by Claim 1. By (4.27), (4.33), and (4.34), the slope is negative in Ω_+, positive in Ω_- and zero on the crest and trough lines.

Claim 3 The pressure gradient P_x at a point in fluid depends the position of the point with respect to the crest line: $P_x = 0$ below the crest, $P_x < 0$ in $\Omega_+ \cup S_+ \cup B_+$, $P_x > 0$ in $\Omega_- \cup S_- \cup B_-$, the component P_y is strictly negative throughout the fluid.

Proof: Using the bound of maximal slope of the surface wave (see the discussion in [8])

$$\eta_x^2(x, \eta(x)) < 1, x \in \mathbb{R} \ . \tag{4.71}$$

Using (2.2) and (4.65) we have

$$P_x = [(c-u)^2 + v^2] u_q \ . \tag{4.72}$$

Since $u_q < 0$ in $\hat{\Omega}_+ \cup \hat{S}_+ \cup \hat{B}_+$, we have $P_x < 0$ on $\Omega_+ \cup S_+ \cup B_+$. Similarly, we have $P_x > 0$ on $\Omega_- \cup S_- \cup B_-$.

Let us consider

$$\frac{d}{dx} \left\{ [c - u(x, \eta(x))]\, u(x, \eta(x)) \right\} = v_x (1 + \eta_x^2)(c-u) \tag{4.73}$$

we also have

$$v_y (c-v)(1-\eta_x^2) + 2v v_x + g \eta_x = 0, \quad \text{on} \quad y = \eta(x) \ . \tag{4.74}$$

Let us now consider $x \in (0, L/2)$ when $\eta'(x) < 0$. Hence, the sixth relation in (2.2) and (4.74) leads to

$$(c-u) \left(\frac{v_y}{\eta_x}(1-\eta_x) - 2v_x \right) + g = 0, \quad \text{on} \quad S_+ \ . \tag{4.75}$$

On using (2.2) and (4.39) we have $\frac{v_y}{\eta_x} > v_x$ on S_+, leading to

$$\frac{v_y}{\eta_x}(1-\eta_x^2) - 2v_x > -v_x(1+\eta_x^2) \quad \text{on} \quad S_+ \tag{4.76}$$

by virtue of (4.71).This combined with (4.73) and (4.75) and symmetry of u and anti-symmetry of v with the crest line gives

$$\frac{d}{dx}\left\{(c-u)v|_{y=\eta(x)}\right\} < g, x \in (-L/2,0) \cup (0,L/2)\ . \tag{4.77}$$

On the flat bed $v = 0$ and $v_x = 0$, so from (2.2), $P_y = -g < 0$ on $y = -d$. Further, P is super harmonic in the fluid domain and attains its minimum everywhere on the free surface $y = \eta(x)$. Hence, Hopf's maximum principle implies P_x is negative all along $y = \eta(x)$.

To investigate the behavior of P_y in Ω_+ we consider

$$f(x,y) = [c-u(x,y)]v(x,y) - gx, (x,y) \in \bar{\Omega}\ . \tag{4.78}$$

We can show

$$\Delta_{x,y} f = 0\ . \tag{4.79}$$

Since f remains harmonic in (q,p)-variables, f_q is harmonic in the strip $\hat{\Omega}_+$. We can get

$$f_q = v_x - \frac{g(c-u)}{(c-u)^2+v^2} \quad \text{in} \quad \mathbb{R}\times[-M/\rho,0]\ . \tag{4.80}$$

On the flat bed $y = -d$, we have $v = 0$ and $v_x(x,-d) = 0$ and from (4.80)

$$f_q = v_x - \frac{g}{c-u} > 0 \quad \text{on} \quad p = -M/\rho\ . \tag{4.81}$$

On the free surface we have $v = (u-c)\eta_x$. Thus, (4.80) gives

$$f_q = \frac{1}{(c-u)(1+\eta_x^2)}\left[v_x(c-u)(1+\eta_x^2) - g\right] \quad \text{on} \quad p = 0$$

and, (4.73), (4.77) give

$$f_q(q,0) > 0 \quad \text{on} \quad q \in (0, cL/2)\ . \tag{4.82}$$

On $\{(cL/2,p) : -M/\rho < p < 0)\}$ we have $v = 0$. As $v_x = 0$ by (2.2) and (4.35), we get from (4.82) that $f_q > 0$ there.

Since f_q is even in the q-variable and harmonic in $(-cL/2,cL/2)\times(-M/\rho,0)$, we obtain from maximum principle using (4.81) and (4.82),

$$f_q(q,0) = v_x - \frac{g(c-u)}{(c-u)^2+v^2} > 0 \quad \text{in} \quad [-cL/2,cL/2]\times[-M/\rho,0]\ . \tag{4.83}$$

Using results from Claim 1 and, (2.2) and (4.27), we can restate $v_y < \frac{vv_x}{u-c}$ in $\Omega_+ \cup S_+ \cup B_+$. Combining this with (4.33) and (2.2) we can show

$$P_y = -g + (c-u)v_x - vv_y < -g + \frac{v_x[(c-u)^2+v^2]}{c-u} \tag{4.84}$$

in Ω_+. From (4.83), this leads to $P_y < 0$ in Ω_+. Since on the crest line ($x = 0$) and on the trough ($x = L$) we have $v = 0$, we get

$$P_y = (c-u)v_x - g = (c-u)f_q < 0 \quad \text{on} \quad x = 0, x = L\ . \tag{4.85}$$

Thus $P_y < 0$ in $\bar{\Omega}_+$ and by evenness of P in the x variable, $P_y < 0$ in $\bar{\Omega}_-$.

5 Analysis of Case B: $k = c$

For the case where $\bar{c} = k - c = 0$, we have

$$\bar{c} = \frac{1}{L} \int_0^L \Psi_y(x, -d) dx = 0 \ . \tag{5.86}$$

Since Ψ is harmonic, derivative of Ψ, i.e., Ψ_y is also harmonic. By invoking mean value theorem for harmonic function, (5.86) implies $\Psi_y = 0$ on some point on the flat bed $y = -d$.

Now, let us consider the mass flux (relative to the uniform current of constant speed c) given in (2.3) expressed as

$$M = \rho \int_{-d}^{\eta(x)} \Psi_y(x, y) dy \ . \tag{5.87}$$

Noting that M is a scalar, three cases are possible: (i) $M = 0$, (ii) $M > 0$, (iii) $M < 0$.

(i) $M = 0$

From (2.12), since Ψ is harmonic, maximum and minimum of Ψ must occur on the boundary of the fluid domain Ω. But from the second and third equations in (2.12), we infer that $\Psi \equiv 0$ throughout Ω.

(ii) $M > 0$

Again maximum principle suggests that maximum and minimum values of the harmonic function Ψ must be on the boundaries, i.e., at the top surface or the bottom bed. The second and third equations of (2.12) imply that the minimum is on the bottom bed and the maximum is on the free top surface. Also, Hopf's maximum principle suggests that if Ψ is not constant throughout the domain Ω, then $\Psi_y > 0$ at the lower boundary where Ψ is minimum. However, by the mean value theorem, there must exist a point on the flat bottom bed where $\Psi_y = 0$, and this is the boundary $y = -d$ where the minimum is attained, leading to a contradiction. Hence, $\Psi \equiv 0$ throughout the domain Ω.

(ii) $M < 0$

Following argument similar to case (ii) with $M > 0$ suggests the occurrence of maximum on the bottom bed $y = -d$ due to maximum principle. Again, the requirement from Hopf's maximum principe of $\Psi_y < 0$ at the bottom flat bed is contrdicted by the existence of a point where $\Psi_y = 0$ on the flat bed, unless $\Psi \equiv 0$ in Ω.

Based on the results from the three cases discussed, we have

$$\begin{aligned} \Delta\Psi =& 0, \quad \text{for} \quad -d \le y \le \eta(x) \\ \Psi =& 0, \quad \text{on} \quad y = -d \\ \Psi =& 0, \quad \text{on} \quad y = \eta(x) \\ |\nabla\Psi|^2 + 2g(y + d) =& 1, \quad \text{on} \quad y = \eta(x) \end{aligned} \tag{5.88}$$

with the solution $\Psi \equiv 0$ throughout the domain Ω. This implies

$$\Psi_y = 0 \ \text{ and } \ \Psi_x = 0 \tag{5.89}$$

which in turn leads to

$$u = c \ \text{ and } \ v = 0 \tag{5.90}$$

i.e., it is a uniform flow with flat surface. The structure of a uniform current with the requirement of a simultaneous wave speed equal to the speed of a current has eliminated any hydrodynamic structure, i.e., simultaneous surface wave propagation at the same speed as of an underlying uniform current are conflicting and the wave propagation has been structurally eliminated to retain uniform current speed.

Remark: It is interesting to point out that the linearized wave propagation solution does admit the possibility of a surface wave with uniform current at the same speed [10].

Since $\psi = 0$, the pressure turns out to be harmonic because of (4.36) as well, i.e., P satisfies

$$\Delta P = 0, -d \leq x \leq \eta(x) \ . \tag{5.91}$$

Hence, using maximum principle the minimum/maximum pressure occurs at the boundaries. Also, from (2.2) we have

$$\begin{aligned} P_x &= 0 \\ P_y &= -g \end{aligned} \tag{5.92}$$

throughout the fluid. This implies

$$P(x, y) = A - gy \tag{5.93}$$

where A is a scalar constant. Since, $P = P_{atm}$ at the top surface, and the top surface is flat ($y = 0$), we have

$$P(x, 0) = A = P_{atm} \tag{5.94}$$

leading to

$$P(x, 0) = P_{atm} - gy \ . \tag{5.95}$$

Hence, the minimum pressure $P = P_{atm}$ is attained all along the surface $y = \eta(x)$ and the maximum pressure at the bed $y = -d$.

6 Analysis of Case C: $k < c$

In this case the strength of the current (uniform) is less than the wave speed. Thus, defining $k - c = \bar{c} < 0$, we have

$$0 = \bar{c} + \frac{1}{L} \int_0^L \psi_y(x, -d) dx \ . \tag{6.96}$$

This is equivalent to a flow with wave speed $\bar{c}$, no current ($k = 0$) and hence can be treated in a similar way as the case with Stokes wave flow without any current. This problem with an appropriate change of variable ($\psi_y = u - \bar{c}, \psi_x = -v$) leads to the condition of

$$\int_0^L u(x, -d) x = 0 \ . \tag{6.97}$$

This corresponds to the swell entering a region of still water, the relation $\frac{1}{L}\int_0^L [\bar{c} - u(x, -d)] dx = \bar{c}$ being Stokes definition of wave speed, the wave velocity in the moving frame of reference in which the wave is stationary. All the results for the case with no current (underlying the surface waves) hold in this case and the mass flux, $M/\rho < 0$; see the discussions in [8, 10].

7 Comments

Some results in this paper, such as the one on impossibility of the existence of Stokes surface wave of non-trivial amplitude and underlying current with identical speed, though apparently counterintuitive are not in contradiction to existing known results as only limited results are available for surface wave and underlying current propagation over finite depths [7, 15]. It may be concluded from the analysis carried out that depending on the relative magnitude of speed of the surface waves and the underlying current, three different qualitative scenario develops. Interestingly, when the speed of the surface wave is equal to the speed of the underlying current, it results in a uniform flow with flat surface. The qualitative nature of the flow fields with surface wave speed less than the speed of current is changed as compared to the case where there is no current and also compared to the case when the speed of current exceeds the speed of the surface waves, while the qualitative nature remains unaffected (and similar to the situation with no current) if the speed of current is less than the speed of the surface waves. In both the cases, irrespective of the relative magnitude of the surface wave and the underlying current speed, the qualitative nature of variation of the pressure field remains unaffected and is the same as that of the case when there is no underlying current present. The bounds on the surface profile derived for the case with an underlying current also holds for the case when no current exists. It may be noted that the results proved here are based on the properties of harmonic functions and use maximum principles, and hence are specific for irrotational flow.

References

[1] C.J. Amick, L.E. Fraenkel, J.F. Toland, On the Stokes conjecture for the wave of extreme form, *Acta Mathematica*, **148(1)** (1982), 193–214.

[2] C.J. Amick, J.F. Toland, On periodic water-waves and their convergence to solitary waves in the long-wave limit, *Phil. Trans. Roy. Soc. London A, Math. Phys. Eng. Sci.*, **303(1481)** (1981), 633–669.

[3] J. Baxter, I. Boyd, M. Cox, A. Donald, S. Malcolm, H. Miles, B. Miller, C. Moffat, "Scotland's Marine Atlas: Information for the national marine plan," *Marine Scotland*, Edinburgh(UK), 2011.

[4] B. Buffoni, É. Séré, J.F. Toland, Minimization methods for quasi-linear problems with an application to periodic water waves, *SIAM J. Math. Anal.*, **36(4)** (2005), 1080–1094.

[5] D. Clamond, Note on the velocity and related fields of steady irrotational two–dimensional surface gravity waves, *Phil. Trans. Roy. Soc. London A, Math. Phys. Eng. Sci.*, **370(1964)** (2012), 1572–1586.

[6] D. Clamond, A. Constantin, Recovery of steady periodic wave profiles from pressure measurements at the bed, *J. Fluid Mech.*, **714** (2013), 463–475.

[7] A. Constantin, The trajectories of particles in Stokes waves, *Invent. Math.*, **166(3)** (2006), 523–535.

[8] A. Constantin, "Nonlinear Water Waves with Applications to Wave-Current Interactions and Tsunamis," CBMS-NSF Conf. Ser. in Appl. Math. vol. 81, SIAM, Philadelphia, 2011.

[9] A. Constantin, Estimating wave heights from pressure data at the bed, *J. Fluid Mech.*, **743** (2014), Art. No. R2.

[10] A. Constantin, "Exact travelling periodic water waves for two-dimensional irrotational flows," in "Nonlinear water waves, Cetaro, Italy 2013", pp 1-82, Editor Adrian Constantin, *Springer Lecture Notes in Mathematics*,Vol. 2158, 2016.

[11] A. Constantin, M. Ehrnström, E. Wahlén, Symmetry of steady periodic gravity water waves with vorticity, *Duke Math. J.*, **140** (2007), 591–603.

[12] A. Constantin, J. Escher, Symmetry of steady periodic surface water waves with vorticity, *J. Fluid Mech.*, **498** (2004), 171–181.

[13] A. Constantin, J. Escher, Analyticity of periodic travelling free surface waves with vorticty, *Annals of Mathematics*, **173** (2011), 559–568.

[14] A. Constantin, W. Strauss, Exact steady periodic water waves with vorticity, *Comm. Pure Appl. Math.*, **57(4)** (2004), 481–527.

[15] A. Constantin, W. Strauss, Pressure beneath a Stokes wave, *Comm. Pure Appl. Math.*, **63(4)** (2010), 533–557.

[16] A. Constantin, G. Villari Particle Trajectories in Linear Water Waves, *J. Math. Fluid Mech.*, **10(1)** (2008), 1–18.

[17] T. Gerkema, F.-P.A. Lam, L.R. Maas, Internal tides in the Bay of Biscay: Conversion rates and seasonal effects, *Deep Sea Res. Part II*, **51(25)** (2004), 2995–3008.

[18] W.D. Grant, O.S. Madsen, Combined wave and current interaction with a rough bottom, *J. Geophys. Res. Oceans*, **84(C4)** (1979), 1797–1808.

[19] D. Henry, The trajectories of particles in deep-water Stokes waves, *Int. Math. Res. Not.*, **2006** (2006), 1 –13.

[20] D. Henry, Pressure in a deep-water Stokes wave, *J. Math. Fluid Mech.*, **13(2)** (2011), 251–257.

[21] R. Johnson, "A modern introduction to the mathematical theory of water waves," *Cambridge University Press*, 1997.

[22] A. Pichon, S. Correard, Internal tides modelling in the Bay of Biscay. Comparisons with observations, *Sci. Mar.*, **70(S1)** (2006), 65–88.

[23] J.F. Toland, Stokes waves, *Topol. Methods Nonlinear Anal*, **7(1)** (1996), 1–48.

[24] J.F. Toland, Stokes waves in Hardy spaces and as distributions, *J. Math. Pures Appl.*, **79(9)** (2000), 901–917.

[25] M. Umeyama, Eulerian–Langrangian analysis for particle velocities and tracjectories in a pure wave motion using particle image velocimetry, *Phil. Trans. Roy. Soc. London A, Math. Phys. Eng. Sci.*, **370(1858)** (2012), 1687–1702.

[26] E. Varvaruca, Bernoulli free-boundary problems in strip-like domains and a property of permanent waves on water of finite depth, *Proc. Royal Soc. Edinburgh A*, **138** (2008), 1345–1362.

On the existence of two dimensional irrotational water waves over finite depth with uniform current

Biswajit Basu

Applicable Analysis, 97(14), 2523-2532, 2017

Abstract

The existence of large amplitude two dimensional water waves with wave speed c, propagating on the surface of an irrotational flow over a flat bed with underlying uniform current, is investigated by means of a bifurcation approach. Two branches of travelling wave solutions exist for a parameter $\mu = (c^3/q_c^3) < 1$ or >1, respectively (where q_c is the flow velocity at the wave crest). The existence of the global bifurcating branch of solution for $\mu < 1$ has not been reported in the literature and can exist in the presence of uniform underlying current, while the other branch of solution for $\mu > 1$ can exist without any underlying current as has been shown by [1].

1 Introduction

This paper is concerned with the problem of proving the existence of two dimensional periodic free surface water waves propagating on an irrotational flow over a flat bed, in the presence of uniform underlying current. [1] had proved the existence of water waves for irrotational flow and, recently [2] and [3] have proved the existence of large amplitude steady water waves with a general vorticity distribution in a flow with no stagnation points and in constant vorticity flows with stagnation points respectively. In this paper, we are particularly interested to investigate the possibility of existence of global bifurcating branch of wave solutions for the case when the speed of wave c is less than the strength (speed) of current k, leading to a case where we have $0 < \mu = (c^3/q_c^3) \leq 1$. [4] had investigated two dimensional free surface water waves (irrespective of small or large amplitude) over finite depth with uniform underlying current and established the properties of the wave flow and pressure fields, assuming their existence. This paper builds upon the work of [1] and [4], and is a closure to the proof of existence of large amplitude wave solutions for two dimensional free surface flows over finite depth with uniform underlying current.

1.1 Formulation of the problem

Let us consider the problem of finding steady periodic surface waves for a two dimensional fluid flow over a constant depth with an underlying uniform current. Even though the current is present, since it is uniform, the flow is still irrotational. Hence, velocity potentials exist. We further concentrate on flows symmetric about the vertical through the crest. [5] showed that for a steady periodic irrotational water wave, there exists a symmetry about the vertical through the crest. For flows with vorticity and without stagnation points, [6] have shown that a profile that is monotone between successive crests and troughs has to be symmetric. Other relevant results on symmetry can be found in [7] for steady periodic surface waves wth vorticity and in [8] for water waves with stagnation points. The geometry of the flow and the co-ordinate axes are shown in

Figure 1. The complex coordinate is $z = x + iy$, the complex potential is $\chi = \phi + i\psi$ and the complex velocity is $w = u - iv$. Let $\Omega = \{\chi = \phi + i\psi | -\infty < \phi < \infty, -Q < \psi < 0\}$. The complex coordinate, the complex potential, the complex velocity and its logarithm are related through the formula

$$\omega = \tau + i\theta = \log \frac{w}{q_c} \tag{1.1}$$

and

$$w = \left(\frac{dz}{d\chi}\right)^{-1} = |w|\, e^{i\theta} = q_c e^{\tau + i\theta} \tag{1.2}$$

where q_c is the speed at the crest C of the wave. The angle formed by the velocity vector with the x-axis is $-\theta$. When w is real and positive ω is real too. Suppose we are given positive numbers L, Q and d (representing the finite depth, which is arbitrary).

Given the physical variables L and Q, and hence given c^3 (where c is the wave speed)

$$c^3 = \frac{gL}{\pi} \tanh \frac{\pi Q}{L} \quad , \tag{1.3}$$

$\alpha \equiv g/c^3$ and k (uniform underlying current), the water-wave problem we consider is to find a non-zero function $\omega(\chi) = \tau + i\theta$ holomorphic in Ω and continuously differentiable on $\bar{\Omega}$, and a number $\mu = c^3/q_c^3$ such that

$$\theta = 0 \text{ on } \psi = -Q, \text{for all } \phi \tag{1.4}$$

$$\frac{\partial \theta}{\partial \psi} = \frac{\partial \tau}{\partial \phi} = \mu\alpha \frac{\sin\theta}{e^{3\tau}} \text{ on } \psi = 0, \text{ for all } \phi \tag{1.5}$$

$$\theta \text{ is odd in } \phi \tag{1.6}$$

$$\omega \text{ is periodic in } \phi, \text{with period } 2L \tag{1.7}$$

$$\omega(0) = 0 \quad . \tag{1.8}$$

This problem is denoted as problem (P) in [1] in absence of the underlying current k.

We can reformulate the problem (Eqs. (1.3)-(1.8)) more concisely in terms of the real function $\theta(\phi)$ (see [1] for details). Knowledge of $\theta(\phi)$, the angle between the tangent to the free surface and the horizontal, is sufficient to define a solution to the free boundary problem as the free surface is the unknown in the problem considered. The reformulated problem can be represented in form of an integral equation as noted by [9], which is known as Nekrasov's integral equation. In this reformulated problem, we seek a non-zero function θ and a real number μ (which is affected by the presence of current with speed k) such that

$$\theta(\phi) = \mathscr{A}(\theta, \mu)(\phi) \tag{1.9}$$

where

$$\mathscr{A}(\theta, \mu)(\phi) = \int_0^L G(\phi, \hat{\phi}) \frac{\mu\alpha \sin\theta(\hat{\phi})}{1 + 3\mu\alpha \int_0^{\hat{\phi}} \sin\theta(\varphi) d\varphi} d\hat{\phi} \tag{1.10}$$

and G is defined by the equation

$$G(\phi, \hat{\phi}) = \frac{2}{\pi} \sum_{j=1}^{\infty} \frac{\tanh(j\pi Q/L)}{j} \sin(j\pi\phi/L) \sin(j\pi\hat{\phi}/L) \quad . \tag{1.11}$$

The reformulated problem is denoted as problem (N) in [1].

Here $\mathscr{A}$ is a positive completely continuous non-linear operator defined on an appropriate subset of $E \times \mathbb{R}$,where E is the function space to be defined in Section 3. The problem in Eqs. (1.9)-(1.11) is a bifurcation problem since $\mathscr{A}(0, \mu) = 0$. The trivial solutions (θ, μ) with $\theta(\phi) \equiv 0$ correspond to uniform flow with flat surface.

2 Influence of underlying uniform current

The current k here is defined as the average of the horizontal velocity over a wavelength, beneath the wave trough level. For further details, see [10], and also refer to [11] for a discussion on the difference between the depth averaged (i.e., vertically averged) and horizontally averaged current. In [4], developing the approaches proposed in [12] and [13], it was shown that for free surface steady waves propagating over a flat bed with uniform underlying currents, three cases can exist depending upon the relative magnitude of the current, k and wave speed, c. Consider the periodic domain (of wavelength $\bar{L}$)

$$\Lambda = \{(x, y) : x \in (-\bar{L}/2, \bar{L}/2), -d < y < \eta(x)\}$$

with its two components

$$\Lambda_+ = \{(x, y) : x \in (0, \bar{L}/2), -d < y < \eta(x)\}$$

and

$$\Lambda_- = \{(x, y) : x \in (-\bar{L}/2, 0), -d < y < \eta(x)\} \ .$$

The crest is located at $(0, \eta(0))$ and the trough at $(\bar{L}/2, \eta(\bar{L}/2))$, where $\eta(x)$ is the free surface profile. In the case of $k > c$, u increases strictly as we go from crest to trough along the lower three sides of $\bar{\Lambda}_+$ resulting in the following strict inequalities

$$\begin{aligned} u_y(0, y) < 0 \quad &\text{for} \quad y \in [-d, \eta(0)] \\ u_x(x, -d) > 0 \quad &\text{for} \quad x \in [0, \bar{L}/2] \\ u_y(\bar{L}/2, y) > 0 \quad &\text{for} \quad y \in [-d, \eta(\bar{L}/2)] \end{aligned} \tag{2.12}$$

on the three sides. Also, in this case

$$u(x, y) > c \quad \text{for} \quad -d \le y \le \eta(x) \ . \tag{2.13}$$

Hence, the velocity at the crest q_c is greater than the non-negative wave speed c, leading to $0 < \mu < 1$.

In the case of $k < c$, u decreases strictly as we go from crest to trough along the lower three sides of $\bar{\Lambda}_+$ resulting in the following strict inequalities

$$\begin{aligned} u_y(0, y) > 0 \quad &\text{for} \quad y \in [-d, \eta(0)] \\ u_x(x, -d) < 0 \quad &\text{for} \quad x \in [0, \bar{L}/2] \\ u_y(\bar{L}/2, y) < 0 \quad &\text{for} \quad y \in [-d, \eta(\bar{L}/2)] \end{aligned} \tag{2.14}$$

on the three sides. Also, in this case

$$u(x, y) < c \quad \text{for} \quad -d \le y \le \eta(x) \ . \tag{2.15}$$

Hence, the velocity at the crest q_c is less than the non-negative wave speed c, leading to $1 < \mu < \infty$.

The case $k = c$ results in a uniform flow with a flat surface with $u = c$. Hence, $q_c = c$ leading to $\mu = 1$ and $\theta = 0$.

We can reformulate the problem in [4] in terms of Nekrasov's integral equation and analyze it in the context of $0 < \mu \le 1$ and $1 \le \mu < \infty$ corresponding to $k \ge c$ and $k \le c$ respectively, with $k = c$ leading to $\mu = 1$ and $\theta = 0$.

The aim of the paper is to show that solutions exist for two dimensional water waves over finite depth with uniform underlying current and that $\mu = 1$ is a bifurcation point. In particular, we prove the existence of a bifurcating branch of solution from $\mu = 1$ for $0 < \mu \le 1$. The proof uses positive operator methods. This approach was used by [1] to prove the existence of irrotational water waves. We extend the results for the case of two dimensional water waves with uniform underlying current and prove the existence of a new bifurcating branch of travelling wave solutions.

Since the case with $\mu = [1, \infty)$ has been already dealt with by [1] (and the approach and the results with current $k \leq c$ will be the same as the irrotational case), we concentrate on the situation with $\mu = (0, 1]$.

3 Positive Operator Results

The results proved in this paper are based on positive operator methods. This approach has been previously used by Keady and Norbury to prove the existence of irrotational travelling water waves in the absence of underlying currents. We extend the results by proving the existence of wave solutions with unform underlying current and showing the existence of an additional bifurcation branch of solutions. We begin with some definitions related to positive operators. Let E be a Banach space whose norm is denoted by $\| \quad \|$. A set $K \subset E$ is called a cone in E if

(i) $u, v \in K \Rightarrow u + v \in K$,

(ii) $u \in K, \alpha \in [0, \infty) \Rightarrow \alpha u \in K$,

(iii) $u \in K, u \neq 0 \Rightarrow -u \notin K$,

(iv) K is closed in E.

We further define $K_\rho \equiv \{x \in K | \|x\| < \rho\}$, and $\bar{K}_\rho \equiv \{x \in K | \ \|x\| \leq \rho\}$. We write $u \leq v$ if and only if $v - u \in K$. Define $E_K = \{u - v | u, v \in K\}$. A cone K is said to be reproducing if $E_K = K$. A linear operator $B : E \to E$ is positive if B maps K into itself. A non-linear operator $A : E \times \mathbb{R} \to E$ is positive if A maps $K \times [0, \infty)$ into K. A linear operator $B : E \to E$ is completely continuous if B is continuous and maps bounded subsets of E to precompact subsets of E. A non-linear operator $A : E \times \mathbb{R} \to E$ is completely continuous if A is continuous and maps bounded subsets of $E \times \mathbb{R}$ to precompact subsets of E.

We will use some theorems in our proof which has been presented in [1], but we restate those (Theorem 3.1 and Lemma 3.2) for the sake of completeness. We then prove Lemma 3.3, which follows from Lemma 3.2, and is needed for our existence proof. Theorem 3.1 is the corollary to Theorem 2 of [14], whose proof depends on the results of [15].

THEOREM 3.1 Let K be a cone in E and suppose $\bar{E}_K = E$. Suppose that $A : E \times \mathbb{R} \to E$ is completely continuous, is positive and has the following properties:

$$A(0, \mu) = 0 \text{ for all } \mu \in \mathbb{R}; \ A(u, 0) = 0 \text{ for all } u \in E; \tag{3.16}$$

$$A(u, \mu) = \mu B u - F(u, \mu) \tag{3.17}$$

where $B : E \to E$ is a completely continuous positive linear operator and for all $\tilde{\mu} > 0$, $F : E \times \mathbb{R} \to E$ satisfies

$$\|F(u, \mu)\| = O(\|u\|) \text{ as } \|u\| \to 0, \tag{3.18}$$

uniformly in μ in some neighbourhood of $\tilde{\mu}$. Suppose also that there exists a unique $(u_0, \mu_0) \in K \times (0, \infty)$ such that

$$u_0 = \mu_0 B u_0 \text{ and } \|u_0\| = 1 \quad . \tag{3.19}$$

Define $\mathscr{D}_K(A) = \{(u,\mu) \in K \times (0,\infty) | u = A(u,\mu), u \neq 0\} \cup \{(0,\mu_0)\}$. Then the component $\mathscr{T}(A)$ of $\mathscr{D}_K(A)$ containing $(0,\mu_0)$ is unbounded in $K \times (0,\infty)$. The sets $\mathscr{T}(A)$ and $\mathscr{D}_K(A)$ are closed in $K \times [0,\infty)$. Moreover $(0,\mu_0)$ is a bifurcation point of A.

LEMMA 3.2 Let K be a reproducing cone in E. Let $B : E \to E$ be a positive completely continuous linear operator on E with a unique positive characteristic value μ_0. Suppose that μ_0 is simple. If there exists a $(u,\mu) \in K \times (0,\infty)$ with $\|u\| \neq 0$ such that

$$\mu Bu \geq u \quad \text{then} \quad \mu \geq \mu_0 \quad . \tag{3.20}$$

For the proof see Lemma 1.2 of [14] or Theorem 2.5 of [16].

In our application, E is the space of all continuous functions θ on $[0,L]$, with $\theta(0) = \theta(L) = 0$ and

$$\|\theta\| = \max_{0 \leq \phi \leq L} |\theta(\phi)| \tag{3.21}$$

and $K = \{\theta \in E | \theta(\phi) \geq 0 \text{ for all } \phi \in [0,L]\}$, where cone K is reproducing in E. In the context of the hydrodynamic problem formulated, we shall establish the existence of waves for which the angle of inclination - $\theta(\phi)$ between the tangent to the free surface and the horizontal is negative at all points between the crest C and trough D (see Figure 1).

We will now prove the following Lemma 3.3, which is needed and will be used later to prove the existence of a new bifurcation branch of solution for $\mu < 1$. The lemma follows from the result of Lemma 3.2.

LEMMA 3.3 Let K be a reproducing cone in E. Let $B : E \to E$ be a positive completely continuous linear operator on E with a unique positive characteristic value μ_0. Suppose that μ_0 is simple. If there exists a $(u,\mu) \in K \times (0,\infty)$ with $\|u\| \neq 0$ such that

$$\frac{1}{\mu} Bu \geq u \quad \text{then} \quad \mu \leq \frac{1}{\mu_0} \ . \tag{3.22}$$

Proof: Since $\frac{1}{\mu}Bu \geq u$, Lemma 3.2 implies $\frac{1}{\mu} \geq \mu_0$. Since both μ and μ_0 are positive, we get $\mu \leq \frac{1}{\mu_0}$ which proves the result.

From Lemma 3.3, for the case when $\mu_0 = 1$, we have $\mu \leq 1$.

4 Bounds on θ_m

We again revisit and restate some of the results from [1] which we need for our proof in this paper. These results are on the bound on θ_m which is defined in Eq. (3.21) as the supremum norm of θ, i.e. the maximum angle of inclination of the tangent to the surface with respect to the horizontal.

PROPOSITION 4.1([1], Proposition 2.4, page 144) Any wave solution (ω,μ) of problem (P) defines a pair $(\theta,\mu) \in K \times [0,\infty)$. Any wave solution for which the corresponding (θ,μ) is in a component of wave solutions $(\theta,\mu) \in K \times [0,\infty)$ containing $(0,\mu_0)$ with $\mu_0 = 1$ has $\theta_m < \pi$.

THEOREM 4.2([1], Theorem 3.2, page 146) Any wave solution of problem (N) or problem (P) with $\theta_m \leq \pi$ has $\theta_m < \frac{1}{2}\pi$.

Proofs for both rely on maximum pinciples (see [17]) and the fact that θ is a harmonic function. Also, see Lemma 3.1 (page 144, [1]) for further details.

5 Main Results for Existence Proof

We now proceed to prove the main results of the paper. We first focus on $0 < \mu \leq 1$ as previously stated. Let us define the following truncation operators which we intend to use in Lemma 5.1. We define a compact extension $\tilde{\mathscr{A}} : E \times \mathbb{R} \to E$ of $\mathscr{A}$ restricted to $\bar{K}_{\frac{1}{2}\pi} \times [0, \infty)$. The choice of the number $\frac{1}{2}\pi$ is motivated by Theorem 4.2.

$$(\mathscr{Q}\theta)(\phi) = \begin{cases} \theta(\phi) & \text{if } |\theta(\phi)| \leq \frac{1}{2}\pi, \\ \frac{1}{2}\pi & \text{if } |\theta(\phi)| > \frac{1}{2}\pi, \end{cases} \tag{5.23}$$

$$(\mathscr{R}\theta)(\phi) = \begin{cases} 0 & \text{if } \theta(\phi) \leq 0, \\ \theta(\phi) & \text{if } 0 \leq \theta(\phi) \leq \frac{1}{2}\pi, \\ \frac{1}{2}\pi & \text{if } \theta(\phi) > \frac{1}{2}\pi \ . \end{cases} \tag{5.24}$$

Also, define

$$\tilde{\mathscr{N}}(\theta, \mu)(\phi) = \frac{\sin(\mathscr{Q}\theta)(\phi)}{1 + 3\alpha|\mu| \int_0^\phi \sin(\mathscr{R}\theta)(\varphi) d\varphi} \ . \tag{5.25}$$

We consider solutions $(\theta, \mu) \in K \times [0, \infty)$ of

$$\theta(\phi) = \tilde{\mathscr{A}}(\theta, \mu)(\phi) \tag{5.26}$$

where

$$\tilde{\mathscr{A}}(\theta, \mu) = \mu \mathscr{B} \tilde{\mathscr{N}}(\theta, \mu) \tag{5.27}$$

and

$$(\mathscr{B}u)(\phi) = \alpha \int_0^L G(\phi, \hat{\phi}) u(\hat{\phi}) d\hat{\phi} \ . \tag{5.28}$$

LEMMA 5.1 Define $\tilde{\mathscr{T}} = \mathscr{T}(\tilde{\mathscr{A}})$ as in Theorem 3.1. Then

$$\theta = \tilde{\mathscr{A}}(\theta, \mu) \tag{5.29}$$

has an unbounded connected set $\tilde{\mathscr{T}}$ of solutions $(\theta, \mu) \in K \times [0, \infty)$ containing $(0, \mu_0)$ with $\mu_0 = 1$. Moreover $(0, \mu_0)$ is a bifurcation point of $\tilde{\mathscr{A}}$.

Proof: We apply Theorem 3.1 and we also use Lemma A.6 from [1] which states that $\tilde{\mathscr{A}} : E \times \mathbb{R} \to E$ is completely continuous. The definition of $\tilde{\mathscr{A}}$ (Eq. (5.27)) implies

$$\tilde{\mathscr{A}}(0, \mu) = 0 \text{ for all } \mu \in \mathbb{R}, \tilde{\mathscr{A}}(\theta, 0) \text{ for all } \theta \in E \ . \tag{5.30}$$

We can write

$$\tilde{\mathscr{A}}(\theta, \mu) = \frac{1}{\mu} \mathscr{B}\theta - \mathscr{F}(\theta, \mu), \tag{5.31}$$

where $\mathscr{B}$ is given by Eq. (5.28). The expression for $\tilde{\mathscr{A}}(\theta, \mu)$ written in this form allows us to apply Theorem 3.1 and is suitable for application of Lemma 3.3. Further, Lemma A.3 from [1] states that $\mathscr{B} : E \to E$ is completely continuous. To verify if Eq. (3.19) in Theorem 3.1 is satisfied, we use Eqs. (1.3) and (5.28) with $\alpha = g/c^3$, to obtain

$$\sin \frac{\pi\phi}{L} = \mu_0 \left(\mathscr{B} \sin \left(\frac{\pi\hat{\phi}}{L} \right) \right) (\phi) \text{ where } \mu_0 = 1. \tag{5.32}$$

Consider $\mathscr{B}$ as an operator on $L_2(0, L)$ (Refer to Lemma A.3 (a) in [1], and [18]). Since the eigenfunctions of $\mathscr{B}$ in $L_2(0, L)$ are $\sin(j\pi\phi/L), j = 1, 2, ...$ with characteristic values

$$(\sinh \pi Q/L)^{-1} \sinh(j\pi Q/L), \tag{5.33}$$

the only eigenfunction in K is $\sin(\pi\phi/L)$, and its associated characteristic value $\mu_0 = 1$ is simple. Let us consider the operator

$$\mathscr{F}(\theta,\mu) = \mathscr{B}\mathscr{G}(\theta,\mu) \tag{5.34}$$

where we can write

$$\mathscr{G}(\theta,\mu) = \frac{1}{\mu}\theta - \frac{\frac{1}{\mu}\sin\mathscr{Q}\theta}{\frac{1}{\mu^2} + \frac{3}{|\mu|}\alpha\int_0^\phi \sin\mathscr{R}\theta(\varphi)d\varphi} \tag{5.35}$$

The operator $\mathscr{F}(\theta,\mu)$ has the property stated in Eq. (3.18). Since $\mu \in [0,\infty)$, we have $1/\mu \in (0,\infty)$. Hence, replacing μ by $1/\mu$, we observe that all conditions of Theorem 3.1 have been satisfied.

The next theorem proves that wave solutions of the problem stated in Eqs. (1.9)-(1.11) have values $0 < \mu < 1$. We thus extend the class of wave solutions to $\mu < 1$ which can occur in the presence of uniform underlying current with $k > c$.

THEOREM 5.2 All wave solutions $(\theta,\mu) \in \bar{K}_{\frac{1}{2}\pi} \times [0,\infty)$ of problem (N), or solutions $(\theta,\mu) \in (K\backslash\{0\}) \times (0,\infty)$ of Eq. (5.26), with uniform current have $\mu < \mu_0 = 1$. Also, $u > c$ and the speed of current is greater than the wave speed, i.e. $k > c$.

Proof: We note that, $\sin\theta < \theta$ for $(\theta,\mu) \in \bar{K}_{\frac{1}{2}\pi} \times [0,\infty)$ (on which $\mathscr{A} = \tilde{\mathscr{A}}$). Let us now assume that $\mu \in (0,1]$, i.e.$\mu \le 1$. Thus, the denominator of the second term in Eq. (5.35) is greater than 1, suggesting

$$\mathscr{A}(\theta,\mu) \le \frac{1}{\mu}\mathscr{B}\theta \quad \text{on} \quad \bar{K}_{\frac{1}{2}\pi} \times (0,1]. \tag{5.36}$$

Hence, from Lemma 3.3, we obtain $\mu \le 1/\mu_0 = 1$. To obtain the strict inequality we proceed as follows. Consider $\mathscr{B}$ as an operator on $L_2(0,L)$. Again by Lemma A.3 (a) of [1] $\mathscr{B}$ is completely continuous and self-adjoint. Hence μ_0 has the variational characterization

$$\frac{1}{\mu_0^2} = \max_{\substack{\theta\in L_2(0,L)\\ \theta\neq 0}} \frac{\int_0^L (\mathscr{B}\theta)^2 d\phi}{\int_0^L \theta^2 d\phi}\ . \tag{5.37}$$

Further, for $0 < \theta < \frac{1}{2}\pi$ we have $0 < \sin\theta < \theta < \frac{1}{2}\pi$. Hence, for wave solutions with $\theta \in K_{\frac{1}{2}\pi}$, we have

$$\theta(\phi) = \mathscr{A}(\theta,\mu)(\phi) < \frac{1}{\mu}\mathscr{B}\theta(\phi) \text{ for } 0 < \phi < L \tag{5.38}$$

implying

$$\int_0^L \theta^2 d\phi < \frac{1}{\mu^2}\int_0^L (\mathscr{B}\theta)^2 d\phi \le \frac{1}{\mu_0^2\mu^2}\int_0^L \theta^2 d\phi \tag{5.39}$$

leading to $\mu\mu_0 < 1$. This yields $\mu < 1/\mu_0 = 1$. Hence, $c < q_c$. Since from [4] (Eq. (35), page 116) we know that q_c the flow velocity at the crest is minimum, we get $c < u$. From [4] (Eq. (27), page 115)) we conclude that this corresponds to $k > c$.

Finally, we prove the main existence and bifurcation result for the two dimensional free surface water waves with unform underlying current, by extending the result for $0 < \mu \le 1$ which corresponds to the case with current speed k either equal to or exceeding the wave speed c.

THEOREM 5.3 Consider the equation

$$\theta = \mathscr{A}(\theta,\mu) \tag{5.40}$$

Define $\mathscr{D}(\mathscr{A}) = \{(\theta,\mu) \in \bar{K}_\pi \times [0,\infty) | \theta = \mathscr{A}(\theta,\mu), \theta \neq 0\} \cup \{(0,1)\}$. Then the component $\mathscr{T}$ of $\mathscr{D}(\mathscr{A})$ containing $(0,\mu_0)$ with $\mu_0 = 1$ is an unbounded subset of $K_{\frac{1}{2}\pi} \times (0,\mu_0]$. All elements of $\mathscr{T}$ are wave solutions except $(0,\mu_0)$. Moreover, $(0,\mu_0)$ is a bifurcation point of $\mathscr{A}$. For any fixed $\mu^* \leq \mu_0$, defining

$$M(\mu*) = \sup_{\mu^* \leq \mu \leq \mu_0} \{\|\theta\| | (\theta,\mu) \in \mathscr{T}\}, \tag{5.41}$$

we have $M(\mu*) < \frac{1}{2}\pi$.

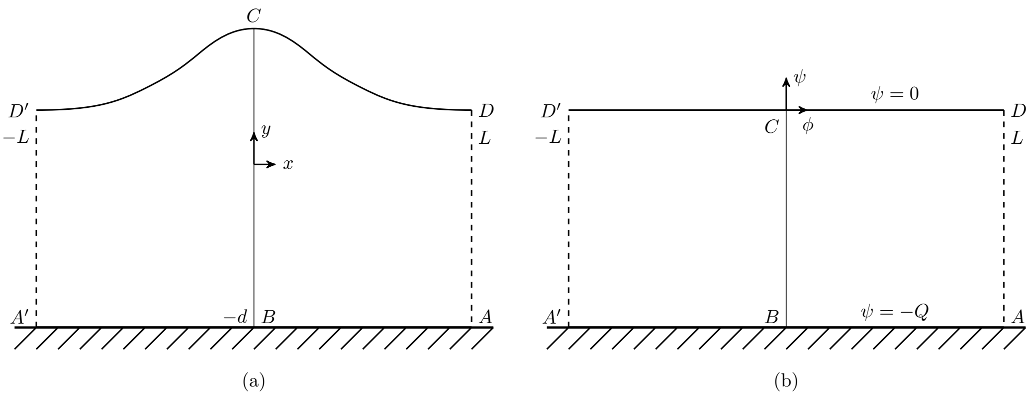

Figure 1: (a) z-plane, (b) χ-plane

Proof: The proof of the first part of this theorem uses the truncation operators in Eqs. (5.23)-(5.24) and some topological properties of $\tilde{\mathscr{T}}$ (also see [1]). We define $\tilde{\mathscr{T}}$ as in Lemma 5.1 and

$$\mathscr{T}_0 \equiv \tilde{\mathscr{T}} \cap \bar{K}_{\frac{1}{2}\pi} \times [0,\infty) \ . \tag{5.42}$$

Since the truncation operators in $\tilde{\mathscr{T}}$ have no effect, all $(\theta,\mu) \in \mathscr{T}_0$ are solutions of Eqs. (1.9)-(1.11). Hence Theorem 4.2 implies that $\|\theta\| < \frac{1}{2}\pi$ whenever $(\theta,\mu) \in \mathscr{T}_0$. The set $\mathscr{T}_0$ is closed, $\mathscr{T}_0 = \tilde{\mathscr{T}}_0$, since $\tilde{\mathscr{T}}$ and $\bar{K}_{\frac{1}{2}\pi} \times [0,\infty)$ are both closed. To prove the theorem we need to show that $\mathscr{T}_0 = \tilde{\mathscr{T}}$. Hence, to show this we define $\mathscr{T}_1 = \tilde{\mathscr{T}} \backslash \mathscr{T}_0$, and let its closure in $E \times \mathbb{R}$ be denoted by $\bar{\mathscr{T}}_1$. Let us denote the empty set by the notation $\varnothing$. Suppose that $\mathscr{T} \neq \varnothing$.Then

$$\bar{\mathscr{T}}_0 \cap \mathscr{T}_1 = \varnothing \text{ and } \mathscr{T}_0 \cap \bar{\mathscr{T}}_1 = \varnothing \ . \tag{5.43}$$

The first of the two relations in Eq. (5.43) follows from the definition of $\mathscr{T}_1$ and the fact that $\mathscr{T}_0$ is closed. The second follows because if $(\theta,\mu) \in \tilde{\mathscr{T}}$ then $\|\theta\| \geq \frac{1}{2}\pi$ so that $(\theta,\mu) \notin \mathscr{T}_0$. Hence $\mathscr{T}_0$ and $\mathscr{T}_1$ are separated. Thus, $\tilde{\mathscr{T}} = \mathscr{T}_0 \cup \mathscr{T}_1$ is not connected, which leads to a contradiction. Hence $\mathscr{T}_1$ is empty and $\mathscr{T}_0 = \mathscr{T}$. With $\mathscr{T} = \mathscr{T}_0$, we now proceed to the next part and the main results of the theorem.

Let us fix μ^* such that $0 < \mu^* \leq \mu_0$. It is obvious that $M(\mu^*) \leq \frac{1}{2}\pi$. We also observe that the fact that $M(\mu^*) < \frac{1}{2}\pi$ is a consequence of the complete continuity of $\mathscr{A}$. Since $\mathscr{A}$ is completely continuous, $\mathscr{T}$ intersects any closed bounded subset of $\bar{K}_\pi \times [0,\infty)$ in a compact set. To derive the strict inequality, let us suppose $M(\mu^*) = \frac{1}{2}\pi$. Because $(0,\mu_0) \in \mathscr{T}$ and $\mathscr{T}$ is connected there exists a sequence $(\theta_n,\mu_n) \in \mathscr{T}$ with $\|\theta_0\| < \frac{1}{2}\pi, \mu^* \leq \mu_n \leq \mu_0$ with $\|\theta_n\| \to \frac{1}{2}\pi$. Since $\mathscr{T} \cap \bar{K}_{\frac{1}{2}\pi} \times [\mu^*,\mu_0]$ is compact, $(\theta_n,\mu_n) \to (\tilde{\theta},\tilde{\mu}) \in \mathscr{T}$. Since $(\tilde{\theta},\tilde{\mu}) \in \mathscr{T}$, Theorem 4.2 ensures that $\|\tilde{\theta}\| < \frac{1}{2}\pi$, leading to a contradiction and hence $M(\mu*) < \frac{1}{2}\pi$, proving the theorem.

The proof of existence for two dimensional water waves propagating along the free surface for the case when the speed of underlying uniform current k is less that of the wave speed c (i..e $\mu \in [\mu_0, \infty)$) is exactly the same as the proof of existence of two dimensional water waves without any current as in [1], and hence is not repeated here. This completes the proof of existence of the two dimensional free surface water waves with uniform underlying current.

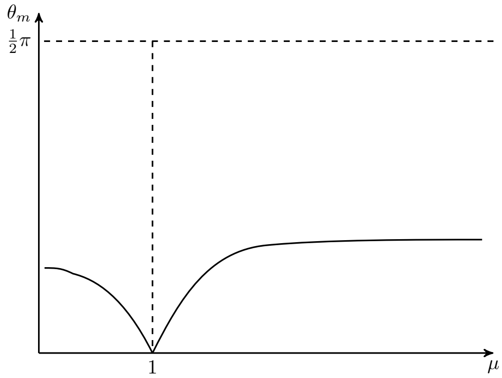

Figure 2: Some possibilities of branches from (0,1) on the bifurcation diagram.

6 Concluding Remarks

In [4], it was shown that if two dimensional travelling water waves over finite depth with uniform underlying current exist, then $\mu = c^3/q_c^3$ can attain a value < 1. In this paper, the existence of two dimensional free suface large amplitude water waves with uniform underlying current for $0 < \mu < 1$ and $\theta < \pi/2$ has been proved. Further, it has been shown that $\mu_0 = 1$ is a bifurcation point and the existence of a new global bifurcating branch of wave solutions for $0 < \mu < 1$ has been established. It may be of interest to note that the proofs and the results by [1] for the existence of two dimensional irrotational water waves for $\mu > 1$) (without underlying current) also hold for the case of wave solution for $\mu > 1$ (with underlying current).

References

[1] Keady G, Norbury J. On the existence theory for irrotational water waves, *Math. Proc. Cambridge Phil. Soc.*, **83** (1978), 137–157.

[2] Constantin A, Strauss W. Exact steady periodic water waves with vorticity, *Comm. Pure Appl. Math.*, **57(4)** (2004), 481–527.

[3] Constantin A, Strauss W, Varvaruca E. Global bifurcation of steady gravity water waves with critical layers, *Acta Mathematica*, **27** (2016), 195-262.

[4] Basu B. Irrotational two-dimensional free-surface steady water flows over a flat bed with underlying currents, *Nonlinear Anal. TMA*, **147** (2016), 110–124.

[5] Garabedian PR. Surface waves of finite depth, *J. d'Analyse Mathématique*, **14(1)** (1965), 161–169.

[6] Constantin A, Ehrnström M, Wahlén E. Symmetry of steady periodic gravity water waves with vorticity, *Duke Math. J.*, **140** (2007), 591–603.

[7] Constantin A, Escher J. Symmetry of steady periodic surface water waves with vorticity, *J. Fluid Mech.*, **498** (2004), 171–181.

[8] Tulzer G. On the symmetry of steady periodic water waves with stagnation points, *Comm. Pure Appl. Math.*, **11(4)** (2012), 1577–1586.

[9] Nekrasov AI. On steady waves, *Izv. Ivanovo-Voznesensk. Politekhn Inst.*, **3** (1921), 52–65.

[10] Constantin A. Mean velocities in a Stokes wave, *Arch. Ration. Mech. Anal.*, **207(3)** (2013), 907–917.

[11] Teles da Silva AF, Peregrine DH. Steep, steady surface waves on water of finite depth with constant vorticity, *J. Fluid Mech.*, **195** (1988), 281–302.

[12] Constantin A. The trajectories of particles in Stokes waves, *Invent. Math.*, **166(3)** (2006), 523–535.

[13] Constantin A, Strauss W. Pressure beneath a Stokes wave, *Comm. Pure Appl. Math.*, **63(4)** (2010), 553–557.

[14] Dancer EN. Global solution branches for positive mappings, *Arch. Ration. Mech. Anal.*, **52(2)** (1973), 181–192.

[15] Rabinowitz PH. Some global results for nonlinear eigenvalue problems, *J. Funct. Anal.*, **7(3)** (1971), 487–513.

[16] Krasnoselskii MA. “Positive solutions of operator equations,” Groningen, Noordhoff, 1964.

[17] Protter MH, Weinberger HF. “Maximum principles in differential equations,” Springer-Verlag, New York, 1984.

[18] Birkhoff G, Zarantonello EH. “Jets, wakes, and cavities” Academic Press, New York, 1957.

Solitary water waves propagating on an underlying uniform current over a finite depth

Biswajit Basu

Nonlinear Anal. 172, 25-35, 2018

Abstract

We investigate the nature of velocity and pressure fields for solitary water waves (without any restriction on amplitude) propagating over finite depth with uniform underlying currents. We show that two cases exist corresponding to the fluid velocities u greater than or less than the solitary wave propagation speed c, and these two cases result in different nature of flow fields. We prove the conditions for existence of solitary waves in 2D with uniform underlying current over finite depth for these two cases. We also derive some bounds on Froude number and maximum amplitude of solitary wave height.

1 Introduction

Originally discovered by Scott Russell from experiments carried out in canals, solitary waves are observed in nature and have been simulated in laboratory. Since its first discovery, solitary waves have attracted the attention of the researchers and a large volume of research has been carried out including some recent revelations about these waves ([10, 11]). Solitary waves are gravity waves as the only restoring force acting on the water in this case is gravity (since surface tension can be ignored if amplitudes are not very small). Solitary waves have a symmetrical profile and propagates on the water surface as a single hump decaying rapidly on either side to almost flat level far ahead and far away from the crest. These waves have a one-dimensional structure as no localized steady gravity waves with a two-dimensional profile (i.e., 3D solitary waves) can exist ([13]).

The rigorous theory of solitary waves was developed by Fredrich and Hyers [16] and was further addressed by Beale [5]. A significant contribution to the analytical theory for solitary waves has been made by Toland and collaborators ([3, 2, 1]) which has provided information about the structure of these waves. Even though a large amount of investigation has been carried out on the solitary waves, properties of the underlying flow, only has been the attention of research in the recent past with only a few papers concentrating on this aspect. A good survey of the literature is available in [8]. Constantin and Escher [10] studied the particle trajectories in solitary waves while Constantin et al. [11] developed the mathematical theory for the pressure beneath a solitary wave including experimental verification of the same. The rigorous analysis of the pressure field in its own right for water waves was initiated in [12], and some interesting further recent developments can be found in the papers [9, 17, 20, 21]. Some studies have focussed on linearized theories for small amplitudes ([14, 23]) and on numerical investigations ([15]). Focus on large amplitude waves has been recent and has been concentrated on by researchers such as Chen et al. [6], Constantin [7], Constantin and Strauss [12] and Hsu et al. [19]. Wheeler [24, 25] constructed large amplitude solutions for solitary waves with vorticity and provided some bounds on Froude number. Henry [18] has developed the pressure transfer function for solitary water waves in the presence of vorticity. Existing literature on solitary waves indicates that inspite of the large volume of research activities in the area, investigations focussing on the flow and pressure fields beneath the water surface for solitary waves of large amplitude over finite depth (including underlying current) are still incomplete. The approach in this paper to study the velocity and pressure field beneath the flow is motivated by the considerations in nonlinear steady periodic Stokes wave of large amplitude ([12]), and the results on existence are influenced by the work of Amick and Toland [2]. Recently, Basu [4] has reported some results on two dimensional irrotational free surface water waves with underlying current and these results also contribute to the proofs and derivations in this paper.

The aim of this paper is to investigate solitary waves of large amplitude propagating on uniform current over flat bed. Some results on velocity and pressure beneath the flow are derived. The existence results for solitary water waves with uniform current have been proved and bounds on Froude number have been established. Finally, bounds on the maximum amplitude of a solitary water wave have also been derived.

2 Preliminaries and Fundamental Equations

We consider a 2D flow described using a Cartesian coordinate system (X, Y). The depth of the fluid medium at rest is $d > 0$ and the flat bed is given by $Y = -d$. The free surface of the water is denoted by $Y = \eta(X - ct)$, where $c > 0$ is the constant speed of the travelling solitary wave.

The governing equations of motion are described by Euler equations

$$\begin{aligned} u_t + uu_X + vu_Y &= -P_X \\ v_t + uv_X + vv_Y &= -P_Y - g \end{aligned} \tag{2.1}$$

where $P(X-ct, Y)$ is the hydrodynamic pressure and g is the acceleration due to gravity. The boundary conditions are

$$v = \eta_t + u\eta_X \quad \text{on} \quad Y = \eta(X - ct) \tag{2.2}$$

and

$$P = P_{atm} \quad \text{on} \quad Y = \eta(X - ct) \tag{2.3}$$

where P_{atm} is the constant atmospheric pressure.

The flat bed is impermeable, i.e.

$$v = 0 \quad \text{on} \quad Y = -d \; . \tag{2.4}$$

The mass conservation equation is expressed as

$$u_X + v_Y = 0 \; . \tag{2.5}$$

We also assume that the flow is irrotational

$$u_Y = v_X \; . \tag{2.6}$$

We further consider a moving frame of reference

$$x = X - ct, \quad y = Y$$

and assume that the crest line is located at $x = 0$.

Velocity potential ϕ is defined as

$$\phi_x = u - c, \quad \phi_y = v, \quad \phi(0, -d) = 0 \; . \tag{2.7}$$

Using $u_y = v_x$

$$\phi(x,y) = \int_0^x [u(l,-d) - c]\, dl + \int_{-d}^y v(x,s)ds, (x,y) \in \bar{\Omega} \tag{2.8}$$

where $\Omega = \Omega_- \cup \Omega_+ = \{(x,y) \in \mathbb{R}^2 : x < 0, -d < y < \eta(x)\} \cup \{(x,y) \in \mathbb{R}^2 : x > 0, -d < y < \eta(x)\}$.

Stream function ψ is defined as

$$\psi_x = -v, \quad \psi_y = u - c, \quad \psi(0, \eta(0)) = 0 \ ; \tag{2.9}$$

leading to

$$\psi(x,y) = m + \int_{-d}^y [u(x,s) - c]\, ds, (x,y) \in \bar{\Omega} \tag{2.10}$$

for a suitable constant $m \in \mathbb{R}$. It follows that $\psi = 0$ on $y = \eta(x)$ and $\psi = m$ on the flat bed $y = -d$. Thus,

$$m = \psi(x,-d) = -\int_{-d}^{\eta(x)} \psi_y(x,s)ds = \int_{-d}^{\eta(x)} [c - u(x,s)]\, ds, x \in \mathbb{R} \ . \tag{2.11}$$

Speed of current is defined as

$$\kappa = \lim_{L\to\infty} \frac{1}{L} \int_{-L/2}^{L/2} u(x,-d)dx \ . \tag{2.12}$$

Since uniform current is considered in this paper, the flow is still irrotational and by virtue of Eq. (2.6) u is harmonic. Hence, the definition of current in Eq. (2.12) is in fact invariant with respect to the depth at which the integral is taken beneath the wave trough - this is also the case with the periodic Stokes wave (see pages 134-135 in [8] for discussions).

We now consider the flow with underlying uniform current. We provide some mathematical results on the properties of flow and pressure field, and on the conditions on the Froude number (defined as $c/\sqrt{gd}$) and current speed for nontrivial finite amplitude solitary waves of elevation to exist.

3 Solitary Waves with Current: Case $\kappa > c$

First of all we investigate the case $\kappa > c$. Define

$$\bar{c} = \kappa - c > 0 \ . \tag{3.13}$$

Hence,

$$\bar{c} = \lim_{L\to\infty} \frac{1}{L} \int_{-L/2}^{L/2} \psi_y(x,-d)dx > 0 \ .$$

We see that ψ is harmonic by virtue of Eqs. (2.6) and (2.9) (the flow is still irrotational as the current is uniform). Strong maximum principle and Hopf's principle suggest

$$\psi_y > 0, \quad (x,y) \in \bar{\Omega} \ . \tag{3.14}$$

Therefore,

$$u > c \ \text{ and } \ m < 0, (x,y) \in \bar{\Omega} \ . \tag{3.15}$$

If the mass flux is defined as

$$M = \rho \int_{-d}^{\eta(x)} [u(x,y) - c]\, dy$$

then $m = -M/\rho$ and $M > 0$.

For the solitary waves as $|x| \to \infty$.

$$M \to \rho \int_{-d}^{0} [\kappa - c]\, dy = \rho[\kappa - c]d > 0 \ . \tag{3.16}$$

3.1 Bernoulli's law

From Euler equations we have

$$\frac{(u-c)^2 + v^2}{2} + \frac{P}{\rho} + g(y+d) = Q \tag{3.17}$$

where Q is a constant throughout the fluid domain. At the free surface, as $|x| \to \infty$

$$\frac{(\kappa - c)^2}{2} + \frac{P_{atm}}{\rho} + gd = Q \ . \tag{3.18}$$

The problem of 2-D irrotational solitary waves propagating over a uniform current above a flat bed is equivalent to the following elliptic free boundary problem

$$\begin{aligned} \Delta\psi = 0, x \in \mathbb{R}, -d \le y \le \eta(x) \\ |\nabla\psi(x,\eta(x))|^2 + 2g\eta(x) = (\kappa - c)^2, x \in \mathbb{R} \\ \psi(x,\eta(x)) = 0, x \in \mathbb{R} \\ \psi(x,-d) = -M/\rho, x \in \mathbb{R} \end{aligned} \tag{3.19}$$

additionally with the asymptotic limits

$$\begin{aligned} &\lim_{|x|\to\infty} \eta(x) = 0 \\ &\lim_{|x|\to\infty} \nabla\psi(x,y) = (k - c, 0) \ \text{ uniformly for } \ -d \le y \le \eta(x) \ . \end{aligned} \tag{3.20}$$

Further, along the free surface we assume η is symmetric about $x = 0$ (crest).

3.2 Mathematical Results

We now proceed to study some of the properties of the velocity field. It may be noted that $v = 0$ on the flat bed $B = \{(x,0) : x \in \mathbb{R}\}$ in view of the kinematic boundary conditions. Since

$$v = (u-c)\eta_x \ \text{ on } \ y = \eta(x) \tag{3.21}$$

using Eq. (3.15) and symmetry of the surface profile we conclude that

$$v > 0 \ \text{ on } \ S_- = \{(x,y) \in \mathbb{R}^2 : x < 0, y = \eta(x)\}$$

as the profile $x \mapsto \eta(x)$ is strictly increasing for $x < 0$, while

$$v = 0 \ \text{ at } \ x = -\infty \ \text{ and on } \ B_- = \{(x,y) \in \mathbb{R}^2 : x < 0, y = 0\}.$$

Maximum principle for harmonic function v, ensures $v > 0$ in Ω. Similar arguments lead to the conclusion

$$v < 0 \ \text{ in } \ \Omega_+ \cup S_+ \ \text{ where } \ S_+ = \{(x,y) \in \mathbb{R}^2 : x > 0, y = \eta(x)\}.$$

Hence, antisymmetry of v leads to the result $v = 0$ for $x = 0$.

Using the stream function and Euler equations we observe that P is super-harmonic, i.e.

$$\Delta P = -2\psi_{xy}^2 - 2\psi_{xx}^2 \leq 0 \ . \tag{3.22}$$

Bernoulli's law (Eq. (3.17) and (3.18)) yields

$$P(x, y) \to P_{atm} - \rho g y > P_{atm} \ \text{ for } \ |x| \to \infty \ . \tag{3.23}$$

Therefore the minimum of P in $\bar{\Omega}$ is attained on the flat bed or on the free surface, since $P = P_{atm}$, on the free surface.

But we have $P_y = -g$ from the Euler equation and using the kinematic condition at the flat bed. Hence, Hopf's maximum principle ensures that the minimum of P is attained everywhere on the free surface (with $P = P_{atm}$) and $P > P_{atm}$ in Ω. Since at the free surface $P = P_{atm}$

$$P_x(x, \eta(x)) > 0 \ \text{ for } \ x < 0 \tag{3.24}$$

while

$$P_x(x, \eta(x)) < 0 \ \text{ for } \ x > 0 \tag{3.25}$$

from the strict monotonicity of the graph S_- and S_+.

The Euler equation and kinematic boundary condition on the surface lead to

$$P_x = (c - u)(u_x + \eta_x u_y) \ \text{ on } \ y = \eta(x) \ .$$

Therefore, Eq. (3.15) yields

$$u_x(x, \eta(x)) + \eta_x(x) u_y(x, \eta(x)) < 0 \ \text{ for } \ x < 0 \ .$$

Hence, we can state

$$\frac{d}{dx} u(x, \eta(x)) < 0 \ \text{ for } \ x < 0 \tag{3.26}$$

and

$$\frac{d}{dx} u(x, \eta(x)) > 0 \ \text{ for } \ x > 0 \ . \tag{3.27}$$

To summarize, along the free surface u decreases strictly from $x = -\infty$ to the crest $x = 0$, and thereafter it is strictly increasing. But u is a harmonic function in Ω, and on the flat bed we have $u_y = v_x = 0$. So Hopf's maximum principle ensures that maximum/minimum of u cannot occur on the flat bed. Since $u \to \kappa(> c)$ as $|x| \to \infty$, and Eq. (3.15) gives $u > c$ throughout $\bar{\Omega}$, u reaches its minimum value (greater than or equal to the wave speed c) at the crest $(0, \eta(0))$.

Based on the result derived, we can state the following lemma.

Lemma 1. At any given time t the horizontal velocity component u is greater than c while the sign of the vertical velocity component v at a point in the fluid depends on the position of the point with respect to the crest: $v = 0$ below the crest and on the flat bed, $v < 0$ if the crest is behind the point located above the bed, and $v > 0$ if the point is above the bed and behind the crest.

Following a similar approach as in [11] we can also state the following theorem.

Theorem 2. The sign of the first component P_x of the pressure gradient at a point in the fluid depends on the position of the point with respect to the crest line:

a) $P_x = 0$ below the crest

b) $P_x < 0$ in $\Omega_+ \cup S_+ \cup B_+$

c) $P_x > 0$ in $\Omega_- \cup S_- \cup B_-$

while the second component P_y in strictly negative throughout the fluid.

Proof. The following results prove Theorem 2.

(i)
$$P_x = ((c-u)^2 + v^2)u_q \tag{3.28}$$
can be verified from the hodograph transform ($q = -\phi(x,y)$; $p = -\psi(x,y)$) and the Euler equation. Introducing the height function $h(q,p) = y$ for $(q,p) \in \mathbb{R} \times [0,-m]$ we have
$$u_q = \frac{(c-u)u_x - vu_y}{(c-u)^2 + v^2} \tag{3.29}$$
since $\partial_q = h_p\partial_x + h_q\partial_y$. The first relation in Eq. (2.1) and Eq. (3.29) give Eq. (3.28).

(ii) To prove $P_x = 0$ below the crest, we use $v(0,y) = 0$ and $v_y = 0\ \forall\ y \in [-d, \eta(0)]$ which implies
$$u_x(0,y) = 0, \forall y \in [-d, \eta(0)] \tag{3.30}$$
leading to the assertion on P_x below the crest using Eq. (3.29).

(iii) To prove the assertion on P_x in $\Omega_+ \cup B_+ \cup S_+$ it suffices to verify
$$u_q(q,p) < 0 \quad \text{for} \quad (q,p) \in (0,\infty) \times [0, M/\rho] \tag{3.31}$$
(see [11] for details).

(iv) A similar argument shows that $P_x > 0$ in $\Omega_- \cup B_- \cup S_-$.

(v) $\frac{d}{dx}((c-u)v|_{y=\eta(x)}) \leq g \forall x \in \mathbb{R}$ can be proved following a similar approach in [11] with different intermediate but same final results.

(vi) Again following [11] we introduce an auxiliary function
$$f(x,y) = (c - u(x,y))v(x,y) - gx, (x,y) \in \bar{\Omega} \tag{3.32}$$
which is a harmonic function, i.e.
$$\Delta f = 0\ . \tag{3.33}$$
We subsequently show that
$$f_q = v_x - \frac{g(c-u)}{(c-u)^2 + v^2} > 0, \quad \text{in} \ \ \mathbb{R} \times [0,-m] \tag{3.34}$$
eventually leading to
$$P_y = -g + (c-u)v_x - vv_y < -g + \frac{v_x[(c-u)^2 + v^2]}{c-u} < 0$$
in $\Omega_+ \cup B_+ \cup S_+$ (since $v_y < -vv_x/(c-u)$) in $\Omega_+ \cup B_+ \cup S_+$ from Eqs. (2.5), (2.6), (3.29) and (3.31)); and
$$P_y = (c-u)v_x - g = (c-u)f_q < 0 \quad \text{on} \quad x = 0$$
i.e. P_y is negative in $\bar{\Omega}_+$ (from Eq. (2.1) and (3.34)), and evenness implies P_y is negative in $\bar{\Omega}_-$ as well.

□

4 Solitary wave with current: Cases $\kappa = c$ and $\kappa < c$

Following a similar approach as in [4] using Eq. (3.19) and maximum principles it can be shown that for $\kappa = c$, there exists no solitary wave of nontrivial amplitude traveling at the same speed as that of an underlying uniform current (with $M = \psi = 0, u = c$).

The case $\kappa < c$, can be treated following the same approach as [10] and [11], with a wave speed defined by $\bar{c} = c - \kappa > 0$.

5 Existence of Solitary Waves with Current

It may be noted that the parameters κ, c and d cannot be arbitrarily chosen for a nontrivial finite amplitude solution of solitary waves of elevation to exist. We now prove the following theorem developing further a theorem (Theorem 4.8, page 66) proved by Amick and Toland [2]. The theorem proved here extends the results to solitary waves propagating over uniform underlying current.

Theorem 3. For nontrivial finite amplitude solution of solitary waves of elevation to exist in a 2-D irrotational fluid domain $\Omega = \{(x, y) \in \mathbb{R}^2 : -d < y < \eta(x)\}$ such that $\eta(x) \to 0$ as $|x| \to \infty$

$$F > 1 + \kappa/\sqrt{gd} \quad \text{when} \quad \kappa < c$$

or

$$F < \kappa/\sqrt{gd} - 1 \quad \text{when} \quad \kappa > c$$

where $F = c/\sqrt{gd}$, is the Froude number.

Proof. For $\kappa > c$, let us define the pressure $p(x, y) = P(x, y) - P_{atm}$ in Ω. Therefore, $p(x, y) = -gy - \frac{1}{2}((u - c)^2 + v^2) + \frac{1}{2}(\kappa - c)^2$. Then $p(x, y) = 0$ on $y = \eta(x)$ from Eq. (2.3) and

$$p(x, y) + (u - c)^2 + gy - (\kappa - c)^2 + v^2 + p + gy = 0, \forall (x, y) \in \bar{\Omega}\ . \tag{5.35}$$

From Eq. (5.35) we have

$$p_x = -(u - c)u_x - vv_x = -\nabla((u - c)((u - c), v))$$

on using the relations $u_x = v_y$ and $u_y = v_x$. Integrating p_x over the domain $\{(x', y') : x \le x' \le \bar{x}, 0 \le y' \le \eta(x') + d\}$ (with $y' = y + d$) for $x \in (-\infty, \infty)$ and $\bar{x} > x$, gives

$$\int_0^{\eta(x)+d} (p(x, y') + (u(x, y') - c)^2)dy' = \int_0^{\eta(\bar{x})+d} (p(\bar{x}, y') + (u(\bar{x}, y') - c)^2)dy' \tag{5.36}$$

since the normal component of (u, v) vanishes on $\partial\Omega$ and $p = 0$ on S. Using Eq. (5.35) in the right hand side of Eq. (5.36) gives

$$\begin{aligned}
&\int_0^{\eta(x)+d} (p(x, y') + (u(x, y') - c)^2)dy' \\
=&\frac{1}{2}\int_0^{\eta(\bar{x})+d} \{(u(\bar{x}, y') - c)^2 - v^2(\bar{x}, y') - 2g(y' - d) + (\kappa - c)^2\}dy' \\
\to &\int_0^{d} \{(\kappa - c)^2 - g(y' - d)\}dy' \quad \text{as} \quad \bar{x} \to \infty\ .
\end{aligned}$$

Hence, for all $x \in \mathbb{R}$

$$\int_0^{\eta(x)+d} (p(x, y') + (u(x, y') - c)^2)dy' = \int_0^{d} ((\kappa - c)^2 - g(y' - d))dy'$$

leading to

$$
\begin{aligned}
&\int_{\Omega}(p(x,y')+(u(x,y')-c)^2+g(y'-d)-(\kappa-c)^2)dxdy' \\
=&\int_{-\infty}^{\infty}dx\int_{d}^{\eta(x)+d}\{g(y'-d)-(\kappa-c)^2\}dy' \\
=&\frac{g}{2}\int_{-\infty}^{\infty}(\eta(x))^2dx-(\kappa-c)^2\int_{-\infty}^{\infty}(\eta(x))dx\ .
\end{aligned}
\tag{5.37}
$$

From Eq. (5.35) we also have

$$
\begin{aligned}
\frac{\partial}{\partial y'}(p+g(y'-d)) =&-(u-c)u_{y'}-vv_{y'}=-(u-c)v_x-vv_{y'} \\
=&-\nabla(v(u-c,v))
\end{aligned}
$$

which gives

$$
\frac{\partial}{\partial y'}(y'p+gy'(y'-d))=v^2+p+g(y'-d)-\nabla(y'v(u-c,u-c))\ .
$$

Hence,

$$
\begin{aligned}
&\int_{-\bar{x}}^{\bar{x}}dx\int_{0}^{\eta(x)+d}(v^2+p+g(y'-d))dy' \\
=&\int_{0}^{\eta(\bar{x})+d}y'v(\bar{x},y')[u(\bar{x},y')-c]dy'-\int_{0}^{\eta(-\bar{x})+d}y'v(-\bar{x},y')\,[u(-\bar{x},y')-c]\,dy' \\
+&\int_{-\bar{x}}^{\bar{x}}(\eta(x)+d)\{p(x,(\eta(x)+d))+g\eta(x)\}dx \\
\to&\int_{-\infty}^{\infty}(\eta(x)+d)\{p(x,(\eta(x)+d))+g\eta(x)\}dx \quad \text{as} \quad \bar{x}\to\infty\ .
\end{aligned}
$$

Since $p=0$ on $y=\eta(x)+d$, we have

$$
\begin{aligned}
\int_{\Omega}(v^2+p+g(y'-d))dxdy' =&g\int_{-\infty}^{\infty}\eta(x)(\eta(x)+d)dx \\
=&g\int_{-\infty}^{\infty}(\eta(x))^2dx+gd\int_{-\infty}^{\infty}\eta(x)dx\ .
\end{aligned}
\tag{5.38}
$$

Using Eqs. (5.37) and (5.38) with Eq. (5.35) gives ($\eta(x)\geq 0\ \ \forall x\in\mathbb{R}$)

$$
\frac{3g}{2}\int_{-\infty}^{\infty}(\eta(x))^2dx+[gd-(\kappa-c)^2]\int_{-\infty}^{\infty}\eta(x)dx=0
$$

which leads to

$$
\frac{(\kappa-c)^2}{gd}=1+\frac{3}{2d}\frac{\int_{-\infty}^{\infty}(\eta(x))^2dx}{\int_{-\infty}^{\infty}\eta(x)dx}>1\ .
\tag{5.39}
$$

Hence,

$$
\kappa>c+\sqrt{gd},\quad \text{or} \quad F<\kappa/\sqrt{gd}-1\ .
$$

For $\kappa<c$, we define $\bar{c}=c-\kappa$. Following a similar approach by Amick and Toland [2], and using the wave speed of $\bar{c}$, we get

$$
c>\kappa+\sqrt{gd}
$$

leading to

$$
F>1+\kappa/\sqrt{gd}\ .
$$

□

6 Some additional results

For the case, $\kappa > c$, we use Eq. (5.39) to arrive at the following inequality

$$\frac{(\kappa - c)^2}{gd} = 1 + \frac{3}{2d} \frac{\int_{-\infty}^{\infty} (\eta(x))^2 dx}{\int_{-\infty}^{\infty} \eta(x) dx} < 1 + \frac{3}{2} \frac{\max \ \eta}{d} \ . \tag{6.40}$$

This inequality was also given by Wheeler [25] based on the exact formula by Starr [22] for irrotational solitary waves. On applying Bernoulli's equation on the crest and on a point on the free surface with ($\eta \to 0$ as $x \to \pm\infty$) respectively, we get

$$\max \ \eta = \frac{(\kappa - c)^2}{2g} \ . \tag{6.41}$$

Using Eq.(6.41) in the inequality given by Eq.(6.40) leads to the following bound on the amplitude of the solitary wave

$$\max \ \eta < 2d \tag{6.42}$$

for the case of non-trvial solution ($\eta \neq 0$). Note the this bound was obtained by Wheeler [25] (but with $u < c$), if we use the condition of uniform current in the expression in Corollary 5.1 in [25].

If we again use Eq.(6.41) in the inequality given by Eq.(6.40), we also get the following

$$\frac{(\kappa - c)^2}{gd} < 4 \tag{6.43}$$

leading to a lower bound on the Froude number

$$F > \kappa/\sqrt{gd} - 2 \ . \tag{6.44}$$

If we redefine the Froude number, $F^{'}$ according to [25] based on a uniform underlying current k, then we have

$$F^{'} < 2 \tag{6.45}$$

for the nontrivial case. A bound was proved by [25] (for $u < c$) which for the case of uniform current leads to $F^{'} < 2$.

For the case, $\kappa < c$, we use the inequality

$$\frac{(c - \kappa)^2}{gd} = 1 + \frac{3}{2d} \frac{\int_{-\infty}^{\infty} (\eta(x))^2 dx}{\int_{-\infty}^{\infty} \eta(x) dx} < 1 + \frac{3}{2} \frac{\max \ \eta}{d} \ . \tag{6.46}$$

Use of Bernoulli's equation

$$\max \ \eta = \frac{(c - \kappa)^2}{2g} \tag{6.47}$$

and the inequality in (6.46) leads to a bound on non-trivial amplitudes of the solitary wave

$$\max \ \eta < 2d \tag{6.48}$$

which is consistent with [25] (Corollary 5.1, on using uniform current κ). Also,

$$\frac{(c - \kappa)^2}{gd} < 4 \tag{6.49}$$

obtained from Eq.(6.47) and inequality (6.46), is an upper bound on the Froude number for the non-trvial case

$$F < 2 + \kappa/\sqrt{gd} \tag{6.50}$$

as proved by [25] (see Theorem 1.2, and use uniform current κ).

7 Remarks

We have shown in this paper that solitary waves of large amplitude in finite water depth over a flat bed can propagate over a uniform current both for the case of $u > c$ or $u < c$ everywhere in the fluid domain. For the case $u < c$, the results are consistent with those proved by [25] for a general vorticity; and by [10], and [11] in the absence of any vorticity.

Acknowledgements

The author would like to thank the referee for the suggestions in improving the quality of the manuscript.

References

[1] C. J. Amick, L.E. Fraenkel, J.F. Toland. On the stokes conjecture for the wave of extreme form. *Acta Mathematica*, 148(1):193–214, 1982.

[2] C.J. Amick, J. F. Toland. On periodic water-waves and their convergence to solitary waves in the long-wave limit. *Phil. Trans. Roy. Soc. of London A: Math., Phys. Eng. Sci.*, 303(1481):633–669, 1981.

[3] C. J. Amick, J. F. Toland. On solitary water-waves of finite amplitude. *Arch. Ration. Mech. Anal.*, 76(1):9–95, 1981.

[4] B. Basu. Irrotational two-dimensional free-surface steady water flows over a flat bed with underlying currents. *Nonlinear Anal. TMA*, 147:110 – 124, 2016.

[5] J. T. Beale. The existence of solitary water waves. *Comm. Pure Appl. Math.*, 30(4):373–389, 1977.

[6] Y.-Y. Chen, H.-C. Hsu. A modified Euler–Lagrange transformation for particle orbits in nonlinear progressive waves. *Ocean Eng.*, 36(9):747–753, 2009.

[7] A. Constantin. The trajectories of particles in Stokes waves. *Invent. Math.*, 166(3):523–535, 2006.

[8] A. Constantin. *Nonlinear Water Waves with Applications to Wave-Current Interactions and Tsunamis.* in : CBMS-NSF Conf. Ser. in Appl. Math., Vol. 81, SIAM, Philadelphia, 2011.

[9] A. Constantin. Extrema of the dynamic pressure in an irrotational regular wave train. *Phy. Fluids.*, 28:113604, 2016.

[10] A. Constantin, J. Escher. Particle trajectories in solitary water waves. *Bull. Amer. Math. Soc.*, 44(3):423 – 431, 2007.

[11] A. Constantin, J. Escher, H.-C. Hsu. Pressure beneath a solitary water wave: Mathematical theory and experiments. *Arch. Ration. Mech. Anal.*, 201:251 – 269, 2011.

[12] A.Constantin, W. Strauss. Pressure beneath a Stokes wave. *Comm. Pure Appl. Math.*, 63(4):533–557, 2010.

[13] W. Craig. Non–existence of solitary water waves in three dimensions. *Proc. Roy. Soc. London A: Math., Phys. Eng. Sci.*, 360(1799):2127–2135, 2002.

[14] J. Escher, T. Schlurmann. On the recovery of the free surface from the pressure within periodic traveling water waves. *J. Nonlinear Math. Phys.*, 15:50 – 57, 2008.

[15] W.A.B. Evans, M.J. Ford. An exact integral equation for solitary waves (with new numerical results for some 'internal' properties). *Proc. Roy. Soc. London A: Math., Phys. Eng. Sci.*, 452:373–390, 1996.

[16] K. O. Friedrichs, D.H. Hyers. The existence of solitary waves. *Comm. Pure and Appl. Math.*, 7(3):517–550, 1954.

[17] D. Henry. Pressure in a deep-water Stokes wave. *J. Math. Fluid Mech.*, 13:251 – 257, 2011.

[18] D. Henry. On the pressure transfer function for solitary water waves with vorticity. *Math. Ann.*, 357:23–30, 2013.

[19] H.-C. Hsu, Y.-Y. Chen, J. R. C. Hsu, W.-J. Tseng. Nonlinear water waves on uniform current in Lagrangian coordinates. *J. Nonlinear Math. Phys.*, 16:47–61, 2009.

[20] T. Lyons. The pressure distribution in extreme Stokes waves. *Nonlinear Anal. RWA*, 31:77 – 87, 2016.

[21] T. Lyons. The pressure in a deep-water Stokes wave of greatest height. *J. Math. Fluid Mech.*, 18:209 – 218, 2016.

[22] V. P. Starr. Momentum and energy integrals for gravity waves of finite height. *J. Mar. Res.*, 6:175 – 193, 1947.

[23] C.-H. Tsai, M.-C. Huang, F.-J. Young, Y.-C. Lin, H. W. Li. On the recovery of surface wave by pressure transfer function. *Ocean Eng.*, 32:1247 – 1259, 2005.

[24] M. H. Wheeler. Large-amplitude solitary water waves with vorticity. *SIAM J. Math. Anal.*, 45(5):2937 – 2994, 2013.

[25] M. H. Wheeler. The Froude number for solitary water waves with vorticity. *J. Fluid Mech.*, 768:91 – 112, 2015.

On some properties of velocity field for two dimensional rotational steady water waves

Biswajit Basu

Nonlinear Anal. 184, 17-34, 2019

Abstract

We investigate the properties of velocity field for steady periodic water waves over a flat bed for a generalized class of C^1 vorticity function γ. Results are proved by exploiting the maximum principles and are based on Dubreil-Jacotin transformation of the fluid domain. Some properties of velocities interior to the fluid domain and the locations of maximum/minimum horizontal fluid velocities are investigated and proved for rotational water waves without any restriction to amplitude. For $u < c$ and a monotonically varying positive vorticity ($\gamma = u_y - v_x \geq 0$), the location of maximal horizontal velocity has been proven to be the crest, generalizing some of the recently proved results.

1 Introduction

Since the systematic investigation by Constantin and Strauss [15], the classical hydrodynamic problem concerning two-dimensional travelling water waves with vorticity has generated considerable interest among researchers. The existence of large amplitude nonlinear water waves and waves with stagnation points was first conjectured by Stokes [33] who undertook an extensive study of the nonlinear governing equations. In the framework of irrotational water waves, significant success has been achieved in the understanding and analysis of large amplitude steady periodic waves in the past few decades (see Toland [34] for properties of the surface waves and Constantin [5] and Constantin and Strauss [18] for the flow beneath the waves). Stokes' conjecture on extreme waves and stagnation point was proved by Amick, Fraenkel and Toland both in the context of irrotational flow in water of finite depth over a flat bed and for infinitely deep water ([1, 2]). The method in [2] was further simplified and extended by Varvaruca [37]. Numerical investigations on the velocity and related fields have been carried out in [4] and results on experimental studies on the velocities and the trajectory of water particles under surface waves using particle image velocimetry (PIV) have been reported in [35]. On the contrary, mathematical theory behind the rotational water waves or water waves with vorticity is at its relative infancy with the major developments taking place only in the last few years.

The existence of global continua of smooth solutions for waves with vorticity was proved by Constantin and Strauss [15] for the finite depth problem and Hur [25] considered the related problem of periodic waves over infinite depth. The solutions in [15] and in [25] have exactly one crest and one trough per period, and are monotone between successive crests and troughs, having a vertical axis of symmetry. Symmetry of steady periodic surface waves with vorticity both for deep water and for water waves over finite depth have been investigated by Constantin and Escher [10, 11]. Variational approach for water waves with vorticity was formulated by Constantin et al. [14] and stability properties of steady water waves with vorticity were studied by Constantin and Strauss [17]. Further, Constantin and Escher [13] proved that periodic travelling free surface waves are analytic in the absence of stagnation points. Constantin and Strauss [16] investigated the location of the point of maximal horizontal velocity for steady periodic water waves with vorticity to provide an insight to water waves near stagnation and a similar investigation was carried out by Varvaruca [38] for a large class of vorticity functions. In both the cases, it was assumed that the horizontal velocity of the fluid, u is less than the travelling wave speed, c. Existence of extreme waves with vorticity and the Stokes conjecture was proved by Varvaruca [39, 40]. Constantin and Strauss [19] investigated the periodic travelling gravity waves in the case of discontinuous vorticity. Regularity and local bifurcation results were proved by Constantin and Varvaruca [21] for constant vorticity. Further, global bifurcation results of steady gravity water waves with critical layers in a flow of constant vorticity were proved by Constantin et al. [20] and some conjectures were put forward based on results available from numerical computations ([22, 36]).

Even though there has been development on water waves with vorticity in the last few years, still very little is known about velocity field in the fluid domain. Numerical evidence ([22, 28]) in the case of constant vorticity suggests that stagnation points exist for negative and small positive vorticity. Also, for large positive vorticity, the solutions can bifurcate from trivial solutions to waves with overhanging profile, without approaching extreme waves. Constantin and Strauss [15] proved that for an arbitrary vorticity distribution and for any given wave speed $c > 0$ with a given relative mass flux, there exists a global continuum of steady periodic water waves travelling at a speed c, such that $u < c$ throughout the fluid. The continuum contains waves with u arbitrarily close to c. In [16], it was shown that the points of maximal horizontal velocity is necessarily the crest for a certain class of waves (with small negative vorticty). This result was further extended by Varvaruca [38] for a larger class of vorticity but with a further condition on the derivative of vorticity function. However, knowledge about location of points of maximum/minimum horizontal velocity or properties of velocity field in the fluid domain for more general classes of vorticity with less restrictions is still lacking. Ehrnström [23] established some results on streamlines, velocity field and particle paths within the fluid domain for rotational flows relying on strong maximum principles. Existing literature suggest that results and knowledge on the behaviour of the flow field within the fluid domain for large amplitude rotational water waves are still far from complete. For example, it was noted in [23] that there are no results available on how the horizontal velocity varied within the domain or on the general control of horizontal velocity in the interior of the fluid; or for that matter even how the slope of the streamlines varied vertically along the depth of the fluid medium.

This paper aims to provide information about location of local/global maximum/ minimum horizontal velocity and properties of velocity field in the fluid domain for 2D large amplitude travelling water waves with vorticity. Several combinations of vorticity functions and their derivatives have been considered to prove the results. In particular, the results on the location of maximum horizontal velocity generalize the previous results of Constantin and Strauss [16] and Varvaruca [38]. The other contribution of this paper is that some information on the horizontal and vertical fluid velocities, u and v respectively, within the fluid domain has been derived for rotational flows under physically realistic conditions.

2 Problem formulation

We consider the governing equations of fluid dynamics for 2D free surface gravity waves represented by the Euler equations with vorticity of fluid flow ω. It is assumed that

(i) the flow velocities u and v, the pressure P and the free surface profile η are periodic

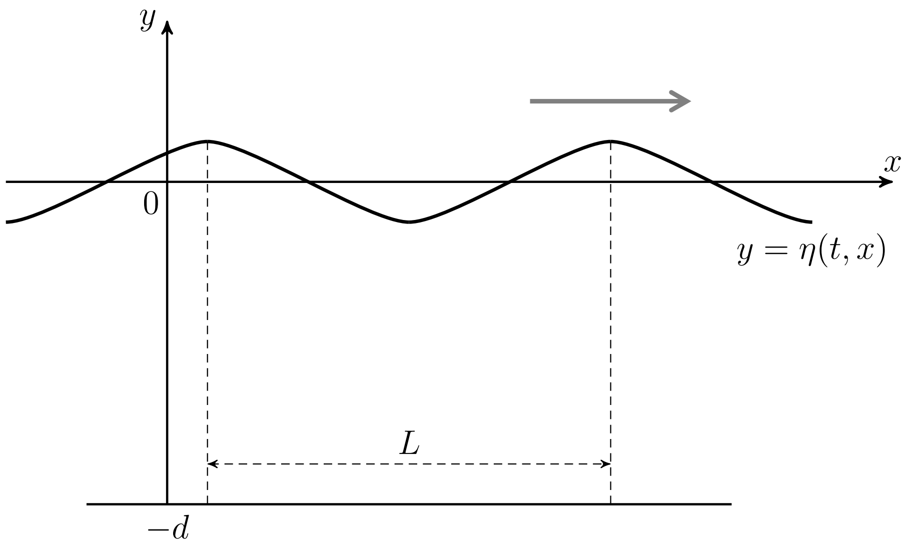

Figure 1: A steady periodic water wave propagating over a flat bed.

along the horizontal axis X with period L ,

(ii) the free surface η is strictly monotonic between successive crests and troughs ,

(iii) η, u, and the pressure P are symmetric about the crest line $X = 0$,

(iv) v is anti-symmetric about the crest line.

We assume all these functions to be smooth: in absence of stagnation points they must be real-analytic (see the discussion in [13]). Further, a profile that is monotone between successive crests and troughs has to be symmetric (see [9, 12, 26]). Under these assumptions, we seek smooth solution(s) for which there exists a period $L > 0$, a wave speed c for a given vorticity of the flow ω such that the free surface profile η, the flow field (u, v) and the pressure P have period L in X variable, η depends on $X - ct$ while u, v, and P are dependent on $X - ct$ and Y, where t is the time variable.

2.1 Governing equations in moving frame

In the moving frame, the flow is steady occupying a fixed region Ω in the (x,y) plane, lying between the horizontal axis $B = \{(x, -d) : x \in \mathbb{R}\}$ which is the flat bed for some $d > 0$ and some apriori unknown free surface $S = \{(x, \eta(x)) : x \in \mathbb{R}\}$, with η a periodic function. Hence, in the moving frame of reference (see Figure 1) with

$$x = X \ - ct \ , \quad y = Y \ , \tag{2.1}$$

the governing equations are

$$
\begin{aligned}
(u-c)u_x + vu_y &= -\frac{1}{\rho}P_x, \quad \text{for} \quad -d \le y \le \eta(x)\\
(u-c)v_x + vv_y &= -\frac{1}{\rho}P_y - g, \quad \text{for} \quad -d \le y \le \eta(x)\\
u_x + v_y &= 0, \quad \text{for} \quad -d \le y \le \eta(x)\\
u_y - v_x &= \omega, \quad \text{for} \quad -d \le y \le \eta(x)\\
v &= 0, \quad \text{on} \quad Y = -d\\
v &= (u-c)\eta_x, \quad \text{on} \quad y = \eta(x)\\
P &= P_{atm}, \quad \text{on} \quad y = \eta(x)
\end{aligned}
\tag{2.2}
$$

where ω represents a non-constant vorticity of the flow.

Since we are dealing with incompressible flow, $\rho = 1$ is assumed for the rest of the paper.

We seek steady classical solutions of Eq. (2.2). Classical solutions of governing equations given in Eq. (2.2) representing periodic travelling water waves, in absence of stagnation points, have to be real-analytic (see [13] for discussions on regularity).

3 Stream function formulation

Let us introduce a stream function $\Psi(x, y)$ such that

$$\Psi_x = -v, \Psi_y = u - c\ . \tag{3.3}$$

Use of stream function enables us to write

$$\Delta\Psi = \omega \tag{3.4}$$

where $\omega = u_y - v_x$ is the vorticity of the flow. Euler's equation implies that Ψ and ω have parallel gradients and same level sets, and are functionally dependent. If either the condition $u < c$ throughout Ω or the condition $u > c$ throughout Ω is satisfied then this functional dependence is global, i.e. $\exists$ a C^1 function γ, called vorticity function, such that

$$\omega = \gamma(\Psi) \tag{3.5}$$

throughout the fluid domain Ω ([15, 16]).

Two particular flow invariants are of interest in this paper in the setting of Eq. (2.2) and are expressed as follows:

(i) Mass flux (flow rate per unit width), relative to uniform flow at constant speed c

$$M = \int_{-d}^{\eta(x)} [u(x, y) - c]\,\mathrm{d}y \tag{3.6}$$

is invariant with x. This follows from the third, fifth and sixth relations in Eq. (2.2) and by differentiation with respect to x.

(ii) Conservation of energy or head follows from the first, second and fourth relations in Eq. (2.2) and by differentiation. The following expression

$$E = \frac{(u-c)^2 + v^2}{2} + P + gy - \int_0^{\Psi} \gamma(s)\mathrm{d}s \tag{3.7}$$

is constant (called hydraulic head) throughout the fluid. This allows us to express the last relation in Eq. (2.2) as a constraint in terms of a physical constant, $Q = 2(E - P_{atm} + gd)$.

The stream function is not harmonic as $\gamma \neq 0$. However, the first relation in Eq. (3.3) and the fifth and sixth relations in Eq. (2.2) ensure that $\Psi_x = 0$ on the flat bed $y = -d$ and $\Psi_x + \Psi_y \eta_x = 0$ on the free surface $y = \eta(x)$. This implies that Ψ must be constant on $y = -d$ and on $y = \eta(x)$. Also, using the second relation in Eq. (3.3) leads to

$$M = \Psi(x, \eta(x)) - \Psi(x, -d) \ . \tag{3.8}$$

Hence, without any loss of generality we can assign $\Psi = 0$ on the free surface and $\Psi = -M$ on the bed. The transformed governing equations are

$$\begin{aligned}
&\Delta\Psi = \gamma(\Psi) \ \text{ in } \ \Omega \ , \\
&\Psi = 0 \ \text{ on } \ S \ , \\
&\Psi = -M \ \text{ on } \ B \ , \\
&\Psi_x^2 + \Psi_y^2 + 2g(y + d) = Q \ \text{ on } \ S \ .
\end{aligned} \tag{3.9}$$

Two cases corresponding to $\gamma > 0$ and $\gamma < 0$ are considered here. For the case $\gamma > 0$ (with $u < c$), we prove results for two different conditions: either $\gamma' \leq 0$ everywhere or $\gamma' \geq 0$ everywhere. However, for $\gamma < 0$ (with $u > c$) we prove results only for $\gamma' \geq 0$ everywhere. Figure 2 shows sketches of some possible profiles for waves with vorticity for three different combinations of γ and γ' considered in this paper.

It may be noted that Constantin and Strauss [16] proved the location of $\max_{\bar{\Omega}} u$ for $\gamma \geq 0$ (with some additional constraints) and Varvaruca [38] gave a proof of the same leading to a less stronger result but valid over a large class of vorticity.

3.1 Flow with vorticity (underlying current)

It is known that in absence of an underlying current, the horizontal fluid velocity u in the flow beneath a smooth Stokes wave propagating at a speed $c > 0$ can never attain a value of c (see [8]), i.e.

$$u(x, y) \neq c \ \text{ for } \ -d \leq y \leq \eta(x) \tag{3.10}$$

or if there is an underlying current then the flow can have a velocity strictly greater than the wave speed, c (see [3]) i.e.

$$u > c \ .$$

In the setting of periodic waves travelling at a constant speed at the surface of water with vorticity γ over flat bed, for a given $y_0 \in [-d, \min_{x\in[0,L]} \{\eta(x)\}]$ we get from Eq.(3.9)

$$\int_0^L \int_{-d}^{y_0} \Psi_{yy}(x, y) \mathrm{d}y \mathrm{d}x = -\int_{-d}^{y_0} \int_0^L \Psi_{xx}(x, y) \mathrm{d}x \mathrm{d}y + \int_{-d}^{y_0} \int_0^L \gamma(\Psi(x, y)) \mathrm{d}x \mathrm{d}y \ . \tag{3.11}$$

We use the periodicity of Ψ in the x-variable, hence

$$\int_0^L u(x, -d) \mathrm{d}x = \int_0^L u(x, y_0) \mathrm{d}x + \int_0^L \int_{-d}^{y_0} \gamma(\Psi(x, s)) \mathrm{d}s \mathrm{d}x \tag{3.12}$$

for any level $y = y_0$ below the trough level $y = \eta(L/2)$; we assume that the crest is located at $x = 0$. Thus, the strength of the depth dependent underlying current can be characterized by

$$k(y) = \frac{1}{L} \int_0^L u(x, y) \mathrm{d}x = \frac{1}{L} \int_0^L u(x, -d) \mathrm{d}x - \frac{1}{L} \int_0^L \int_{-d}^{y} \gamma(\Psi(x, s)) \mathrm{d}s \mathrm{d}x \tag{3.13}$$

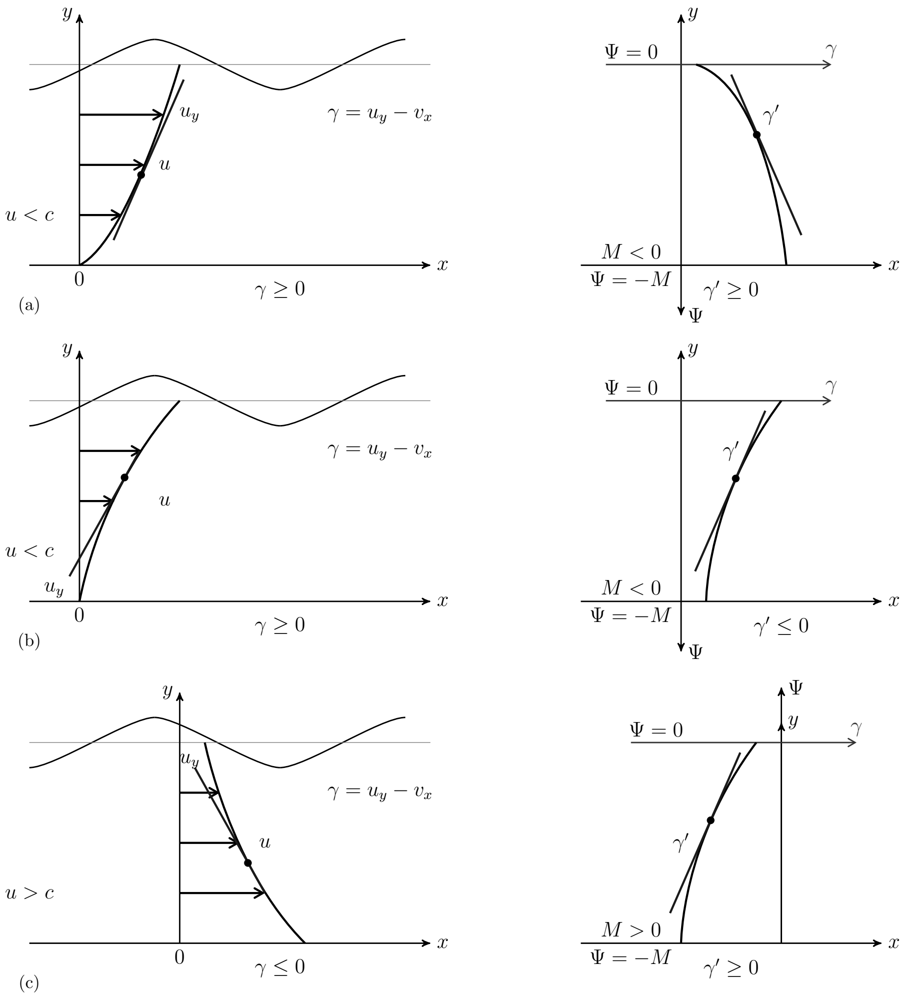

Figure 2: Various combinations of γ and $\gamma^{'}$.

which leads to

$$k(y) = \frac{1}{L}\int_0^L \Psi_y(x,-d)\mathrm{d}x - \frac{1}{L}\int_0^L \int_{-d}^{y} \gamma(\Psi((x,s))\mathrm{d}s\mathrm{d}x + c \ . \tag{3.14}$$

Note that in absence of any underlying current (due to absence of vorticity), i.e. $k(y) = 0$ and $\gamma = 0$; the wave speed is obtained as the mean of $-\Psi_y$ over the flat bed which is consistent with the Stokes' first definition of wave speed (see [6, 8]). Stokes' second definition of the wave speed is the depth-averaged horizontal fluid velocity (or "mass-transport velocity"). An in-depth discussion on these two definitions of wave speed is available in [7].

Based on the assumption that critical points are absent (i.e., $u \neq c$) in the fluid domain, the fluid velocity u is either strictly less than or strictly greater than the wave speed c, i.e. $u < c$ or $u > c$ everywhere in the fluid domian. Hence, from Eq. (3.3) we assume $M \neq 0$.

4 Analysis in transformed domain

We now prove some more results related to the properties of velocity field. It may be noted that due to the presence of vorticity the flow is rotational. Hence, an underlying current exists. A conformal mapping is not possible as velocity potential does not exist. Instead we take recourse to a different approach which was proposed by Constantin and Strauss [15]. One of the main difficulties associated with the problem in Eq. (2.2) is that the free surface $y = \eta(x)$ is unknown. This can be overcome by introducing co-ordinate transformation designed by Dubreil-Jacotin. It should be noted that because of vorticity, it is not possible to convert the problem to an integral equation on the boundary as in [1, 27, 29, 31, 34]. By noting that $\Psi(x, y)$ is a constant on the free surface and on the bottom, Constantin and Strauss [15] introduced independent variables to transform the water wave problem into a problem in fixed domain. Since, by assumption $\Psi(x, y)$ is a strictly monotonic function of y, hence for every fixed x at the height above the flat bottom is a single-valued function of Ψ. This and the fact that Ψ is constant both on the fixed bed and the free surface, naturally lead to the introduction of the transformation

$$q = x, \quad p = -\Psi(x, y) \ . \tag{4.15}$$

The new domain R under this transformation is rectangular and is known apriori since we assume that the (relavtive) mass flux is known. The dependent variables can be replaced by a single function $h(q, p)$, periodic in q, where

$$h(q, p) = y + d \tag{4.16}$$

is the height above the flat bottom. Then,

$$h_q = \frac{v}{u-c}, \quad h_p = \frac{1}{c-u} \ . \tag{4.17}$$

Thus, we have

$$v = -\frac{h_q}{h_p}, \quad u = c - \frac{1}{h_p} \ , \tag{4.18}$$

$$\partial_q = \partial_x - \frac{v}{c-u}\partial_y, \quad \partial_p = \frac{1}{c-u}\partial_y \tag{4.19}$$

and

$$\partial_x = \partial_q - \frac{h_q}{h_p}\partial_p, \quad \partial_y = \frac{1}{h_p}\partial_p \ . \tag{4.20}$$

Constantin and Strauss [15] showed by an explicit calculation that $h(p,q)$ satisfies the following second-order, quasi-linear elliptic equation with nonlinear oblique boundary conditions

$$(1+h_q^2)h_{pp} - 2h_p h_q h_{pq} + h_p^2 h_{qq} = \gamma(\Psi) h_p^3 \ , \quad p \in (0, M) \tag{4.21}$$

$$1 + h_q^2 + (2gh - Q)h_p^2 = 0 \ , \quad p = 0 \tag{4.22}$$

$$h = 0 \ , \quad p = M \tag{4.23}$$

where h is even and periodic in q-variable. The image of the fluid domain $\Omega_+ = \{(x,y) : x \in (0, L/2), y \in (-d, \eta(x))\}$, and the four sides (top S_+, bottom B_+, left R_{l+} and right R_{r+}) of the corresponding boundary (with the exception of the four corner points) under the transformation becomes

$$\begin{aligned}
\hat{\Omega}_+ &= (0, cL/2) \times (M, 0) \ , \\
\hat{S}_+ &= (0, cL/2) \times 0 \ , \\
\hat{B}_+ &= (0, cL/2) \times M \ , \\
\hat{R}_{l+} &= 0 \times (M, 0) \ , \\
\hat{R}_{r+} &= cL/2 \times (M, 0) \ .
\end{aligned} \tag{4.24}$$

$\hat{\Omega}_+$ is an open rectangle with the sides $\hat{S}_+$, $\hat{B}_+$, $\hat{R}_{l+}$ and $\hat{R}_{r+}$. Following the reformulation of the water-wave problem (Eq.(9)) and using bifurcation and degree theory, and given $M < 0$, $c > 0$ and $\gamma \in C^2$, Constantin and Strauss [15] proved the existence of a global connected set $\mathscr{C}$ of smooth solutions. Each solution in this continuum of $\mathscr{C}$ has certain properties which are specfied now.

For the open rectangle $\hat{\Omega}_+$, Constantin and Strauss [15] (see also [16]) proved that for every wave in $\mathscr{C}$, the following strict inequalities hold

$$\begin{aligned}
h_q < 0 \ \text{ in } \ \hat{\Omega}_+ \ \cup \ \hat{S}_+ \ , \quad h_{qp} < 0 \ \text{ on } \ \hat{B}_+ \\
h_{qq} < 0 \ \text{ on } \ \hat{R}_{l+} \ , \quad h_{qq} > 0 \ \text{ on } \ \hat{R}_{r+}
\end{aligned} \tag{4.25}$$

on the four sides.

For the case, $u > c$, we have $M > 0$. In such a situation, the bottom boundary of the transformed rectangular fluid domain $\hat{\Omega}_+$, corresponds to $\Psi = -M < 0$ while $\Psi = 0$ at the top boundary. Hence, $p = -\Psi$ is > 0 at the bottom and $p = 0$ at the top, implying p decreases with increasing y, i.e. the direction of positive p axis is opposite to that for the case $M < 0$ (or $u < c$). This has implications in terms of the inequalitiy involving axis p, proved by Constantin and Strauss [15] for the wave solution in $\mathscr{C}$ for the bottom boundary of the open rectangle $\hat{\Omega}_+$. The new inequality can be stated as

$$h_{qp} > 0 \ \text{ on } \ \hat{B}_+ \ . \tag{4.26}$$

4.1 Vertical velocity

Let us now consider the vertical velocity v. From the sixth relation of Eq. (2.2) we know that $v = (u-c)\eta_x$ on $y = \eta(x)$. Using $u < c$ and that $\eta_x(x) \le 0$ for $x \in [0, L/2]$ ensures $v(x, \eta(x)) \ge 0$ for $x \in [0, L/2]$. Correspondingly, for $u > c$ and $\eta_x(x) \le 0$ for $x \in [0, L/2]$ we have $v(x, \eta(x)) \le 0$ for $x \in [0, L/2]$. Also, $v(x, -d) = 0$ for $x \in [0, L/2]$ from the fifth relation of Eq. (2.2). Further, $v = 0$ on $x = 0$ and $x = L/2$, since v is odd and periodic in x-variable throughout Ω.

We prove the following theorem based on the results of Constantin and Strauss [15, 16].

Theorem 4.1. Let $v \in C^2(\bar{\Omega})$ be the vertical fluid velocity over the fluid domain $\bar{\Omega}$. Then the following holds for v in $\Omega = \Omega_+ \bigcup \Omega_-$ where $\Omega_+ = \{(x,y) : x \in (0, L/2), y \in (-d, \eta(x))\}$, $\Omega_- = \{(x,y) : u \in (-L/2, 0), y \in (-d, \eta(x))\}$,

(i) If $u < c$, then $v > 0$ in Ω_+ and $v < 0$ in Ω_-

(ii) If $u > c$, then $v < 0$ in Ω_+ and $v > 0$ in Ω_-

Proof. (i) If $u < c$ then from the results in Eq. (4.25) we have $h_q < 0$ in $\hat{\Omega}_+ \bigcup \hat{S}_+$ leading to $v > 0$ in Ω_+. Since v is odd and periodic in x variable we have $v < 0$ in Ω_-, which proves (i).

(ii) To prove (ii), we use similar arguements, and since $u > c$ and v is odd in x varable, we arrive at the results. □

Note that along the crest line, trough line and on the flat bed we always have $v = 0$. Also observe, that the results here are independent of γ and γ'.

4.2 Horizontal velocity along the flat bed

We next consider the variation of the horizontal velocity along the flat bed. We prove the following lemma which is a straightforward consequence of the result from the last theorem.

Lemma 4.2. The horizontal fluid velocity u satisfies the following relationship

$$u_x(x, -d) < 0 \quad \text{for} \quad x \in [0, L/2], \text{if } u < c \tag{4.27}$$

$$u_x(x, -d) > 0 \quad \text{for} \quad x \in [0, L/2], \text{if } u > c \tag{4.28}$$

on $B^+ = \{(x,y) : 0 < x < L/2, y = -d\}$.

Proof. Using the relation $h_{qp} < 0$ on $\hat{B}_+$ from Eq. (4.25) we conclude that $u_x(x, -d) < 0$ for $x \in [0, L/2]$ (assuming $u < c$) which is the first of the two results in the lemma. Alternatively, Constantin and Strauss [16] in Proposition 3.2 defined a function f and studied its monotonicity properties along the boundary of the fluid domain Ω_+ (i.e. along the vertical crest line, flat bed and the vertical trough line). Using the monotonicity properties they proved $u_x(x, -d) < 0$ for $x \in [0, L/2]$ (assuming $u < c$).

For proving the second relation, note the diuscussion for $u > c$ following Eq. (4.25) and the condition in Eq. (4.26) $h_{qp} > 0$ on $\hat{B}_+$. Thus, on $B^+ = \{(x,y) : 0 < x < L/2, y = -d\}$ we have

$$0 < h_{qp} = \partial_q h_p = \left(\frac{1}{c-u}\right)_x - \frac{v}{c-u}\left(\frac{1}{c-u}\right)_y = \frac{u_x}{(c-u)^2} \tag{4.29}$$

leading to $u_x(x, -d) > 0$ for $x \in [0, L/2]$.

□

Again, the results are not dependent on vorticity γ and γ'.

4.3 Pressure in the fluid domain

We again consider two cases in this section corresponding to $\gamma \leq 0$ and $\gamma \geq 0$ and investigate how the horizontal fluid velocity profile varies along the free surface.

(a) $\gamma \geq 0$ and $u < c$

In order to study the horizontal fluid velocity profile along the surface let us first consider the function

$$R = \frac{1}{2}|\nabla\Psi|^2 + g(y+d) - \frac{1}{2}Q - \hat{\Gamma}(\Psi) \tag{4.30}$$

which is the negative of the pressure in the fluid domain upto a constant (see Constantin and Strauss [16]). The expression for $\hat{\Gamma}(\Psi) : [0, -M] \to \mathbb{R}$ is given by $\hat{\Gamma}(\Psi) = \int_0^\Psi \gamma(s)ds \;\; \forall \;\; \Psi \in [0, -M]$. It was proved by Constantin and Strauss [16] that $R \le 0$ in $\bar{\Omega}$ i.e., in the closure of the fluid domain and this result has significance in relation to pressure within the fluid domain and horizontal velocity of the fluid along the surface (see discussions in [15], [16] and [38]). It has been proved by Constantin and Strauss [16] under certain conditions and by Varvaruca [38] under a more general condition that the fluid pressure within the fluid domain is greater than the atmospheric pressure P_{atm} (see Proposition 3.4, Constantin and Strauss [16] and Theorem 2.1, Varvaruca [38]). We now use this result for our proof in this paper. We restate the theorem in Varvaruca [38] in a way that is compatible with our notation and sign convention.

Theorem 4.3. (Theorem 2.1, [38]) Suppose that $\gamma(\Psi) \ge 0 \;\; \forall \;\; \Psi \in [0, -M]$. Then $R \le 0$ in $\bar{\Omega}$.

From the result of Theorem 2.1 of Varvaruca [38], we can state that for the case $u < c$ and $\gamma > 0$, we have

$$R_y \ge 0 \tag{4.31}$$

in $\bar{\Omega}$, since $R = 0$ everywhere on the free surface and $R \le 0$ in $\bar{\Omega}$. Also, noting that R is the negative of the pressure (up to constant) we get

$$P_y \le 0 \tag{4.32}$$

on the free surface (i.e., on $y = \eta(x)$).

(b) $\gamma \le 0$ and $u > c$

We again consider the function R in Eq. (4.30). Our next result shows that when γ is everywhere nonpositive, the pressure in the fluid domain is larger than the atmospheric pressure. In this case we however assume $u > c$. The relation between the monotonicity of Ψ_y along the free surface and the inequality $R \le 0$ was first recognized by Constantin and Strauss [16] (Proposition 3.4). The following theorem generalizes the result.

Theorem 4.4. Suppose $\gamma(\Psi) \le 0 \; \forall \Psi \in [-M, 0]$ and $u > c$. Then $R \le 0$ in $\bar{\Omega}$.

Proof. From Eq. (4.30) we have the following relations everywhere in $\bar{\Omega}$

$$\begin{aligned} R_x &= \Psi_y \Psi_{xy} - \Psi_x \Psi_{yy} \;, \\ R_y &= \Psi_x \Psi_{xy} - \Psi_y \Psi_{xx} + g \;, \\ \Delta R &= 2\Psi_{xy}^2 - 2\Psi_{xx}\Psi_{yy} \;. \end{aligned}$$

Also Eq.(4.30) leads to $R = 0$ everywhere on the free surface S. We claim that the maximum of R in $\bar{\Omega}$ must occur on S.

Since $R_y = g > 0$ everywhere on the flat surface B, maximum of R can not be attained anywhere on B.

Let us now assume that maximum of R is attained at some point A in the interior of the domain, i.e. in Ω. This implies

$$R_x(A) = 0, \;\; R_y(A) = 0, \;\; \Delta R(A) \le 0$$

resulting in

$$\Psi_y(A)\Psi_{xy}(A) = \Psi_x(A)\Psi_{yy}(A) \tag{4.33}$$

$$\Psi_x(A)\Psi_{xy}(A) < \Psi_y(A)\Psi_{xx}(A) \tag{4.34}$$

$$\Psi_{xy}^2(A) \le \Psi_{xx}(A)\Psi_{yy}(A)\ . \tag{4.35}$$

Since $u > c$, if follows that $\Psi_y(A) > 0$. Let us now consider two cases corresponding to $\Psi_{yy}(A) = 0$ and $\Psi_{yy}(A) \neq 0$.

If $\Psi_{yy}(A) = 0$, then Eq. (4.33) implies $\Psi_{xy}(A) = 0$. Subsequently from Eq. (4.34) this yields $\Psi_{xx}(A) > 0$ and hence $\Psi_{yy}(A) > 0$ (from Eq. (4.35)), leading to $\Delta\Psi(A) = \gamma(\Psi(A)) > 0$. This leads to a contradiction.

If $\Psi_{yy}(A) \neq 0$, then Eq. (4.33) and (4.34) give

$$\frac{\Psi_y(A)\Psi_{xy}^2(A)}{\Psi_{yy}(A)} < \Psi_y(A)\Psi_{xx}(A)\ . \tag{4.36}$$

Hence, Eqs. (4.35) and (4.36) yield $\Psi_{yy}(A) > 0$, and Eq. (4.35) gives $\Psi_{xx}(A) > 0$. Hence, we have $\Delta\Psi(A) = \gamma(\Psi(A)) > 0$ which again leads to a contradiction.

Thus, we conclude that the maximum of R over $\bar{\Omega}$ cannot be in Ω and must be attained on S, leading to the result that $R \le 0$ in $\bar{\Omega}$. □

Since $R = 0$ everywhere on the free surface and $R \le 0$ in $\bar{\Omega}$ we then deduce that

$$R_y \ge 0 \tag{4.37}$$

on the free surface S, leading to

$$P_y \le 0 \tag{4.38}$$

on the free surface S expressed by $y = \eta(x)$, which is the same result we obtained for $\gamma \ge 0$ and $u < c$.

4.4 Horizontal velocity profile along the surface

We now proceed further using the results of the theorems in the last subsection and examine the horizontal velocity profile along the free surface.

Differentiating P with respect to the x-variable along the free surface along $(x, \eta(x))$ and using the monotonicity of the wave profile on the top free surface of Ω_+ i.e. along S_+ results in

$$P_x(x, \eta(x)) = -\eta'(x)P_y(x, \eta(x)) \le 0 \tag{4.39}$$

for $x \in [0, L/2]$, since $P_y \le 0$ on the free surface, recalling Eq. (4.38).

From the first and sixth relation in (2.2) we can deduce

$$\begin{aligned} P_x(x, \eta(x)) &= [c - u(x, \eta(x))] \cdot [u_x(x, \eta(x)) + \eta'(x)u_y(x, \eta(x))] \\ &= [c - u(x, \eta(x))]\partial_x u(x, \eta(x)) \end{aligned} \tag{4.40}$$

From (4.39), we conclude that on S_+

$$\partial_x(u(x, \eta(x))) \le 0 \quad \text{for} \quad x \in [0, L/2] \tag{4.41}$$

and

$$\partial_x(u(x, \eta(x))) \ge 0 \quad \text{for} \quad x \in [0, L/2] \tag{4.42}$$

corresponding to $u < c$ and $u > c$ respectively.

Resulting from Theorems 4.3 and 4.4, and Eq. (4.41) and (4.42) we state the following Lemma.

Lemma 4.5. The horizontal fluid velocity u is a non-increasing or non-decreasing function of x along the surface S from the crest to the trough, depending on the condition, $(\gamma > 0, u < c)$ or $(\gamma < 0, u > c)$ respectively.

The result of Lemma 4.5 will be used in proving the main results in Section 5.

4.5 Maximal horizontal velocity for $\gamma \geq 0, \gamma' \leq 0$, $u < c$

We now present an alternate proof of the theorem on the location of the point of maximal horizontal velocity for the case $\gamma \geq 0$ and $\gamma' \leq 0$. The location of point of maximal horizontal velocity was proved by Constantin and Strauss [16] under a restrictive class of wave profiles and a less stronger result was subsequently proved by Vararuca [38] for a more general class of vorticity. We now provide a slightly different proof of the result by Varvaruca[38].

Theorem 4.6. Suppose $\gamma(\Psi) \geq 0$ and $\gamma' \leq 0,\ \forall \Psi \in [0, -M]$. If $u < c$ then crest must be the point of maximum horizontal velocity.

Proof. Consider the equation $\Delta\Psi = \gamma(\Psi)$. We further deduce

$$\Delta\Psi_y = \gamma'\Psi_y \ . \tag{4.43}$$

If $\Psi_y < 0$ and $\gamma' \leq 0$, then $\Delta\Psi_y \geq 0$. Hence, the maximum principle ensures that no maximum of Ψ_y can be attained at an interior point in Ω. Also, Corollary 3.2 in Constantin and Strauss [16], requiring the condition $\gamma \geq 0$, suggests that the maximum can not be attained on the horizontal bed either. Hence, the maximum has to occur on the surface S. Further, we use Theorem 2.3 by Vararuca [38] which is re-stated as follows for the sake of completeness.

Theorem 2.3.[[38]] Let $\eta : \mathbb{R} \to \mathbb{R}$ be such that there exists $N \in \mathbb{N}$ and points $x_0 < x_1 < \cdots < x_{2N} = x_0 + 2L$ with the property that $\eta'(x_j) = 0$ for all $j \in \{0, \cdots, 2N\}$, η is strictly increasing on $[x_{2j}, x_{2j+1}]$ for all $j \in \{0, \cdots, N-1\}$ and η is strictly decreasing on $[x_{2j-1}, x_{2j}]$ for all $j \in \{1, \cdots, N\}$. Suppose that $R \leq 0$ in $\bar{\Omega}$. Then the function $x \mapsto \psi_y(x, \eta(x))$ is increasing on $[x_{2j}, x_{2j+1}]$ for all $j \in \{0, \cdots, N-1\}$ and decreasing on $[x_{2j-1}, x_{2j}]$ for all $j \in \{1, \cdots, N\}$. Therefore, $\max_{\mathcal{S}} \psi_y$ is attained at the points of maximal height on $\mathcal{S}$.

Using this theorem, we note that on the surface the maximum of Ψ_y is attained at the point of maximum height on S (i.e. is a decreasing function from crest to trough). Thus, we conclude that crest is necessarily the point of maximum horizontal velocity. $\square$

We will consider the case $\gamma \geq 0$ and $\gamma' \geq 0$ in the next section based on Dubreil-Jacotin transformation and properties along stream function. Further, the case of $\gamma \leq 0$ with the condition $u > c$ will be dealt with in the next section.

5 Main results on properties of velocity field

We now proceed to prove the main results of the paper related to the properties of the velocity field including results along streamlines within the fluid domain. If we consider the first component of the flow field, i.e. $u(x, y)$, which is the horizontal velocity in the x-direction, then from the third and fourth relation in Eq. (2.2) we observe that

$$\partial_x^2 u + \partial_y^2 u = \gamma'(\Psi)\Psi_y = \gamma'(\Psi)(u - c) \quad \text{for} \quad -d \leqslant y \leqslant \eta(x) \ . \tag{5.44}$$

If $(x, y(x))$ is the parametric equation of some streamline, then by definition

$$\partial_x[\Psi(x, y(x))] = 0 \ . \tag{5.45}$$

Using Eq. (5.45) we note that on a streamline

$$\Psi_x + y'\Psi_y = 0 \tag{5.46}$$

which leads to

$$y' = -\frac{\Psi_x}{\Psi_y} = \frac{v}{u - c} = h_q \tag{5.47}$$

from Eq. (2.17). Hence, we have

$$\Psi_x + h_q \Psi_y = 0 \; . \tag{5.48}$$

We observe from Eq. (5.44) that

$$\partial_x^2 u_q + \partial_y^2 u_q = \{\gamma'(\Psi)(u-c)\}_q \; . \tag{5.49}$$

Further, we note that

$$\{\gamma'(\Psi)(u-c)\}_q = \gamma' u_q \tag{5.50}$$

since from Eqs. (5.45) and (5.48), along a streamline

$$\Psi_q(x, y(x)) = \Psi_x + h_q \Psi_y = 0 \; . \tag{5.51}$$

Hence, from Eq. (5.49) we can write

$$\partial_x^2 u_q + \partial_y^2 u_q = \gamma' u_q \; . \tag{5.52}$$

Using Eq. (4.20) in Eq. (5.52), we have

$$\left(\partial_q - \frac{h_q}{h_p}\partial_p\right)\left\{\left(\partial_q - \frac{h_q}{h_p}\partial_p\right) u_q\right\} + \left(\frac{1}{h_p}\partial_p\right)\left\{\left(\frac{1}{h_p}\partial_p\right) u_q\right\} = \gamma' u_q \; . \tag{5.53}$$

Eq. (5.53) leads to

$$(u_q)_{qq} - \frac{2h_q}{h_p}(u_q)_{pq} + \frac{(1+h_q^2)}{h_p^2}(u_q)_{pp} - \frac{(1+h_q^2)h_{pp} - 2h_p h_q h_{pq} + h_p^2 h_{qq}}{h_p^3}(u_q)_p = \gamma' u_q \; . \tag{5.54}$$

Using Eq. (4.21) in Eq. (5.54), and since $h_p \neq 0$ (i.e. $u \neq c$), we arrive at

$$h_p^2(u_q)_{qq} - 2h_p h_q (u_q)_{pq} + (1+h_q^2)(u_q)_{pp} - \gamma(\Psi)h_p^2(u_q)_p = \gamma' h_p^2 u_q \; , \quad p \in (0, M) \tag{5.55}$$

which is also a quasi-linear second order elliptic equation in u_q.

On using the definition of streamline (Eq.(5.47)) we also have

$$\partial_x[u(x, y(x))] = u_x + y' u_y = u_x + h_q \cdot u_y = u_q \tag{5.56}$$

from Eq.(4.20), on a streamline.

For proving a following lemma based on Eq. (5.56) we will use Hopf's maximum principle. While Hopf's principle is generally understood to be applicable to linear equation, it is also in fact useful in nonlinear theories, such as the one under consideration here (see Pucci and Serrin [32]).

Let $w \in C^2$ satisfy the differential inequality

$$Lw = \sum_{i,j} a_{ij} \frac{\partial^2 w}{\partial x_i \partial x_j} + \sum_i b_i \frac{\partial w}{\partial x_i} \geq 0 \tag{5.57}$$

in a domain Ω, where matrix a_{ij} is locally uniformly positive definite in Ω and the coefficients a_{ij}, b_i are locally bounded. The requirement of $w \in C^2$ is essential, although w could be only measurable (see Littman [30]) for the case of C^1 distributive solution).

Hopf observes (Section II of Hopf [24]) that one can allow the coefficients to depend on the solution w itself (see [32]) for discussion).

We state a theorem based on the conclusion of Hopf's formulation and two theorems presented in [32] which we will use in the following Lemma.

Theorem 5.1. (Theorem 2.1 and 2.2, [32]) Let w be a C^2 function satisfying the differential inequality

$$Lw + cw \geq 0 (\leq 0) \tag{5.58}$$

in a domain Ω, where the coefficients of L satisfy the previously mentioned conditions, and $c = c(x)$ is a nonpositive locally bounded function on Ω. If w takes a non-negative maximum (non-positive minimum) value M in Ω, then $w \equiv M$.

We now proceed to prove a lemma which together with the results proved in Section 4 will be used to prove the main results in the paper.

Lemma 5.2. Suppose $\gamma' \geq 0$. Then the horizontal fluid velocity u, even in x, is a strictly decreasing or a strictly increasing function of x along any streamline in $\bar{\Omega}_+$, if $u < c$ and $\gamma \geq 0$; or $u > c$ and $\gamma \leq 0$ respectively.

Proof. Considering the restriction of u_q to $\hat{\Omega}_+$ we have

$$u_q = u_x + \frac{v}{u-c} u_y \ . \tag{5.59}$$

From (5.59), we deduce that along the lateral sides of $\hat{\Omega}_+$ (images of crest and trough lines), we have

$$u_q = u_x = -v_y = 0, \quad \text{for} \quad q = 0 \tag{5.60}$$

and similarly

$$u_q = 0 \ , \quad \text{for} \quad q = cL/2 \tag{5.61}$$

as $v = v_y = 0$ along these sides. On the boundary B^+, $v = 0$, so

$$u_q = u_x \quad \text{if} \quad q \in (0, cL/2) \tag{5.62}$$

which leads to

$$\begin{aligned} u_q < 0 \quad \text{if} \quad u < c \\ u_q > 0 \quad \text{if} \quad u > c \end{aligned} \tag{5.63}$$

on using Eq. (4.27) and Eq.(4.28). On the top boundary, S^+, we have $p = 0$, so

$$\begin{aligned} u_q = \partial_x[u(x,\eta(x))] \leq 0 \ , \quad u < c \quad (\text{and } \gamma \geq 0 \quad \text{everywhere}) \\ u_q = \partial_x[u(x,\eta(x))] \geq 0 \ , \quad u > c \quad (\text{and } \gamma \leq 0 \quad \text{everywhere}) \end{aligned} \tag{5.64}$$

for $p = 0$, $q \in (0, cL/2)$, using Eq. (5.56), and Eq.(4.41) and Eq.(4.42).

Note that $\gamma^{'} \geq 0$ and so application of Hopf's maximum principle to u_q (Theorem 5.1) suggests that unless u_q is constant it cannot have either a non-negative maxima or a non-positive minima within the fluid domain. Hence from Eqs. (5.60)-(5.64) we conclude that $u_q < 0$ or $u_q > 0$ in the open rectangle $\hat{\Omega}_+$ depending upon whether $u < c$ or $u > c$ respectively. Thus, (5.56) ensures that u is a strictly decreasing or a strictly increasing function of x along any streamline in $\bar{\Omega}_+$ depending upon whether $u < c$ or $u > c$ respectively. Since u is even in x, the function u is a strictly increasing or a strictly decreasing function of x along any streamline in $\bar{\Omega}_-$ for $u < c$ or $u > c$ respectively. $\square$

For $u < c$, Ehrnström [23] proved a similar result for the waves in the neighbourhood of bifurcation point from the laminar flow (see [15] for the bifurcation results), and with the assumption $\eta^{'}$ and $\eta^{''}$ small enough. We do not need such restrictions here and the results hold generally.

We will use this result in Lemma 5.2 to prove the theorems on the location of maximum/minimum horizontal velocities, to follow. We now prove two other lemma which follows from our previous result in this section, but will not be used for proving the results on the maximum/minimum horizontal velocities.

Lemma 5.3. Along any fixed vertical line in the moving frame the absolute value of the slope of a streamline decreases or inceases with depth corresponding to $u < c$ or $u > c$ respectively.

Proof. The slope of a streamline $y = y(x)$ is given by $y' = \frac{v}{u-c}$. The derivative of the slope is

$$\partial_y \frac{v}{u-c} = \frac{u_q}{c-u} \quad \text{in} \quad \Omega_+ \tag{5.65}$$

using Eq. (4.20) . Hence, Lemma 5.2 proves Lemma 5.3. □

We focus our attention to the vertical velocity v, within the fluid domain. From the third and fourth relation in Eq. (2.2) we observe that

$$\partial_x^2 v + \partial_y^2 v = -\gamma'(\Psi)\Psi_x = \gamma'(\Psi)v \quad \text{for} \quad -d \leqslant y \leqslant \eta(x) \tag{5.66}$$

which further leads to

$$\partial_x^2 v_p + \partial_y^2 v_p - \gamma'(\Psi)v_p = -\gamma'' v \tag{5.67}$$

The following lemma provides some information on the variation of v along the depth of the fluid domain.

Lemma 5.4. Suppose $\gamma' \geq 0$ and $\gamma'' \geq 0$. Also, assume $u < c$. Then the vertical fluid velocity, v along any fixed vertical line in the moving frame is a strictly decreasing or a strictly increasing function of depth within the fluid domain $\hat{\Omega}_+$ or $\hat{\Omega}_-$ respectively .

Proof. If $\gamma'' \geq 0$, on using the result $v > 0$ in $\hat{\Omega}_+$ from Theorem 4.1 for $u < c$, we arrive at the following differential inequality from Eq. (5.67)

$$\partial_x^2 v_p + \partial_y^2 v_p - \gamma'(\Psi)v_p \leq 0 \ . \tag{5.68}$$

Along the lateral sides of $\hat{\Omega}_+$ (images of crest and trough lines), we have

$$v_y = 0 = v_p, \quad \text{for} \quad q = 0 \tag{5.69}$$

on using Eq. (4.19). Similarly,

$$v_p = 0 \quad \text{for} \quad q = cL/2 \tag{5.70}$$

as $v_y = 0$ along these sides. On the flat bed, i.e. on the boundary B^+, we have

$$v_y = -u_x = -u_q > 0 \quad \text{if} \quad u < c \tag{5.71}$$

from the result of Lemma 4.2, leading to

$$v_p = \frac{v_y}{(c-u)} > 0 \quad \text{if} \quad u < c \tag{5.72}$$

on using Eq. (4.19). On the top boundary, S^+ for $u < c$, we have

$$v_p = \frac{1}{(c - u(x,\eta(x)))}\partial_y[v(x,\eta(x))] = \frac{1}{(u(x,\eta(x)) - c)}\partial_x[u(x,\eta(x))] \geq 0 \ , \tag{5.73}$$

for $p = 0$, $q \in (0, cL/2)$, using Eqs. (2.2), (4.19) and the results from Lemma 4.5 (Eq. (4.41)).

Note that $\gamma' \geq 0$ and so application of Hopf's maximum principle to v_p in Eq. (5.68) (Theorem 5.1) suggest that v_p cannot have a non-positive minima within the fluid domain. Hence from Eqs. (5.69)-(5.73) we conclude that $v_p > 0$ in the open rectangle $\hat{\Omega}_+$ for $u < c$. Hence, Eq. (4.19) ensures that $v_y > 0$, i.e. v is a strictly increasing function of y or a strictly decreasing function of depth along any vertical line in $\bar{\Omega}_+$. Since v is odd in x, the function v is a strictly decreasing function of y in $\bar{\Omega}_-$ for $u < c$. □

We now prove the following proposition.

Proposition 5.1. Consider the restriction of the horizontal fluid velocity u along the vertical line below the crest.

(i) If $\gamma \geq 0, u < c$, then the velocity u is strictly monotone on the crest line AB with the maximum at the crest A.

(ii) If $\gamma \leq 0, u > c$, then the velocity u is strictly monotone on the crest line AB with the minimum at the crest A.

Proof. Consider Figure 3.

(i) Along AB we have $(u-c)_y = \Psi_{yy} = -\Psi_{xx} + \gamma > -\Psi_{xx} = v_x > 0$ since $v > 0$ in Ω_+ and v is antisymmetric about x-axis (from Theorem 4.1) (also see the result in Proposition 3.3 (i) in [16]).

(ii) Again along AB we have $u_y = v_x + \gamma < 0$ since $v < 0$ in Ω_+ for $u > c$, and v is antisymmetric about $x = 0$ (see Theorem 4.1).

□

We now state and prove two theorems on the locations of maximum/minimum horizontal velocities in the fluid domain.

Theorem 5.5. Let $\eta : \mathbb{R} \to \mathbb{R}, c > 0$, $u \in C^2(\bar{\Omega})$, $v \in C^2(\bar{\Omega})$ and $\gamma \in C^1([0, -M])$. Suppose $\gamma \geq 0$, $\gamma' \geq 0, \forall\ \Psi \in [0, -M]$ and $u < c$ throughout the fluid domain. Then, in the fluid domain $\bar{\Omega}$, (i) the point of maximum horizontal velocity $u_{\max}$ is the crest A; (ii) the point C on the flat bed directly below the trough is a point of local minimum horizontal velocity $u_{\min(\text{loc})}$; (iii) the point of local minimum horizontal velocity C becomes the point of global minimum horizontal velocity, $u_{\min(\text{global})}$ if γ is sufficiently large (strong vorticity), and (iv) the trough D becomes a point of local minimum horizontal velocity $u_{\min(\text{loc})}$, if γ is sufficiently small (weak vorticity).

Proof. Consider Figure 3(a).

(i) From Lemma 5.2 we infer that maximum horizontal velocity has to be on the crest line. Further, proposition 5.1 states that for $\gamma \geq 0$, u is monotonic along the crest line with a maximum at the crest. Hence, crest must be the point of maximum u.

(ii) Again from Lemma 5.2 we conclude that the minimum value of u must be on the trough line, as u is strictly decreasing along any streamline in $\bar{\Omega}_+$ for $u < c$. This is applicable to flat bed which is further confirmed from Lemma 4.2, that the velocity u is strictly decreasing along the flat bed. On the other hand at the point C, we observe $v_x = 0$ and hence $u_y = \gamma + v_x = \gamma \geq 0$. Thus, we conclude that C is a point of local minimum for u.

Remark: Note however, we still have no inference on the location of global minimum for u. We now try to deduce the condition which yields further information on the location of global minimum u.

(iii) Again observe from $u_y = \gamma + v_x$ that $\gamma \geq 0$ and $v_x < 0$ along the trough line (from Theorem 4.1, $v > 0$ in Ω_+, $v = 0$ along $x = L/2$ and v is antisymmetric about $x = L/2$, leading to $v_x < 0$ on $(L/2, y), y \in (-d, \eta(L/2))$). Thus, if γ is sufficiently large (such that $|v_x|$ is always smaller than γ on $(L/2, y), y \in (-d, \eta(L/2))$), then the fourth relation in Eq. (2.2) yields $u_y > 0$ on the trough line leading to a minimum value of u at C on the bed directly below the trough. Using the result from Lemma 4.2, point C must be the point of global minimum horizontal velocity $u_{\min(\text{global})}$.

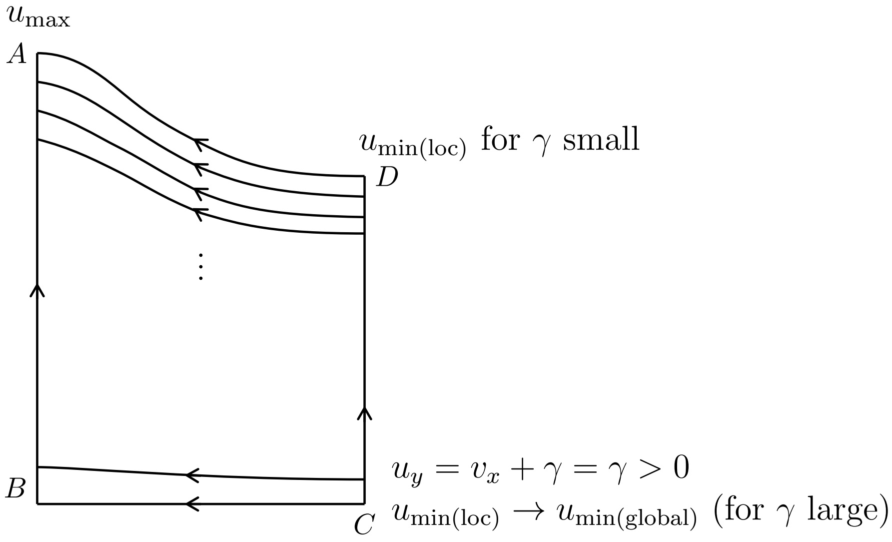

(a)

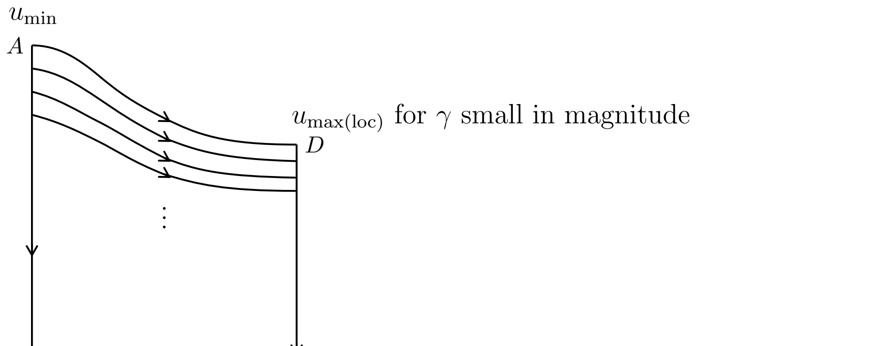

(b)

Figure 3: Velocity profile showing increasing path (a) $\gamma > 0$, $u < c$ and (b) $\gamma < 0$, $u > c$.

(iv) We again use the relation $u_y = \gamma + v_x$ on the trough point D which leads to the condition $u_y < 0$ if $\gamma = 0$. Hence, if γ is sufficiently small, it would lead to the same condition. Further, Lemma 5.2 states that u is strictly decreasing along the free surface. Hence, D is a point of local minimum horizontal velocity, $u_{\min(\text{loc})}$.

□

Theorem 5.6. Let $\eta : \mathbb{R} \to \mathbb{R}, c > 0, u \in C^2(\bar{\Omega}), v \in C^2(\bar{\Omega})$ and $\gamma \in C^1([-M, 0])$. Suppose $\gamma \leq 0$, $\gamma' \geq 0, \forall\ \Psi \in [0, -M]$ and $u > c$. Then, in the fluid domain $\bar{\Omega}$ (i) the point of minimum horizontal velocity $u_{\min}$ is the crest A, (ii) the point C on the flat bed directly below the trough is a point of local maximum horizontal velocity $u_{\max(\text{loc})}$, (iii) the point of local maximum horizontal velocity C becomes the point of global maximum horizontal velocity, if γ is sufficiently large in magnitude (strong vorticity), and (iv) the trough D becomes a point of local maximum horizontal velocity $u_{\max(\text{loc})}$ if γ is sufficiently small in magnitude(weak vorticity).

Proof. Consider Figure 3(b).
Following similar type of arguments and proceeding along the line of proof of Theorem 5.5, we can prove this theorem. □

Remark: From the results of Lemma 4.5 and Theorem 5.5 we can state the following theorem.

Theorem 5.7. Suppose $\gamma(\Psi) \geq 0$ and is monotonic. Then the maximum horizontal velocity is attained at the crest.

Proof. If γ is monotonic then either $\gamma'(\Psi) \geq 0\ \forall\ \ \Psi[0, -M]$ or $\gamma'(\Psi) \leq 0\ \forall\ \ \Psi[0, -M]$. The proof is straightforward as combining Lemma 4.5 and Theorem 5.6 we arrive at the result. □

6 Observations

1. For the case $\gamma \geq 0$, Constantin and Strauss [15] proved that for a certain class of waves (satisfying an inequality in γ representing small vorticity), the point of maximum velocity must be the crest.

2. Varvaruca [38] generalized the results mentioned in the previous observation for a larger class of vortcity but with a slightly less stronger result requiring $\gamma' \leq 0$ everywhere.

3. The final theorem stated and proved in this paper, considering Thereom 5.5 and the result in [38] together, generalizes the previous results by removing the restriction in [15] on the class of vorticity and the requirement on γ' in [38]. Hence, the final result in Theorem 5.7 in this paper is stronger than each of the individual results proved in Theorem 4.1 in [15] or Theorem 2.4 in [38] or Theorem 5.5 in this paper.

4. This paper also provides some information on the behaviour of fluid velocities (both horizontal and vertical) within the fluid domain (Lemma 5.2 and 5.4) and on streamlines (Lemma 5.3) under certain conditions.

7 Acknowledgements

The author would like to thank the reviewer for the helpful suggestions.

References

[1] C.J. Amick, J. F. Toland. On periodic water-waves and their convergence to solitary waves in the long-wave limit. *Phil. Trans. Roy. Soc. London A, Math. Phys. Eng. Sci.*, 303(1481):633–669, 1981.

[2] C. J. Amick, L.E. Fraenkel, J.F. Toland. On the stokes conjecture for the wave of extreme form. *Acta Mathematica*, 148(1):193–214, 1982.

[3] B. Basu. Irrotational two-dimensional free-surface steady water flows over a flat bed with underlying currents. *Nonlinear Anal. TMA*, 147:110–124, 2016.

[4] D. Clamond. Note on the velocity and related fields of steady irrotational two-dimensional surface gravity waves. *Phil. Trans. Roy. Soc. London A, Math. Phys. Eng. Sci.*, 370(1964):1572–1586, 2012.

[5] A. Constantin. The trajectories of particles in stokes waves. *Invent. Math.*, 166(3):523–535, 2006.

[6] A. Constantin. *Nonlinear water waves with applications to wave-current interactions and tsunamis*, CBMS-NSF Conf. Ser. in Appl. Math. vol. 81. SIAM, Philadelphia, 2011.

[7] A. Constantin. Mean velocities in a stokes wave. *Arch. Ration. Mech. Anal.*, 207(3):907–917, 2013.

[8] A. Constantin. *Exact travelling periodic water waves in two-dimensional irrotational flows in "Nonlinear water waves, Cetaro, Italy 2013", pp 1-82.* Editor Adrian Constantin, Springer Lecture Notes in Mathematics, vol.2158, 2016.

[9] A. Constantin, M. Ehrnström, E. Wahlén. Symmetry of steady periodic gravity water waves with vorticity. *Duke Math. J.*, 140(3):591–603, 2007.

[10] A. Constantin, J. Escher. Symmetry of steady deep-water waves with vorticity. *Eur. J. Appl. Math.*, 15(6):755–768, 2004.

[11] A. Constantin, J. Escher. Symmetry of steady periodic surface water waves with vorticity. *J. Fluid Mech.*, 498:171–181, 2004.

[12] A. Constantin, J. Escher. Particle trajectories in solitary water waves. *Bull. Amer. Math. Soc.*, 44(3):423–431, 2007.

[13] A. Constantin, J. Escher. Analyticity of periodic traveling free surface water waves with vorticity. *Annals of Mathematics*, 173(1):559–568, 2011.

[14] A. Constantin, D. Sattinger, W. Strauss. Variational formulations for steady water waves with vorticity. *J. Fluid Mech.*, 548:151–163, 2006.

[15] A. Constantin, W. Strauss. Exact steady periodic water waves with vorticity. *Comm. Pure Appl. Math.*, 57(4):481–527, 2004.

[16] A. Constantin, W. Strauss. Rotational steady water waves near stagnation. *Phil. Trans. Roy. Soc. London A, Math. Phys. Eng. Sci.*, 365(1858):2227–2239, 2007.

[17] A. Constantin, W. Strauss. Stability properties of steady water waves with vorticity. *Comm. Pure Appl. Math.*, 60(6):911–950, 2007.

[18] A. Constantin, W. Strauss. Pressure beneath a stokes wave. *Comm. Pure Appl. Math.*, 63(4):533–557, 2010.

[19] A. Constantin, W. Strauss. Periodic traveling gravity water waves with discontinuous vorticity. *Arch. Ration. Mech. Anal.*, 202(1):133–175, 2011.

[20] A. Constantin, W. Strauss, E. Vărvărucă. Global bifurcation of steady gravity water waves with critical layers. *Acta Mathematica*, 217(2):195–262, 2016.

[21] A. Constantin, E. Varvaruca. Steady periodic water waves with constant vorticity: regularity and local bifurcation. *Arch. Ration. Mech. Anal.*, 199(1):33–67, 2011.

[22] A.F. Teles da Silva, D.H. Peregrine. Steep, steady surface waves on water of finite depth with constant vorticity. *J. Fluid Mech.*, 195:281–302, 1988.

[23] M. Ehrnström. On the streamlines and particle paths of gravitational water waves. *Nonlinearity*, 21(5):1141, 2008.

[24] E. Hopf. *Elementare Bemerkungen über die Lösungen partieller Differentialgleichngen zweiter Ordnung vom elliptischen Typus.* Sitzungsber. Preuss. Akad. Wiss. , Berlin, pp 147-152, 1927.

[25] V. M. Hur. Global bifurcation theory of deep-water waves with vorticity. *SIAM J. Math. Anal.*, 37(5):1482–1521, 2006.

[26] V. M. Hur. Exact solitary water waves with vorticity. *Arch. Ration. Mech. Anal.*, 188(2):213–244, 2008.

[27] G. Keady, J. Norbury. On the existence theory for irrotational water waves. *Math. Proc. Cambridge Phil. Soc.*, 83:137–157, 1978.

[28] J. Ko, W. Strauss. Large-amplitude steady rotational water waves. *Eur. J. Mech.-B/Fluids*, 27(2):96–109, 2008.

[29] M.A. Krasnoselskii. *Positive solutions of operator equations*, Noordhoff, Groningen, 1964.

[30] W. Littman. A strong maximum principle for weakly l-subharmonic functions. *J. Math. Mech.*, 8(5):761–770, 1959.

[31] A.I. Nekrasov. On steady waves. *Izv. Ivanovo-Voznesensk*, 3:52–65, 1921.

[32] P. Pucci, J. Serrin. The strong maximum principle revisited. *J. Differential Equations*, 196(1):1–66, 2004.

[33] G.G. Stokes. On the theory of oscillating waves. *Trans. Camb. Phil. Soc.* 8: 441-445, 1847.

[34] J. F. Toland. Stokes waves. *Topol. Methods Nonlinear Anal.*, 7(1):1–48, 1996.

[35] M. Umeyama. Eulerian–Lagrangian analysis for particle velocities and trajectories in a pure wave motion using particle image velocimetry. *Phil. Trans. Roy. Soc. London A, Math. Phys. Eng. Sci.*, 370(1964):1687–1702, 2012.

[36] J.-M. Vanden-Broeck. Some new gravity waves in water of finite depth. *Phys. Fluids*, 26(9):2385–2387, 1983.

[37] E. Varvaruca. Singularities of bernoulli free boundaries. *Comm. Partial Differential Equations*, 31(10):1451–1477, 2006.

[38] E. Varvaruca. On some properties of traveling water waves with vorticity. *SIAM J. Math. Anal.*, 39(5):1686–1692, 2008.

[39] E. Varvaruca. On the existence of extreme waves and the Stokes conjecture with vorticity. *J. Differential Equations*, 246(10):4043–4076, 2009.

[40] E. Varvaruca, G. S. Weiss. The Stokes conjecture for waves with vorticity. In *Ann. Inst. H. Poincaré Anal. Non Linéaire* , 29: 861–885, 2012.

Estimation of wave heights from pressure data at the bed in the presence of uniform underlying currents

Biswajit Basu

Nonlinear Anal. 156, 82 -89, 2017

Abstract

We provide some bounds on the estimated wave heights (valid for all ranges of amplitudes) from pressure measurements at the flat bed for steady water waves flowing over underlying uniform currents. The derived upper bound for the wave height for the case when the speed of the underlying current is greater than the wave speed is different from the one when there is no current. The results in this paper also confirm that waves of nontrivial amplitudes cannot exist where the speed of the underlying current is same as the wave speed, a result that was previously proved by Basu [1] in a different context following another approach.

1 Introduction

Wave heights play an important role in estimating forces on maritime and offshore structures, estimating power generated by wave energy devices and designing possible means of flood control at costal regions. Observations of sea waves can be either done remotely by satellite measurements or by in situ measurements. Remote-sensing techniques being an indirect way of measurement require ground-truth verification. Recovery of wave heights from pressure data at the bed is a practical means to estimate wave heights from in-situ measurements which can be also used for such verifications. Use of pressure sensors among other types of sensors are widespread in practice due to their low costs, ease of installation and relatively less liability in the event of damage [18]. Pressure sensors are usually deployed underwater at fixed loactions on the rigid bed. These sensors provide accurate measurement of the pressure at the bed, but recovery of wave heights from these pressure measurements requires some additional considerations to unfold the pressure-wave height relationship.

Researchers in the past have developed expressions for recovering the wave height from the pressure at the bed, e.g. [20] used the hydrostatic formula for tsunami detection and [16] developed explicit expressions for pressure and surface waves in the setting of linear wave theory. However, these studies either did not consider the wave effects or are valid for waves of small amplitude. In fact, linear theory may overestimate wave heights by over 10% even for waves of moderate amplitude when compared with observed data [22]. Since most waves relevant in ocean engineering do not fall into the category of small amplitude theory, it is necessary to consider the governing equations without approximations. Researchers such as [20], [15], [7], [4], [3], [11] and [12] have pursued further investigations in this direction. Considering the presence of vorticity, Henry [17] showed that pressure function on the flat bed prescribes a unique surface profile for the resulting solitary waves. The conclusion derived from these investigations was that an exact recovery of the wave profile from the pressure at the flat bed is indeed possible. However, in this context the only explicit results for the recovery of surface profile is due to [7] for solitary waves while others such as [4] and [3] require either the solution of either a non-linear differential equation or an implicit functional equation for periodic traveling waves. Constantin [10] recently developed another approach to provide simple, explicit but accurate estimates of wave heights for the fully nonlinear large amplitude 2D traveling gravity waves which differed from some of the previously proposed approaches and results.

Inspite of several results available on the wave height recovery problem, simple and accurate expressions for the recovery of wave heights from the pressure data at the bed for the case of large amplitude surface waves with underlying currents, are not available in the literature currently, which is the contribution of this paper. Recently, Basu [1] reported some new results on flow fields and pressure distribution for the case of 2D wave-uniform current interactions using maximum principles for elliptic partial differential equations. This paper further builds upon the work by Basu [1] in exploiting some of those results and the extends the work by Constantin [10], by developing bounds on wave heights for 2D periodic travelling waves from pressure data at the bed with wave-uniform current interaction, which are equally valid for all ranges of amplitude (small and large).

2 Basic equations

We consider a 2D flow represented in the Cartesian co-ordinate (X,Y) with the direction of wave propagation along the X-axis and the Y-axis pointing vertically upwards. The depth of water at rest is denoted by $d > 0$ which leads to the equation of the flat bed as $Y = -d$. The free surface is given by $Y = \eta(X - ct)$, where $c > 0$ is the speed of propagation of the periodic travelling waves. The surface waves are assumed to propagate over a uniform underlying current of speed k. The flow is irrotational and it may be noted that the uniform underlying current does not introduce any vorticity to the flow.

We investigate periodic travelling waves of wave lenght L, with profile η moving at constant speed c. The wave crest is assumed to be located at $X = 0$. Also, let the flow field (u,v) have a space-time dependence of the form $(X-ct)$, i.e. $u := u(X-ct, Y)$ $v := v(X - ct, Y)$. To analyze this problem let us introduce a co-ordinate transformation to a moving frame $x = X - ct, y = Y$. Flows without stagnation points are considered, so that, by regularity results discussed in [13], all functions are real analytic. The only waves that are thus excluded are the so-called Stokes waves of greatest height (see the discussions in [21, 8, 19]).

The governing equations for the water waves under the inviscid, incompressible conditions are given by the Euler's equation

$$\begin{aligned} (u-c)u_x + vu_y &= -\frac{1}{\rho}P_x \quad \text{for} \quad -d \le y \le \eta(x) \\ (u-c)v_x + vv_y &= -\frac{1}{\rho}P_y - g \quad \text{for} \quad -d \le y \le \eta(x) \end{aligned} \tag{2.1}$$

where $P(x, y)$ is the hydrodynamic pressure, ρ is the density and g is the acceleration due to gravity.

The mass conservation equation for a homogeneous, incompressible fluid is

$$u_x + v_y = 0 \quad \text{for} \quad -d \le y \le \eta(x) \tag{2.2}$$

and irrotationality imples

$$u_y = v_x \quad \text{for} \quad -d \le y \le \eta(x)\ . \tag{2.3}$$

The kinematic boundary conditions at the flat bed and at the free surface are respectively given by

$$v = 0 \quad \text{on} \quad y = -d \tag{2.4}$$

and

$$v = (u-c)\eta(x) \quad \text{on} \quad y = \eta(x) \ . \tag{2.5}$$

The dynamic boundary condition of constant atmospheric pressure at the surface is

$$P = P_{atm} \quad \text{on} \quad y = \eta(x) \ . \tag{2.6}$$

Mass flux (relative to the uniform flow speed c) is a constant and is expressed as

$$M = \rho \int_{-d}^{\eta(x)} [u(x,y) - c] dy \ . \tag{2.7}$$

Conservation of energy leads to Bernoulli's law which states that

$$\frac{(u-c)^2 + v^2}{2} + g(y+d) + \frac{1}{\rho} P = Q \tag{2.8}$$

where Q is a constant throughout the fluid domain.

Let us define stream functions

$$\psi_x = -v, \quad \psi_y = u - c$$

and set (see [6], [1])

$$\psi(x,-d) = -\frac{M}{\rho} \quad \text{and} \quad \psi(x,\eta(x)) = 0 \quad \forall \quad x \in \mathbb{R} \ .$$

Equivalent form of governing equations (Eq. (2.1)) can be expressed in terms of stream functions

$$\begin{aligned}
&\psi_{xx} + \psi_{yy} = 0 \qquad \text{for} \qquad -d \le y \le \eta(x) \ , \\
&\psi = 0 \quad \text{on} \quad y = \eta(x) \ , \\
&\psi = -\frac{M}{\rho} \quad \text{on} \ \ y = -d \ , \\
&\psi_x^2 + \psi_y^2 + 2g(y+d) = 2Q - \frac{2}{\rho} P_{atm} \quad \text{on} \quad y = \eta(x) \ .
\end{aligned} \tag{2.9}$$

The expression for uniform underlying current is

$$k = \frac{1}{L} \int_{\frac{-L}{2}}^{\frac{L}{2}} u(x,-d) dx = \frac{1}{L} \int_{\frac{-L}{2}}^{\frac{L}{2}} u(x,y_0) dx \quad , \quad -d \le y_0 \le \eta(x) \tag{2.10}$$

which can be written as [1]

$$k = c + \frac{1}{L} \int_{\frac{-L}{2}}^{\frac{L}{2}} \psi_y(x,-d) dx \ . \tag{2.11}$$

The expression in Eq. (2.11) may be compared with the two definitions of the Stokes wave speed (see the discussion in [9]). In the absence of current (i.e. $k = 0$), c is equal to the mean of $-\psi_y$ along the flat bed, so that, the wave speed can be recovered from the wave pattern in the reference frame in which the wave is at rest (this is Stokes first definition of the wave speed (refer to [9])). Three cases may arise consequently from Eq. (2.11) corresponding to $k > c$, $k = c$ and $k < c$, strength (average speed) of the current greater than, equal to and less than the wave speed respectively, as shown and discussed in [1]. In the following sections these three cases will be considered separately as they lead to different nature of flow fields as has been shown by Basu [1].

3 Case I: $k > c$

We first consider the case where the speed of the current is great than the wave velocity, i.e. $k > c$. This case results in flow fields (see [1] for details) different from what has been known previously about flow fields when there is no underlying current (e.g., see [5, 14, 23, 2]). The results are summarized as follows in the present paper for completeness .

Let $\bar{c} = k - c > 0$, leading to

$$\bar{c} = \frac{1}{L} \int_{\frac{-L}{2}}^{\frac{L}{2}} \psi_y(x, -d) dx > 0$$

and from Basu [1]

$$u > c \quad \text{and} \quad M > 0 \tag{3.12}$$

throughout the fluid domain.

Further, use of properties of harmonic functions and maximum principles results in (see [1])

$$\begin{aligned} u_y(0, y) < 0 \quad &\text{for} \quad -d < y < \eta(0) \ , \\ u_y(\frac{L}{2}, y) > 0 \quad &\text{for} \quad -d < y < \eta(\frac{L}{2}) \ , \\ u_x(x, -d) > 0 \quad &\text{for} \quad 0 < x < \frac{L}{2} \ . \end{aligned} \tag{3.13}$$

3.1 Lower bounds for wave height

Evaluating Bernoulli's law (Eq.2.8) at the wave crest ($x = 0$), at the wave trough ($x = \frac{L}{2}$) and on the flat bed at $x = 0$ and $x = \frac{L}{2}$, respectively, we have

$$\begin{aligned} \frac{(u_{min} - c)^2}{2} + g(\eta(0) + d) + \frac{1}{\rho} P_{atm} &= Q \ , \\ \frac{(u_{max} - c)^2}{2} + g(\eta(\frac{L}{2}) + d) + \frac{1}{\rho} P_{atm} &= Q \ , \\ \frac{(u(0, -d) - c)^2}{2} + \frac{1}{\rho} P(0, -d) &= Q \ , \\ \frac{(u(\frac{L}{2}, -d) - c)^2}{2} + \frac{1}{\rho} P(\frac{L}{2}, -d) &= Q \ , \end{aligned} \tag{3.14}$$

where $u_{min} = u(0, \eta(0))$ and $u_{max} = u(L/2, \eta(L/2))$ are the minimum and maximum fluid velocites at $(0, \eta(0))$ and $(L/2, \eta(L/2))$ respectively. The first and third relations in Eq. (3.14) lead to

$$\eta(0) + d = \frac{P(0, -d) - P_{atm}}{\rho g} + \frac{(u(0, -d) - c)^2 - (u_{min} - c)^2}{2} > \frac{P(0, -d) - P_{atm}}{\rho g} \tag{3.15}$$

and the second and fourth relations in Eq.(3.14) lead to

$$\eta(\frac{L}{2}) + d = \frac{P(\frac{L}{2}, -d) - P_{atm}}{\rho g} + \frac{(u(\frac{L}{2}, -d) - c)^2 - (u_{max} - c)^2}{2} < \frac{P(\frac{L}{2}, -d) - P_{atm}}{\rho g} \tag{3.16}$$

on using Eqs. (3.12) and (3.13).

From Eqs. (3.15) and (3.16), the lower bound for the estimate of wave height $H = \eta(0) - \eta(L/2)$ is obtained as

$$H = \eta(0) - \eta(\frac{L}{2}) > \frac{P(0,-d) - P(\frac{L}{2},-d)}{\rho g} \ . \tag{3.17}$$

It is interesting to point out that [10] also arrived at the same lower bound for the case of surface waves propagating without any underlying currents. It may be noted that the right hand side of the inequality in Eq.(3.15) exceeds d while the right hand side of the inequality in Eq.(3.16) is less than d. This is because of the fact that fluid pressure is maximal at $(0,-d)$, while $P(L/2,-d)$ is the minimum value of the pressure along the flat bed with the average pressure on the flat bed equal to $P_{atm} + \rho g d$ (see [14] for detail discussion) and this nature of pressure remains unchanged in the presence of uniform currents [1].

It is also worth noting that estimates given by Eqs.(3.15) and (3.16) show that hydrostatic formula always underestimates the wave elevation while overestimating the wave trough level, as was also concluded by Constantin [11] for the case without any underlying currents.

3.2 Upper bounds for wave height

To obtain the upper bounds on the wave heights it is convenient to formulate the problem and carry out the derivations in a transformed domain. Transforming by means of conformal change of variables (since the problem is irrotational)

$$q = -\phi(x,y), \quad p = -\psi(x,y) \ ,$$

the free boundary problem given by Eq. (2.9) has an equivalent boundary value problem

$$\begin{aligned} \Delta_{q,p} h = 0 \quad \text{for} \quad \frac{M}{\rho} > p > 0 \ , \\ h = 0 \quad \text{on} \quad p = \frac{M}{\rho} \ , \\ 2(Q - \frac{1}{\rho} P_{atm} - gh)(h_q^2 + h_p^2) = 1 \quad \text{on} \quad p = 0 \end{aligned} \tag{3.18}$$

for the function

$$h(q,p) = y + d \tag{3.19}$$

(see [14], [10]).

Let us also define $P_*(q,p) = P(x,y), \quad u_*(q,p) = u(x,y) \quad .$

Since $q = 0$ corresponds to $x = 0$, so if we define

$$\alpha = \frac{P_*(0,\frac{M}{\rho}) - P_{atm}}{\frac{M}{\rho}} = \frac{P(0,-d) - P_{atm}}{\frac{M}{\rho}} > 0 \tag{3.20}$$

then Eqs.(3.12),(3.13) and (3.18) lead to

$$
\begin{aligned}
P_*(q, M/\rho) =& \rho Q - \frac{\rho(u_*(q, M/\rho) - c)^2}{2} \\
\leq& \rho Q - \frac{\rho(u_*(0, M/\rho) - c)^2}{2} \\
=& P_*(0, M/\rho) \\
=& P_{atm} + (M/\rho)\alpha, \quad \forall q \in [0, cL/2] \ .
\end{aligned} \tag{3.21}
$$

Since from Eq. (2.1) and Eq.(3.19) we can deduce

$$
\frac{1}{\rho}\Delta(q,p)P_* = -2(u_{*q}^2 + u_{*p}^2), \qquad M/\rho > p > 0
$$

the function

$$
f(q,p) = \frac{P_*(q,p) - \alpha p}{\rho} \tag{3.22}
$$

is superharmonic in the strip $M/\rho > p > 0$. It may be noted that f equals P_{atm}/ρ on the upper surface $p = 0$, and from Eq. (3.21) it is observed that f does not attain higher values than P_{atm}/ρ on the lower boundary $p = M/\rho$. Hence, from the strong maximum principle we infer that the maximum of f is attained on the upper boundary $p = 0$ and Hopf's principle ensures $f_p(q, 0) > 0 \ \forall \ q \in R$. Hence from Eqs. (2.1), (2.2), (2.5) and (3.19), we have

$$
f_p(q,0) = \frac{1}{\rho}P_{*p}(q,0) - \frac{\alpha}{\rho} > 0
$$

leading to

$$
-\frac{\alpha}{\rho} > \frac{2(u-c)^2 u_x \eta_x + (u-c)^2 u_y(\eta_x^2 - 1) - g(u-c)}{(u-c)^2(1+\eta_x^2)} \tag{3.23}
$$

on $y = \eta(x)$.

On differentiating the fourth relation in Eq. (2.9) along the free surface w.r.t x-variable we also get

$$
0 = (u-c)u_x + (u-c)u_y\eta_x + vv_x + vv_y\eta_x + g\eta_x \quad \text{on} \quad y = \eta(x) \ .
$$

Further, from the last equation and Eqs. (2.2), (2.3) and (2.5) we obtain

$$
(u-c)u_x(1-\eta_x^2) + 2(u-c)u_y\eta_x + g\eta_x = 0 \quad \text{on} \quad y = \eta(x) \ . \tag{3.24}
$$

Using Eqs. (3.12), (3.23), (3.24) and the fact that $\eta_x(x) < 0$ for $x \in (0, L/2)$, we get

$$
-\frac{\alpha}{\rho}\eta_x < u_x(x,\eta(x)) + u_y(x,\eta(x))\eta_x(x), \quad 0 < x < L/2
$$

which on integration on $[0, L/2]$ leads to

$$
\frac{\alpha}{\rho}\left[\eta(L/2) - \eta(0)\right] > u(0,\eta(0)) - u(L/2,\eta(L/2)) \ . \tag{3.25}
$$

Evaluating Eq. (2.8) at the wave crest and the wave trough, and from Eq. (3.25) we can deduce

$$
\frac{\alpha}{2\rho g}\left[\{u(0,\eta(0)) - c\}^2 - \{u(L/2,\eta(L/2)) - c\}^2\right] > u(0,\eta(0)) - u(L/2,\eta(L/2)) \tag{3.26}
$$

which further yields

$$u(0,\eta(0)) + u(L/2,\eta(L/2)) - 2c < \frac{2\rho g}{\alpha} \tag{3.27}$$

since from Eq. (3.13) we have $u(L/2,\eta(L/2)) > u(0,\eta(0)) > c$. Further, since $\eta(L/2) \leq 0$, we have

$$ML = \int_{-L/2}^{L/2} M dx = \rho \int_{-L/2}^{L/2} \int_{-d}^{\eta(L/2)} (u-c) dx dy \leq \rho \int_{-L/2}^{L/2} \int_{-d}^{0} (u-c) dx dy = \rho(k-c)Ld\,.$$

Thus,

$$M \leq \rho(k-c)d\,. \tag{3.28}$$

Combining Eqs. (3.20), (3.27) and (3.28) we obtain

$$u(0,\eta(0)) + u(L/2,\eta(L/2)) - 2c \leq \frac{2\rho g(k-c)d}{P(0,-d) - P_{atm}}\,. \tag{3.29}$$

On evaluating Eq. (2.8) at wave crest/trough and using Eq.(2.6) we obtain

$$\begin{aligned} H = \eta(0) - \eta(L/2) = & \frac{[u(L/2),\eta(L/2)) - c]^2 - [u(0),\eta(0)) - c]^2}{2g} \\ < & \frac{[u(0),\eta(0)) + u(L/2),\eta(L/2)) - 2c]^2}{2g}\,. \end{aligned} \tag{3.30}$$

Hence, from Eqs. (3.29) and (3.30) we obtain the upper bound

$$H \leq \frac{2\rho^2 g(k-c)^2 d^2}{[P(0,-d) - P_{atm}]^2} \tag{3.31}$$

on the wave height. An interesting observation is that where $k = c$, the bound in Eq. (3.31) leads to a Stokes wave of trivial amplitude which amounts to the fact that a Stokes wave of the same speed as an underlying uniform current can only co-exist if the top surface is flat, as proved by [1]. Hence, the case $k = c$ needs no further attention.

4 Case 2: $k < c$

To deal with this case, let us define $\bar{c} = c - k > 0$. The case can be treated in a similar way as in [10] with a wave speed of $\bar{c}$, resulting in similar bounds on wave heights.

5 Concluding Remarks

The bounds dervied in this paper hold for all Stokes waves irrespective of the amplitude, travelling over uniform current on a finite depth. The lower bound for the case $k > c$ is exactly the same as derived by Constantin [10] without any current. The upper bound in the same case (i.e. for $k > c$) however is a function of the speed of current (Eq. (3.31). Eq. (3.31) also leads to consistent results for the case $k = c$ as has been proved by Basu [1]. The case $k < c$ leads to similar bounds as have been obtained by Constantin [10] for the case without any underlying currents.

Acknowledgments

The author is grateful to the reviewers for the useful suggestions.

References

[1] B. Basu Irrotational two-dimensional free-surface steady water flows over a flat bed with underlying currents, *Nonlinear Anal. TMA*, **147** (2016),110–124.

[2] D. Clamond Note on the velocity and related fields of steady irrotational two-dimensional surface gravity waves, *Phil. Trans. Roy. Soc. London A*, **370(1964)** (2012), 1572–1586.

[3] D. Clamond New exact relations for easy recovery of steady wave profiles from bottom pressure measurements, *J. Fluid Mech.*, **726** (2013), 547–558.

[4] D. Clamond, A. Constantin Recovery of steady periodic wave profiles from pressure measurements at the bed, *J. Fluid Mech.*, **714** (2013), 463–475.

[5] A. Constantin The trajectories of particles in Stokes waves, *Invent. Math.*, **166(3)** (2006), 523–535.

[6] A. Constantin *Nonlinear Water Waves with Applications to Wave-Current Interactions and Tsunamis*, CBMS- NSF Reg. Conf. Ser. Appl. Math., 81, SIAM, Philadelphia, (2011).

[7] A. Constantin On the recovery of solitary wave profiles from pressure measurements, *J. Fluid Mech.*, **699** (2012), 376–384.

[8] A. Constantin Particle trajectories in extreme Stokes waves, *IMA J. Applied Math.*, **7** (2012), 293-307.

[9] A. Constantin Mean velocities in a Stokes wave, *Arch. Ration. Mech. Anal.*, **207(3)** (2013), 907–917.

[10] A. Constantin Estimating wave heights from pressure data at the bed, *J. Fluid Mech.*, **743** (2014), R2.

[11] A. Constantin Stokes waves in water with a non-flat bed, *J. Fluid Mech.*, **740** (2014), 17–27.

[12] A. Constantin Extrema of the dynamic pressure in an irrotational regular wave train, *Phys. Fluids*, **28(11)** (2016), 113604.

[13] A. Constantin, J. Escher Analyticity of periodic traveling free surface water waves with vorticity, *Annals of Mathematics*, **173(1)** (2011), 559–568.

[14] A. Constantin, W. Strauss Pressure beneath a Stokes wave, *Comm. Pure Appl. Math.*, **63(4)** (2010), 533–557.

[15] B. Deconinck, K.L. Oliveras, V. Vasan Relating the bottom pressure and the surface elevation in the water wave problem, *J. Nonlin. Math. Phys.*, **19(Suppl. 1)** (2012), 179–189.

[16] J. Escher, T. Schlurmann On the recovery of the free surface from the pressure within periodic traveling water waves, *J. Nonlin. Math. Phys.*, **15** (2008), 50–57.

[17] D. Henry On the pressure transfer function for solitary water waves with vorticity, *Math. Ann.*, **357** (2013), 23–30.

[18] N. L. Jones, S. G. Monismith Measuring short-period wind waves in a tidally forced environment with a subsurface pressure gauge, *Limnol. Oceanogr. Methods*, **5** (2007), 317–327 .

[19] T. Lyons The pressure in a deep-water Stokes wave of greatest height, *J. Math. Fluid Mech.*, **18** (2016), 209–218.

[20] K. L. Oliveras, V. Vasan, B. Deconinck, D. Henderson Recovering the water-wave profile from pressure measurements, *SIAM J. Appl. Math.*, **72(3)** (2007), 897–918.

[21] J. F. Toland Stokes waves, *Topol. Methods Nonlinear Anal.*, **7(1)** (1996),1–48.

[22] C. Tsai, M.Huang, F. Young, Fu-Ji Y. Lin, H. Li On the recovery of surface wave by pressure transfer function, *Ocean Eng.*, **32(10)** (2005), 1247–1259.

[23] M. Umeyama Eulerian–Lagrangian analysis for particle velocities and trajectories in a pure wave motion using particle image velocimetry, *Phil. Trans. of Roy. Soc. London A*, **370(1964)** (2012), 1687–1702.

Wave height estimates from pressure and velocity data at an intermediate depth in the presence of uniform currents

Biswajit Basu

Phil. Trans. Roy. Soc. London A, 376, 2017.0087, 2017

Abstract

Bounds on estimates of wave heights (valid for large amplitudes) from pressure and flow measurements at an arbitrary intermediate depth has been provided. Two-dimensional irrotational steady water waves over a flat bed with finite depth in the presence of underlying uniform currents have been considered in the analysis. Five different upper bounds based on a combination of pressure and velocity field measurements have been derived, though there is only one available lower bound on the wave height in the case of the speed of current greater than the wave speed.

1 Introduction

Importance of wave height estimates in the fields of ocean energy, coastal engineering and ocean science is well known. The problem of recovering wave heights from measured pressure data at the bed is a practical way to estimate wave heights which can also be used for ground truth verification of indirect remote observations. The use of pressure sensors at the bed for this so called recovery problem is popular due to low cost and convenience in installations [20]. Several researchers have addressed this problem in the past, such as [23] and [17].

As most waves relevant in ocean engineering do not fall into the category of small amplitude theory and, in fact, linear theory may overestimate wave heights by over 10% even for waves of moderate amplitude when compared with observed data [25], investigations have been carried out to relax the approximations of linearity and small amplitudes by researchers such as [23], [16], [8], [5], [4], [12] and [13]. Even though there has been investigations to consider large amplitude waves, exact results are rare in the literature. It has been shown in [18] that it is possible to have exact recovery of wave heights from the pressure data at the bed even for flows with vorticity, and [11] developed an approach to provide simple, explicit but accurate estimates of wave heights for the fully nonlinear large amplitude two-dimensional travelling gravity waves. This was followed by Basu [2] to provide bounds on estimated wave heights from pressure measurements at flat bed for water waves with uniform current using some results from the properties of pressure and flow fields [1].

The aim of this paper is to address the recovery problem, i.e. provide estimates of wave height from pressure and flow velocity measurements at an intermediate arbitrary (known) depth instead of measurements at the bed, without any limitation on the amplitude of wave height. The driver for this is mainly due to the convenience of implementation and flexibility in operation. The other aspect we also consider is a uniform underlying current, which still retains the irrotational structure of the two-dimensional problem.

2 Governing equations

The governing equations and the boundary conditions, including the description of current, are similar to what has been considered and presented in [2]. However, for the sake of completeness we re-present these in this section.

We consider a two-dimensional flow represented in the Cartesian co-ordinate (X,Y) with the direction of wave propagation along the X-axis and the Y-axis pointing vertically upwards. The depth of water at rest is denoted by $d > 0$ which leads to the equation of the flat bed as $Y = -d$. The free surface is given by $Y = \eta(X - ct)$, where $c > 0$ is the speed of propagation of the periodic travelling waves. The surface waves are assumed to propagate over a uniform underlying current of speed k. The flow is irrotational and it may be noted that the uniform underlying current does not introduce any vorticity to the flow.

We investigate periodic travelling waves of wavelength L, with profile η moving at constant speed c. The wave crest is assumed to be located at $X = 0$. Also, we assume that the flow field (u, v) have a space-time dependence of the form $(X - ct)$, i.e. $u := u(X - ct, Y)$ $v := v(X - ct, Y)$. To analyse this problem we introduce a moving frame co-ordinate transformation such that $x = X - ct, y = Y$. Flows without stagnation points are considered, so that, by regularity results discussed in [14], all functions are real analytic. The only waves that are thus excluded are the so-called Stokes waves of greatest height (see the discussions in [24, 9, 22]).

The governing equations for the water waves under inviscid, incompressible conditions are given by the Euler's equation

$$\begin{aligned} (u-c)u_x + vu_y &= -\frac{1}{\rho}P_x \quad \text{for} \quad -d \le y \le \eta(x) \\ (u-c)v_x + vv_y &= -\frac{1}{\rho}P_y - g \quad \text{for} \quad -d \le y \le \eta(x) \ , \end{aligned} \tag{2.1}$$

where $P(x, y)$ is the hydrodynamic pressure, ρ is the density and g is the acceleration due to gravity.

The mass conservation equation for a homogeneous, incompressible fluid is

$$u_x + v_y = 0 \quad \text{for} \quad -d \le y \le \eta(x) \tag{2.2}$$

and, due to irrotationality we have

$$u_y = v_x \quad \text{for} \quad -d \le y \le \eta(x) \ . \tag{2.3}$$

The kinematic boundary conditions at the flat bed and at the free surface are respectively given by

$$v = 0 \quad \text{on} \quad y = -d \tag{2.4}$$

and

$$v = (u-c)\eta(x) \quad \text{on} \quad y = \eta(x) \ . \tag{2.5}$$

The dynamic boundary condition of constant atmospheric pressure at the surface is

$$P = P_{atm} \quad \text{on} \quad y = \eta(x) \ . \tag{2.6}$$

Mass flux (relative to the uniform flow speed c) is a constant and is expressed as

$$M = \rho \int_{-d}^{\eta(x)} [u(x,y) - c] dy \ . \tag{2.7}$$

Conservation of energy leads to Bernoulli's law, which states that

$$\frac{(u-c)^2+v^2}{2}+g(y+d)+\frac{1}{\rho}P=Q\ , \tag{2.8}$$

where Q is a constant throughout the fluid domain.

Let us define stream functions

$$\psi_x=-v,\quad \psi_y=u-c$$

and set (see [7], [1])

$$\psi(x,-d)=-\frac{M}{\rho}\quad \text{and}\quad \psi(x,\eta(x))=0\quad \forall\quad x\in\mathbb{R}\ .$$

The equivalent form of governing equations (Eq. (2.1)) can be expressed in terms of stream functions

$$\begin{aligned}
&\psi_{xx}+\psi_{yy}=0 \qquad \text{for} \qquad -d\le y\le \eta(x)\\
&\psi=0 \quad \text{on} \quad y=\eta(x)\\
&\psi=-\frac{M}{\rho} \quad \text{on} \;\; y=-d\\
&\psi_x^2+\psi_y^2+2g(y+d)=2Q-\frac{2}{\rho}P_{atm} \quad \text{on} \quad y=\eta(x)\ .
\end{aligned} \tag{2.9}$$

The expression for uniform underlying current is

$$k=\frac{1}{L}\int_{\frac{-L}{2}}^{\frac{L}{2}}u(x,-d)dx=\frac{1}{L}\int_{\frac{-L}{2}}^{\frac{L}{2}}u(x,y_0)dx \quad , \quad -d\le y_0\le \eta(x)\ , \tag{2.10}$$

which can be written as [1]

$$k=c+\frac{1}{L}\int_{\frac{-L}{2}}^{\frac{L}{2}}\psi_y(x,-d)dx\ . \tag{2.11}$$

The expression in Eq. (2.11) may be compared with the two definitions of the Stokes wave speed (see the discussion in [10]). In the absence of current (i.e. $k=0$), c is equal to the mean of $-\psi_y$ along the flat bed, so that the wave speed can be recovered from the wave pattern in the reference frame in which the wave is at rest (this is Stokes first definition of the wave speed (see [10])). Three cases may arise consequently from Eq. (2.11) corresponding to $k>c$, $k=c$ and $k<c$; these are the strength (average speed) of the current greater than, equal to and less than the wave speed, respectively, as shown and discussed in [1]. In the following sections these three cases will be considered separately as they lead to different nature of flow fields, as has been shown by Basu [1].

3 Estimates on wave heights: $k>c$

We first consider the case where the speed of the current is greater than the wave velocity, i.e. $k>c$. The other two cases i.e. $k=c$ and $k<c$ will be dealt with subsequently.

The case with $k>c$ results in flow fields (see [1] for details) different from what has been known previously about flow fields when there is no underlying current (e.g., see [6],[15], [26],[3]). The results are summarized as follows for completeness .

Let $\bar{c} = k - c > 0$, leading to

$$\bar{c} = \frac{1}{L}\int_{\frac{-L}{2}}^{\frac{L}{2}} \psi_y(x, -d)dx > 0$$

and from Basu [1]

$$u > c \quad \text{and} \quad M > 0 \tag{3.12}$$

throughout the fluid domain.

Further, the use of properties of harmonic functions and maximum principles results in (see [1])

$$\begin{aligned} u_y(0, y) < 0 \quad &\text{for} \quad -d < y < \eta(0) \ , \\ u_y(\frac{L}{2}, y) > 0 \quad &\text{for} \quad -d < y < \eta(\frac{L}{2}) \ , \\ u_x(x, -d) > 0 \quad &\text{for} \quad 0 < x < \frac{L}{2} \ . \end{aligned} \tag{3.13}$$

3.1 Lower bounds for wave height

Evaluating Bernoulli's law (Eq.(2.8)) at the wave crest ($x = 0$), at the wave trough ($x = \frac{L}{2}$) and, at a depth (d_{int} from the still water level) below the wave crest and the wave trough respectively, we have

$$\begin{aligned} \frac{(u_{min} - c)^2}{2} + g(\eta(0) + d) + \frac{1}{\rho}P_{atm} &= Q \ , \\ \frac{(u_{max} - c)^2}{2} + g(\eta(\frac{L}{2}) + d) + \frac{1}{\rho}P_{atm} &= Q \ , \\ \frac{(u(0, -d) - c)^2}{2} + g(d - d_{int}) + \frac{1}{\rho}P(0, -d_{int}) &= Q \ , \\ \frac{(u(\frac{L}{2}, -d) - c)^2}{2} + g(d - d_{int}) + \frac{1}{\rho}P(\frac{L}{2}, -d_{int}) &= Q \ , \end{aligned} \tag{3.14}$$

where $u_{min} = u(0, \eta(0))$ and $u_{max} = u(L/2, \eta(L/2))$ are the minimum and maximum horizontal fluid velocities at $(0, \eta(0))$ and $(L/2, \eta(L/2))$ respectively. The first and third relations in Eq. (3.14) lead to

$$\eta(0)+d_{int} = \frac{P(0, -d_{int}) - P_{atm}}{\rho g} + \frac{(u(0, -d_{int}) - c)^2 - (u_{min} - c)^2}{2} > \frac{P(0, -d_{int}) - P_{atm}}{\rho g} \tag{3.15}$$

and the second and fourth relations in Eq.(3.14) lead to

$$\eta(\frac{L}{2})+d_{int} = \frac{P(\frac{L}{2}, -d_{int}) - P_{atm}}{\rho g} + \frac{(u(\frac{L}{2}, -d_{int}) - c)^2 - (u_{max} - c)^2}{2} < \frac{P(\frac{L}{2}, -d_{int}) - P_{atm}}{\rho g} \tag{3.16}$$

on using Eqs. (3.12) and (3.13).

From Eqs. (3.15) and (3.16), the lower bound for the estimate of wave height $H = \eta(0) - \eta(L/2)$ is obtained as

$$H = \eta(0) - \eta(\frac{L}{2}) > \frac{P(0, -d_{int}) - P(\frac{L}{2}, -d_{int})}{\rho g} \ . \tag{3.17}$$

It is interesting to observe that the lower bound is independent of the current speed. Further, the lower bounds arrived at by [11] and [2] in the case of surface waves propagating without any underlying currents can be recovered by substituting $d_{int} = d$. It may also be noted that the right hand side of the inequality in Eq.(3.15) exceeds d_{int} while the right hand side of the inequality in Eq.(3.16) is less than d_{int}. This is because fluid pressure is maximal at $(0, -d_{int})$, while $P(L/2, -d_{int})$ is the minimum value of the pressure along the depth d_{int} with the average pressure at a depth d_{int} from the still water level equal to $P_{atm} + \rho g d_{int}$ (see [15] for detail discussion on pressure on the flat bed); this nature of pressure remains unchanged in the presence of uniform currents [1]. This was also observed by [2] in the context of pressure data on the flat data.

Another point to note from Eq. (3.17) is that as the depth of the points at which pressures are measured decreases, the bound becomes less sharp and is trivially true when pressures are measured at the surface. The sharpest bound is obtained for the pressure measured at the flat bed.

3.2 Upper bounds for wave height

To obtain the upper bounds on the wave heights, it is convenient to formulate the problem and carry out the derivations in a transformed domain. Transforming by means of conformal change of variables (since the problem is irrotational)

$$q = -\phi(x, y), \quad p = -\psi(x, y)$$

the free boundary problem given by Eq. (2.9) has an equivalent boundary value problem

$$\begin{aligned} \Delta_{q,p} h = 0 \quad \text{for} \quad \frac{M}{\rho} > p > 0 \ , \\ h = 0 \quad \text{on} \quad p = \frac{M}{\rho} \ , \\ 2(Q - \frac{1}{\rho} P_{atm} - gh)(h_q^2 + h_p^2) = 1 \quad \text{on} \quad p = 0 \ , \end{aligned} \tag{3.18}$$

for the function

$$h(q, p) = y + d \tag{3.19}$$

(see [15, 11]).

Let us also define $P_*(q, p) = P(x, y), \quad u_*(q, p) = u(x, y) \quad .$
As $q = cL/2$ corresponds to $x = L/2$, we define

$$\alpha = \frac{P_*(cL/2, M/\rho) - P_{atm}}{\frac{M}{\rho}} = \frac{P(cL/2, -d) - P_{atm}}{\frac{M}{\rho}} \tag{3.20}$$

and

$$\alpha_0 = \frac{P_*(cL/2, M_0/\rho) + \rho(u_*(cL/2, M_0/\rho) - c)^2 - P_{atm}}{\frac{M}{\rho}} \tag{3.21}$$

where

$$M_0 = \rho \int_{-d_{int}}^{\eta(x)} [u(x, y) - c] dy < M \tag{3.22}$$

From Eqs. (3.20) and (3.21),

$$\alpha > 0, \alpha_0 > 0$$

and choose a depth such that the condition $\alpha \geq \alpha_0$ is satisfied.

Eqs. (3.12), (3.13) and (3.18) lead to

$$\begin{aligned} P_*(q, M/\rho) &= \rho Q - \frac{\rho(u_*(q, M/\rho) - c)^2}{2} \\ &\geq \rho Q - \frac{\rho(u_*(cL/2, M/\rho) - c)^2}{2} \\ &= P_*(cL/2, M/\rho) \\ &= P_{atm} + \alpha M/\rho, \qquad \forall q \in [0, cL/2] \ . \end{aligned}$$

From Eq. (2.1) and Eq.(3.19) we can deduce

$$\frac{1}{\rho}\Delta(q,p)P_* = -2(u_{*q}^2 + u_{*p}^2), \qquad M/\rho > p > 0$$

and the function

$$f(q,p) = \frac{P_*(q,p) - \alpha_0 p}{\rho} \tag{3.23}$$

is superharmonic in the strip $M/\rho > p > 0$. Also, we note that

$$\begin{aligned} f(q, M/\rho) &= \frac{P_*(q, M/\rho) - \alpha_0 M}{\rho} \\ &\geq \frac{P_{atm} + \alpha M/\rho - \alpha_0 M/\rho}{\rho} \\ &> \frac{P_{atm}}{\rho} \quad (\because \ \alpha, \quad \alpha_0, \quad M > 0) \ . \end{aligned} \tag{3.24}$$

It may be noted that f equals P_{atm}/ρ on the upper surface $p = 0$, and from Eq. (3.24) it is observed that f always attain higher values than P_{atm}/ρ on the lower boundary $p = M/\rho$. Hence, from the strong maximum principle we infer that the mimnimum of f is attained on the upper boundary $p = 0$ and Hopf's principle ensures $f_p(q, 0) > 0 \ \forall \ q \in R$. Hence from Eqs. (2.1), (2.2), (2.5) and (3.19), we have

$$f_p(q,0) = \frac{1}{\rho}P_{*p}(q,0) - \frac{\alpha_0}{\rho} > 0$$

leading to

$$-\frac{\alpha_0}{\rho} > \frac{2(u-c)^2 u_x \eta_x + (u-c)^2 u_y(\eta_x^2 - 1) - g(u-c)}{(u-c)^2(1+\eta_x^2)} \tag{3.25}$$

on $y = \eta(x)$.

On differentiating the fourth relation in Eq. (2.9) along the free surface w.r.t x-variable we also obtain

$$0 = (u-c)u_x + (u-c)u_y\eta_x + vv_x + vv_y\eta_x + g\eta_x \quad \text{on} \quad y = \eta(x) \ .$$

Furthermore, from the last equation and Eqs. (2.2), (2.3) and (2.5) we obtain

$$(u-c)u_x(1-\eta_x^2) + 2(u-c)u_y\eta_x + g\eta_x = 0 \quad \text{on} \quad y = \eta(x) \ . \tag{3.26}$$

Using Eqs. (3.12), (3.25), (3.26) and the fact that $\eta_x(x) < 0$ for $x \in (0, L/2)$, we get

$$-\frac{\alpha_0}{\rho}\eta_x < u_x(x,\eta(x)) + u_y(x,\eta(x))\eta_x(x), \quad 0 < x < L/2 \ ,$$

which on integration on $[0, L/2]$ leads to

$$\frac{\alpha_0}{\rho}\left[\eta(L/2)-\eta(0)\right]\ .> u(0,\eta(0))-u(L/2,\eta(L/2))\ . \tag{3.27}$$

Evaluating Eq. (2.8) at the wave crest and the wave trough, and from Eq. (3.27) we can deduce

$$\frac{\alpha_0}{2\rho g}\left[\{u(0,\eta(0))-c\}^2-\{u(L/2,\eta(L/2))-c\}^2\right] > u(0,\eta(0))-u(L/2,\eta(L/2))\ , \tag{3.28}$$

which further yields

$$u(0,\eta(0))+u(L/2,\eta(L/2))-2c < \frac{2\rho g}{\alpha_0}\ . \tag{3.29}$$

From Eq. (3.13) we have $u(L/2,\eta(L/2)) > u(0,\eta(0)) > c$. Furthermore, as $\eta(L/2) \leq 0$, we have

$$ML = \int_{-L/2}^{L/2} M dx = \rho\int_{-L/2}^{L/2}\int_{-d}^{\eta(L/2)}(u-c)dxdy \leq \rho\int_{-L/2}^{L/2}\int_{-d}^{0}(u-c)dxdy = \rho(k-c)Ld\,.$$

Thus

$$M \leq \rho(k-c)d\ . \tag{3.30}$$

Combining Eqs. (3.21), (3.29) and (3.30), we obtain

$$u(0,\eta(0))+u(L/2,\eta(L/2))-2c < \frac{2\rho g(k-c)d}{P(L/2,-d_{int})+\rho\left\{u(L/2,-d_{int})-c)\right\}^2-P_{atm}}. \tag{3.31}$$

On evaluating Eq. (2.8) at wave crest/trough and using Eq.(2.6), we obtain

$$\begin{aligned} H=\eta(0)-\eta(L/2) =& \frac{\left[u(L/2),\eta(L/2))-c\right]^2-\left[u(0),\eta(0))-c\right]^2}{2g} \\ <& \frac{\left[u(0),\eta(0))+u(L/2),\eta(L/2))-2c\right]^2}{2g}\ . \end{aligned} \tag{3.32}$$

Hence, from Eqs. (3.31) and (3.32) we obtain the upper bound

$$H < \frac{2\rho^2 g(k-c)^2 d^2}{[P(L/2,-d_{int})+\rho\left\{u(L/2,-d_{int})-c)\right\}^2-P_{atm}]^2} \tag{3.33}$$

on the wave height. An alternative bound is obtained on using the Bernoulli's law (Eq. (2.8)) at a depth $y=-d_{int}$ as follows

$$H < \frac{2\rho^2 g(k-c)^2 d^2}{[P(0,-d_{int})+\rho\left\{u(0,-d_{int})-c)\right\}^2-P_{atm}]^2}\ . \tag{3.34}$$

If velocity measurements are not available then the bound in Eq. (3.33) can be modified based on pressure measurement alone, and can be given as

$$H < \frac{2\rho^2 g(k-c)^2 d^2}{[P(L/2,-d_{int})-P_{atm}]^2}\ . \tag{3.35}$$

Eq. (3.35) can also be obtained by defining α_0 in Eq. (3.21) by

$$\alpha_0 = \frac{P_*(L/2,M_0/\rho)-P_{atm}}{\frac{M}{\rho}} > 0 \tag{3.36}$$

and proceeding following a similar approach as before, exploiting maximum principles and the govering equations of the water waves.

Eq. (3.35) provides a bound less sharper than the one given by Eq. (3.34). In fact, a sharper bound is obtained from Eq. (3.34) and is given by

$$H < \frac{2\rho^2 g(k-c)^2 d^2}{[P(0,-d_{int}) - P_{atm}]^2} \ , \tag{3.37}$$

if velocity measurements are not available and cannot be used.

If pressure measurements are not available and only velocity measurements are available instead, then the following bound is obtained from Eq. (3.33) (since $P(L/2,-d_{int}) > P_{atm}$, see [1])

$$H < \frac{2g(k-c)^2 d^2}{[u(L/2,-d_{int}) - c]^4} \ . \tag{3.38}$$

It may be noted that if measurements at the flat bed are available, then bounds based on pressure measurements become sharper bounds than those based on velocity measurements, while velocity measurements should be used to arrive at sharper bounds when measurements are taken closer to the free surface.

Another interesting point to note, as was also observed in [1] is that, when $k = c$, the bounds in Eqs. (3.33)-(3.35) and Eqs. (3.37)-(3.38) all lead to a Stokes wave of trivial amplitude. This is equivalent to the fact that a Stokes wave of the same speed as an underlying uniform current can only co-exist if the top surface is flat. Hence, the case $k = c$ needs no further persual.

4 Estimates on wave heights: $k < c$

To deal with this case, let us define $\bar{c} = c - k > 0$. The case can be treated in a similar way as in [11] with a wave speed of $\bar{c}$ and no current. However, we need to make appropriate modifications to account for measurements at an arbitrary depth. We proceed to obtain the bounds on wave heights.

The case with $k < c$ results in flow fields (see [1] for details) similar to the flow fields when there is no underlying current (e.g., see [6],[15], [26],[3]). The results are summarized as follows.

Let $\bar{c} = c - k > 0$, leading to

$$\bar{c} = \frac{1}{L}\int_{\frac{-L}{2}}^{\frac{L}{2}} \psi_y(x,-d)dx > 0$$

and, from Basu [1]

$$u < c \quad \text{and} \quad M < 0 \tag{4.39}$$

throughout the fluid domain.

Further, the use of properties of harmonic functions and maximum principles results in (see [1])

$$\begin{aligned} u_y(0,y) > 0 \quad &\text{for} \quad -d < y < \eta(0) \ , \\ u_y(\frac{L}{2},y) < 0 \quad &\text{for} \quad -d < y < \eta(\frac{L}{2}) \ , \\ u_x(x,-d) < 0 \quad &\text{for} \quad 0 < x < \frac{L}{2} \ . \end{aligned} \tag{4.40}$$

4.1 Lower bounds for wave height

Evaluating Bernoulli's law (Eq.(2.8)) at the wave crest ($x = 0$), at the wave trough ($x = \frac{L}{2}$) and, at a depth (d_{int} from the still water level) below the wave crest and the wave trough, respectively, we have

$$
\begin{aligned}
\frac{(u_{max}-c)^2}{2} + g(\eta(0)+d) + \frac{1}{\rho}P_{atm} &= Q \ , \\
\frac{(u_{min}-c)^2}{2} + g(\eta(\frac{L}{2})+d) + \frac{1}{\rho}P_{atm} &= Q \ , \\
\frac{(u(0,-d_{int})-c)^2}{2} + g(d-d_{int}) + \frac{1}{\rho}P(0,-d_{int}) &= Q \ , \\
\frac{(u(\frac{L}{2},-d_{int})-c)^2}{2} + g(d-d_{int}) + \frac{1}{\rho}P(\frac{L}{2},-d_{int}) &= Q \ ,
\end{aligned}
\tag{4.41}
$$

where $u_{max} = u(0, \eta(0))$ and $u_{min} = u(L/2, \eta(L/2))$ are the maximum and minimum horizontal fluid velocities, respectively. The first and third relations in Eq. (4.41) lead to

$$
\eta(0)+d_{int} = \frac{P(0,-d_{int})-P_{atm}}{\rho g} + \frac{(u(0,-d_{int})-c)^2-(u_{max}-c)^2}{2} > \frac{P(0,-d_{int})-P_{atm}}{\rho g}
\tag{4.42}
$$

and the second and fourth relations in Eq.(4.41) lead to

$$
\eta(\frac{L}{2})+d_{int} = \frac{P(\frac{L}{2},-d_{int})-P_{atm}}{\rho g} + \frac{(u(\frac{L}{2},-d_{int})-c)^2-(u_{min}-c)^2}{2} < \frac{P(\frac{L}{2},-d_{int})-P_{atm}}{\rho g}
\tag{4.43}
$$

on using Eqs. (4.39) and (4.40).

From Eqs. (4.42) and (4.43), the lower bound for the estimate of wave height $H = \eta(0) - \eta(L/2)$ is obtained as

$$
H = \eta(0) - \eta(\frac{L}{2}) > \frac{P(0,-d_{int}) - P(\frac{L}{2},-d_{int})}{\rho g}
\tag{4.44}
$$

arriving at the same lower bound as in Eq. (3.17). In fact this is exactly the same lower bound as in the case of wave heights for surface waves without any underlying current [11] if the depth of observation 'd' is replaced by '$-d_{int}$'.

As also observed for the case $k > c$, the bound becomes less sharp and is trivially true when pressures are measured at the surface, and the sharpest bound is obtained for the pressure measured at the flat bed.

4.2 Upper bounds for wave height

Using the same transformations as in Section 3, we obtain

$$
\begin{aligned}
\Delta_{q,p} h = 0 \quad &\text{for} \quad \frac{M}{\rho} < p < 0 \ , \\
h = 0 \quad &\text{on} \quad p = \frac{M}{\rho} \ , \\
2(Q - \frac{1}{\rho}P_{atm} - gh)(h_q^2 + h_p^2) = 1 \quad &\text{on} \quad p = 0 \ ,
\end{aligned}
\tag{4.45}
$$

for the function

$$h(q,p) = y + d \tag{4.46}$$

(see [15], [11]).

Let us also define $P_*(q,p) = P(x,y), \quad u_*(q,p) = u(x,y) \quad .$

As $q = cL/2 \quad$ corresponds to $x = L/2, \quad$ we define

$$\alpha = \frac{P_*(cL/2, M/\rho) - P_{atm}}{\frac{M}{\rho}} = \frac{P(cL/2, -d) - P_{atm}}{\frac{-M}{\rho}} \tag{4.47}$$

and

$$\alpha_0 = \frac{P_*(cL/2, M_0/\rho) + \rho(u_*(cL/2, M_0/\rho) - c)^2 - P_{atm}}{\frac{-M}{\rho}} \ , \tag{4.48}$$

where M_0 has been defined in Section 3. Again, from Eqs. (4.47) and (4.48), we infer

$$\alpha > 0, \alpha_0 > 0,$$

and choose a depth such that the condition $\alpha \geq \alpha_0$ is satisfied. Eqs. (4.39), (4.40) and (4.45) lead to

$$\begin{aligned}
P_*(q, M/\rho) &= \rho Q - \frac{\rho(u_*(q, M/\rho) - c)^2}{2} \\
&\geq \rho Q - \frac{\rho(u_*(cL/2, M/\rho) - c)^2}{2} \\
&= P_*(cL/2, M/\rho) \\
&= P_{atm} - \alpha M/\rho, \qquad \forall q \in [0, cL/2].
\end{aligned}$$

Consider the function

$$f(q,p) = \frac{P_*(q,p) + \alpha_0 p}{\rho} \ . \tag{4.49}$$

Then, we have

$$\begin{aligned}
f(q, M/\rho) &= \frac{P_*(q, M/\rho + \alpha_0 M}{\rho} \\
&\geq \frac{P_{atm} - \alpha M/\rho + \alpha_0 M/\rho}{\rho} \\
&> \frac{P_{atm}}{\rho}
\end{aligned} \tag{4.50}$$

as $\alpha > 0$, $\alpha_0 > 0$ and $M < 0$. From Eq. (2.1) and Eq.(4.46) we can deduce

$$\frac{1}{\rho}\Delta(q,p)P_* = -2(u_{*q}^2 + u_{*p}^2), \qquad M/\rho > p > 0 \ .$$

The function $f(q,p)$ is superharmonic in the strip $M/\rho < p < 0$.

It may be noted that f equals P_{atm}/ρ on the upper surface $p = 0$, and from Eq. (4.50) it is observed that f always attain higher values than P_{atm}/ρ on the lower boundary $p = M/\rho$. Hence, from the strong maximum principle we infer that the minimum of f is attained on the upper boundary $p = 0$ and Hopf's principle ensures $f_p(q,0) < 0 \ \forall \ q \in R$. Hence from Eqs. (2.1), (2.2), (2.5) and (4.46), we have

$$f_p(q,0) = \frac{1}{\rho} P_{*p}(q,0) + \frac{\alpha_0}{\rho} < 0$$

leading to

$$\frac{\alpha_0}{\rho} < \frac{2(u-c)^2 u_x \eta_x + (u-c)^2 u_y(\eta_x^2 - 1) - g(u-c)}{(u-c)^2(1+\eta_x^2)} \tag{4.51}$$

on $y = \eta(x)$. A similar inequality was derived in [11]. Following a similar approach as in [11] we have

$$|u(0, \eta(0) - c| + |u(L/2, \eta(L/2)) - c| < \frac{2\rho g}{\alpha_0} \; . \tag{4.52}$$

Furthermore, as $\eta(L/2) \leq 0$, we have

$$ML = \int_{-L/2}^{L/2} M dx = \rho \int_{-L/2}^{L/2} \int_{-d}^{\eta(L/2)} (u-c) dx dy \geq \rho \int_{-L/2}^{L/2} \int_{-d}^{0} (u-c) dx dy = \rho(k-c)Ld.$$

Thus,

$$M \geq \rho(k-c)d \; . \tag{4.53}$$

Combining Eqs. (4.48), (4.52) and (4.53) we obtain

$$|u(0, \eta(0)) - c| + |u(L/2, \eta(L/2)) - c| < \frac{|2\rho g(k-c)d|}{P(L/2, -d_{int}) + \rho \left\{u(L/2, -d_{int}) - c)\right\}^2 - P_{atm}}. \tag{4.54}$$

On evaluating Eq. (2.8) at wave crest/trough and using Eq.(2.6), we obtain

$$\begin{aligned} H = \eta(0) - \eta(L/2) = & \frac{[u(L/2), \eta(L/2)) - c]^2 - [u(0), \eta(0)) - c]^2}{2g} \\ < & \frac{[|u(0), \eta(0)) - c| + |u(L/2), \eta(L/2)) - c|]^2}{2g} \; . \end{aligned} \tag{4.55}$$

Hence, from Eqs. (4.54) and (4.55) we obtain the upper bound

$$H < \frac{2\rho^2 g(k-c)^2 d^2}{[P(L/2, -d_{int}) + \rho \left\{u(L/2, -d_{int}) - c)\right\}^2 - P_{atm}]^2} \tag{4.56}$$

on the wave height. Similar approaches, followed as in Section 3, lead to four other upper bounds,

$$H < \frac{2\rho^2 g(k-c)^2 d^2}{[P(0, -d_{int}) + \rho \left\{u(0, -d_{int}) - c\right\}^2 - P_{atm}]^2}, \tag{4.57}$$

$$H < \frac{2g(k-c)^2 d^2}{[u(0, -d_{int}) - c]^4}, \tag{4.58}$$

$$H < \frac{2\rho^2 g(k-c)^2 d^2}{[P(L/2, -d_{int}) - P_{atm}]^2} \tag{4.59}$$

and

$$H < \frac{2\rho^2 g(k-c)^2 d^2}{[P(0, -d_{int}) - P_{atm}]^2} \; . \tag{4.60}$$

Again, if velocity measurements are not available then the last two bounds based on pressure measurements are useful, and out of the two bounds the last one is sharper.

5 Remarks

The following remarks pertains to the analysis in this paper and results obtained.

1. The derived bounds on wave heights in this paper hold for all levels of amplitudes and thus can be applied to water waves of large amplitudes.

2. The lower bounds in this paper are independent of the speed of the underlying uniform current, while the upper bounds depend on the current speed. This was also the case in Basu [1] and is consistent with the bounds provided by Constantin [11] in the case without any current. Hence, this seems to be generally true for two-dimensional irrotational flow with uniform underlying current or flows without any current.

3. The lower bounds with current approach the lower bounds for the case without any current when the pressure measurement at the flat bed is used to obtain the bounds.

4. Use of a combination of pressure and velocity measurements can make the bounds on the wave heights sharper.

5. It is worth pointing out that the considerations in this paper are of great interest also in the case of non-uniform currents. This setting corresponds to waves with non-zero vorticity and one cannot rely on a harmonic velocity potential, so that the approach used in the present paper does not apply. However, the existence theory for travelling periodic water waves with vorticity of small and large amplitude is quite well-developed theoretically for a general vorticity in flows without critical layers (see [27]), for constant vorticity in flows with critical layers (see [28]) and there are quite accurate numerical simulations (see [29]). Some considerations dealing with the pressure recovery for linear and weakly nonlinear waves were recently made in [19]. Further, existence and bounds on the amplitude of water waves over finite depth have been also derived by Kogelbauer [21] in terms of a number of flow parameters.

The author(s) declare that they have no competing interests.

References

[1] Basu B. 2016 Irrotational two-dimensional free-surface steady water flows over a flat bed with underlying currents. *Nonlinear Anal. TMA* **147**, 110–124.

[2] Basu B. 2017 Estimation of wave heights from pressure data at the bed in the presence of uniform underlying currents. *Nonlinear Anal.* **156**, 82–89.

[3] Clamond D. 2012 Note on the velocity and related fields of steady irrotational two-dimensional surface gravity waves. *Phil. Trans. Roy. Soc. London A* **370**(1964), 1572–1586.

[4] Clamond D. 2013 New exact relations for easy recovery of steady wave profiles from bottom pressure measurements. *J. Fluid Mech.* **726**, 547–558.

[5] Clamond D, Constantin A. 2013 Recovery of steady periodic wave profiles from pressure measurements at the bed. *J. Fluid Mech.* **714**, 463–475.

[6] Constantin A. 2006 The trajectories of particles in Stokes waves. *Invent. Math.* **166** (3), 523–535.

[7] Constantin A. 2011 *Nonlinear water waves with applications to wave-current interactions and tsunamis.* CBMS- NSF Reg. Conf. Ser. Appl. Math., vol. 81, SIAM, Philadelphia.

[8] Constantin A. 2012. On the recovery of solitary wave profiles from pressure measurements. *J. Fluid Mech.* **699**, 376–384.

[9] Constantin A. 2012. Particle trajectories in extreme Stokes waves. *IMA J. Appl. Math.* **77**, 293–307.

[10] Constantin A. 2013 Mean velocities in a Stokes wave. *Arch. Ration. Mech. Anal.* **207**(3), 907–917.

[11] Constantin A. 2014 Estimating wave heights from pressure data at the bed. *J. Fluid Mech.* **743**, R2.

[12] Constantin A. 2014 Stokes waves in water with a non-flat bed. *J. Fluid Mech.* **740**, 17–27.

[13] Constantin A. 2016 Extrema of the dynamic pressure in an irrotational regular wave train. *Phys. Fluids* **28**(11), 113604.

[14] Constantin A, Escher J. 2011 Analyticity of periodic traveling free surface water waves with vorticity. *Annals of Mathematics* **173**(1), 559–568.

[15] Constantin A, Strauss W. 2010 Pressure beneath a Stokes wave. *Comm. Pure Appl. Math.* **63**(4), 533–557.

[16] Deconinck B, Oliveras K, Vasan V. 2012 Relating the bottom pressure and the surface elevation in the water wave problem. *J. Nonlinear Math. Phys.* **19**(sup1), 179–189.

[17] Escher J, Schlurmann T. 2008 On the recovery of the free surface from the pressure within periodic traveling water waves. *J. Nonlinear Math. Phys.* **15**, 50–57.

[18] Henry D. 2013 On the pressure transfer function for solitary water waves with vorticity. *Math. Ann.* **357**(1), 23–30.

[19] Henry D, Thomas GP. 2017 Prediction of the free-surface elevation for rotational water waves using the recovery of pressure at the bed. *Phil. Trans. Roy. Soc. London A* **376**, 20170102. (doi:10.1098/rsta.2017.0102)

[20] Jones NL, Monismith SG. 2007 Measuring short-period wind waves in a tidally forced environment with a subsurface pressure gauge. *Limnol. Oceanogr. Methods* **5**, 317–327.

[21] Kogelbauer F. 2017 Existence and amplitude bounds for irrotational water waves in finite depth. *Phil. Trans. Roy. Soc. London A* **376**, 20170094. (doi:10.1098/rsta/2017.0094)

[22] Lyons T. 2016 The pressure in a deep-water Stokes wave of greatest height. *J. Math. Fluid Mech.* **18**, 209–218.

[23] Oliveras KL, Vasan V, Deconinck B, Henderson D. 2012 Recovering the water-wave profile from pressure measurements. *SIAM J. Appl. Math.* **72**(3), 897–918.

[24] Toland JF. 1996 Stokes waves. *Topol. Methods Nonlinear Anal.* **7**(1), 1–48.

[25] Tsai CH, Huang MC, Young FJ, Lin YC, Li HW. 2005 On the recovery of surface wave by pressure transfer function. *Ocean Eng.* **32**(10), 1247–1259.

[26] Umeyama M. 2012 Eulerian–Lagrangian analysis for particle velocities and trajectories in a pure wave motion using particle image velocimetry. *Phil. Trans. Roy. Soc. London A* **370**(1964), 1687–1702.

[27] Constantin A, Strauss W. 2004 Exact steady periodic water waves with vorticity. *Comm. Pure Appl. Math.* **57**(4): 481–527.

[28] Constantin A, Strauss W, Vărvărucă E. 2016 Global bifurcation of steady gravity water waves with critical layers. *Acta Mathematica* **217**(2): 195–262.

[29] Ribeiro R, Milewski PA, Nachbin A. 2017 Flow structure beneath rotational water waves with stagnation points. *J. Fluid Mech.* **812**, 792-814.

A Flow Force Reformulation of Steady Irrotational Water Waves

Biswajit Basu

submitted for review

Abstract

The classical irrotatioal water wave problem described by Euler equations with a nonlinear free surface boundary condition and influenced by gravity over a flat bed is considered. Exploiting the monotonicity property of the flow force lines with depth, the unknown boundary problem is transformed into a problem with fixed domain. A flow force function formulation of the irrotational water wave problem is developed. Variational approach is used to prove the existence of small amplitude irrotational travelling wave solutions. Local bifurcation results have been proved relying on Crandall-Rabinowitz bifurcation theorem.

1 Introduction

Studies on irrotational periodic travelling water waves including some of their nonlinear approximations were initiated by Stokes in 1847 [28]. Further research were carried out by Nekrasov, Levi-Civita and Struik [27, 25, 29] in 1920s on local solution of these waves with profiles which were almost flat. Large amplitude irrotational waves were constructed by Krasovskii [24] in 1961 and were further refined by Keady and Norbury [19] in 1978 using global bifurcation techniques. Subsequently, research by Toland and McLeod [30, 26] showed the exsistence of waves with stagnation points.

With regard to rotational flows, only recently, the existence of large amplitude water waves with vorticity was proved rigourously in the seminal paper by Constantin and Strauss [9]. Following this, large amplitude waves in the presence of discontinuous vorticity, stratification and surface tension were also proved to exist [11, 31, 32]. Other relevant research in this area can be found in [6, 7, 14, 10, 13, 5, 8, 12].

Typically, in previous studies related to existence of water waves, an essential approach is to formulate an equivalent problem in a fixed domain. Bifurcation theory is then used as the most successful tool to prove the existence results. For example, in the case of irrotational flows, hodograph transform is used to map the unknown domain occupied by the fluid to a fixed horizontal strip in a complex plane, where the variable is the complex potential of the fluid flow. In these transformed coordinates, a nonlinear integral equation is formulated for a function of one variable, which is the angle of inclination between the tangent to the free surface and the horizontal [1, 30, 19]. Another approach which also works for water waves with vorticity, under the assumption that the streamfunction ψ is monotone in the vertical direction, is a streamfunction formulation with a transform $(X, Y) \mapsto (X, -\psi)$ which can be used [9] to convert the problem into a nonlinear boundary value problem with quasilinear elliptic equation in a strip.

The studies by [3, 20] have mentioned in their papers about a quantity called flow force, related to flow of fluid with free surface over a flat bed. The quantity flow force has the property that it is zero on the flow bed and is invariant on the free surface. This opens up a possibility to transform the free unknown boundary problem to a fixed domain with a suitable transformation involving the flow force. In addition, it also turns out that the level curves of the flow force function within the fluid domain (which we define as ‘flow force lines’) are monotone in the vertical direction. This then is the motivation for us to reformulate the free surafce nonlinear boundary value problem for water waves by using a ‘flow force’ function leading to a novel formulation.

In almost all of the mentioned previous studies, either on irrotational or rotational waves, the mass flux has been defined as a given fixed constant, alongwith constant depth. Numerical investigations [21, 22] have revealed that the depth varies throughout the continuum [9] of solutions for fixed mass flux. To address this, Henry [17, 18] formulated a fixed depth formulation for large amplitude steady periodic waves. However, the definition and properties of ‘flow force’ lines; and the transformed flow force formulation provide us the option of making the flow force as a fixed constant, instead of the mass flux. This is not just mathematically consistent, but also physically relevant as it is natural to hold the flow force constant with a fixed depth, which is the driver of the fluid flow, letting the mass flux to adjust accordingly.

The aim of the paper is to reformulate the steady periodic irrotational water wave problem in terms of the ‘flow force’ functions. In this framework, the existence of small-amplitude irrotational steady periodic water waves propagating over a flat bed, with a given flow force is proved using a variational approach. Local bifurcation results are also proved using the theorem of Crandall-Rabinowitz.

2 Stream function formulation of the water wave problem

Let us consider the water wave profile oscillating about the flat surface $y = 0$. The two-dimensional periodic steady waves traveling at speed c, has a space-time dependence of the free surface, of the velocity field and of the pressure of the form $(X - ct)$ and is periodic with period $L > 0$. The flat bed is given by $y = -d$ and the oscillating wave profile is represented by $y = \eta(X - ct)$ where y is the vertical axis. The free boundary problem can be simplified by the change of reference frame from a stationary to a moving one, $(X - ct, y) \mapsto (x, y)$; thus coverting the wave to a stationary wave. Let (u, v) denote the velocity field. The stream function $\psi(x, y)$ upto an additive constant is defined given by the following equations

$$\psi_x = -v, \psi_y = u - c \; . \tag{2.1}$$

For the irrotational flow in absence of vorticity, we have

$$\Delta\psi = u_y - v_x = 0 \; . \tag{2.2}$$

The mass flux (relative to the uniform flow c) is defined as

$$p_0 = \int_{-d}^{\eta(x)} \psi_y dy \; . \tag{2.3}$$

We assume that $u < c$ (i.e. $p_0 < 0$) throughout the closed fluid domain.

From the Euler equation, we get the Bernoulli’s law which states

$$E = \frac{(c-u)^2 + v^2}{2} + gy + P \tag{2.4}$$

is a constant (called hydrualic head) throughout the flow, where P is the pressure. The dynamic boundary condition at the surface can be stated as

$$\frac{\psi_x^2 + \psi_y^2}{2} + g(y + d) = Q \quad \text{on} \quad y = \eta(x) \tag{2.5}$$

where $Q = E - P_{atm} + gd$ is a constant for any given flow, with P_{atm} denoting the atmospheric pressure on the free surface.

We can formulate the free surface irrotational water wave problem represented by the governing equations [9]

$$\begin{aligned} \Delta\psi = 0 \quad &\text{in} \quad -d < y < \eta(x) \\ |\nabla\psi|^2 + 2g(y+d) = Q \quad &\text{on} \quad y = \eta(x) \\ \psi = 0 \quad &\text{on} \quad y = \eta(x) \\ \psi = -p_0 \quad &\text{on} \quad y = -d \end{aligned} \tag{2.6}$$

which is to be solved for functions which are L-periodic in the $x-$variable over a fluid domain $\bar{D}_\eta$. Let $\bar{D}_\eta$ be the closure of the open fluid domain

$$D_\eta = \{(x,y) \in \mathbb{R}^2 : x \in \mathbb{R}, -d < y < \eta(x)\} \ .$$

For $m \geq 1, m \in \mathbb{I}$ and $\alpha \in (0,1)$, a domain $D \subset \mathbb{R}^2$ is a $C^{m,\alpha}$ domain if each point on its boundary ∂D has a neighborhood in which ∂D is the graph of a function with Hölder-continuous derivative (of exponent α) upto oder m. For the solution of the problem considered, we define the space $C^{m;\alpha}_{per}(D)$ of function $f : \bar{D} \to R$ with Hölder continuous derivative exponent α, upto order m, which also satisfies the $L-$periodicity condition.

We set $L = 2\pi$ without any loss of generality and consider one wavelength of the periodic domain. By introducing a height function (see constantin2004exact) for every fixed x

$$h = y + d$$

which is a single valued function of ψ and using a Dubreil-Jacotin transformation with

$$q = x \quad , p = -\psi$$

the unknown fluid domain is transformed into a rectangular domain

$$R = (-\pi, \pi) \times (p_0, 0) \ . \tag{2.7}$$

We also choose the location of the crest of the wave at $(0, \eta(0))$.

3 Flow force reformulation

We now reformulate the governing equations in Section 2 using a different and novel approach based on flow force function. Let us define the flow force function denoted by S using the following integral expression

$$S(x,y) = \int_{-d}^{y} [p(x,r) + (u(x,r) - c)^2] \mathrm{d}r \tag{3.8}$$

where $p(x,y) = P(x,y) - P_{atm}$. The pressure at (x,y) is denoted by the function $P(x,y)$ and P_{atm} is the atmospheric pressure at the surface. Hence, from the definition of $S(x,y)$ we have

$$S = 0 \quad \text{ on the bottom } y = -d \ ,$$

and let us denote

$$S = S_0 \quad \text{ on the free surface } y = \eta(x) \quad .$$

The expression for S on the free surface $y = \eta(x)$ (denoted by S_0) is thus given by

$$S_0 = S(x, \eta(x)) = \int_{-d}^{\eta(x)} [p + (u - c)^2] dy \quad .$$

Let us assume

$$p(x, r) + (u(x, r) - c)^2 = F_r(x, r) \quad .$$

$$\therefore S(x, y) = \int_{-d}^{y} F_\omega d\omega = F(x, y) - F(x, -d) \tag{3.9}$$

On differentiating Eq.(3.9), we have the differential of the flow force function as

$$S_y(x, y) = F_y(x, y) = p(x, y) + (u(x, y) - c)^2 \; .$$

It may be noted that the term S_0 is independent of x which can verified by the following calculation

$$\frac{dS_0}{dx} = \eta'(x)[p(x, \eta(x)) + (u(u, \eta(x) - c)^2] + [v(u - c)]_{\eta(x)}^{-d} = 0 \quad . \tag{3.10}$$

The result in (3.10) has been derived using the following relation

$$S_{yx} = P_x + 2(u - c)u_x = -(u - c)v_y - vu_y = -\{(u - c)v\}_y \quad , \tag{3.11}$$

which can be obtained by using the continuity equation

$$u_x + v_y = 0 \; , \tag{3.12}$$

the kinematic boundary conditions at the surface and at the flat bed respectively, i.e. $v = \eta_x(u - c)$ and $v = 0$; and also the dynamic boundary condition at the free surface, $p = 0$. Eq. (3.11) leads to

$$S_x = (c - u)v \; . \tag{3.13}$$

It can be shown for irrotational flows (see [2]) that for $u \neq c$, the pressure $P(x, y)$ increases as we go down within the fluid domain. Thus, $p_y < 0$; and since $p = 0$ at the surface we infer that $S_y = p + (u - c)^2 > 0$ throughout the fluid domain.

The main difficulties associated with the classical water wave problem are that the equations are nonlinear and also the free surface, $y = \eta(x)$, forming a boundary of the domain is unknown. The latter difficulty is proposed to be circumvented by the use of the flow force function which possesses certain properties which are suitable to transfrom the unknown domain to a problem with fixed domain. In this regard, we notice that S is constant both on the free surface and on the flat bed. Also, for $u \neq c$ we observe that $S_y = p + (u - c)^2 > 0$ throughout the fluid domain, which implies that $y \mapsto S(x, y)$ is strictly increasing. So, for every fixed x, the height

$$h = y + d \tag{3.14}$$

above the flat bed is a single-valued function of S. This allows us to change the variables, by defining a set of two new independent variables

$$q = x \quad , s = S \tag{3.15}$$

and in the process transform the unknown fluid domain, for one wavelength, to a known rectangular domain

$$R_s = (-\pi, \pi) \times (0, S_0) \; .$$

We also choose the location of the wave crest at $(0, \eta(0))$.

3.1 Governing equations based on flow force

Recalling that the following two equations relating to the derivatives of the flow force function

$$S_x = (c-u)v \ , \tag{3.16}$$

$$S_y(x,y) = F_y(x,y) = p(x,y) + (u(x,y)-c)^2 \ ;$$

and differentiating the first one with respect to x and the second one with respect to y, we have

$$s_{xx} + s_{yy} = -g - 2(c-u)(u_y - v_x) \tag{3.17}$$

in the absence of any vorticity leads to the superharmonic equation

$$\Delta s = -g \ , \tag{3.18}$$

with $s = 0$ on the flat bed $y = -d$ and $s = S_0$ on the free surface $y = \eta(x)$. The nonlinear dynamic boundary condition on the free surface may be expressed as

$$\frac{|\nabla s|^2}{s_y} + 2g(y+d) = Q \ . \tag{3.19}$$

3.2 Depth function formulation with flow force

We one again consider the previously discussed transformation of the variables $q = x$ and $s = S$; and the depth function $h(q,s) = y + d$ for the purpose of a depth function formulation of the flow force function. We consider the level set of the functions $S(x,y)$ within the fluid domain, which we term 'flow force lines', in analogy with 'streamlines'. This motivates us to proceed with a depth function formulation utilizing the 'flow force lines'. Notice that the flat bed and the (unknown) free surface coincide with two 'flow force lines', defining the bottom and the top bundary.

Since by definition, the value of a flow force function is invariant along a 'flow force line', we have

$$S_x + S_y.h_q = 0 \tag{3.20}$$

leading to

$$h_q = -\frac{S_x}{S_y} \ . \tag{3.21}$$

In view of the fact that $p + (c-v)^2 > 0$, we can write the following relations

$$h_q = -\frac{S_x}{S_y} = -\frac{s_x}{s_y} = \frac{(u-c)v}{p+(c-u)^2} \tag{3.22}$$

and

$$h_s = \frac{1}{s_y} = \frac{1}{S_y} = \frac{1}{p+(c-u)^2} \tag{3.23}$$

$$\therefore \partial_x = \partial_q + s_x.\partial_s = \partial_q - \frac{h_q}{h_s}\partial_s \tag{3.24}$$

and

$$\partial_y = s_y.\partial_s = \frac{1}{h_s}\partial_s \ . \tag{3.25}$$

Consequently, we have

$$(c-u)v = -\frac{h_q}{h_s} \ ; \tag{3.26a}$$

$$p + (c-u)^2 = \frac{1}{h_s} \ . \tag{3.26b}$$

On differentiating (3.26a) with respect to the x-variable and on differentiating (3.26b) with respect to the y-variable, we have the following two equations:

$$-u_x v + (c-u)v_x = \left(\partial_q - \frac{h_q}{h_s}\partial_s\right)\left(-\frac{h_q}{h_s}\right) \tag{3.27}$$

and

$$P_y - 2(c-u)u_y = \frac{1}{h_s}\partial_s\left(\frac{1}{h_s}\right) \ . \tag{3.28}$$

Further from Eqs. (3.27) and (3.28), on using the Euler equation and the condition for irrotational flow with vorticity $u_y - v_x = 0$, we have

$$\psi_{xx}\psi_y + \psi_x\psi_{xy} = \left(\partial_q - \frac{h_q}{h_s}\partial_s\right)\left(-\frac{h_q}{h_s}\right) \tag{3.29}$$

and

$$-\psi_x\psi_{xy} - \psi_y\psi_{xx} - g = \frac{1}{h_s}\partial_s\left(\frac{1}{h_s}\right) \ . \tag{3.30}$$

Adding Eqs. (3.29) and (3.30), yields

$$-\left(\partial q - \frac{h_q}{h_s}\partial_s\right)\left(\frac{h_q}{h_s}\right) + \frac{1}{h_s}\partial_s\left(\frac{1}{h_s}\right) = -g \ , \tag{3.31}$$

which on further simplification leads to

$$(1+h_q^2)h_{ss} - 2h_s h_q h_{sq} + h_s^2 h_{qq} = g h_s^3 \ , \tag{3.32}$$

which is a second order quasi-linear elliptic partial differential equation.

For the boundary condition at the free surface, we consider the following equation (from Eq.(2.6))

$$|\nabla\psi|^2 + 2g(y+d) = Q \quad \text{on } y = \eta(x), \quad \text{i.e. } s = S_0 \ ,$$

which on using the following relations (from Eqs. (3.26a) and (3.26b))

$$\psi_x^2 = \frac{h_q^2}{h_s}(1 - p h_s)^{-1}, \qquad \psi_y^2 = \frac{1}{h_s} - p \ ;$$

and noting that $p = 0$ on the free surface (i.e. on $s = S_0$), leads to the first order fully nonlinear oblique boundary condition

$$(1+h_q^2) + (2gh - Q)h_s = 0 \quad \text{on } s = S_0 \ . \tag{3.33}$$

On the flat bed, corresponding to $y = -d$, we have

$$h = 0 \quad \text{on } s = 0 \ . \tag{3.34}$$

Thus, the reformulated irrotational steady water wave problem in the flow force framework becomes

$$\begin{cases} (1+h_q^2)h_{ss} - 2h_s h_q h_{sq} + h_s^2 h_{qq} = g h_s^3 \text{ in } \quad (0, S_0), \\ (1+h_q^2) + (2gh - Q)h_s = 0 \text{ on } \quad s = S_0, \\ h = 0 \text{ on } \ s = 0 \ ; \end{cases} \tag{3.35}$$

which is to be solved in the class of functions that are even and and 2π-periodic; i.e. for h of period 2π in the q-variable satisfying

$$\frac{1}{2\pi}\int_{-\pi}^{\pi} h(q,0)\mathrm{dq} = \mathrm{d} \ , \tag{3.36}$$

with $h \in C^{2,\alpha}_{per}(\bar{R_s})$ for some $\alpha \in (0,1)$.

3.3 Equivalence of formulations

Lemma 1. Problem (3.18) is equavalent to problem (3.35).

Proof. It has been already shown from direct calculation that (3.18) implies (3.35). To prove the equivalence result, we need to show the converse holds. If R_s denotes the rectangle $(-\pi,\pi)\times(0,S_0)$, let h be a solution to (3.35) of class $C^2_{per}(\overline{R_s})$, where $\overline{R_s}$ is the closure of R_s. Let us define the $C^1_{per}(\overline{R_s})$ functions

$$F(q,s) = \frac{1}{h_s(q,s)}, G(q,s) = -\frac{h_q(q,s)}{h_s(q,s)} \quad . \tag{3.37}$$

The commutative relation for differential, $h_{sq} = h_{qs}$ implies

$$F_q + F_s G - G_s F = 0 \text{ in } R_s \tag{3.38}$$

while the partial differential equation in (3.35) gives

$$G_q + G G_s + F F_s = -g \text{ in } R_s \quad . \tag{3.39}$$

The free surface of the flow is given by the equation $\eta(x) = h(x,0) - d$.

Our intention is to recover s. For fixed $x_0 \in \mathbb{R}$, we can solve the ordinary differential equation

$$s_y(x_0, y) = F(x_0, s(x_0, y)) \tag{3.40}$$

with initial data $s(x_0, \eta(x_0)) = S_0$. Given the smoothness of F, there is a unique local solution $s(x_0, y)$ to (3.40). Moreover, since $F \geq \delta > 0$ throughout R_s for some $\delta > 0$, we deduce that as long as it defined, the function $s(x_0, y)$ is decreasing at a rate faster than δ as y decreases. Therefore, (3.40) is solvable until $s(x_0, y)$ becomes 0, and correspondingly we find some $y(x_0) < \eta(x_0)$ with $s(x_0, y(x_0)) = 0$. This shows that for every $x \in \mathbb{R}$ we can define $s(x,y)$ on some interval $[y(x), \eta(x)]$ with $y(x) < \eta(x)$. By uniqueness for (3.40), s is periodic in x.

We now claim that $y(x) = -d$ for all $x \in \mathbb{R}$. To prove this, the first step is to show that

$$s_x(x,y) = G(x, s(x,y)) \tag{3.41}$$

for all $y \in [y(x), \eta(x)]$. Let us set $H(x,y) = G(x, \psi(x,y))$ for $y \in [y(x), \eta(x)]$. Then from (3.38)and (3.40) we get,

$H_y = G_s s_y = G_s F = F_q + F_s G = F_q + F_s H \quad .$

On the other hand, (3.40) and the C^1-dependence of its solution on the parameter x implies

$(s_x)_y = F_q + F_s s_x$.

Thus, we conclude that H and s_x satisfy the same ordinary differential equation. We have by definition $s(x, \eta(x)) = S_0$, so that (3.40) leads to

$$s_x(x, \eta(x)) = -s_y(x, \eta(x))\eta'(x) = -F(x, s(x, \eta(x))\eta'(x) \ .$$

On the other hand, we have

$$H(x, \eta(x)) = G(x, -s(x, \eta(x))) = -\eta'(x)F(x, -s(x, \eta(x))$$

if we take into account (3.37) and the fact that $h(q, S_0) = \eta(x) + d$. Thus, H and s_x have identical initial data at $y = \eta(x)$, yielding $H \equiv s_x$ and (3.41) follows.

We now exploit the C^1-dependence of $y(x)$ upon x, enabling us to differentiate the relation $s(x, y(x)) = 0$ to give

$$s_x(x, y(x)) + s_y(x, y(x))\frac{dy(x)}{dx} = 0, x \in \mathbb{R} \ .$$

On using (3.40) and (3.41), this becomes

$$G(x, 0) + F(x, 0)\frac{dy(x)}{dx} = 0, x \in \mathbb{R} \ .$$

But $G(x, 0) \equiv 0$ if we take (3.35) and (3.37) into account, while $F(x, 0) \geq \delta > 0$ on $\mathbb{R}$. Hence, we infer that $y(x)$ is a constant y_0, $\forall x \in \mathbb{R}$.

On using (3.22) and (3.23), together with (3.37) and (3.40), taking $x_0 = 0$, and since $h \equiv 0$ on $s = 0$ and $h(0, S_0) = \eta(0) + d$, we get

$$\begin{aligned}
\eta(0) + d = h(0, S_0) = \int_0^{S_0} h_s(0, s)ds &= \int_0^{S_0} \frac{1}{F(0, s)} ds \\
&= \int_{y_0}^{\eta(0)} \frac{1}{F(0, s(0, y))}[ds(0, y)] \\
&= \int_{y_0}^{\eta(0)} 1 dy = \eta(0) - y_0.
\end{aligned}$$

This indeed leads to the conclusion that the flat bottom is precisely $y = -d$.

It remains to be shown that the constructed s is a solution to (3.18). It is known to us that $s = 0$ on $y = -d$ and $s = S_0$ on $y = \eta(x)$. It may be noted that $F^2 + G^2 = |\nabla s|^2$ in view of (3.40) and (3.41). On the other hand, the boundary condition on $s = S_0$ in (3.35) combined with (3.41) yields $F^2 + G^2 + (2gh - Q)F = 0$ on $y = \eta(x)$, i.e. for $s = S_0$. Since $q = x$ and $h(q, p) = y + d$, we get $\frac{|\nabla s|^2}{s_y} + 2g(y + d) = Q$ at $y = \eta(x)$. Finally, we observe that differentiating (3.40) with respect to y, and (3.37) with respect to x, and then adding up, we arrive at $\Delta s = G_q + GG_s + FF_s$. Now taking (3.39) into account, we can verify that $\Delta s = -g$ throughout the fluid domain. Therefore s indeed is a solution to (3.18).

Defining u and v by means of (3.26a) and (3.26b); and recalling that the moving frame was obtained by means of the transformation $(x - ct, y) \mapsto (x, y)$, we obtain a solution $(u, v, \eta) \in C^1_{per}(\overline{D}_\eta) \times C^1_{per}(\overline{D}_\eta) \times C^2_{per}(\mathbb{R})$ to the original problem (3.18).

Further note that if $h \in C^{2,\alpha}_{per}(\overline{R})$ for some $\alpha \in (0, 1)$, then the solution $(u, v, \eta) \in C^{1,\alpha}_{per}(\overline{D}_\eta) \times C^{1,\alpha}_{per}(\overline{D}_\eta) \times C^{2,\alpha}_{per}(\mathbb{R})$.

4 Steady periodic waves of small amplitude

Given $S_0 > 0$, we seek solutions $h \in C^{2,\alpha}_{per}(\overline{R_s})$ to the problem (3.35). Such solutions correspond to solutions

$$\eta \in C^{2,\alpha}_{per}(\overline{D}_\eta), u, v \in C^{1,\alpha}_{per}(\overline{D}_\eta), P \in C^{0,\alpha}_{per}(\overline{D}_\eta)$$

of the governing equations (3.35). It may be noted that a solution h which corresponds to an non-flat free surface are q-dependent, while q-independent solutions of h correspond to laminar flow, i.e. parallel shear flows with a flat free surface. In case of laminar flows, the particles moves horizontally with a speed that depends on the height of the particle above the flat bed. This represents the presence of a pure current (i.e., with no vertical motions).

The existence of small amplitude wave solutions of (3.35) is stated by the following theorem of local bifurcation.

Theorem 2. (Local bifurcation) Let $S_0 > 0$, $c > 0$ and $\alpha \in (0, 1)$. Further, assume that

$$\frac{g}{2}(1 + 3S_0/2g)\left[\sqrt{1 + 3S_0/2g} - 1\right] + \frac{g}{6}\sqrt{1 + 3S_0/2g}\left[(1 + 3S_0/2g)^2 - 1\right] < g\ .$$

Consider travelling wave solutions of speed c and flow force S_0 evaluted at the surface $y = \eta(x)$ of the irrotational water wave problem (3.35) such that $u < c$ throughout the fluid domain. Then there exists a C^1-curve $\mathcal{C}_{loc}$ of small-amplitude solutions $h \in C^{2,\alpha}_{per}(\bar{R}_s)$ and $(u, v, \eta) \in C^{1,\alpha}_{per}(\bar{D_\eta}) \times C^{1,\alpha}_{per}(\bar{D_\eta}) \times C^{2,\alpha}_{per}(\mathbb{R})$. Moreover, the solution curve $\mathcal{C}_{loc}$ contains precisely one function that is independent of q corresponding to the trivial flow with ($\eta \equiv 0$).

Remark 1. Note that the left hand side of the inequality in Theorem 2 is a monotonically increasing function of S_0 with a value equal to zero when $S_0 = 0$ and infinity when $S_0 \to \infty$. Hence, it puts a constraint on the strength of the flow force.

Remark 2. Benjamin and Lighthill [3] had shown that there are some feasible combinations of mass flux, total head and flow force which allow the wave trains to exist. The feasible combinations were represented with a diagram with barriers beyond which no stationary or other steady waves were possible. Kozlov et al. [23] also used the flow force to uniquely parametrise the subset of waves with crests located on a fixed vertical and verified the Benjamin-Lighthill conjecture with values of Bernoulli's constant close to critical one.

The proof of the result relies on applying the Crandall-Rabinowitz theorem and for this it is necessary to identify the bifurcating parameter which can be used to investigate the bifurcating wave solution from the laminar flow.

4.1 Laminar flow

We proceed to find the laminar flow solutions and their properties.

Lemma 3. (Trivial solution) The trivial solutions (representing parallel shear flow with flat surface $\eta \equiv 0$) are $h(q, s) = H(s)$ with

$$H(s) = H(s; \lambda) = -\int_s^{S_0} \frac{ds}{\sqrt{\lambda^2 + 2g(S_0 - s)}} + \frac{Q - \lambda}{2g} \tag{4.42}$$

where $\lambda > 0$ and is related to Q.

Proof. Trivial solutions belong to the class of laminar flows and hence are independent of q. Thus, (3.35) reduces to the solution of the following differential equation

$$H_{ss} = gH_s^3 \ . \tag{4.43}$$

It has the solution

$$H_s(s, \lambda) = [\lambda^2 + 2g(S_0 - s)]^{-1/2} \tag{4.44}$$

where $\lambda > 0$ is defined as

$$\lambda = \frac{1}{H_s(S_0, \lambda)} = (c - u)^2|_{\text{surface}} \tag{4.45}$$

considered as the bifurcation parameter denoting the square of the surface velocity relative to the wave speed.

The nonlinear surface boundary condition $1 + (2gH(S_0, \lambda) - Q)H_s(S_0, \lambda) = 0$ then leads to (4.42). The bottom boundary condition $H(0) = 0$ becomes

$$0 < g\left\{(\lambda^2 + 2gS_0)^{1/2} - \lambda\right\} = \frac{Q - \lambda}{2g} \tag{4.46}$$

which is the relation between λ and Q. We have $S_0 > 0$ and $\lambda < Q$. Note that λ is not a single-valued function of Q. For every $\lambda > 0$, there is a unique $Q(\lambda)$ satisfying (4.46) since

$$Q = (1 - 2g^2)\lambda + 2g^2[(\lambda^2 + 2gS_0)]^{1/2} \ . \tag{4.47}$$

On differentiating (4.47), we have

$$\frac{dQ}{d\lambda} = (1 - 2g^2) + \frac{2g^2\lambda}{\sqrt{\lambda^2 + 2gS_0}} \ , \quad \lambda > 0 \ . \tag{4.48}$$

Therefore the function $\lambda \mapsto Q(\lambda)$ is strictly convex for $\lambda > 0$ (see Fig. 1). The minimum value on $(0, \infty)$ is attained at some λ_0 where

$$\int_0^{S_0} \frac{ds}{[\lambda^2 + 2g(S_0 - s)]^{3/2}} = \frac{1}{2g\lambda_0}$$

leading to

$$\lambda_0 = \frac{(2g^2 - 1)\sqrt{2gS_0}}{\sqrt{4g^2 - 1}} \ . \tag{4.49}$$

For every $Q > Q(\lambda_0)$ there is exactly one $\lambda > \lambda_0$ satisfying (4.47) and for certain $Q > 0$ there is another solution of (4.47) for $\lambda \in (0, \lambda_0)$. Note also that (4.42) can be written is

$$H(s) = \int_0^s \frac{ds}{\sqrt{\lambda^2 + 2g(S_0 - s)}} = g\left\{\sqrt{\lambda^2 + 2gS_0} - \sqrt{\lambda^2 + 2g(S_0 - s)}\right\} \ .$$

□

5 Linearization

In order to find waves of small amplitude we first linearize (3.35) about a laminar solution. We seek solutions $h \in C^{2;\alpha}_{per}(\bar{R}_s)$ even in the $q-$ variable and zero on $s = 0$, with perturbation from the laminar solution and represented in the form

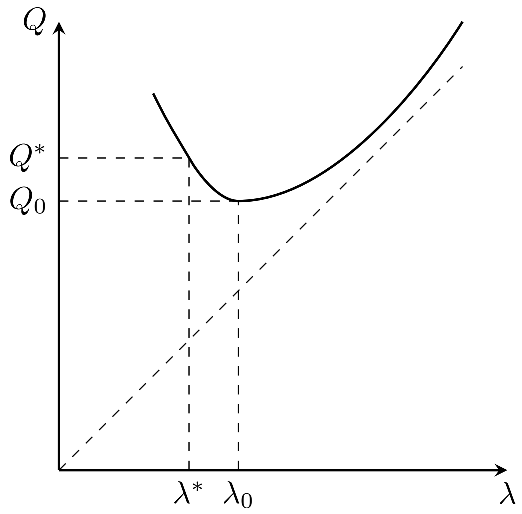

Figure 1: Functional dependence for laminar flows

$$h = H + \varepsilon m \ .$$

The symmetry on the wave is expressed by the requirement of m to be even. Denoting

$$a(s, \lambda) = \sqrt{\lambda^2 + 2g(S_0 - s)} \tag{5.50}$$

we linearize (3.35) around H and use the fact that the terms involving H_q are zero. Hence, we also have $H_{qq} = 0$ and $H_{sq} = 0$ for laminar flow.

Therefore, at order ϵ^0, we obtain the laminar flow. Subsequently, at order ϵ, we obtain, for $m \in C^{2,\alpha}_{per}(\bar{R}_s)$ and even in the q- variable,

$$m_{ss} + H_s^2 m_{qq} = 3gH_s^2 m_s \ .$$

$$\because a = \frac{1}{H_s} \therefore a_s = -\frac{H_{ss}}{H_s^2} \ ;$$

we therefore have,

$$3a^2 a_s = 3.\frac{1}{H_s^2}.\left(-\frac{H_{ss}}{H_s^2}\right) = \frac{-3gH_s^3}{H_s^4} = \frac{-3g}{H_s}$$

eventually leading to

$$m_{ss} + H_s^2 m_{qq} = 3gH_s^2 m_s \ \text{ in } \ R_s \ . \tag{5.51}$$

Next we consider the boundary condition on the free surface, yielding

$$[1 + (H_q + \varepsilon m_q)^2] + [2g(H + \varepsilon m) - Q](H_s + \varepsilon m_s) = 0 \text{ on } s = S_0 \ ,$$

which at order ε^0 and ε^1 leads to

$$(2gH - Q) = -\frac{1}{H_s}$$

and

$$2gH_s m + (2gH - Q)m_s = 0 \ ,$$

respectively. Hence, we get the boundary conditions on the free surface $s = S_0$ and the flat bed $s = 0$ as follows

$$\begin{array}{ll} 2gm = \lambda^2 m_s & \text{on } s = S_0 \ ; \\ m = 0 & \text{on } s = 0 \ . \end{array}$$

For a fixed λ, let $a_\lambda(s) = a(s;\lambda) = \{\lambda^2 + 2g(S_0 - s)\}^{1/2}$. Then $H_s^2 = a^{-2}$ and hence, the linearized boundary value problem can be written in the self-adjoint form as

$$\begin{aligned} \{a^3 m_s\}_s + \{a m_q\}_q = 0 \ \text{ in } \ R_s \\ a^2 m_s = 2gm \ \text{ on } \ s = S_0 \\ m = 0 \ \text{ on } \ s = 0 \end{aligned} \tag{5.52}$$

with evenness and periodicity in q.

We claim that $m \in C^{2,\alpha}_{per}(\bar{R}_s)$ even in $q-$variable can be represented by a Fourier series

$$m(q,s) = \sum_{k=0}^{\infty} m_k(s)\cos(kq) \ \text{ in } \ C^2_{per}(\bar{R}_s) \tag{5.53}$$

with $C^{3,\alpha}_{per}[0, S_0]$ coefficients

$$m_0(s) = \frac{1}{2\pi}\int_{-\pi}^{\pi} m(q,s)dq, \quad m_k(s) = \frac{1}{2\pi}\int_{-\pi}^{\pi} m(q,s)\cos(kq)dq, \ \ k \geq 1 \ . \tag{5.54}$$

Since the other cases are similar, it is sufficient for us to show that $\sum_{k=0}^{\infty} m_k''(s)\cos(kq)dq$ converges in $C_{per}(\bar{R}_s)$. It may be noted that

$$|m_0''(s)| = \left|\frac{1}{2\pi}\int_{-\pi}^{\pi} m_{ss}(q,s)dq\right| \leq ||m||C^2_{per}(\bar{R}_s) \quad ,$$

and on integration by parts

$$m_k''(s) = \frac{1}{2\pi}\int_{-\pi}^{\pi} m_{ss}(q,s)\cos(kq)dq = -\frac{1}{k\pi}\int_{-\pi}^{\pi} m_{ssq}(q,s)\sin(kq)dq \quad , \ \ k \geq 1 \ .$$

We thus have for $N \geq n \geq 1$

$$\begin{aligned} |\sum_{k=n}^{N} m_k''(s)\cos(kq)|^2 \leq (\sum_{k=n}^{N} |m_k''(s)|)^2 \\ \leq \{\sum_{k=n}^{N}\frac{1}{k^2}\}\{\sum_{k=n}^{N}(\frac{1}{\pi}\int_{-\pi}^{\pi} m_{ssq}(q,s)\sin(kq)dq)^2\} \\ \leq \frac{\pi^2}{6}\{\frac{1}{\pi}\int_{-\pi}^{\pi} m_{ssq}^2(q,s)dq\} \leq \frac{\pi}{3} \parallel m \parallel^2_{C^3_{per}(\bar{R}_s)} \ . \end{aligned} \tag{5.55}$$

Thus, we see that $\sum_{k=0}^{\infty} \ m_k''(s)\cos(kq)$ converges in $C_{per}(\bar{R}_s)$. Also, $m(q,s) = \sum_{k=0}^{\infty} \ m_k(s)\cos(kq)$ is in $C_{per}(\bar{R}_s)$, since $\sum_{k=0}^{\infty} m_k(s)\cos(kq)$ converges in $C_{per}(\bar{R}_s)$

and by $L^2[-\pi,\pi]$ covergence of the right hand side of (5.53) to $m(.,s)$ for every fixed $s \in [0,S_0]$. Thus, $\sum_{k=0}^{\infty} m_k''(s)\cos(kq)$ converges in the sense of distribution to $m_{ss}(q,s)$, permitting us to identify the limit of $\sum_{k=0}^{\infty} m_k''(s)\cos(kq)$ in $C_{per}(\bar{R}_s)$ precisely as $m_{ss}(q,s)$. Similar procedure will lead to the validity of (5.52).

From (5.52) we can derive that m is a solution to (5.51), if and only if each m_k solves the Sturm-Liouville problem

$$\begin{cases} (a^3 M_s)_s = k^2 a M & \text{in } (0,S_0) \\ a^2 M_s = 2gM & \text{on } s = S_0 \\ M = 0 & \text{on } s = 0 \end{cases} \tag{5.56}$$

with $m_k \neq 0$ for some $k \geq 1$.

We seek solutions of period 2π and hence we consider the case corresponding to $k = 1$.

5.1 Variational approach

Since from (5.56),

$$\begin{aligned} -\int_0^{S_0} (a^3 M_s)_s M ds &= \int_0^{S_0} a^3 M_s^2 ds - a^3 M_s\, M|_0^{S_0} \\ &= \int_0^{S_0} a^3 M_s^2 ds - 2gaM^2(S_0) \\ &= -k^2 \int_0^{S_0} aM^2 ds \ , \end{aligned}$$

we now associate with (5.56) for $k = 1$, the following minimization problem

$$\mu(\lambda) = \inf\{F(\varphi,\lambda)\} \tag{5.57}$$

over the space of functions satisfying

$$\varphi \in H^1(0,S_0), \varphi(0) = 0, \varphi \not\equiv 0 \ \ ,$$

with

$$F(\varphi,\lambda) = \frac{-2ga(S_0)\varphi^2(S_0) + \int_0^{S_0} a^3 \varphi_s^2 ds}{\int_0^{S_0} a\varphi^2 ds} \quad . \tag{5.58}$$

This is suggested by the fact that for a solution M of (5.56) we have $F(M,\lambda) = -k^2$, and the choice of the function space stems from the motivation to search for the largest possible Hilbert space for which F is well defined, with the boundary condition on $s = 0$ satisfied, while the condition $s = S_0$ is inherent in the form of $F(. \ ,\lambda)$. For $\lambda > 0$, the existence of μ is ensured as will be seen from the following result.

Lemma 4. (Eigenvalue problem) There exists $\lambda^* > 0$ and a solution $m(q,s) \not\equiv 0$ of (5.52) which is even and 2π - periodic in q.

Proof. Consider the minimization problem in (5.57). Let

$$\varepsilon(\lambda) = \ \inf\{a(s,\lambda)\} > 0 \ \ , s \in [0,S_0] \ \ .$$

Now,

$$\begin{aligned} &\int_0^{S_0} a^3 \varphi_s^2 ds + \tfrac{16g^2}{\varepsilon^2(\lambda)} \int_0^{S_0} a\varphi^2 ds \geq \varepsilon(\lambda) \int_0^{S_0} a^2 \varphi_s^2 ds + \tfrac{16g^2}{\varepsilon(\lambda)} \int_0^{S_0} \varphi^2 ds \\ &\geq 8g \int_0^{S_0} a\varphi\varphi_s ds \geq 4ga(S_0)\varphi^2(S_0) \end{aligned}$$

where $\phi \in H'(0, S_0)$ satisfies $\varphi(0) = 0$. Thus,

$$\mu(\lambda) \geq -\frac{16g^2}{\varepsilon^2(\lambda)} \quad . \tag{5.59}$$

We now claim that the infimum in (5.57) is attained by a function $M \in C^{3,\alpha}[0, S_0]$. Consider a minimizing sequence $\varphi_n \in H'(0, S_0)$ with $\varphi_n(0) = 0$ such that $F(\varphi_n, \lambda) \to \mu(\lambda)$. We can then have

$$F(\varphi_n, \lambda) = -2ga(S_0)\varphi^2(S_0) + \int_0^{S_0} a^3(\partial_s\varphi_n)^2 ds$$
$$\geq \frac{1}{2}\int_0^{S_0} a^3(\partial_s\varphi_n)^2 ds - \frac{8g^2}{\epsilon^2(\lambda)} \geq \frac{\varepsilon^3(\lambda)}{2}\int_0^{S_0}(\partial_s\varphi_n)^2 ds - \frac{8g^2}{\varepsilon^2(\lambda)}$$

on normalizing the sequence $\{\varphi_n\}_{n\geq 1}$ by a scalar, setting $\int_0^{S_0} a\varphi^2 ds = 1$. Note that normalization of φ by a scalar $\theta \neq 0$, leads to $F(\theta\ \varphi, \lambda) = F(\varphi, \lambda)$. Since $F(\varphi_n, \lambda) \to \mu(\lambda)$, we conclude that $\{\int_0^{S_0}(\partial_s\varphi_n)^2 ds\}_{n\geq 1}$ is bounded. Also, we have

$$\frac{1}{\varepsilon(\lambda)} = \frac{1}{\varepsilon(\lambda)}\int_0^{S_0} a\varphi^2 ds \geq \int_0^{S_0} {\varphi_n}^2 ds \quad , n \geq 1 \quad .$$

Hence, $\{\varphi_n\}_{n\geq 1}$ is bounded in the Hilbert space $H^1(0, S_0)$ and as a consequence has a weakly convergent subsequence $\{\varphi_{n_k}\}$ with limit $M \in H^1(0, S_0)$. Also, note $\partial_s\varphi_{n_k} \rightharpoonup M_s$ weakly in $L^2(0, S_0)$ and $\varphi_{n_k}(0) = 0$ resulting in

$$\varphi_{n_k}(s) = \int_0^s \partial_s\varphi_{n_k}(r)dr \to \int_0^s M_s(r)dr = M(s) \text{ at every } s \in [0, S_0] \quad . \tag{5.60}$$

A weak convergence in general does not lead to a.e. convergence of some subsequence as wild oscillations are possible and nonlinear operations with weakly convergent sequence are not allowed. Hence, $\partial_s\varphi_{n_k} \rightharpoonup M_s$ does not lead to a.e. convergence. However, we use the fact that the sequence $\{\varphi_{n_k}\}$ is minimizing and use some structural properties of $F(., \lambda)$ as follows:

$$\int_0^{S_0} a^3 {M^2}_s ds \leq \liminf_{n_k\to\infty}\int_0^{S_0} a^3(\partial_s\varphi_{n_k})^2 ds \tag{5.61}$$

since

$$\int_0^{S_0} a^3(\partial_s\varphi_{n_k})^2 ds - \int_0^{S_0} a^3 M_s^2 ds = \int_0^{S_0} a^3(\partial_s\varphi_{n_k} - M_s)^2 ds$$

$$+2\int_0^{S_0} a^3(\partial_s\varphi_{n_k})ds - 2\int_0^{S_0} a^3 M_s^2 ds \ ,$$

and $a^3 M_s \in L^2(0, S_0)$ together with $\partial_s\varphi_{n_k} \rightharpoonup M_s$ weakly in $L^2(0, S_0)$ ensure that the sum of the last two terms converge toward zero as $n_k \to \infty$. Then, from (5.60) and (5.61), we have

$$2gaM^2(S_0) - \int_0^{S_0} a^3 M_s^2 ds \leq \liminf_{n_k\to\infty}\left[2ga(S_0){\varphi^2}_{n_k}(S_0) - \int_0^{S} a^3(\partial_s\varphi_{n_k})^2 ds\right] \quad .$$

Since the sequence $\{\varphi_{n_k}\}$ is minimizing for $F(.,\lambda)$, the infimum is a minimum attained at $M \in H^1(0,S_0)$. In fact, $M \in C^{3,\alpha}[0,S_0]$.

The associated Euler-Lagrange equation corresponding to the variational problem,

$$\frac{d}{d\varepsilon}F(M+\varepsilon\varphi,\lambda)|_{\varepsilon=0} = 0 \tag{5.62}$$

is satisfied by M as a minimum for every $\varphi \in H^1(0,S_0)$ with $\varphi(0) = 0$. It may be observed that $F(M,\lambda) = \mu(\lambda)$, and $\int_0^{S_0} aM^2 ds = 1$ by the dominated convergence theorem in view of (5.60), and that the sequence $\{\varphi_{n_k}\}$ is bounded in $H^1(0,S_0)$. This ensures an $L^\infty[0,S_0]$ uniform bound for $\{\varphi_{n_k}\}$. Therefore,

$$-2ga(S_0)M(S_0)\varphi(S_0) + \int_0^{S_0} a^3 M_s\varphi_s ds = \mu(\lambda)\int_0^{S_0} aM\varphi ds \tag{5.63}$$

$\forall\varphi \in H^1(0,S_0)$ with $\varphi(0) = 0$. With a smooth and compactly supported φ in the support $(0,S_0)$, we conclude that

$$(a^3M_s)_s = -\mu aM \text{ in } H^1(0,S_0) \tag{5.64}$$

Since $a \in C^{2,\alpha}[0,S_0] \subset H^2(0,S_0)$ and $M \in H^1(0,S_0)$, we have $aM \in H^1(0,S_0)$ and hence, $a^3M_s \in H^2(0,S_0)$ and $M_s \in H^2(0,S_0)$, which means $M \in H^3(0,S_0) \subset C^2[0,S_0]$. As a result, (5.64) holds classically and $a \in C^{2,\alpha}[0,S_0]$ gives $M \in C^{3,\alpha}[0,S_0]$. Multiplying (5.64) by some $\varphi \in H^1(0,S_0)$ with $\varphi(0) = 0$ and integrating yields

$$-a^3(S_0)M_s(S_0)\varphi(S_0) + \int_0^{S_0} a^3\varphi_s M_s ds = \mu(\lambda)\int_0^{S_0} aM\varphi ds \quad . \tag{5.65}$$

From (5.63) and (5.65), and choosing $\varphi(s) = s$, we have the missing boundary condition

$$a^2M_s = 2gM \text{ on } s = S_0$$

and the minimum $M \in C^{3,\alpha}[0,S_0]$ is a classical solution of the (weighted) Sturm-Liouville problem

$$\begin{array}{ll} (a^3M_s)_s = -\mu aM & \text{in } (0,S_0) \\ a^2M_s = 2gM & \text{on } s = S_0 \\ M = 0 & \text{on } s = 0 \end{array} \tag{5.66}$$

For the existence of the linear waves, it is necessary that $\mu(\lambda) = -1$ for some $\lambda > 0$. □

5.2 Monotonicity of the ground state

In this subsection we intend to prove the analyticity result, i.e. $\lambda \mapsto \mu(\lambda)$ for $\lambda > \bar{\lambda} > 0$, with $\mu(\lambda)$ depending monotonically on $\lambda > \bar{\lambda}$ whenever we have $\mu(\lambda) < 0$.

Let $M(s,\lambda)$ be the $C^{3,\alpha}[0,S_0]$ eigenfunction corresponding to the eigenvalue problem with eigenvalue $\mu(\lambda)$. We normalize by setting $M(S_0,\lambda) = 1$. It may be noted that

$$M(s,\lambda) = \varphi(s,\lambda,\mu(\lambda)) \quad ,$$

where $\varphi(s,\lambda,\mu)$ is the unique solution of the linear differential equation

$$(a^3\varphi_s)_s = -\mu a\varphi \text{ in } (0, S_0) \tag{5.67}$$

with initial data

$$\begin{array}{l} \varphi(S_0) = 1 \\ \varphi'(S_0) = \frac{2g}{a^2(S_0)} \end{array} \tag{5.68}$$

depending analytically on (λ, μ) as the solutions continuously depend on the parameters. The variational approach showing the existence resulted in

$$2ga(S_0) - \int_0^{S_0} a^3 M_s^2 ds + \mu \int_0^{S_0} aM^2 ds = 0 \tag{5.69}$$

which is a functional relation between $\mu(\lambda)$ and λ. Differentiating (5.67) with respect to μ and multiplying by $\varphi = M$ and integrating over $[0, S_0]$ (using $M(0, \lambda, \mu) = 0$) yields

$$-\int_0^{S_0} a^3 M_{s\mu} M_s ds + \mu \int_0^{S_0} aMM_\mu ds = -\int_0^{S_0} aM^2 ds \ .$$

Therefore, we obtain the partial derivative with respect to μ of the function (μ, λ) on the left hand side of (5.69) as

$$\int_0^{S_0} aM^2 ds - 2\int_0^{S_0} a^3 M_{s\mu} M_s ds + 2\mu \int_0^{S_0} aMM_\mu ds = -\int_0^{S_0} aM^2 ds < 0$$

By implicit function theorem we deduce the real analytic dependence of $\mu(\lambda)$ on $\lambda > 0$.

Denote $\dot{a} = \frac{\partial a}{\partial \lambda}$, hence we get

$$\dot{a} = \frac{\lambda}{a}, \dot{a}_s = -\frac{\lambda a_s}{a^2}$$

Thus from (5.66), we find that $\dot{M}$ satisfies

$$\begin{array}{l} (a^3\dot{M}_s)_s + 3\lambda(aM_s)_s = -\dot{\mu}aM - \frac{\lambda}{a}\mu M - \mu a\dot{M} \text{ in } (0, S_0) \\ 2\lambda M_s + a^2\dot{M}_s = 2g\dot{M} \text{ at } s = S_0 \\ \dot{M} = 0 \text{ at } s = S_0 \ . \end{array} \tag{5.70}$$

Multiplying the differential equation (5.70) by M and the differential equation in (5.66) by $\dot{M}$, integrating over $(0, S_0)$, and subtracting the result of one from the other, we arrive at

$$\dot{\mu}\int_0^{S_0} aM^2 ds = -\lambda\mu \int_0^{S_0} a^{-1} M^2 ds + 3\lambda \int_0^{S_0} aM_s^2 ds - 2g \ . \tag{5.71}$$

Hence, we can state the following proposition.

Proposition: If $\lambda \longmapsto \mu(\lambda)$ is increasing for $\lambda > \bar{\lambda} > 0$ on any interval where it is negative, then it continues to increase monotonically on the interval and the solution λ^* to $\mu(\lambda) = -1$, if it exists, is unique. Moreover, a solution exists in the interval if and only if $\lim_{\lambda \uparrow \lambda^*} \mu(\lambda) < -1$.

5.3 Existence of nonlinear waves of small amplitude

We prove the existence of nontrivial solutions to the linearized problem (5.52). To this end we need to prove that for some $\lambda > 0$ we have $\mu(\lambda) \leq -1$.

Lemma 5. (Location of λ^*) The solution λ^* of $\mu(\lambda^*) = -1$ is unique. Furthermore, $\lambda^* < \lambda_0$.

Proof. We know that

$$S_0 = \max\{s \in [0, S_0]\} \tag{5.72}$$

We set $\lambda = \bar{\lambda}$. Thus, from

$$a(s, \bar{\lambda}) = \sqrt{\bar{\lambda}^2 + 2g(S_0 - s)} = \sqrt{2g}\sqrt{\bar{S} - s}$$

with $\bar{S} = S_0 + \frac{\bar{\lambda}^2}{2g}$, we get

$$a(s, \bar{\lambda}) \leq \sqrt{\bar{\lambda}^2 + 2gS_0}\ , s \in [0, S_0]. \tag{5.73}$$

Define for $k > 1/4$ and $n \geq 1$ the function

$$\varphi_n(s) = \begin{cases} 0, & 0 \leq s \leq s_n, \\ (\bar{S} - s)^k, & s_n \leq s \leq S_0, \end{cases} \tag{5.74}$$

where

$$s_n = \left(\frac{S_0}{n}\right) > 0 \quad . \tag{5.75}$$

Clearly $\varphi_n \in H^1(S_0, 0)$ is such that $\varphi_n(0) = 0$ and $\varphi_n \not\equiv 0$. Hence, we have

$$\begin{aligned}
&\int_0^{S_0} a^3(s, \bar{\lambda})\left(\partial_s \varphi_n(s)\right)^2 ds + \int_0^{S_0} a(s, \bar{\lambda})\varphi_n^2(s) ds \\
&\leq \sqrt{\bar{\lambda}^2 + 2gS_0}\left\{\int_{s_n}^{S_0} a^2(s, \bar{\lambda})k^2(\bar{S} - s)^{2k-2} ds + \int_{s_n}^{S_0} (\bar{S} - s)^{2k} ds\right\} \\
&\leq \sqrt{\bar{\lambda}^2 + 2gS_0}\left\{\int_{s_n}^{S_0} \sqrt{\bar{\lambda}^2 + 2gS_0}\sqrt{2g}(\bar{S} - s)^{1/2}k^2(\bar{S} - s)^{2k-2} ds + \int_{s_n}^{S_0} (\bar{S} - s)^{2k} ds\right\} \\
&= \sqrt{\bar{\lambda}^2 + 2gS_0}\left\{\int_{s_n}^{S_0} \sqrt{\bar{\lambda}^2 + 2gS_0}\sqrt{2g}k^2(\bar{S} - s)^{2k-3/2} ds + \int_{s_n}^{S_0} (\bar{S} - s)^{2k} ds\right\} \quad .
\end{aligned} \tag{5.76}$$

The last expression can be computed explicitly as

$$\begin{aligned}
&\sqrt{\bar{\lambda}^2 + 2gS_0}\left\{\sqrt{\bar{\lambda}^2 + 2gS_0}\sqrt{2g}k^2\left[\frac{(\bar{S} - s_n)^{2k-1/2} - (\bar{S} - S_0)^{2k-1/2}}{2k - 1/2}\right]\right. \\
&\left. + \left[\frac{(\bar{S} - s_n)^{2k+1} - (\bar{S} - S_0)^{2k+1}}{2k + 1}\right]\right\} \\
&= \frac{1}{\bar{\lambda}}a(S_0, \bar{\lambda})\varphi_n^2(S_0)\sqrt{\bar{\lambda}^2 + 2gS_0}\left\{\sqrt{\bar{\lambda}^2 + 2gS_0}\sqrt{2g}\frac{k^2}{2k - 1/2}\right. \\
&\left.\left[\frac{(\bar{S} - s_n)^{2k-1/2}}{(\bar{S} - S_0)^{2k}} - (\bar{S} - S_0)^{-1/2}\right] + \frac{1}{2k + 1}\left[\frac{(\bar{S} - s_n)^{2k+1}}{(\bar{S} - S_0)^{2k}} - (\bar{S} - S_0)\right]\right\}
\end{aligned} \tag{5.77}$$

since $\varphi_n^2(S_0) = (\bar{S} - S_0)^{2k}$. On the other hand, by construction we have

$$\frac{s_n}{S_0} \leq 1 \tag{5.78}$$

while $\lim_{n\to\infty}(\bar{S} - s_n) = \bar{S}$ which can be used in (5.77). We can find a $k > 1/4$ and some integer N such that for some S_0 the following condition holds, i.e.

$$\begin{aligned}
&\frac{1}{\bar{\lambda}}\sqrt{\bar{\lambda}^2 + 2gS_0}\left\{\sqrt{\bar{\lambda}^2 + 2gS_0}\sqrt{2g}\frac{2k^2}{4k-1}\left[(S_0 + \frac{\bar{\lambda}^2}{2g})^{2k-1/2}\frac{(2g)^{2k}}{\bar{\lambda}^{4k}} - \frac{(2g)^{1/2}}{\bar{\lambda}}\right]\right. \\
&\left. + \frac{1}{2k+1}\left[(S_0 + \frac{\bar{\lambda}^2}{2g})^{2k+1}\frac{(2g)^{2k}}{\bar{\lambda}^{4k}} - \frac{\bar{\lambda}^2}{2g}\right]\right\} < 2g\ .
\end{aligned} \tag{5.79}$$

Notice that if we choose $\bar{\lambda} = 2g/\sqrt{3}$ and $k = 1/2$, the condition in (5.79) is precisely the condition in Theorem 2, providing a restriction on maximum flow force S_0. This provides us with φ_n satisfying

$$\int_0^{S_0} a^3(s,\bar{\lambda})\left(\partial_s\varphi_n(s)\right)^2 ds + \int_0^{S_0} a(s,\bar{\lambda})\varphi_n^2(s)ds < 2ga(S_0,\bar{\lambda})\varphi_n^2(S_0)\ . \tag{5.80}$$

To see that $\mu(\lambda_0) = 0$, note that $F(\int_0^s a^{-3}(r,\lambda_0)dr, \lambda_0) = 0$ yields $\mu(\lambda_0) \leq 0$. On the other hand, $\mu(\lambda_0) \geq 0$ since $F(\varphi, \lambda_0) \geq 0$ for any $\varphi \in H^1(0, S_0)$ such that $\varphi(0) = 0$, as

$$\begin{aligned}
2g\lambda_0\varphi^2(S_0) &= 2g\lambda_0\left(\int_0^{S_0}\varphi_s(s)ds\right)^2 \\
&= 2g\lambda_0\left(\int_0^{S_0} a^{3/2}(s,\lambda_0)\varphi_s(s)a^{-3/2}(s,\lambda_0)ds\right)^2 \\
&\leq 2g\lambda_0\left(\int_0^{S_0} a^3(s,\lambda_0)\varphi_s^2(s)ds\right)\left(\int_0^{S_0} a^{-3}(s,\lambda_0)ds\right) \\
&= \int_0^{S_0} a^3(s,\lambda_0)\varphi_s^2(s)ds\ .
\end{aligned} \tag{5.81}$$

Since a depends continuously on λ, the inequality in (5.80) ensures that $F(\varphi_n, \lambda) = -1$ for some $\lambda > \bar{\lambda}$. At this specific λ we have $\mu(\lambda) = -1$.

□

6 Setting for local bifurcation

We now apply the Crandall-Rabinowitz theorem on bifurcation from a simple eigenvalue.

Let $T = \{(q,s) : q \in [-\pi,\pi], s = S_0\}$ be the top, and $B = \{(q,s) : q \in [-\pi,\pi], s = 0\}$ be the bottom, of the closed rectangular domain $\bar{R}_s$ in order to check that Crandall-Rabinowitz theorem can be applied in our setting.

We define the Banach spaces

$$X = \{w \in C^{2,\alpha}_{per}(\bar{R}_s) : w = 0 \ \text{ on } \ B\}$$

and

$$Y = C^{0,\alpha}_{per}(\bar{R}_s) \times C^{1,\alpha}_{per}(T)\ .$$

The subscript 'per' refers to 2π-periodicity and even in $q-$variable. If $H(s,\lambda)$ is the laminar flow, set

$$h(q,s) = H(s,\lambda) + w(q,s)$$

with $w \in X$ and we write the following set of equations

$$
\begin{aligned}
(1+h_q^2)h_{ss} - 2h_s h_q h_{sq} + h_s^2 h_{qq} = gh_s^3 \ \text{ in } \ 0 < s < S_0 \\
(1+h_q^2) + (2gh - Q)h_s = 0 \ \text{ on } \ s = S_0 \\
h = 0 \ \text{ on } \ s = 0
\end{aligned}
\tag{6.82}
$$

in an operator form

$$\mathcal{F}(\lambda, w) = 0 \ \text{ with } \ w \in X$$

where $\mathcal{F} : (0, \infty) \times X \to Y$ is given by

$$\mathcal{F} = (\mathcal{F}_1, \mathcal{F}_2) \ \text{ with}$$

$$\mathcal{F}_1(\lambda, w) = (1+w_q^2)(H_{ss} + w_{ss}) - 2w_q(H_s + w_s)w_{sq} + (H_s + w_s)^2 w_{qq} - g(H_s + w_s)^3$$

and

$$\mathcal{F}_2(\lambda, w) = (1 + w_q^2 + [2g(H+w) - Q](H_s + w_s))|_T \ .$$

By the equation for laminar flow satisfied by H, we have

$$\mathcal{F}(\lambda, 0) = 0 \ \text{ with } \ \forall \ \ \lambda > 0$$

The linearized operator $\mathcal{F}_w = (\mathcal{F}_{1w}, \mathcal{F}_{2w})$ at $w = 0$ is given by

$$
\begin{aligned}
\mathcal{F}_{1w}(\lambda, 0) = \partial_s^2 + H_s^2 \partial_q^2 - 3gH_s^2 \partial_s \ \text{ in } \ R_s \\
\mathcal{F}_{2w}(\lambda, 0) = \left(2\lambda^{-1} g - \lambda \partial_s\right)\big|_T \ .
\end{aligned}
\tag{6.83}
$$

The linear eigenvalue problem

$$
\begin{aligned}
(a^3 M_s)_s = -\mu a M \ \text{ in } \ (0, S_0) \\
a^2 M_s = 2gM \ \text{ on } \ s = S_0 \\
M = 0 \ \text{ on } \ s = 0
\end{aligned}
\tag{6.84}
$$

with $\mu = -1$, expresses the fact that the function $M(s)\cos(q)$ belongs to the null space of $\mathcal{F}_w(\lambda, 0)$.

6.1 Null space

Lemma 6. For $\lambda = \lambda^*$, the solution space of (5.52) is one-dimensional. Equivalently, the null space of $\mathcal{F}_w(\lambda^*, 0)$ is one-dimensional.

Proof. We know that there is a unique $\lambda^* > 0$ with $\mu(\lambda^*) = -1$ so that the null space $ker\{\mathcal{F}_w(\lambda^*, 0)\}$ contains at least one element $w(q, s) = M(s)\cos(q)$, where $M \in C^{3,\alpha}[0, S_0]$ is the unique eigenfunction of (5.66) corresponding to the eigenvalue $\mu(\lambda^*) = -1$, normalized by $M(S_0) = 1$. The null space is one-dimensional. If $m \in C^{3,\alpha}_{per}(\bar{R}_s)$ belongs to the null space, then we proved before that its Fourier coefficients m_k satisfy (5.56) so that $m_1(s)$ is a constant multiple of $M(s)$. Further, if $m_k \not\equiv 0$ for some $k \geq 2$, then we would have

$$\frac{-2ga(S_0)m_k^2(S_0) + \int_0^{S_0} a^3(\partial_s m_k)^2 ds}{\int_0^{S_0} a m_k^2 ds} = -k^2 < -1. \tag{6.85}$$

This contradicts the fact that a minimum is attained corresponding to $\mu(\lambda^*) = -1$. As for m_0, from the differential equation and from the boundary condition at $s = 0$ in (5.56) with $k = 0$ we get

$$m_0(s) = A_0 \int_0^s a^{-3}(r, \lambda^*) dr, s \in [0, S_0], \tag{6.86}$$

for some $A_0 \in \mathbb{R}$, and the boundary condition at $s = S_0$ yields $A_0 = 0$ unless

$$\frac{1}{2g} = \lambda^* \int_0^{S_0} a^{-3}(s, \lambda^*) ds \tag{6.87}$$

which is impossible. The last relation is the defining condition of λ_0 as the point where, in the context of laminar flows, the strictly convex function $\lambda \mapsto Q(\lambda)$ attains its minimum. However,

$$\lambda^* < \lambda_0, \tag{6.88}$$

by the monotonicity property of $\mu(\lambda)$ and the fact that $\mu(\lambda^*) = -1$ while $\mu(\lambda_0) = 0$. □

6.2 The range

The operator $\mathcal{F}_w(\lambda^*, 0) : X \to Y$ has a closed range of codimension one. This is ensured by proving the following lemma.

Lemma 7. The pair $(\mathcal{A}, \mathcal{B}) \in Y$ belongs to the range of the linear operator $F_w(\lambda^*, 0)$ if and only if it satisfies the orthogonality condition

$$\int\int_{R_s} \mathcal{A}(q, s) a^3(s, \lambda^*) \varphi^*(q, s) dq ds + \int_T \mathcal{B}(q) a^2(S_0, \lambda^*) \varphi^*(q, s) dq = 0, \tag{6.89}$$

where

$$\varphi^*(q, s) = M(s) \cos(q) \in X \tag{6.90}$$

generates the null space $ker\{\mathcal{F}_w(\lambda^*, 0)\}$.

Proof. Assuming the validity of the characterization (6.89), the range $\mathcal{R}(\mathcal{F}(\lambda^*, 0))$ is clearly closed in Y. Notice that $\lambda^* > 0$. On the other hand, $a(s, \lambda^*) > 0$ for $s \in [0, S_0]$ and $F(M, \lambda^*) = -1$ ensure $M(0) \neq 0$. Since $a(S_0, \lambda^*) = \lambda^*$, we deduce from (6.89) that $(0, \cos(q)) \notin \mathcal{R}(\mathcal{F}_w(\lambda^*, 0))$. Notice that if $(\mathcal{A}_1, \mathcal{B}_1), (\mathcal{A}_2, \mathcal{B}_2) \in Y \backslash \mathcal{R}(\mathcal{F}_w(\lambda^*, 0))$, then

$$(\mathcal{A}_1, \mathcal{B}_1) - c(\mathcal{A}_2, \mathcal{B}_2) \in \mathcal{R}(\mathcal{F}_w(\lambda^*, 0)) \tag{6.91}$$

for

$$c = \frac{\int\int_R \mathcal{A}_1 a^3 \varphi^* dq dp + \int_T \mathcal{B}_1 a^2 \varphi^* dq}{\int\int_R \mathcal{A}_2 a^3 \varphi^* dq dp + \int_T \mathcal{B}_2 a^2 \varphi^* dq}, \tag{6.92}$$

with a nonzero denominator as $(\mathcal{A}_2, \mathcal{B}_2) \notin \mathcal{R}(\mathcal{F}_w(\lambda^*, 0))$. Therefore, the Banach space $Y/\mathcal{R}(\mathcal{F}_w(\lambda^*, 0))$ is one-dimensional, so $\mathcal{R}(\mathcal{F}_w(\lambda^*, 0))$ has codimension one.

As for the necessity of (6.89), if $\mathcal{F}_w(\lambda^*, 0)\varphi = (\mathcal{A}, \mathcal{B})$, then multiplying the partial differential equation

$$\mathcal{A} = \mathcal{F}_{1w}(\lambda^*, 0)\varphi = \varphi_{ss} + H_s^2 \varphi_{qq} - 3g H_s^2 \varphi_s \tag{6.93}$$

by $a^3 \varphi^*$, integrating by parts, and using the fact that

$$\mathcal{B} = \mathcal{F}_{2w}(\lambda^*, 0)\varphi = \Big(2\frac{g}{\lambda^*}\varphi - \lambda^* \varphi_s\Big)\Big|_T \tag{6.94}$$

in combination with $\mathcal{F}_w(\lambda^*,0)\varphi^*=0$ and $H_s=a^{-1}$, we get (6.89).

The proof of the sufficiency of (6.89) is technically more intricate. To ensure a coercivity condition, let us introduce the closed subspaces

$$
\begin{aligned}
X_0 &= \left\{\phi \in X : \int_{-\pi}^{\pi} \phi(q,s)dq = 0 \ \text{ for all } \ s\in[0,S-0]\right\} \subset X,\\
Y_0 &= \left\{(\mathcal{A},\mathcal{B}) \in Y : \int_{-\pi}^{\pi} \mathcal{A}(q,s)dq = 0 \ \text{ for all } \ s\in[0,S_0], \int_T \mathcal{B}dq = 0\right\} \subset Y.
\end{aligned}
$$

The following relations hold

$$
H_s = a^{-1}, a_s = -ga^{-1}, a(S_0) = \lambda^* \; . \tag{6.95}
$$

Hence, given $(\mathcal{A},\mathcal{B})\in Y$ such that (6.89) holds, and on using (6.83), we observe that $\mathcal{F}_w(0,\lambda^*)\phi=(\mathcal{A},\mathcal{B})$ for some $\phi\in X$ if and only if

$$
\begin{cases}
(a^3\partial_s\phi_0)_s = a^3\mathcal{A}_0 \ \text{ in } \ (0,S_0),\\
2ga\phi_0 - a^3\partial_s\phi_0 = a^2\mathcal{B}_0 \ \text{ at } \ s=S_0,\\
\phi_0 = 0 \ \text{ at } \ s=0
\end{cases} \tag{6.96}
$$

and

$$
\begin{cases}
(a^3\varphi_s)_s + a\varphi_{qq} = a^3(\mathcal{A}-\mathcal{A}_0) \ \text{ in } \ R_s,\\
2ga\varphi - a^3\varphi_s = a^2(\mathcal{B}-\mathcal{B}_0) \ \text{ on } \ T,\\
\varphi = 0 \ \text{ on } \ B
\end{cases} \tag{6.97}
$$

for

$$
\varphi = \phi - \phi_0 \in X_0, (\mathcal{A}-\mathcal{A}_0, \mathcal{B}-\mathcal{B}_0) \in Y_0, \tag{6.98}
$$

where $\mathcal{B}_0\in\mathbb{R}, \phi_0\in C^{3,\alpha}[0,S_0]$, $\mathcal{A}_0\in C^{1,\alpha}[0,S_0]$ are given by

$$
\mathcal{B}_0 = \frac{1}{2\pi}\int_T \mathcal{B}dq, \phi_0(s) = \frac{1}{2\pi}\int_{-\pi}^{\pi}\phi(q,s)dq, \mathcal{A}_0(s) = \frac{1}{2\pi}\int_{-\pi}^{\pi}\mathcal{A}(q,s)dq. \tag{6.99}
$$

Claim 1. For any $(\mathcal{A},\mathcal{B})\in C^{1,\alpha}[0,S_0]\times\mathbb{R}$ the problem (6.96) has a unique solution $\phi_0\in C^{3,\alpha}[0,S_0]$.

From the differential equation in (6.96) we infer that

$$
a^3(s)\phi_0'(s) = C + \int_0^s a^3(s,\lambda^*)\mathcal{A}_0(r)dr, s\in[0,S_0], \tag{6.100}
$$

for some constant $C\in\mathbb{R}$. Therefore, the boundary condition at $s=0$ yields

$$
\phi_0(s) = C\int_0^s a^{-3}(r,\lambda^*)dr + \int_0^s a^{-3}(r,\lambda^*)\left(\int_0^r a^3(\tau,\lambda^*)\mathcal{A}_0(\tau)d\tau\right)dr, \quad s\in[0,S_0]. \tag{6.101}
$$

The boundary condition at $s=S_0$ becomes

$$
\begin{aligned}
&C\left\{1-2g\lambda^*\int_0^{S_0} a^{-3}(s,\lambda^*)ds\right\}\\
&= 2g\lambda^*\int_0^{S_0} a^{-3}(s,\lambda^*)\left(\int_0^s a^3(\tau,\lambda^*)\mathcal{A}_0(\tau)d\tau\right)ds\\
&- \int_0^{S_0} a^3(\tau,\lambda^*)\mathcal{A}_0(\tau)d\tau - a^2(S_0,\lambda^*)\mathcal{B}_0.
\end{aligned} \tag{6.102}
$$

We have already proved (in the analysis of the null space) that

$$\frac{1}{2g} = \lambda^* \int_0^{S_0} a^{-3}(s, \lambda_0) ds < \lambda^* \int_0^{S_0} a^{-3}(s, \lambda^*) ds. \tag{6.103}$$

Consequently, the constant C is always uniquely determined and Claim 1 is proved.

The above considerations reduce the proof of the sufficiency of (6.89) to showing that if (6.89) holds, then (6.97) has a solution $\varphi \in X_0$. Notice that both integrals in (6.89) vanish if they are evaluated on $\mathcal{A}_0$, respectively, $\mathcal{B}_0$. Consequently, we have to prove that if $(\mathcal{A}_0, \mathcal{B}_0) \in Y_0$ are satisfying (6.89), then (6.97) has a solution $\varphi \in X_0$.

Claim 2. With $a = a(s, \lambda^*)$ and $(\mathcal{A}, \mathcal{B}) \in Y_0$, we claim that for every $\varepsilon \in (0, 1)$ the approximate problem

$$\begin{cases} -\varepsilon a^3 v^{(\varepsilon)} + (1+\varepsilon)\left(a^3 v_s^{(\varepsilon)}\right)_s + (1+\varepsilon) a v_{qq}^{(\varepsilon)} = a^3 \mathcal{A} \ \text{ in } \ R_s, \\ 2gav^{(\varepsilon)} - (1+\varepsilon) a^3 v_s^{(\varepsilon)} = a^2 \mathcal{B} \ \text{ on } \ T, \\ v^{(\varepsilon)} = 0 \ \text{ on } \ B \end{cases} \tag{6.104}$$

has a unique solution $v^{(\varepsilon)} \in X_0$.

To prove this claim we introduce the space

$$\mathbb{H} = \left\{ \varphi \in H^1_{per}(R_s) : \varphi \ \text{ even in } \ q, \int_{-\pi}^{\pi} \varphi(q, s) dq = 0, \ \text{ a.e. in } \ [0, S_0], \varphi = 0 \ \text{ a.e. on } B \right\}. \tag{6.105}$$

Notice that $\varphi \mapsto \int_{-\pi}^{\pi} \varphi(q, s) dq$ is a bounded linear map from $\mathbb{H}^1_{per}(R_s) \subset L^1(R_s)$ to $L^1[0, S_0]$ (by Fubini's theorem). Hence, the trace operator is also bounded from $\mathbb{H}^1_{per}(R_s)$ to $L^2(B)$ ([15]) so that $\mathbb{H}$ is a Hilbert space, being a closed subspace of the Hilbert space $H^1_{per}(R_s)$. A function $\varphi \in \mathbb{H}$ is a weak solution to (6.104) if

$$\begin{aligned} (1+\varepsilon) \int\!\!\int_{R_s} a^3 \varphi_s \phi_p dq ds + (1+\varepsilon) \int\!\!\int_{R_s} a \varphi_q \phi_q ds dq + \varepsilon \int\!\!\int_{R_s} a^3 \varphi \phi dq ds \\ -2g \int_T a \varphi \phi dq = - \int_T \mathcal{B} a^2 \phi dq - \int\!\!\int_{R_s} \mathcal{A} a^3 \phi dq ds \end{aligned} \tag{6.106}$$

for all $\phi \in \mathbb{H}$. For $\varphi \in \mathbb{H} \cap C^{3,\alpha}_{per}(\bar{R}_s)$ we have

$$\varphi(q, s) = \sum_{k=1}^{\infty} \varphi_k(s) \cos(kq) \ \text{ in } \ C^2_{per}(\bar{R}_s), \tag{6.107}$$

with $\varphi_k \in C^3[0, S_0]$ given by

$$\varphi_k(s) = \frac{1}{\pi} \int_{-\pi}^{\pi} \varphi(q, s) \cos(kq) dq, s \in [0, S_0], k \geq 1 \tag{6.108}$$

Clearly $\varphi_k(0) = 0$ for any $k \geq 1$, and

$$\int\!\!\int_{R_s} a^3 \varphi_s^2 dq ds = \pi \sum_{k=1}^{\infty} \int_0^{S_0} a^3 (\partial_s \varphi_k)^2 ds \tag{6.109}$$

while

$$\int\!\!\int_{R_s} a \varphi_q^2 dq ds = \pi \sum_{k=1}^{\infty} k^2 \int_0^{S_0} a \varphi_k ds, \int_T \varphi^2 dq = \pi \sum_{k=1}^{\infty} \varphi_k^2(S_0). \tag{6.110}$$

Taking into account the minimization problem (5.57), we derive that

$$\begin{aligned}\int\int_{R_s} a^3\varphi_s^2 dqds + \int\int_{R_s} a\varphi_q^2 dqds &\geq \pi \sum_{k=1}^{\infty}\int_0^{S_0}\left\{a^3(\partial_s\varphi_k)^2 + a\varphi_k^2\right\} ds \\ &\geq \pi 2g\lambda^* \sum_{k=1}^{\infty}\varphi_k^2(S_0) = 2g\lambda_* \int_T \varphi^2 dq\end{aligned} \tag{6.111}$$

Consequently

$$\int\int_{R_s} a^3\varphi_s^2 dqds + \int\int_{R_s} a\varphi_q^2 dqds \geq 2g\lambda^* \int_T \varphi^2 dq\ . \tag{6.112}$$

Moreover, since $\mathbb{H}\cap C^{3;\alpha}_{per}(\bar{R}_s)$ is dense in $\mathbb{H}$, (6.112) holds for $\varphi\in\mathbb{H}$.

Since $\inf_{s\in[0,S_0]}\{a(s,\lambda^*)\}>0$, using (6.112) we see that the left-hand side of (6.106) defines a bounded and coercive bilinear form in $\mathbb{H}$, while the right-hand side defines a bounded linear functional on $\mathbb{H}$. An application of the Lax-Milgram theorem (see, e.g., [15]) yields the existence and uniqueness of a weak solution $v^{(\varepsilon)}\in\mathbb{H}$ to (6.104). Using standard elliptic regularity theory (see [4]) we conclude that $v^{(\varepsilon)}\in X_0$. Moreover, we have the Schauder estimates (see [Chapter 8][16])

$$||v^{(\varepsilon)}||_{C^{1,\alpha}_{per}(\bar{R}_s)} \leq C\left(||\mathcal{A}||_{C^{0,\alpha}_{per}(\bar{R}_s)} + ||\mathcal{B}||_{C^{1,\alpha}_{per}(T)} + ||v^{(\varepsilon)}||_{L^\infty(R_s)}\right) \tag{6.113}$$

with the constant C depending only on $||a||_{C^{1,\alpha}_{per}(\mathbb{R})}$ and on $\inf_{s\in[0S,0]}\{a(s,\lambda^*)\}$.

Claim 3. If $(\mathcal{A},\mathcal{B})\in Y_0$ satisfy (6.89), then for any sequence $\varepsilon_k\downarrow 0$ the sequence $\{v^{(\epsilon_k)}\}_{k\geq 1}$ is bounded in $C^{1,\alpha}_{per}(\bar{R}_s)$.

The existence of some $\varepsilon_k\downarrow 0$ with $||v^{(\varepsilon_k)}||_{C^{1,\alpha}_{per}(\bar{R}_s)}\to\infty$ implies by (6.113) that $||v^{(\varepsilon_k)}||_{L^\infty(R_s)}\to\infty$. But then (6.113) ensures that the normalized functions

$$v_k = \frac{v^{(\varepsilon_k)}}{||v^{(\varepsilon_k)}||_{L^\infty(R_s)}} \tag{6.114}$$

are bounded in $C^{1;\alpha}_{per}(\bar{R}_s)$. The compact embedding $C^{1;\alpha}_{per}(\bar{R}_s)\subset C^1_{per}(\bar{R}_s)$ enables us to extract a subsequence $\{v_{n_k}\}$ that converges in $C^1_{per}(\bar{R}_s)$ to some v with $||v||_{L^\infty(R_s)}=1$. Now consider (6.106) with $\varepsilon=\varepsilon_{n_k}$ and $\varphi=v^{(\varepsilon_{n_k})}$, divided by $||v^{\varepsilon_k}||_{L^\infty(R_s)}$, and pass to the limit $n_k\to\infty$ to obtain

$$\int\int_{R_s} a^3 v_s\phi_s dqds + \int\int_{R_s} a v_q\phi_q dqds = 2g\int_T av\phi dq, \quad \phi\in\mathbb{H} \tag{6.115}$$

Thus $v\in C^{1,\alpha}_{per}(\bar{R}_s)$ is a weak solution (in $\mathbb{H}$) of the problem

$$\begin{cases} (a^3v_s)_s + av_{qq} = 0 \ \text{ in } \quad R_s, \\ 2gav - a^3v_s = 0 \ \text{ on } \quad T, \\ v = 0 \ \text{ on } \ B\ . \end{cases} \tag{6.116}$$

By elliptic regularity $v\in X_0$. It may be noted that (6.116) is exactly (5.52). So $v\in ker\{\mathcal{F}_w(0,\lambda^*)\}$. Since $ker\{\mathcal{F}_w(0,\lambda^*)\}$ is one-dimensional. The function v can be written as a multiple of $\varphi^*(q,s)=M(s)\cos(q)$, where $M\in C^{3,\alpha}[0,S_0]$ is eigenfunction of (5.66) corresponding to $\mu(\lambda)=-1$, that is,

$$v = \delta\varphi^* \tag{6.117}$$

for some $\delta \in \mathbb{R}$. If $(\mathcal{A}, \mathcal{B}) \in Y_0$ satisfy (6.89), we can infer more about this limit v. We consider (6.106), with $\varepsilon = \varepsilon_{n_k}, \varphi = v^{(\varepsilon_{n_k})}, \phi = \varphi^*$, and perform an integration by parts. Now, using the fact that φ^* solves (6.116) and (6.89) holds true, we arrive at

$$\int\int_{R_s} a^3 \varphi^* v^{(\varepsilon_{n_k})} dqds + 2g \int_T a\varphi^* v^{(\varepsilon_{n_k})} dq = 0 \ . \tag{6.118}$$

Dividing by $||v^{\varepsilon_{n_k}}||_{L^\infty(R_s)}$ and pass to the limit $n_k \to \infty$, we get from the previous relation

$$\int\int_{R_s} a^3 \varphi^* v dqds + 2g \int_T a\varphi^* v dq = 0 \ . \tag{6.119}$$

But then (6.117) forces $v \equiv 0$, which contradicts $||v^{\varepsilon_{n_k}}||_{L^\infty}(R_s) = 1$ and proves Claim 3.

Claim 3 and the compactness of $C^{1,\alpha}_{per}(\bar{R}_s) \subset C^1_{per}(\bar{R}_s)$ yield the existence of a subsequence $\{v^{\epsilon_{n_k}}\}$ converging to some limit w in $C^1_{per}(\bar{R}_s)$. Passing to the limit $n_k \to \infty$ in (6.106) with $\varepsilon = \varepsilon_{n_k}, \varphi = v^{\epsilon_{n_k}}$, we thus obtain that w is a weak solution (in $\mathbb{H}$), and by regularity a classical solution $w \in X_0$, of

$$\begin{cases} (a^3 w_s)_s + a w_{qq} = a^3 \mathcal{A} \ \text{ in } \ R_s, \\ 2gaw - a^3 w_s = a^2 \mathcal{B} \ \text{ on } \ T, \\ w = 0 \ \text{ on } \ B, \end{cases} \tag{6.120}$$

which is exactly (6.97). This completes the proof of the sufficiency of (6.89). □

6.3 The transversality condition: Proof of Theorem 2 (Local Bifurcation)

Proof. In order to ensure that the Crandall–Rabinowitz theorem is applicable, it is sufficient to check the transversality condition

$$[\mathcal{F}_{\lambda w}(\lambda^*, 0)](1, \varphi^*) \notin \mathcal{R}(\mathcal{F}_w(\lambda^*, 0)).$$

Since $a_s = -ga^{-1}$, where $a = a(\cdot, \lambda^*)$, from (6.83) we obtain

$$\mathcal{F}_{\lambda w}(\lambda^*, 0) = -\left(2\lambda a^{-4} \partial_q^2 + 6\lambda a_s a^{-3} \partial_s, \left\{ 2g \left(\frac{1}{\lambda^*} \right)^2 + \partial_s \right\} \Big|_T \right) \ .$$

Based on the characterization of the range $\mathcal{R}(\mathcal{F}_w(\lambda^*, 0))$, it suffices to verify that

$$\int\int_{R_s} a^3 \varphi^* 2\lambda^* \left\{ a^{-4} \varphi^*_{qq} + 3a_s a^{-3} \varphi^*_s \right\} dqds + \int_T \left\{ 2g(\varphi^*)^2 + {\lambda^*}^2 \varphi^* \varphi^*_s \right\} dq \neq 0 \tag{6.121}$$

It may be recalled that

$$\varphi^*(q, s) = M(s) \cos(q) \tag{6.122}$$

With $M \not\equiv 0$ solving (5.66) with $\mu = -1$, and $a(S_0) = \lambda^*$, we have the following

$$\begin{cases} a^3 \varphi^*_{ss} + 3a^2 a_s \varphi^*_s - a\varphi^* = 0 \ \text{ in } \ (0, S_0), \\ {\lambda^*}^2 \varphi^*_s = 2g\varphi^* \ \text{ at } \ s = S_0, \\ \varphi^* = 0 \ \text{ at } \ s = 0, \end{cases} \tag{6.123}$$

Thus we have

$$\begin{aligned} \int\int_{R_s} a_s \varphi^* \varphi^*_s dqds &= \int_T a\varphi^* \varphi^*_s dq - \int\int_{R_s} a\varphi^* \varphi^*_{ss} dqds - \int\int_{R_s} a(\varphi^*_s)^2 dqds \\ &= \int_T a\varphi^* \varphi^*_s dq + \int\int_{R_s} \varphi^* \left(3a_s \varphi^*_s - a^{-1} \varphi^* \right) dqds - \int\int_{R_s} a(\varphi^*_s)^2 dqds \end{aligned}$$

leading to

$$\int\int_{R_s} a_s\varphi^*\varphi^*_s dqds = -\frac{1}{2}\int_T a\varphi^*\varphi^*_s dq + \frac{1}{2}\int\int_{R_s}\left\{a^{-1}(\varphi^*)^2 + a(\varphi^*_s)^2\right\} dqds.$$

Hence we need to show (from (6.121))

$$2\lambda^*\int\int_{R_s} a^{-1}\varphi^*\varphi^*_{qq} dqds + 3\lambda^*\int\int_{R_s}\left\{a^{-1}(\varphi^*)^2 + a(\varphi^*_s)^2\right\} dqds$$
$$+\int_T\left\{2g(\varphi^*)^2 - 2(\lambda^*)^2\varphi^*\varphi^*_s\right\} dq \neq 0\ .$$

Since $a(S_0) = \lambda^*$ and $\varphi^*_{qq} = -\varphi^*$ we deduce that (6.121) equals

$$(\lambda^* - 2g/\sqrt{3})\int\int_{R_s} a^{-1}(\varphi^*)^2 dqds + 3(\lambda^* - 2g/\sqrt{3})\int\int_{R_s}\left\{a(\varphi^*_s)^2\right\} dqds > 0$$

for $\lambda^* > 2g/\sqrt{3}$ on using the boundary condition at $s = S_0$ to evaluate the boundary integral expression. This completes the proof of the transversality condition and of Theorem 2.

□

7 The dispersion relation

We now further proceed to derive the dispersion relation in order to confirm that we are able to recover the classical relation for the irrotational periodic gravity waves. Since for the laminar flow

$$H_s^{-1}(0,\lambda) = (c-u)^2\big|_{\text{at the flat surface}} = \lambda$$

we see that waves of small amplitude occur exactly when the velocity of the laminar flows reaches the critical speed $\sqrt{\lambda^*}$ at the flat surface.

The problem (5.66) with $\mu = -1$ becomes

$$\begin{cases} (a^3M_s)_s = aM \quad \text{on} \quad (0, S_0), \\ M_s = 2g\lambda^{-2}M \quad \text{at} \quad s = S_0, \\ M = 0 \quad \text{at} \quad s = 0\ . \end{cases} \tag{7.124}$$

With $M(s)$ assumed to be of the form

$$M(s) = \frac{1}{\sqrt{\lambda^2 + 2g(S_0 - s)}}.M_0\left(\frac{\sqrt{\lambda^2 + 2g(S_0 - s)}}{g}\right)\ , \tag{7.125}$$

we obtain

$$M_0'' = M_0\ . \tag{7.126}$$

from (7.124). Thus, the general solution of the differential equation in (7.124) with the boundary condition at $s = 0$ is

$$M(s) = \delta\frac{1}{\sqrt{\lambda^2 + 2g(S_0 - s)}}\sinh\left(\frac{\sqrt{\lambda^2 + 2g(S_0 - s)} - \sqrt{\lambda^2 + 2gS_0}}{g}\right)$$

with $\delta \in \mathbb{R}$. For $\delta \neq 0$ the boundary condition at $s = S_0$ is equivalent to the implicit equation

$$\lambda + g\tanh\left(\frac{\lambda - \sqrt{\lambda^2 + 2gS_0}}{g}\right) = 0. \tag{7.127}$$

As a function of λ, the left-hand side can be easily seen to be a strictly increasing function from $(0, \infty)$ onto $(-g \tanh\left(\sqrt{\frac{2S_0}{g}}\right), \infty)$, so that $\lambda^* > 0$ is its unique root. We can compute λ^* explicitly in terms of the flow force S_0 of the laminar water flow at which bifurcation occurs. In terms of the the physical variables we get the uniform current

$$(c - u(x,y))^2 \equiv \lambda^*, v(x,y) \equiv 0, -d \leq y \leq 0. \tag{7.128}$$

Now, from the definition of the flow force variable, we have

$$S_0 = \int_{-d}^{0} \left[-yg + (u(x,y) - c)^2\right] dy \tag{7.129}$$

which yields

$$S_0 = \lambda^* d + \frac{gd^2}{2} \ , \tag{7.130}$$

leading to the relevant solution of d from the quadratic equation as

$$d = \frac{-\lambda^* + \sqrt{{\lambda^*}^2 + 2gS_0}}{g} > 0 \ . \tag{7.131}$$

Hence, the dispersion relation for 2π-periodic irrotational gravity water waves with a flow force S_0 becomes

$$(c - u)|_{\mathrm{attheflatsurface}} = \sqrt{g \tanh(d)} \ , \tag{7.132}$$

which is precisely the dispersion relation for the irrotational periodic gravity waves over a flat bed of depth d.

8 Uniform currents

Since we have considered the irrotational case in our analysis, the case with uniform currents satisfying the condition that the current speed k, is less than wave speed c, can be treated in a similar way (see [2]); and the analyses carried out and the results derived hold.

References

[1] C.J. Amick, J. F. Toland. On periodic water-waves and their convergence to solitary waves in the long-wave limit. *Phil. Trans. Roy. Soc. London A*, 303(1481):633–669, 1981.

[2] B. Basu. Irrotational two-dimensional free-surface steady water flows over a flat bed with underlying currents. *Nonlinear Anal. TMA*, 147:110–124, 2016.

[3] T.B. Benjamin, M.J. Lighthill. On cnoidal waves and bores. *Proc. R. Soc. London A*, 224:448–460, 1954.

[4] H. Brézis. *Functional Analysis, Sobolev Spaces and Partial Differential Equations* Springer, New York, 2011.

[5] A. Constantin. *Nonlinear water waves with applications to wave-current interactions and tsunamis*, CBMS-NSF Conf. Ser. in Appl. Math. vol. 81. SIAM, Philadelphia, 2011.

[6] A. Constantin, J. Escher. Symmetry of steady deep-water waves with vorticity. *Eur. J. Appl. Math.*, 15(6):755–768, 2004.

[7] A. Constantin, J. Escher. Symmetry of steady periodic surface water waves with vorticity. *J. Fluid Mech.*, 498:171–181, 2004.

[8] A. Constantin, J. Escher. Analyticity of periodic traveling free surface water waves with vorticity. *Annals of Mathematics*, 173(1):559–568, 2011.

[9] A. Constantin, W. Strauss. Exact steady periodic water waves with vorticity. *Comm. Pure Appl. Math.*, 57(4):481–527, 2004.

[10] A. Constantin, W. Strauss. Stability properties of steady water waves with vorticity. *Comm. Pure Appl. Math.*, 60(6):911–950, 2007.

[11] A. Constantin, W. Strauss. Periodic traveling gravity water waves with discontinuous vorticity. *Arch. Ration. Mech. Anal.*, 202(1):133–175, 2011.

[12] A. Constantin, E. Varvaruca. Steady periodic water waves with constant vorticity: Regularity and local bifurcation. *Arch. Ration. Mech. Anal.*, 199(1):33–67, 2011.

[13] A. Constantin, M. Ehrnström, E. Wahlén. Symmetry of steady periodic gravity water waves with vorticity. *Duke Math. J.*, 140(3):591–603, 2007.

[14] A. Constantin, D. Sattinger, W. Strauss. Variational formulations for steady water waves with vorticity. *J. Fluid Mech.*, 548:151–163, 2006.

[15] L.C.Evans. *Partial Differential Equations* Amer. Math. Soc., Providence, RI, 1998.

[16] D.Gilbarg, N.S.Trudinger. *Elliptic Partial Differential Equations of Second Order* Springer-Verlag, Berlin, 2001.

[17] D. Henry. Large amplitude steady periodic waves for fixed-depth rotational flows. *Comm. Partial Differential Equations*, 38:1015–1037, 2013.

[18] D. Henry. Steady periodic waves bifurcating for fixed-depth rotational flows. *Quart. Appl. Maths.*, 71:455–487, 2013.

[19] G. Keady, J. Norbury. On the existence theory for irrotational water waves. *Math. Proc. Cambridge Phil. Soc.*, 83:137–157, 1978.

[20] G. Keady, J. Norbury. Waves and conjugate streams with vorticity. *Mathematika*, 25:129–150, 1978.

[21] J. Ko, W. Strauss. Effect of vorticity on steady water waves. *J. Fluid Mech.*, 608:197–215, 2008.

[22] J. Ko, W. Strauss. Large-amplitude steady rotational water waves. *Eur. J. Mech.-B/Fluids*, 27(2):96–109, 2008.

[23] V.Kozlov, N. Kuznetsov, E. Lokharu. On the Benjamin–Lighthill conjecture for water waves with vorticity. *J. Fluid Mech.*, 825:961–1001, 2017.

[24] Y.P.Krasovskii. On the theory of steady-state waves of finite amplitude. *U.S.S.R. Comp. Math. and Math. Phys.*, 1:996–1618, 1961.

[25] T.Levi-Civita. Determinazione rigorosa delle onde irrotazionali periodiche in acqua profonda. *Rend. Acad. Lincei.*, 33:141–150, 1924.

[26] J.B.McLeod. Stokes and Krasovskii's conjectures for the wave of greatest height. *Stud. Appl. Maths.*, 98(4):311–334, 1980.

[27] A.I. Nekrasov. On steady waves. *Izv. Ivanovo-Voznesensk*, 3:52–65, 1921.

[28] G.G. Stokes. On the theory of oscillating waves. *Trans. Camb. Phil. Soc.*. 8: 441-445, 1847.

[29] D.J. Stuik. Détermination rigoureuse des ondes irrotationelles périodiques dans un canal à profondeur finie. *Mathematische Annalen.* 95(1): 595–634, 1926.

[30] J. F. Toland. Stokes waves. *Topol. Methods Nonlinear Anal.*, 7(1):1–48, 1996.

[31] S. Walsh. Stratified steady periodic water waves. *SIAM J. Math. Anal.*, 41(3):1054–1105, 2009.

[32] S. Walsh. Steady stratified periodic gravity waves with surface tension II: Global bifurcation. *Discr. Cont. Dyn. Sys. Ser. A*, 8:3241–3285, 2014.

Some numerical investigations into a nonlinear three-dimensional model of the Pacific equatorial ocean flows

Biswajit Basu

Deep Sea Part II, 160, 7-15, 2019

Abstract

This study focusses on some numerical investigations into a recently developed nonlinear, three-dimensional Pacific equatorial undercurrent model. The development of the model has been motivated by observations and the model is able to capture some essential properties of the flow in Pacific equatorial region. The present investigation verifies some of the results related to single and multiple cellular flow structures obtained from the theoretical model by carrying out numerical investigations and further explores additional features that may be present. In addition to streamlines, to examine the flow behavior, velocity amplitude maps have also been obtained. The maps assess the relative strength of the flow in the individual cells. Numerical results indicate that the flow configuration evolves along the line of the Equator as evidenced from streamlines and velocity maps.

1 Introduction

Equatorial ocean dynamics present some rich features pertaining to waves and ocean currents [35]. Presence of equatorial undercurrents is its hallmark. Since the observation of these undercurrents in 1950s by Cromwell, several investigations have been carried out [28]. Although significant progress has been made to explain its observed features, primarily based on linear theory, there are still a number of other aspects which are yet to be resolved. This calls for development of suitable nonlinear theories as the ocean dynamics is essentially three-dimensional and nonlinear [12].

1.1 Equatorial current and dynamics

The apparent lack of features of the surface equatorial currents in contrast to the gyres of the mid-latitudes is deceptive. Equatorial Under Currents (EUCs) are driven across basins and in conjunction with thermocline is also the cause of the dramatic El-Niño variability. The presence of strong currents in the Pacific equatorial region is well established and they play a major role in the equatorial ocean dynamics [28]. The main characteristics of the equatorial dynamics are:

(1) A shallow westward surface current (typically within the top 50 m depth), which is mainly confined to a few degrees on either side of the equator.

(2) A strong coherent eastward undercurrent, which is much faster in speed compared to the surface current. This is primarily responsible for the vertically integrated transport. Beneath this undercurrent, the flow is relatively weak.

(3) Flow in the westward direction on either side of the Equatorial Under Current (EUC), with eastward countercurrents poleward of this. This current is strongest in the Northern hemisphere and reaches the surface.

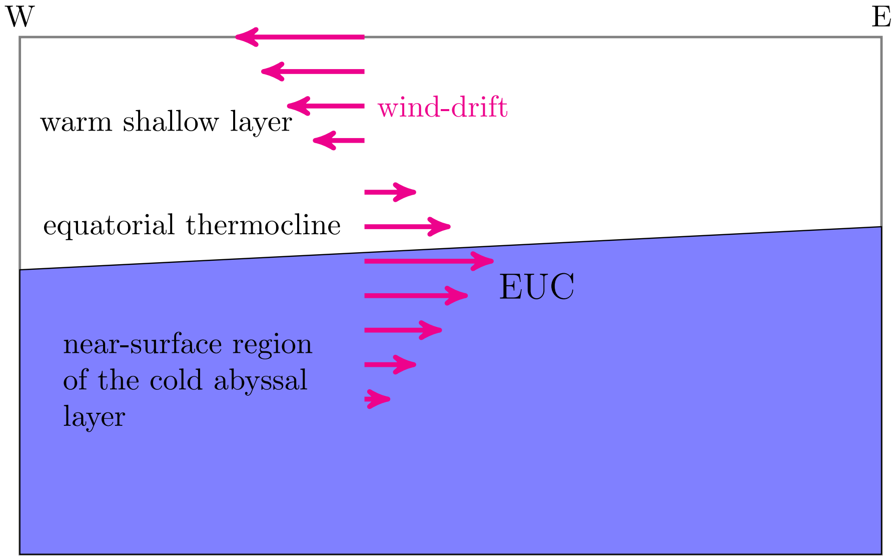

Figure 1: Schematic of equatorial flow in Pacific.

The flow structure is nonlinear and complex with regions of upwelling and downwelling superimposed on the EUC. This makes the flow three dimensional rising to the surface, though the upwelling may be restricted to certain specific zones. As a consequence, while flow at the surface moves predominantly to the west driven by wind, and some flows moving to the north or to the south, farther down little is known about flow structures [20, 21, 22]. Based on observations, the following describes the basic flow patterns (Fig. 1).

Close to the equator the meridional component of the Coriolis force is negligible (vanishing at the equator), and geostrophy breaks down; in these ocean regions the flow is basically wind-driven: by the easterly trade winds in the Pacific and Atlantic, and by the seasonally reversing monsoonal winds in the Indian Ocean (see the discussion in [33]). In addition, due to the breakdown of the geostropic balance in the equatorial region [24] frequency-scale separation between slow potential vortex dynamics and gravity induced fast oscillatory effects is not possible. In fact, the vanishing of the meridional component of the Coriolis force has the effect of the equator working as a natural (fictitous) boundary forcing azimuthal flow propagation [14].

Further, there is pronounced stratification in the equatorial region (about 150 km on either side) near the surface where a pycnocline/thermocline exists. This stratification present in the equatorial ocean region is greater than anywhere else in the ocean (see [14]). There is a separation of warm water with less density from a deeper layer of colder, denser water. The difference in density across this line is small and is about 0.5%.

1.2 El-Niño

El-Niño phenomenon, one of the most dramatic effects of oceanic flows on climate variability, is the aperiodic warming of the sea surface in the eastern equatorial Pacific. The interval between the two warm events are irregular (typically ranging between two to seven years). El-Niño is also associated with the weakening of the trade winds and eastward shift of the region of convection, measured by the pressure difference between

Darwin and Tahiti, and is known as the the Southern Oscillation. The two together are known as El-Niño-Southern Oscillation (ENSO). The phenomenon of El-Niño has a counterpart La Niña, which is an anomolous, weaker warming of the western equatorial Pacific. Among others, the interaction of the equatorial flows, especially the undercurrents with the thermoclines leading to upwelling of water is the cause of El-Niño events. The nonlinear, three-dimensional model proposed by [9] for the Pacific Equatorial Undercurrent and thermocline provides information about and explains some of the observed complex flow structures which are believed to contribute to the El-Niño phenomenon. Following this nonlinear three-dimensional model, further numerical investigations have been carried out in this paper to explore the complex flow structures in more detail and to see if additional insights can be obtained. Particular attention is given to the presence of the multi-cellular flow structures in the vertical plane perpendicular to the zonal plane. In fact, the variability (irregular oscillation) in the El-Niño effects could also be in part attributed to the presence of complex nonlinear, three-dimensional oceanic flow with possible local multi-cellular structures of upwelling and downwelling, supplementing the natural stochastic uncertainty of the atmosphere on shorter time scales.

1.3 Models of undercurrent

Undercurrents play a significant role in the Pacific equatorial dynamics [25, 28, 11, 8]. Various aspects of undercurrents such as termination, source, divergence and upwelling [23, 34, 20] have been the focus of research in the last few decades. Measurements and obeservations have been the basis of modelling the nature of undercurrents and discussions on modelling are available in the literature [28, 35]. Recent studies using global models have also shown that the Pacific EUC will strengthen in future [13] which then is expected to have profound influence on equatorial ocean dynamics.

The simplest model of the EUC consists of a homogeneous fluid subject to uniform westward stress at the surface. This local model in a rudimentary form is unstratified and can be further developed to account for the effect of horizontal viscosity. More realistic models can also consider effects of stratification leading to a layered model of undercurrents. Other non-local and physical models involve a pressure head which acts on the undercurrent and has an extra-equatorial origin. Observations indicate that some of the water in the EUC flows from sub-tropical gyres as the temperature in the core of the undercurrent ranges between $16 - 22^0$ C, much lower than the surface equatorial temperatures except at the eastern end of the ocean basin where the undercurrent ends. A two layer inertial model of undercurrents can account for equatorial and extra-equatorial dynamics and aspects of vorticity.

Local theories of undercurrents were initiated by [10] and were developed further [32, 36, 31]. Other linear non-dissipative models can be found in [16, 17, 29]. Significant extensions to linear models including effects of continuous stratification are due to [26]. Some nonlinear models have also been developed [3, 1, 2, 29]. Inertial theories began with the work of [15] and were further advanced by [30]. [27] reconciled the inertial approach with the local perspective who considered the EUC as a part of a larger and more complex subtropical current system, with both local and inertial effects. However, in order to have a complete model of the integrated dynamics one has to resort to numerical approaches.

While the basic depth variation of the azimuthal flow of the EUC can be modelled in the spherical geometry of a rotating Earth [7], to capture the fine structure it is advantageous to rely on the familiar beta-plane approximation. Explicit solutions to the nonlinear governing equations in the equatorial beta-plane, without recourse to further approximations of any sort, were recently obtained in the Lagrangian framework [4, 6, 5, 18, 19], but these are realistic representations of the flow only for the region near the surface and in the neighbourhood of the thermocline, respectively, and they do not cope satisfactorily with the entire vertical extent of the equatorial flow due to the limitations on the permissible underlying currents.

Recently, [9] have proposed a systematic approach which is mathematically consistent capturing the essential properties of the nature of flow observed in the Pacific EUC. The model is based on fundamentals of fluid dynamics and is non-linear and three dimensional. The analytical model refrains from oversimplification leading to linear models. The model, for example, accounts for the Coriolis effects due to the rotation of the Earth and non-traditional terms arising in the formulation are not ignored. The model is based on the assumption that the two-layer flow in the equatorial direction evolves slowly. Asymptotic solutions have been developed for the model.

Inspired by the Constantin-Johnson model, this study investigates the model further based on numerical simulations. The intention is to numerically examine the structures such as cellular flows, both single and multiple; carry out numerical investigation to see the influence of the small parameter approximation of the non-dimensional rotational speed in the asymptotic solutions and finally explore in further detail if the numerical simulations indicate the existence of any other structures or features in the flow field.

2 Theory

2.1 Governing equations

A co-ordinate system that rotates with the Earth is chosen, with $\bar{x}$ axis pointing towards east, $\bar{y}$ axis pointing towards north and $\bar{z}$ pointing vertically upwards (see Fig. 2). It should be noted that this description of co-ordinate system is associated with tangent plane approximation and also consistent with the β-plane approximation.

The two set of governing equations (Euler equations and conservation equations) may be written as

$$\frac{D\bar{\mathbf{u}}}{D\bar{t}} + 2\bar{\mathbf{\Omega}} \times \bar{\mathbf{u}} = -\frac{1}{\bar{\rho}}\bar{\nabla}\bar{p} + \bar{\mathbf{F}} \quad , \bar{\nabla} \cdot \bar{\mathbf{u}} = 0 \quad ,$$

where $\bar{\mathbf{u}} = (\bar{u}, \bar{v}, \bar{w})$ is the velocity of the fluid at $\bar{\mathbf{x}}$ at time $\bar{t}$. The operator $D/D\bar{t}$ is the material derivative, while $\bar{p}$ and $\bar{\rho}$ are the pressure and the (constant) density, respectively. The body force is represented by $\bar{\mathbf{F}}$ and $\bar{\mathbf{\Omega}} = \bar{\Omega}(0, \cos\theta, \sin\theta)$ is the angular velocity vector decsribing the rotation of the Earth with $|\bar{\mathbf{\Omega}}| = \bar{\Omega} \approx 7.29 \times 10^{-5}$ rads^{-1} and θ the angle of latitude. Under suitable approximation of the Coriolis term close to the equator and the assumption of slow variation of the flow along the equator the following formulation has been developed by [9].

2.2 Nondimensionalized equations with a slow scale of evolution

For a suitable nondimensionalisation of the variables, we write

$$\begin{aligned}
\mathbf{x} &= (\bar{x}, \bar{y}, \bar{z}) = (\bar{L}x, \bar{l}y, \bar{h}z) \ , \\
\mathbf{u} &= (\bar{u}, \bar{v}, \bar{w}) = \bar{U}\Big(u, \frac{\bar{l}}{\bar{L}}v, \frac{\bar{h}}{\bar{L}}w\Big), \\
\bar{p} &= \bar{\rho}_0 \bar{U}^2 p \ ,
\end{aligned}$$

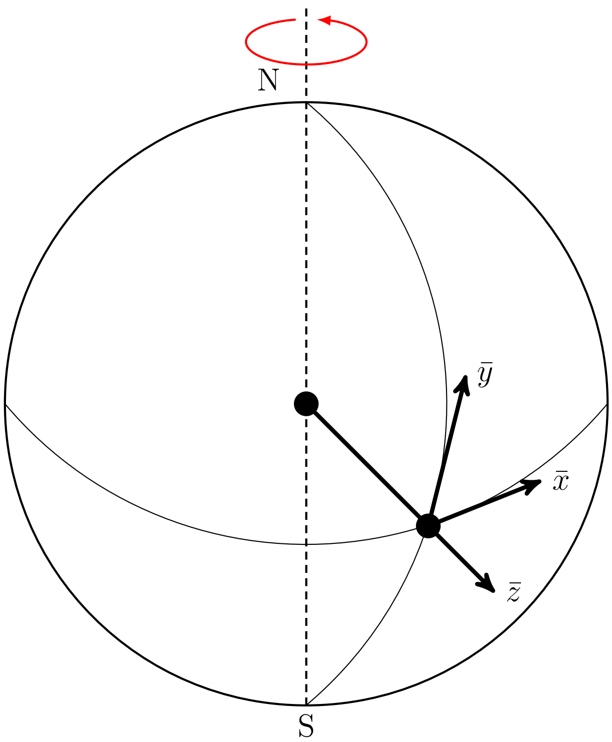

Figure 2: The rotating frame of reference for the Earth with the North pole, South pole and the Equator indicated (as well as the rotation direction around the polar axis).

where the length scales are $\bar{L}, \bar{l}, \bar{h}$; $\bar{U}$ is an appropriate speed scale and $\bar{\rho_0} \approx 1027$ kg m^{-3} an average constant density of the ocean. The pressure is measured relative to the ambient hydrostatic pressure by setting

$$p(x, y, z) = \frac{-\bar{g}\bar{h}}{\bar{u}^2} z + P(x, y, z) \ .$$

where $\bar{g}$ is the acceleration due to gravity. The size of some of the parameters involved in the formulation has been taken guided by the flow associated with the Pacific equator. The length is about 13×10^3 km, the typical value of the depth to the bottom of EUC is about 200 m and the width is about 300 km. With these values as mentioned, and with a speed scale of $\bar{U} = 0.5 \ \ ms^{-1}$ (a typical speed at the surface), the non-dimensional parameter $\omega = \bar{\Omega}\bar{h}/\bar{U} \approx 0.03$.

The governing equations invoking the limiting process described by $(\bar{h}/\bar{L})^2 \to 0$ with $(\bar{l}/\bar{L})^2 \to 0$ are given by

$$\begin{aligned} &uu_x + vu_y + wu_z + 2\omega(w - yz) = -P_x \ , \\ &2\omega yu = -P_y, \ 2\omega u = P_z \ , \end{aligned} \tag{2.1}$$

$$u_x + v_y + w_z = 0 \tag{2.2}$$

with the boundary conditions

$$\left.\begin{aligned} &P(x, y, z) = P_0(x, y) + \kappa\eta(x, y) \\ &w = u\eta_x + v\eta_y \end{aligned}\right\} \ \text{on} \ \ z = \eta(x, y), \tag{2.3}$$

corresponding to pressure and a kinematic condition at the surface ($z = \eta(x, y)$), and

$$w = uT_x + vT_y \ \ \text{on} \ \ z = T(x, y) \tag{2.4}$$

corresponding to a kinematic condition at the thermocline ($z = T(x, y)$) where, $\omega = \bar{\Omega}\bar{h}/\bar{u}$ and $\kappa = \bar{g}\bar{h}/\bar{u}^2$.

The choice of scale can be interpreted such that in the flow direction $0 \le x \le 1$, with $x = 0$ corresponding to the western end, away from any shorelines and $x = 1$ corresponding to the eastern end. The width is restricted to $-y_0 < y < y_0$ by virtue of β-plane approximation, for suitable finite y_0.

The density of the region above the thermocline is ρ_0 and that of the region below is $(1+\text{r})\rho_0$. The pressure is continuous across the thermocline. The governing equation corresponding to (2.1) and (2.2), and valid below the thermocline, are written with $P/(1 + r)$ instead of P.

An important point to mention is that equations in the formulation contain all the Coriolis contributions associated with the rotation of the Earth. Some studies have revealed that ignoring non-traditional components of the Coriolis force has a significant impact on the equatorial ocean dynamics.

2.3 Constantin-Johnson model

The equations for a simplified three-dimensional nonlinear model under the following three assumptions.

1. small r,
2. free surface and thermocline sitting on planes parallel to tangent plane, and
3. constant pressure on the surface along $y = 0$,

take the form

$$\begin{aligned} uu_x + vu_y + wu_z + 2\omega(w - yz) &= -2\ w\phi_x\ , \\ u_x + v_y + w_z &= 0 \end{aligned} \tag{2.5}$$

with $w = yz$ on $z = \frac{1}{2}y^2$ and $w = -ut'$ on $z = -t(x) + \frac{1}{2}y^2$, where the prime denotes the derivative with respect to x. The function ϕ is introduced such that

$$u = u(x, z - \frac{1}{2}y^2) = \phi_\zeta(x, \zeta) \quad \text{with} \quad \zeta = z - \frac{1}{2}y^2\ . \tag{2.6}$$

The function ϕ is related to the pressure (see [9] for details).

The thermocline is set to

$$T(x, y) = -t(x) + \frac{1}{2}y^2\ . \tag{2.7}$$

2.4 Method of solution

By choosing $\phi(x, 0) = 0$ [9], it is inferred from Eq. (2.6) that

$$\phi(x, \zeta) = -\int_\zeta^0 u(x, \zeta')d\zeta' \quad \text{for} \quad \zeta < 0\ . \tag{2.8}$$

The velocity components (v, w) are given by

$$\begin{aligned} v &= \frac{1}{(2\omega + u_\zeta)^2}\Big[(2\omega + u_\zeta)uu_{x\zeta} - (uu_x + 2\omega\phi_x)u_{\zeta\zeta}\Big]y, \\ w &= yv - \frac{uu_x + 2\omega\phi_x}{2\omega + u_\zeta}\ . \end{aligned}$$

The solution of the velocity field is for the fluid region

$$\{(x, \zeta) : 0 < x < 1\ , \zeta_0 < \zeta = z - \frac{1}{2}y^2 < 0 \text{ with} - \mathrm{y}_0 < \mathrm{y} < \mathrm{y}_0\}\ .$$

2.5 Modelling the undercurrent

The nature of the u-velocity profile or the background undercurrent is non-unique. These are mostly based on observations. The profiles also could be transient. For the solution of the equations, we need to specify a profile for the undercurrent u. Following one of the proposals by [9], which mimics observations, we consider the quadratic-quartic profile for investigations in this work. The profile extends down to zero and also has a second zero which replicates the switch from westward to eastward flow near the surface. The model assumes no flow (stagnant conditions) below the bottom zero of the chosen profile. The expression can be written as

$$\begin{aligned} u(x, \zeta) &= U(x) - \gamma(x)[\zeta + \lambda(x)]^2 - \delta(x)[\zeta + \lambda(x)]^4 \quad , 0 \geq \zeta \geq -\mu(x)\ , \\ &= 0\quad ,\quad -\mu(x) > \zeta \end{aligned}$$

where

$$\mu = \lambda + \sqrt{-\frac{\gamma}{2\delta} + \sqrt{\frac{U}{\delta} + \frac{\gamma^2}{4\delta^2}}}\ . \tag{2.9}$$

We also set $\lambda(x) = 1 - \Lambda x, 0 \leq x \leq 1$. We assume that $U > 0, \gamma > 0, \delta > 0$, and $\mu > \lambda > 0$. It may be noted that there is some freedom available in the model leading, for example, to the choice of $\lambda(x)$. The path of the EUC, if that is what is desired to be modelled is represented by the function $\lambda(x)$. Hence, by setting the function $\lambda(x)$ we prescribe the path taken (eastwards) by the line of maximum speed below the surface. The function $\lambda(x)$ considered here is motivated by observation, it is taken to be a straight line that rises to the east. However, other choices are possible and can be easily accommodated within the model. The uniform maximum azimuthal flow below the surface is located in $-\lambda(x) > \zeta \geq -\mu(x)$ and it is assumed that for the model the thermocline is situated somewhere within this maximum azimuthal flow region and not on its boundary.

3 Results

For carrying out the numerical investigations, it is necessary to choose a specific setting with parameters of an appropriate profile of the Pacific EUC. For this purpose we consider parameters settings from examples presented in [9]. Numerical codes written in MATLAB have been used for performing the numerical simulations.

We take the parameters considered in Example 3 in [9]. A linear function is used for γ_0 given by

$$\gamma_0 = A + Bx \tag{3.10}$$

with $A = 0.03$ and $B = 2.4$, approximating γ in Eq.(2.9). We also set $\hat{U_0} = 2$ and $V_0 = 1$ leading to $c_0 = \hat{U_0} + V_0 = 3$. The value of Λ is taken as 0.18. The function δ in Eq.(2.9) is approximated by δ_0 which is given by

$$\delta_0 = c_0/\lambda^4(x) - \gamma_0(x)/\lambda^2(x). \tag{3.11}$$

This is an example where a two-cell structure of the flow field was observed by [9]. We plot the horizontal (v-component) and the vertical (w-component) of the velocities in the y - ζ plane at $x = 0.5$ in Fig. 3(a) and Fig. 3(b) respectively. The flows described here are symmetric about the Equator, and hence the flow properties on only one side of the Equator are presented. It is observed that the horizontal (v-component) velocity changes direction from positive near the equatorial surface to negative just below the surface along the y direction. Farther down, it reverses direction again. These features are consistent with the flow patterns reported in [9]. The change in magnitude for flow reversal is more pronounced near the western end. For the vertical (w-component) velocity, there is change in flow direction from downward at the surface to upward below the surface. The magnitude of change again is observed to be more pronounced at the western end.

The streamlines for the flow projected on the (y-z) plane can be computed by solving the differential equation

$$\frac{\mathrm{d}z/\mathrm{dt}}{\mathrm{d}y/\mathrm{dt}} = \frac{w}{v}\ .$$

Transforming onto the (y - ζ) plane on using $\zeta = z - \frac{1}{2}y^2$, we have the differential equation

$$\frac{\mathrm{d}z}{\mathrm{d}\zeta} = \frac{-uu_x + 2\omega\phi_x}{v(2\omega + u_\zeta)}\ .$$

Numerical solution of this differential equation produces the streamlines on the (y - ζ) plane.

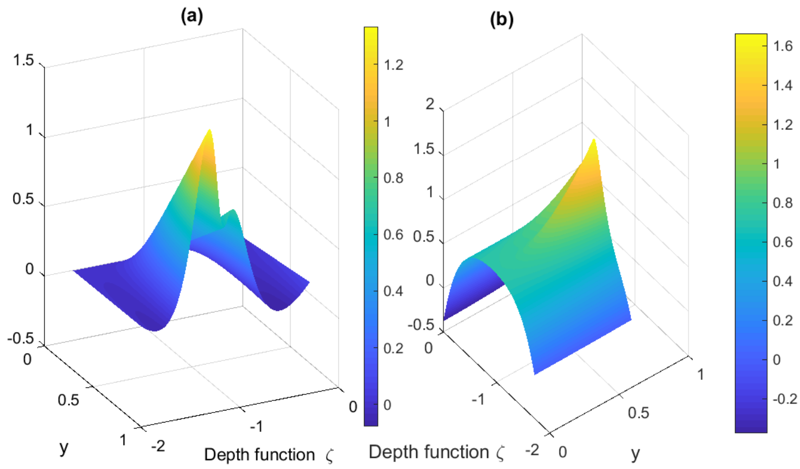

Figure 3: (a) Horizontal velocity, u in the y - ζ plane at x = 0.5 for (Example 3, Constantin and Johnson) and $\omega = 0.03$
(b) Vertical velocity, v in the y - ζ plane at x = 0.5 for (Example 3, Constantin and Johnson) and $\omega = 0.03$.

To compare with the exact streamlines obtained by asymptotic methods in [9] we plot the streamlines obtained numerically for a value of $\omega = 0.03$ in Fig. 4. The streamlines obtained numerically closely match the exact ones and also confirm a two-cell structure of the flow.

Even though streamlines provide an overview of the flow pattern and the nature of flow fields, we need additional information for assessing the strength of flow within the fluid medium. To this end, we plot the in-plane velocity amplitudes defined by $u_{amp} = \sqrt{v^2 + w^2}$ in the y - ζ plane at x = 0.5 in Fig. 5. It is interesting to observe that two relatively strong flow regions emerge, both near the western end at around y = 0.5 and 0.8 respectively. However, it is further interesting to note that one region is relatively weak compared to the other. To explore this aspect in further detail, a more detailed investigation is carried out in relation to the velocity amplitude maps at various locations along the azimuthal x direction.

While keeping all the other parameters constant, the in-plane velocity amplitude maps are computed in the y - ζ plane for various different values of x and are plotted in Fig. 6. It has been found that two strong flow regions exist at the western end (corresponding to $x = 0$). However, one out of these two regions disappears as x approaches 0.1 and eventually the velocity field turns into a flow field with a single region until at about x = 0.15 when the second region of relatively stronger flow starts to reappear. This disappearance and re-emergence of the second flow region is both intriguing and is again strong evidence of the 3D non-linear nature of the flow regime. In addition, it also shows the capability of the Constantin-Johnson model to capture such kind of complex nonlinear features. With the progress along x direction, the two flow regions become more evident and are quite distinct at around x = 0.35 and beyond. However, as we approach the eastern end, distortions are observed in the flow patterns and the two regions approach each other showing a tendency to merge at the eastern end. The velocity amplitude maps are shown in Fig. 6 for x = 0 (two-region flow), 0.11 (one

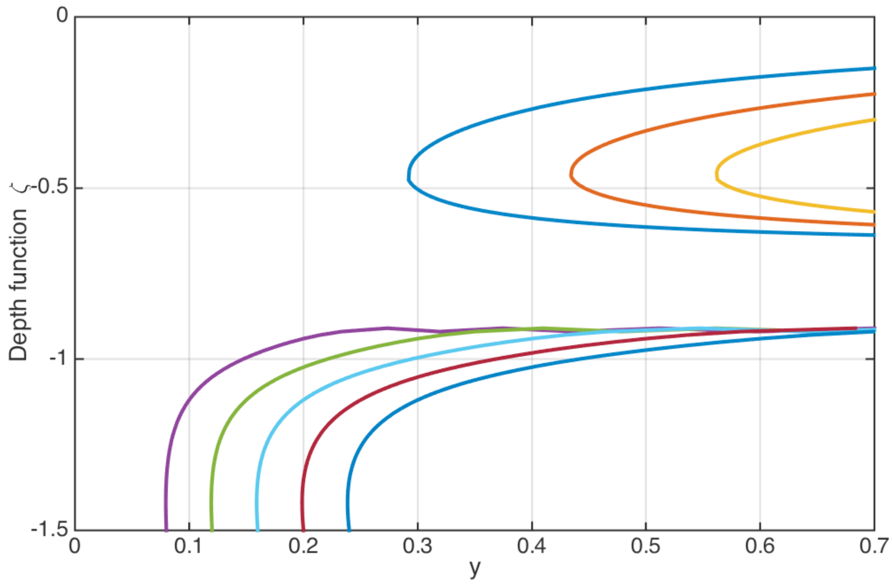

Figure 4: Streamlines in the y - ζ plane at $x = 0.5$ for $\omega = 0.03$ (Scale: 0.1 along meridional y axis corresponds to 15 km, 0.1 along depth i.e. z axis $\sim$ 20 m).

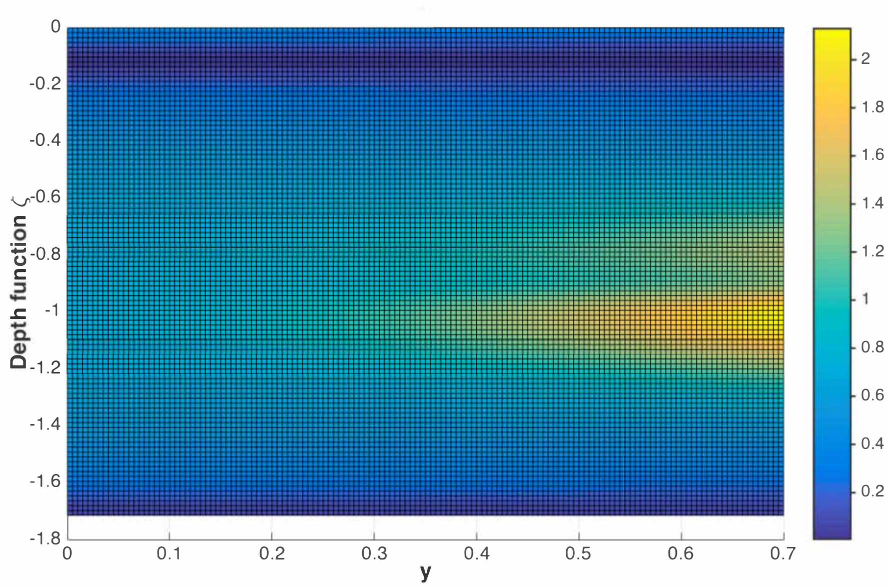

Figure 5: In-plane velocity amplitude u_{amp} map in the y - ζ plane at $x = 0.5$ for $\omega = 0.03$ (Scale: 0.1 along meridional y axis corresponds to 15 km, 0.1 along depth i.e. z axis $\sim$ 20 m).

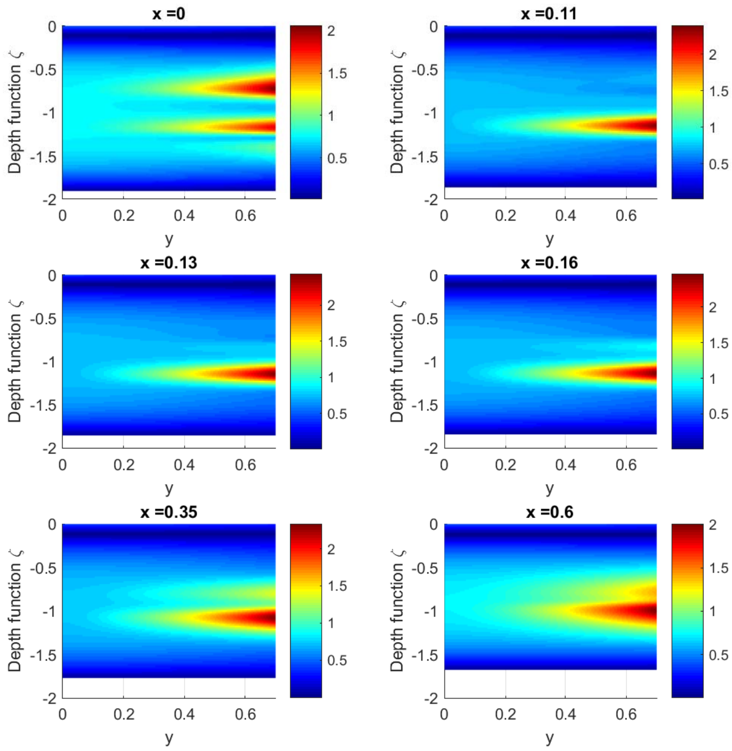

Figure 6: Evolution of in-plane velocity amplitude u_{amp} maps in the y - ζ plane along the azimuthal x axis for $\omega = 0.03$.

region flow), 0.16 (a weak second region appears), 0.35 and 0.6. To provide insight into the flow structure, streamlines are plotted in Fig. 7 for $x = 0.11$, 0.13, 0.16 and 0.35. It is noticed that at $x = 0.11$ the streamlines for the two-cells almost merge with each other. Hence, even though there is a two-cell structure (from a streamline perspective), the flow pattern has merged into a complex single region flow. This fascinating flow structure is clearly a hallmark of the nonlinear, complex flow of the Pacific EUC. Starting around $x = 0.15$ and then subsequently from $x = 0.2$, the two cells start separating gradually, finally becoming distinct as evident from the plot for $x = 0.35$.

Numerical computations so far had been carried out with the value of $\omega = 0.03$. To study the sensitivity to the value of ω, we carried out the numerical computations with a very small value of $\omega = 0.001$ which is close enough to the formal case of $\omega = 0$ and can also be somewhat comparable to the asymptotic results. We carried out similar numerical investigations to generate results corresponding to Figs. 3-7 and produce Figs. 8-12. Observations from the velocity field plots in Fig. 8 are similar in nature to Fig. 3, except for the fact that the presence of two region of flow is more strongly evident in Fig. 8 for x =0.5. The existence of the two regions is evident in Fig. 8 from the two peaks. The fact that there are two regions is also seen from Fig. 10. The streamlines in Fig. 9 show similar patterns and hence again confirm the two-cell flow structure. To further look into the detail, the in-plane velocity amplitude maps are plotted in Fig. 11 and the streamlines are shown in Fig. 12. It is observed that for $x = 0$, 0.11 and 0.35,

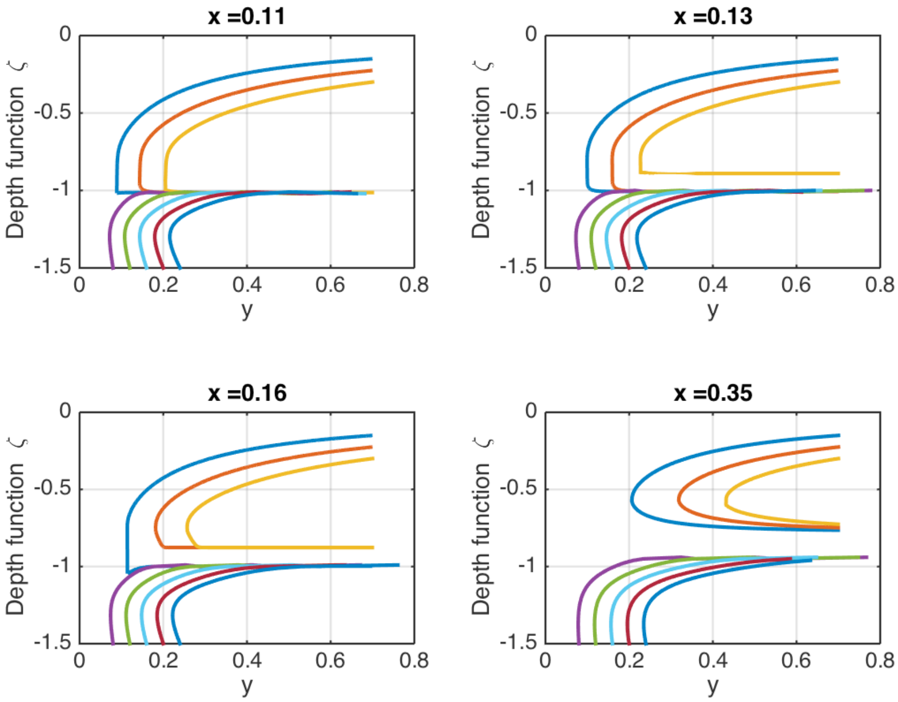

Figure 7: Evolution of streamlines in the y - ζ plane along the azimuthal x axis for ω = 0.03. As x increases one moves eastward along the Equator (Scale: 0.1 along x axis corresponds to 1000 km, 0.1 along meridional y axis corresponds to 15 km, 0.1 along depth i.e. z axis corresponds to 20 m).

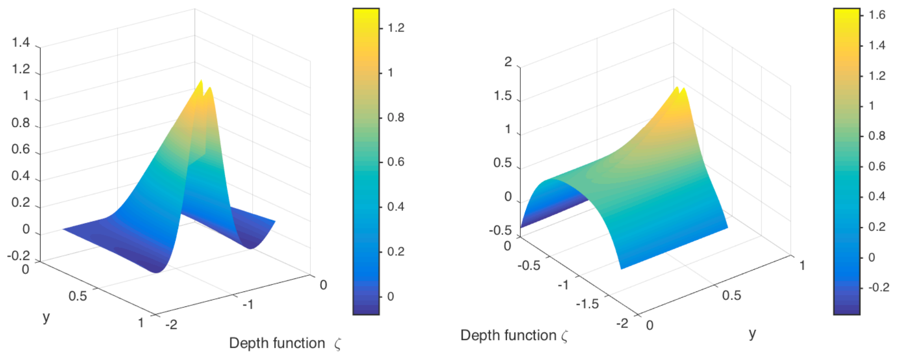

Figure 8: (a) Horizontal velocity, u in the y - ζ plane at x = 0.5 for ω = 0.001 (b) Vertical velocity, v in the y - ζ plane at x =0.5 for ω = 0.001.

the two region flow patterns are much more evident and the streamlines for x = 0.11, 0.13, 0.16 and 0.35 do not show the same kind of merging/separating behavior as seen for the case with ω = 0.03. Hence, it may be inferred that the detail flow patterns are indeed sensitive to values of ω, while the overall flow patterns and structures (such as two-cell flows) are still preserved.

Further, numerical investigation has been carried out on a single cell structure of flow pattern in the (y - ζ) plane for Example 2 [9] at x = 0.5 and for a value of ω = 0.03. Plots for the case concerned, similar to those in Figs. 3-5 have been provided as supplementary information. Some minor kinks in the streamlines have been observed which disappear for ω = 0.001 and the streamlines approach the smooth streamlines obtained using asymptotics in [9]. Further investigations are necessary to ascertain if this is indicative of some more fundamental phenomenon of relevance to the flow field.

4 Discussion and Conclusions

The numerical investigations carried out in this paper have confirmed the presence of cellular structures of flow pattern in the equatorial ocean dynamics. In addition, the existence of multiple cells has also been verified. There is indication of upwelling and downwelling. A sensitivity of the flow patterns and the cellular structures to the non-dimensional rotational parameter ω has been carried out to examine the effect of ω and further confirm the asymptotic results. It has been observed that the overall flow structures and the features are unchanged though some minor details may be affected. Hence, the theory and the exact results based on asymptotic approximation of small parameters are valid for all practical purpose. It has been revealed from the simulations executed using the three-dimensional fully nonlinear model proposed by Constantin and Johnson that these cellular patterns and associated flow structures evolve in the azimuthal direction along the equator. This has been reflected in the streamline patterns and velocity maps. Further, the strength of the flow fields corresponding to the cells vary. In other words, flow in some cells are stronger than others. This is also evidenced in the computed velocity maps showing the strength (or vector amplitude) of the $(v - w)$ velocity fields. In fact, another spectacular revelation is that the flow cells can merge. This is also reinforced from the plots of the streamlines. The effects of this may lead to phenomenon such as disappearance and re-emergence of flow cells. This seems to suggest that, in the future, further numerical work should be undertaken, as the model

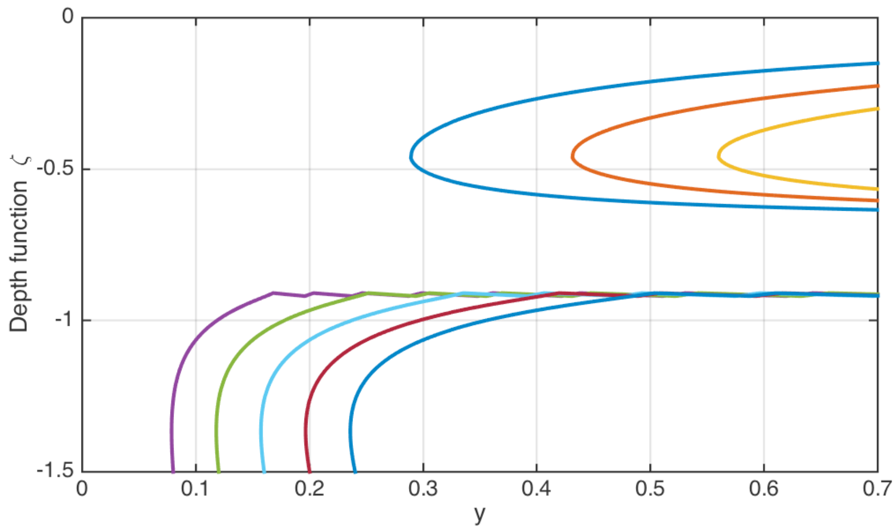

Figure 9: Streamlines in the y - ζ plane at x = 0.5 for ω = 0.001 (Scale: 0.1 along meridional y axis corresponds to 15 km, 0.1 along depth i.e. z axis $\sim$ 20 m).

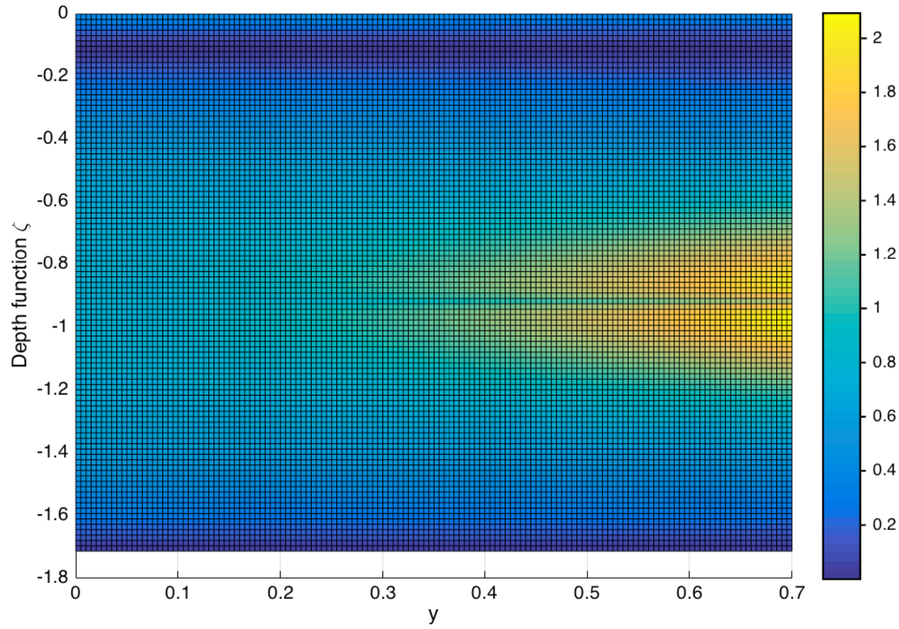

Figure 10: In-plane velocity amplitude u_{amp} map in the y - ζ plane at x = 0.5 for ω = 0.001 (Scale: 0.1 along meridional y axis corresponds to 15 km, 0.1 along depth i.e. z axis $\sim$ 20 m).

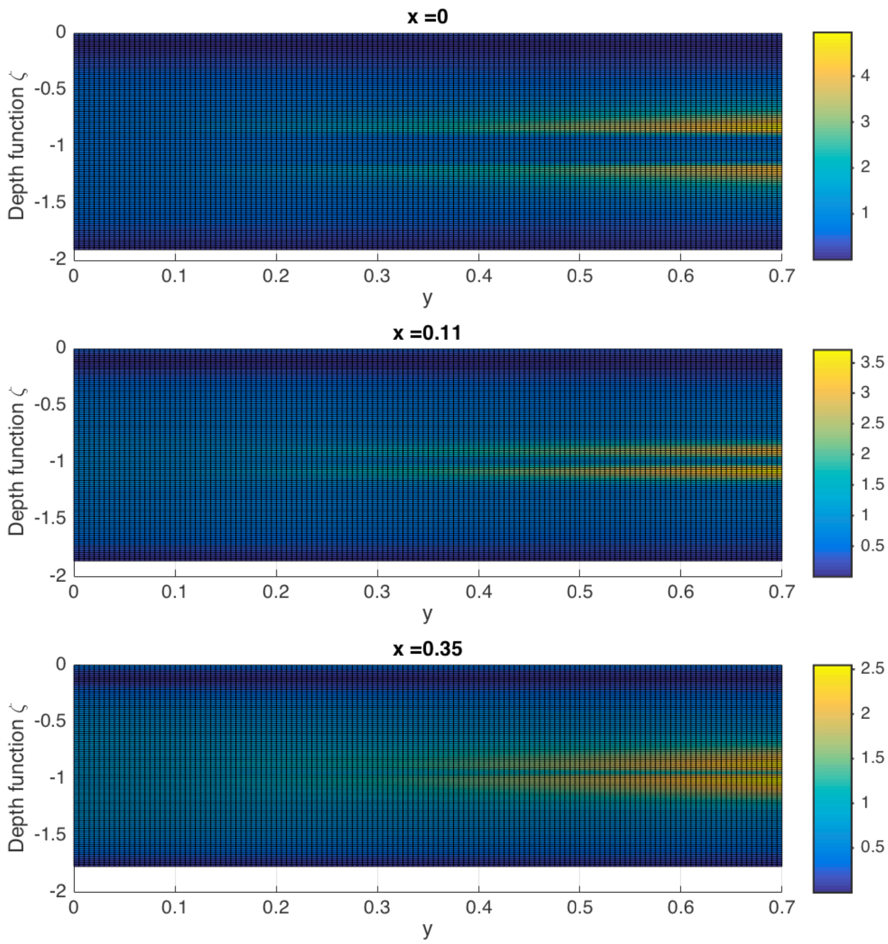

Figure 11: Evolution of in-plane velocity amplitude u_{amp} maps in the y - ζ plane along the azimuthal x axis for $\omega = 0.001$.

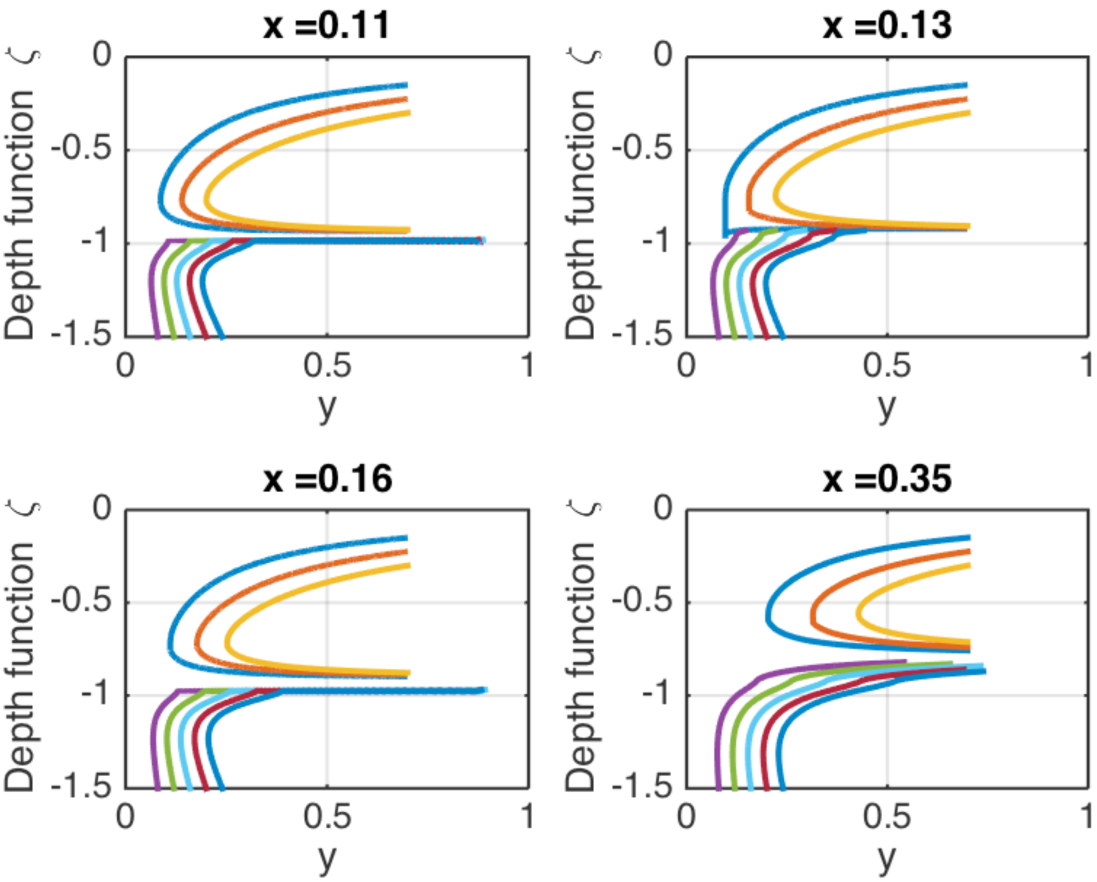

Figure 12: Evolution of streamlines in the y - ζ plane along the azimuthal x axis for ω = 0.001. As x increases one moves eastward along the Equator (Scale: 0.1 along x axis corresponds to 1000 km, 0.1 along meridional y axis corresponds to 15 km, 0.1 along depth i.e. z axis $\sim$ 20 m.

appears to contain hidden and intriguing details. Some future development exploiting the potential of the Johnson-Constantin model could be in the following areas -

1. The model could be used to investigate flow paths in more detail, and integrated with other models to explore the transfer of nutrients, heat transfer and sea surface temperatures, and carbon sequestration phenomenon.

2. The model can be used to analyse similar flows encountered in the equatorial regions of the Atlantic and Indian Ocean.

3. The availability of a suitable background flow opens up promising opportunities for the investigation of the effects on wave propagation, including wave-current interactions in the context of non-traditional corrections.

4. The model could also be used in conjunction with other computationally intensive ocean circulation models, for validation with exact results or for improving the computational efficiency with coupled models.

Acknowledgement

Insightful discussions with Prof Robin Stanley Johnson, Newcastle University, UK and his suggestions during the course of this work leading to some interesting observations and results are gratefully acknowledged. The author also gratefully acknowledges the support from the Erwin Schrödinger Institute in Vienna for this work, during the thematic programme on 'Mathematical Aspects of Physical Oceanography'.

The author would also like to thank the reviewers for their helpful suggestions.

Supplemental material

The following files have been included as supplementary information: (1) A movie file showing the evolution of the in-plane velocity amplitude maps along the x-axis from west to east, for Example 3 [9] and $\omega = 0.03$.(2) FigS1.pdf, Example 2 [9] (a) Horizontal velocity in the y - ζ plane at $x = 0.5$ for $\omega = 0.03$ (b) Vertical velocity in the y - ζ plane at x =0.5 for $\omega = 0.03$ (Fig. 13). (3) FigS2.pdf, Example 2 [9] Streamlines in the y - ζ plane at $x = 0.5$ for $\omega = 0.03$ (Fig. 14). (4) FigS3.pdf, Example 2 [9] In-plane velocity amplitude u_{amp} map in the y - ζ plane at $x = 0.5$ for $\omega = 0.03$ (Fig. 15).

References

[1] M. A. Cane The response of an equatorial ocean to simple wind stress patterns: I. model formulation and analytical results. *J. Mar. Res.*, 37:232–252, 1979.

[2] M. A. Cane The response of an equatorial ocean to simple wind stress patterns: Ii. numerical results. *J. Mar. Res.*, 6:355–398, 1979.

[3] J. G. Charney Non-linear theory of a wind-driven homogeneous layer near the equator. *Deep Sea Res.*, 6:303–310, 1960.

[4] A. Constantin An exact solution for equatorially trapped waves. *J. Geophys. Res.: Oceans*, 117:C05029, 2012.

[5] A. Constantin Some nonlinear, equatorially trapped, nonhydrostatic internal geophysical waves. *J Phys. Oceanogr.*, 44:781–789, 2014.

[6] A. Constantin, P. Germain Instability of some equatorially trapped waves. *J. Geophys. Res.: Oceans*, 118:2802–2810, 2013.

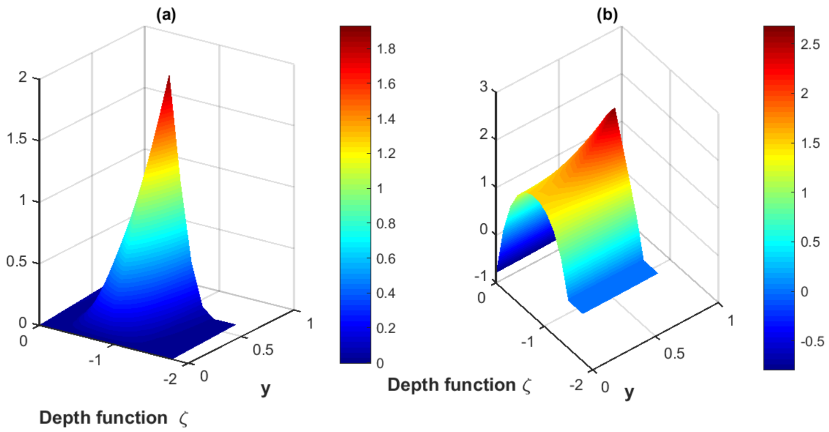

Figure 13: Supplementary file (2), FigS1.pdf. Example 2 [9] (a) Horizontal velocity in the y - ζ plane at $x = 0.5$ for $\omega = 0.03$ (b) Vertical velocity in the y - ζ plane at x =0.5 for $\omega = 0.03$.

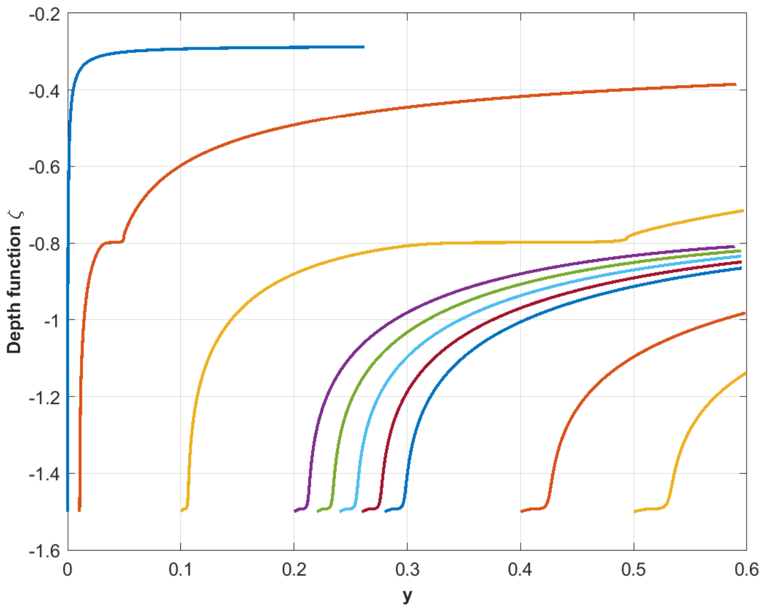

Figure 14: Supplementary file (3), FigS2.pdf. Example 2 [9] Streamlines in the y - ζ plane at $x = 0.5$ for $\omega = 0.03$.

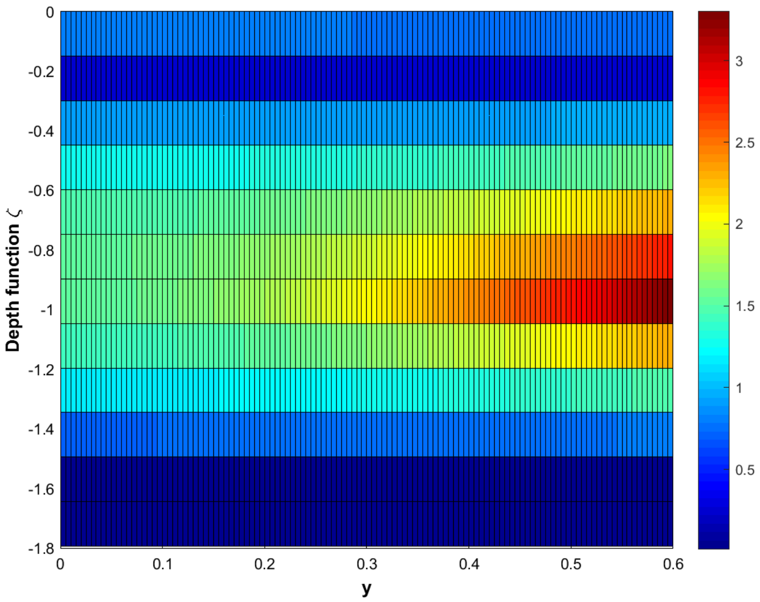

Figure 15: Supplementary file (4), FigS3.pdf. Example 2 [9] In-plane velocity amplitude u_{amp} map in the y - ζ plane at $x = 0.5$ for $\omega = 0.03$.

[7] A. Constantin, R. S. Johnson An exact, steady, purely azimuthal equatorial flow with a free surface. *J Phys. Oceanogr.*, 46:1935–1945, 2016.

[8] A. Constantin, R. S. Johnson The dynamics of waves interacting with the equatorial undercurrent. *Geophys. Astrophys. Fluid Dyn.*, 109(4):311–358, 2015.

[9] A. Constantin, R. S. Johnson A nonlinear, three-dimensional moel for ocean flows, motivated by some observations of the Pacific equatorial undercurrent and thermocline. *Phys. of Fluids*, 29:1–21, 2017.

[10] T. Cromwell Circulation in a meridional plane in the central euqatorial Pacific. *J. Mar. Res.*, 12:196–213, 1953.

[11] M. F. Cronin, W. S. Kessler Near-surface shear flow in the tropical Pacific cold tongue front. *J. Phys. Oceanogr.*, 39(5):1200–1215, 2009.

[12] H. A. Dijkstra *Nonlinear physical oceanography: a dynamical systems approach to the large scale ocean circulation and El Nino*, Vol. 28. Springer Science & Business Media, 2005.

[13] E. J. Drenkard, K. B. Karnaukas Strengtheing of Pacific equatorial undercurrent in the soda reanalysis: Mechanics, ocean dynamics, and implications. *J. Amer. Meteorol. Soc.*, 27: 2405–2415, 2014.

[14] A. V. Fedorov, J. N. Brown *'Equatorial waves' in Encyclopeida of Ocean Sciences, edited by Steele, J.* Academic Press, San Diego, pp. 3679–3695, 2009.

[15] N. P. Fofonoff, R. B. Montgomery The equatorial undercurrent in the light of the vorticity equation. *Tellus*, 7:518–521, 1955.

[16] A. E. Gill The equatorial current in a homogeneous ocean. *Deep Sea Res.*, 18:421–431, 1971.

[17] A. E. Gill Models of equatorial currents. *Proc. Numerical Models of Ocean Circulation*, pp. 181– 203, 1975.

[18] D. Henry An exact solution for equatorial geophysical water waves with an underlying current. *Eur. J. Mech.-B /Fluids*, 38:18–21, 2013.

[19] D. Henry Equatorially trapped nonlinear water waves in a beta-plane approximation with centripetal forces. *J. Fluid Mech.*, 804:R1, 2016.

[20] G. C. Johnson, M. J. McPhaden, E. Firing Equatorial Pacific ocean horizontal velocity, divergence, and upwelling. *J. Phys. Oceanogr.*, 31(3):839–849, 2001.

[21] G. C. Johnson, B. M. Sloyan, W. S. Kessler, K. E. McTaggart Direct measurements of upper ocean currents and water properties across the tropical Pacific during the 1990s. *Prog. Oceanogr.*, 52(1):31–61, 2002.

[22] W. S. Kessler The circulation of the eastern tropical Pacific: A review. *Prog. Oceanogr.*, 69(2-4):181–217, 2006.

[23] R. Lukas The termination of the equatorial undercurrent in the eastern Pacific. *Prog. Oceanogr.*, 16:63–90, 1986.

[24] A. J. Majda Climate science, waves and PDEs for the tropics. In *Nonlinear Partial Differential Equations*, pp. 223–230. Springer, 2012.

[25] S. A. Maslowe Critical layers in shear flows. *Annu. Rev. Fluid Mech.*, 18(1):405–432, 1986.

[26] J. P. McCreary A linear stratified ocean model of the equatorial undercurrent. *Phil. Trans. Roy. Soc. London A: Math. Phys. Eng. Sci.*, 298:603– 635, 1981.

[27] J. P. McCreary, P. Lu Interaction between the subtropical and equatorial ocean circulations: the subtropical cell. *J. Phys. Oceanogr.*, 24:466– 497, 1994.

[28] J. P. McCreary Jr Modeling equatorial ocean circulation. *Annu. Rev. Fluid Mech.*, 17(1):359–409, 1985.

[29] W. D. McKee The wind-driven equatorial circulation in a homogeneous ocean. *Deep Sea Res.*, 20:889–899, 1973.

[30] J. Pedlosky Thermocline theories. In *General Circulation of the Ocean*, pp. 55–101. Springer, 1987.

[31] A. R. Robinson An investigation into the wind as the cause of the equatorial undercurrent. *J. Mar. Res.*, 24:179 − 204, 1966.

[32] H. Stommel Wind-drift near the equator. *Deep Sea Res.*, 6:298 − 302, 1960.

[33] L. D. Talley, G. L. Pickard, W. J. Emery, J. H. Swift *Descriptive physical oceanography: An introduction.* Elsevier, London, 2011.

[34] M. Tsuchiya, R. Lukas, F. A. Fine Source waters of the Pacific equatorial undercurrent. *Prog. Oceanog.*, 23:101–147, 1989.

[35] G. K. Vallis *Atmospheric and Oceanic Fluid Dynamics.* Cambridge University Press, 2006.

[36] G. Veronis An approximate theoretical analysis of the equatorial undercurrent. *Deep Sea Res.*, 6:318– 327, 1960.

On a three-dimensional nonlinear model of Pacific equatorial ocean dynamics: Velocities and flow paths

Biswajit Basu

Oceanography 31(3), 51-58, 2018

Abstract

We investigate the velocity field and the three dimensional flow paths obtained from a recently developed three dimensional, nonlinear model that can simulate observed features of the Pacific Equatorial Undercurrent. The sensitivity of the flow field and the paths to the undercurrent are examined. The flow path or the trajectories used in the model were obtained from the exact solution of the velocity field. Nonlinear, three-dimensional features that can be simulated by the model include upwelling/downwelling, cellular flow structures, divergence of flow from the equator and extra-equatorial flows, subsurface ocean 'bridge' in the equatorial direction and sharp changes in gradient of the flow path.

1 Introduction

Understanding of the Pacific Equatorial Undercurrent (EUC) is important because contributions to it from various sources profoundly influence the temperature, salinity, and nutrient enrichment of the equatorial thermocline and impact biological productivity, atmospheric carbon exchange, and the El-Niño Southern Oscillation (ENSO). Known history of the EUC began in the 1950s with its first observations [12] and measurements [26]. McCreary [29, 30] provided early models of the current, and among mapping studies, one worthy of mention is the Hawaii-to-Tahiti Shuttle Experiment [43] conducted as a part of the World Ocean Circulation Experiment. Investigations using global observational models suggest that the Pacific EUC will strengthen in the future [13], and in turn is expected to impact the equatorial ocean dynamics.

The EUC is the Pacific cold tongue's major source of water in the eastern Pacific equatorial region [43]. It is also the primary supplier of the limiting nutrient iron, whose source is sediments from the continental shelf of Papua New Guinea [35]. The supply of iron is vital to phytoplankton production that modulates CO_2 fluxes in the equatorial Pacific and controls the export of carbon to the deep ocean [13, 15, 25].

The EUC has also been associated with long-term (decadal) climate variability. Extratropical sea surface temperature (SST) anomalies are transmitted to the Tropics by way of intergyre exchange, reappearing along the equator after several years of incorporation into the EUC and then resufacing. Existence of a subsurface ocean 'bridge" is a possible connection between the warm SST anomoly in the North Pacific during the early 1970s and the susequent warm SST anomoly along the equator in the 1980s. However, the possible contribution of low latitude wind stresses to equatorial warming cannot be ignored [37, 21].

Equatorial ocean dynamics has some striking features. Close to the equator, the meridional component of the Coriolis force is negligible, and it vanishes at the equator. This leads to the breakdown of geostrophy. The flow in this region is essentially driven by winds, the easterly trade winds in the Pacific and Atlantic, and the seasonally reversing monsoonal winds in the Indian Ocean [39]. Equatorial ocean regions also exhibit pronounced stratification, greater than anywhere else in the ocean [14].

Subjects of undercurrent research include termination, source, divergence and upwelling [28, 40, 24], undercurrent modelling has employed measurements and observations [30, 41]. The simplest model of the EUC is based on a homogeneous fluid subject to uniform westward stress at the surface. While this local model is unstratified, more realistic models considering effects of sratification lead to layered models of undercurrents. Other non-local and physical models include a pressure head that is of extra-equatorial origin. Observations indicate that some of the water in the EUC flows from sub-tropical gyres. A two layer inertial model of undercurents can account for equatorial and extra-equatorial dynamics. Initial local theories of undercurrent formation proposed by Cromwell [11] were developed further by [38, 42, 36], and linear non-dissipative models followed [17, 18, 32]. Subsequently, linear models were significantly extended to include the effects of continuous stratification [29], and some nonlinear models were also developed [4, 2, 3, 32]. Inertial theories of Fofonoff and Montgomery [16] were further advanced by Pedlosky [33], and McCreary and Lu [31] reconciled the inertial approach with a local perspective that considered the EUC as a part of a larger and more complex subtropical current system that has both local and inertial effects. A complete model that captures the integrated dynamics, however, requires numerical computations.

To capture the fine structure of the EUC, the basic variation with depth of its main azimuthal flow can be modeled in the spherical geometry of a rotating Earth [9], However, there are advantages to using the standard β-plane approximation. It permits capture of variations in the meridional direction (in particular, following the Earth's curvature) that are not available within the f-plane approximation framework. (See [8], for an overview of ocean dynamics in the equatorial Pacific in the f-plane setting.) Without further approximations, explicit solutions to the nonlinear governing equations in the equatorial β-plane, were recently obtained in the Lagrangian framework [5, 7, 6, 22, 23]. These solutions represent realistic flow only for the region near the surface or in the neighbourhood of the thermocline. The model does not perform well within the entire vertical extent of the equatorial flow due to the limitations on the permissible underlying currents.

Constantin and Johnson [10] propsoed a model based on fundamentals of fluid mechanics. This nonlinear three-dimensional model, called herein the Constantin-Johnson model, is developed following a systematic approach that is mathematically consistent, captures the essential flow properties observed for the Pacific EUC, and avoids any oversimplification. The model is nonlinear and three dimensional in nature. The analytical model developed by [10] avoids any oversimplication. For example, the model accounts for the Coriolis effects due to the rotation of the Earth and retains non-traditional terms arising in the formulation. The model is based on the assumption of slow evolution of a two-layer flow in the equatorial direction, and successfully provides asymptotic solutions.

This article has two goals. One is to study the sensitivity of the EUC model to oceanic flows. The other is to obtain and study Pacific EUC flow paths /trajectories based on the Constantin-Johnson model by identifying the nonlinear three-dimensional nature of the flow, comparing the model with known observations, and exploring the unknowns. Past studies have used trajectory analysis to look at various aspects of Pacific EUC. A 3 $\frac{1}{2}$ layer model was used to study the tropical cells and quantitatively estimate of source of the EUC waters [27]. A relatively coarse resolution Oceanic General Circulation Model (OGCM) simulation was carried out to quantify local exchanges as EUC flows from Indonesia to Peru [1]. Other studies examined the mean-time composition of EUC waters [19, 20] and variability in pathways of Pacific EUC [34]. While increasing computing resources and parametrizing subgrid-scale phenomena have resulted in more realistic simulations, analytically tractable and mathematically consistent models such as the one proposed by Constantin and Johnson, arising out of and satisfying the fluid dyanmics equations and principles, are valuable for providing insight to complex nonlinear phenomena. The Constantin-Johnson model has the potential to become an OGCM and to be integrated with other OGCMs for computational efficiency.

This paper focusses on the Constantin-Johnson model and investigates one example [10] in detail. The two EUC models considered here, polynomial and quadratic-quartic, both reasonably represent the EUC. The velocity field for the equatorial flow is computed for these two cases, and the results are compared to assess their sensitivity to the model. Three-dimensional flow paths are then derived from the velocity field, and computed trajcetories or flow paths are then examined to identify features and structures indicative of nonlinear three-dimensional flow.

2 Results

Here we investigate the Constantin-Johnson model. To express the governing equations, we choose a coordinate system that rotates with the Earth, with the $\bar{x}$ axis pointing toward the east, the $\bar{y}$ axis pointing due north, and the $\bar{z}$ axis pointing vertically upwards (see Figure 1). This description of co-ordinate system, in fact, is associated with tangent plane approximation and is also consistent with β-plane approximation.

In this co-ordinate system the two set of governing equations (Euler and conservation equations) may be written as

$$\frac{D\bar{\mathbf{u}}}{D\bar{t}} + 2\bar{\mathbf{\Omega}} \times \bar{\mathbf{u}} = -\frac{1}{\rho}\bar{\nabla}\bar{p} + \bar{\mathbf{F}} \quad , \bar{\nabla} \cdot \bar{\mathbf{u}} = 0 \quad ,$$

where $\bar{\mathbf{u}} = (\bar{u}, \bar{v}, \bar{w})$ is the velocity of the fluid at $\bar{\mathbf{x}}$ at time $\bar{t}$. The operator $D/D\bar{t}$ is the material derivative, the pressure is $\bar{p}$, the (constant) density is $\bar{\rho}$ and the body force is represented by $\bar{\mathbf{F}}$. The angular velocity vector is $\bar{\mathbf{\Omega}} = \bar{\Omega}(0, \cos\theta, \sin\theta)$ describing the rotation of the Earth with $|\bar{\mathbf{\Omega}}| = \bar{\Omega} \approx 7.29 \times 10^{-5}\text{rads}^{-1}$ and θ the angle of latitude.

2.1 Preliminary considerations

With a suitable nondimensionalisation of the variables, we can write

$$\mathbf{x} = (\bar{x}, \bar{y}, \bar{z}) = (\bar{L}x, \bar{l}y, \bar{h}z) \ ,$$
$$\mathbf{u} = (\bar{u}, \bar{v}, \bar{w}) = \bar{U}\Big(u, \frac{\bar{l}}{\bar{L}}v, \frac{\bar{h}}{\bar{L}}w\Big) \ .$$

We provide some guidelines on the size of some of the parameters. The length is about 13×10^3 km, the typical value of the depth to the bottom of EUC is about 200 m and the width is about 300 km. With these values, and a speed at the surface $\bar{U} = 0.5ms^{-1}$, the non-dimensional angular speed of rotation of Earth is $\omega = \bar{\Omega}\bar{h}/\bar{U} \approx 0.03$. The choice of scale can be interpreted such that in the flow direction $0 \leq x \leq 1$, with $x = 0$ corresponding to the western end, and $x = 1$ corresponding to the eastern end. The width is restricted to $-y_0 < y < y_0$ by virtue of β-plane approximation, for a suitable finite value of y_0.

A simplified three-dimensional nonlinear model is derived and a solution is proposed using a suitable approximation of the Coriolis term close to the equator, assuming slow variation of a two-layered flow along the equator and some appropriate simplifying assumptions [10], such as:

1. Small r (thermocline [pycnocline] is a line of discontinuity in density; above the density is ρ_0 and below the density is $(1 + r)\rho_0$)

2. Free surface and thermocline sitting on planes parallel to tangent plane

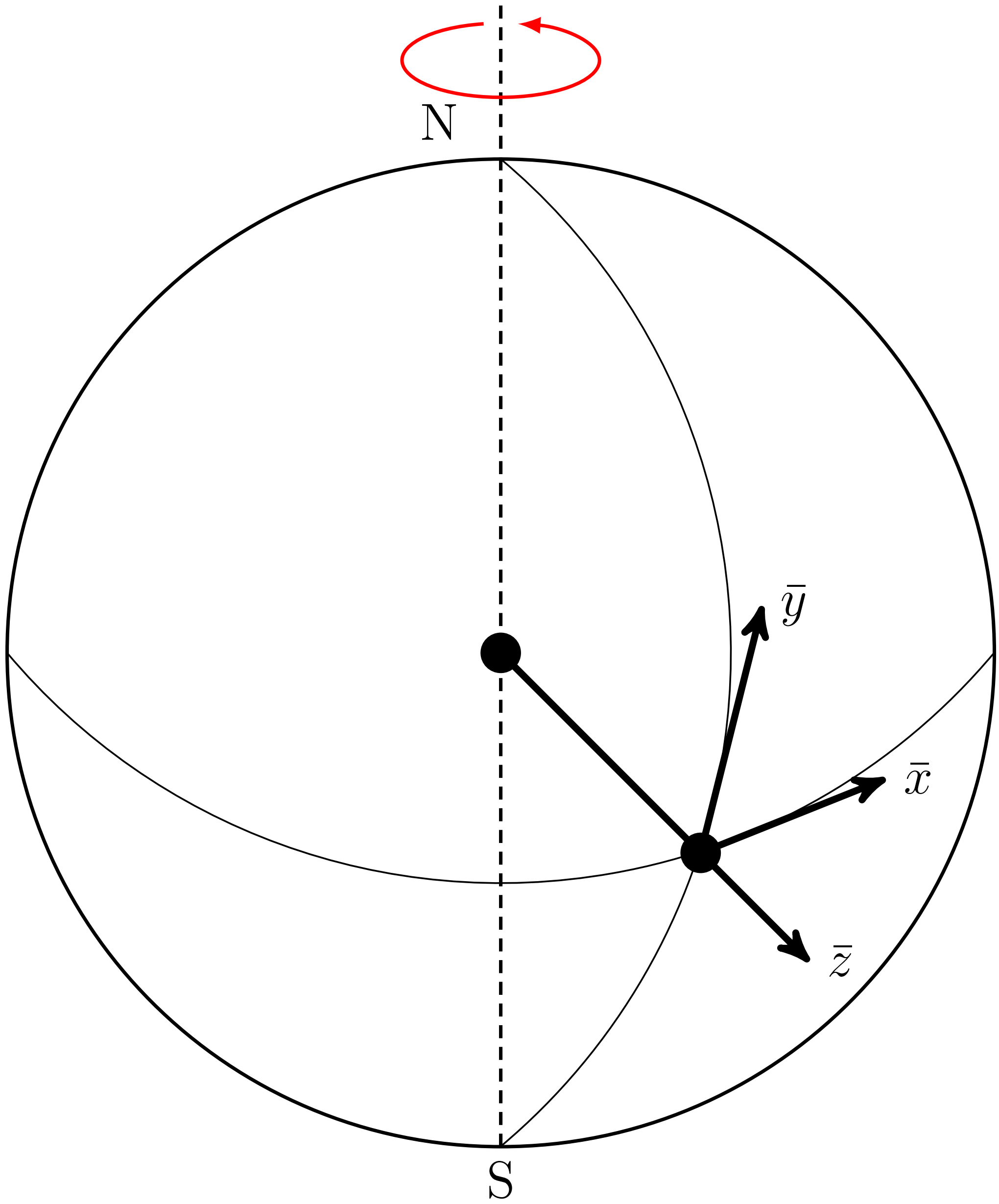

Figure 1: The rotating frame of reference for the Earth with the North pole, South pole, the Equator and the rotational axis around the pole indicated.

3. Constant pressure on the surface along $y = 0$.

Importantly, the formulation considers all of the Coriolis contributions associated with Earth's rotation (see [10] for more details on the model). Studies have indicated that ignoring nonraditional components of the Coriolis force has influence on the equatorial ocean dynamics. Constantin and Johnson [10] provide the solution of the non-dimensional velocity field $(v - w)$ for the fluid region:

$$\{(x, \zeta) : 0 < x < 1 \ , \zeta_0 < \zeta = z - \frac{1}{2}y^2 < 0\}$$

with $-\ \mathrm{y}_0 < \mathrm{y} < \mathrm{y}_0$. The solution of the velocity field (v, w) is dependent on the nature of velocity profile u or the background undercurrent. The models for background current are mostly based on observations and measurements. For the solution of the equations, we need to specify a profile for the undercurrent u. Following the proposals by [10] which mimic observations, we consider two EUC profiles for our investigations: qudratic-quartic profile and polynomial profile. The profiles extend down to zero and also has a second zero which replicates the switch from westward to eastward flow near the surface.

The expression for quadratic-quartic profile can be written as

$$\begin{aligned} u(x, \zeta) &= U(x) - \gamma(x)[\zeta + \lambda(x)]^2 \\ &\quad - \delta(x)[\zeta + \lambda(x)]^4 \ , \ 0 \geq \zeta \geq -\mu(x) \ , \\ &= 0 \quad , \quad -\mu(x) > \zeta \end{aligned}$$

while the expression for polynomial profile can be written as

$$\begin{aligned} u(x, \zeta) &= U(x) - \gamma(x)[\zeta + \lambda(x)]^2 \\ &\quad - \delta(x)[\zeta + \lambda(x)]^4 \quad , \ 0 \geq \zeta \geq -\lambda(x) \ , \\ &= U(x) \, , -\lambda(x) \geq \zeta \geq -\mu(x) \\ &= 0 \quad , \quad -\mu(x) \geq \zeta \end{aligned}$$

where

$$\mu = \lambda + \sqrt{-\frac{\gamma}{2\delta} + \sqrt{\frac{U}{\delta} + \frac{\gamma^2}{4\delta^2}}} \tag{2.1}$$

and $\lambda(x) = 1 - \Lambda x$. We assume that $U > 0, \gamma > 0, \delta > 0$, and $\mu > \lambda > 0$. The uniform maximum azimuthal flow below the surface is located in $-\lambda(x) > \zeta \geq -\mu(x)$, and it is assumed that for the model the thermocline is situated somewhere within this maximum azimuthal flow region and not on its boundary.

A complete description of the 3D flow paths requires the solution of the following differential equations simultaneously:

$$\mathrm{d}x/\mathrm{dt} = u \ , \ \mathrm{d}y/\mathrm{dt} = v \ , \ \mathrm{d}z/\mathrm{dt} = w$$

Transforming to the ζ variable on using $\zeta = z - \frac{1}{2}y^2$, we have the following differential equations:

$$\mathrm{d}x/\mathrm{dt} = u \ , \ \mathrm{d}y/\mathrm{dt} = v \ , \ \mathrm{d}\zeta/\mathrm{dt} = w - v \ .$$

Numerical integration of the set of differential equations yields three-dimensional streamlines from the three-dimensional velocity field (u, v, w). Note that no approximation is made regarding small ω in this analysis.

2.2 Example

To carry out the numerical investigations, it is necessary to choose a specific setting with parameters appropriate to a Pacific EUC profile. For this purpose, we consider parameter settings from examples presented in [10]. The value of ω is taken as 0.03 for numerical computations in this paper.

We use the parameters consided in Example 3 in [10]. A linear function is used for γ_0 given by

$$\gamma_0 = A + Bx$$

with $A = 0.03$ and $B = 2.4$, approximating γ in Equation (2.1). We also set $\hat{U_0} = 2$ as an approximation of U, and $V_0 = 1$ leading to $c_0 = \hat{U_0} + V_0 = 3$. The value of Λ is taken as 0.18. The function δ in Equation (2.1) is approximated by δ_0 which is given by

$$\delta_0 = c_0/\lambda^4(x) - \gamma_0(x)/\lambda^2(x).$$

In a three-dimensional plot, Figure 2 shows the horizontal velocity v and vertical velocity w in the (ζ - y) plane for the quadratic-quartic profile of the EUC for a point on the equator corresponding to $x = 0.0$ (i.e. at the western end). The variations of the velocity magnitude are plotted vertically as a function of depth function ζ and tangential distance due north from the equator y, at $x = 0.0$. As expected, the velocity field exhibits complex structures (see [10]). The horizontal velocity, v changes sign from positive to neagtive near the surface, and then asumes a large positive value at an intermediate depth, followed again by a neagtive value prior to approaching zero deeper down. This fluctuating pattern, clearly evident in Figure 2a, is more pronounced away from the equator. Along the equatorial direction, there is relatively little variation in horizontal velocity. Figure 2b also shows the transformation of negative values of vertical velocity w near the surface to positive at an intermediate depth, subsequenty leading to negative values at a greater depth. Local troughs and peaks in the vertical velocity profile increase away from the equator. Along the equatorial direction, the vertical velocity values take on a convex shape, with a maximum positive value at an intermediate depth and negative values both near the surface and deep down. These observations indicate the existence of cellular structures in the oceanic flow [10]. To investigate the strength of the flow in the (ζ-y) domain, we plot the in-plane velocity amplitude maps ($u_{in-amp} = \sqrt{v^2 + w^2}$) on the ($\zeta$ - y) plane. Figure 3 potrays two clear regions of strong flow that are located away from the equator at intermediate depth.

To compare the results displayed in Figures 2 and 3 to the case where we consider the polynomial EUC profile, and to examine the sensitivity of the results to two different but reasonable representations of EUC, similar results are plotted in Figures 4 and 5 for polynomial EUC profile. Figures 4 and 5 demonstrate that the type of EUC profile used affects the results. Figure 4 shows the horizontal velocity v and vertical velocity w for the polynomial profile of the EUC in a three-dimensional plot, as in Figure 2, for a point on the equator corresponding to $x = 0.0$ (i.e. at the western end). It is observed from Figure 4a that variation of the horizontal velocity v is less compared to that seen in Figure 2a, though the broad nature is somewhat similar. Further, it is observed from Figure 4a that horizontal velocities are predominantly negative. Again, as in Figure 2a, we infer that fluctuations in horizontal velocities along the equator are marginal, as seen in Figure 4a. We also observe from Figure 4b that the vertical velocities are similar in nature to those in Figure 2b, with the exception that the vertical velocities at greater depth in Figure 4b tend to have negative values of higher magnitude. Not much difference is observed in the results between Figures 3 and 5, as both display two strong regions of flow away from the equator at intermediate depth.

Exercises leading to similar types of results as those in Figures 2-5, are produced in Figures 6-9. The results in Figures 6-9 correspond to a point along the equator

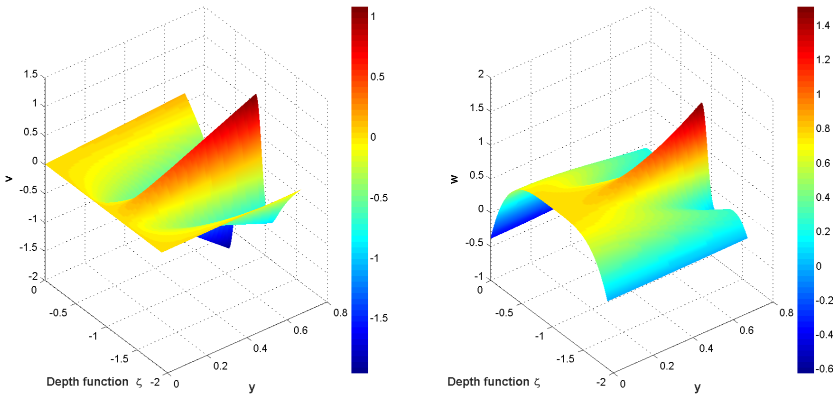

Figure 2: (a) Horizontal velocity v (b) Vertical velocity w, for quadratic-quartic profile of EUC at x = 0.0.

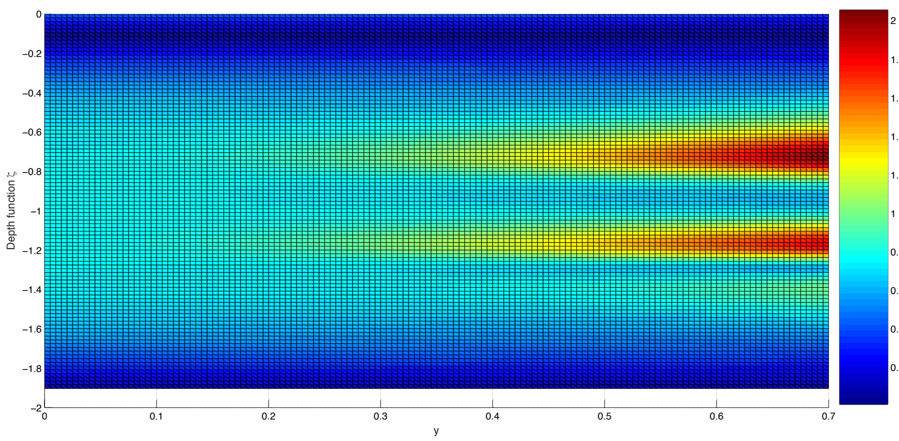

Figure 3: In-plane velocity amplitude u_{in-amp} map for quadratic-quartic profile of EUC for x =0.0.

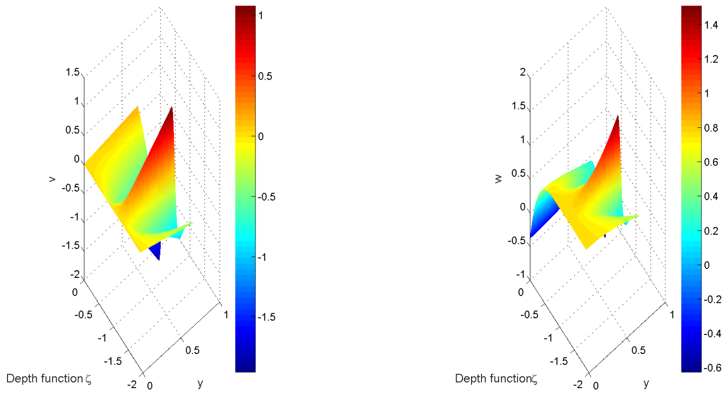

Figure 4: (a) Horizontal velocity v (b) Vertical velocity w, for polynomial profile of EUC at x = 0.0.

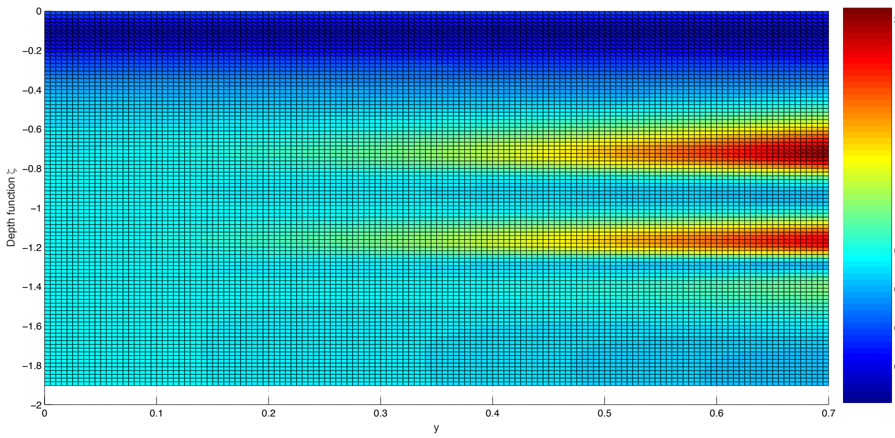

Figure 5: In-plane velocity amplitude u_{in-amp} map for polynomial profile of EUC for x =0.0.

at x = 0.25. Broad conclusions from Figures 6-9 derived from the analysis remain unchanged with respect to what was inferred from Figures 2-5, there are some minor differences. For example, the vertical velocities for the case of polynomial profile of EUC attain positive values deep down (around $\zeta \approx$ -1.7 to -1.8; see Figure 8) in contrast to negative values for the case of quadratic-quartic profile of EUC (see Figure 6).

Next, we use the velocity field to compute the flow path or the trajectories. Because the profile of EUC has some impact locally on the velocity (though the broad features of the velocity field are unchanged), we decide to use both the profiles of EUC once again. We consider the quadratic-quartic profile of the EUC first. The results for the three-dimensional flow paths are plotted in Figures 10-12 using the Eulerian velocites in three-dimension obtained previously and performing time integration. We strategically chose nine different initial points at the western end of the equator, i.e. x = 0.0. These nine points represent three groups. The first group chosen is representative of the flow originating from near surface, hence ζ = -0.1 (i.e. at a depth of 20 m). The second, representing flows originating at intermediate depth, corresponds to ζ = -0.6 (i.e. at a depth of 120 m). The third group at ζ = -1.2 (i.e., at a depth of 240 m) initiates flow at greater depth. For each of the groups, the y position of the initial points are chosen to be 0.0, 0.3 and 0.6 respectively (i..e, at the equator, approximately 45 km away from the equator, and approximately 90 km away from the equator, respectively).

Figure 10 is a plot of the three-dimensional flow paths from the three initial locations close to the surface (ζ = -0.1) on the (ζ - y) plane, corresponding to y = 0.0, 0.3 and 0.6, respectively. The figure clearly shows the complex three-dimensional nonlinear nature of the paths. Following an initial downward descent, there is a sudden ascent, which is subsequently followed by a sudden sharp drop. This happens around x = 0.3 and for all the trajectories. The final phase of the trajectories are monotonically descending in nature, with a gentler slope. The trajectories provide evidence of downwelling, in which waters originating at the western end of the EUC move to the eastern end in a downward-sloping direction. The paths initiated away from the equator also show some (though marginal) amount of flow toward the equator - demonstrating real three-dimensional structures and confirming that the flow is forced toward the equatorial region.

The three flow paths orginating from the (ζ - y) plane shown in Figure 11, corresponding to an intermediate depth of ζ = -0.6, potray the existence of a subsurface ocean 'bridge" in the west-to-east direction. This concept [44] has been used to explain the relationship between the North Pacific and the equator in terms of SST anomoly. In Figure 11, the source water from the western end of the Pacific travels downward prior to resurfacing at the eastern end. The trajectories in this figure have the tendency to move outward from the equator.

The extra-equatorial flow patterns produced in Figure 11 is amplified in Figure 12, where the originating points of the flow paths at the western end of the equator are located at a relatively greater depth of ζ = -1.2 and corresponding to y = 0.0, 0.3 and 0.6. The presence of an extra-equatorial poleward flow path is evident. In fact, originating points farther from the equator show greater amount of flow divergence from the equator. In addition, we find flows that originate deep down (240 m) at the western boundary of the equator move upward as they move toward the eastern boundary.

Figures 13-15 show results similar to those in Figures 10-12, but for the case of the polynomial EUC profile. The qualitative results in these figures are close to the results as observed in Figures 10-12. This is not unexpected as the velocity fields for the two cases of EUC profiles have similar broad nature though differ in some details. This is translated in the results for flow paths. Hence, the trajectories in Figures 13-15 are similar to the trajectories in Figures 9-12, though there may be some variation in numerical details.

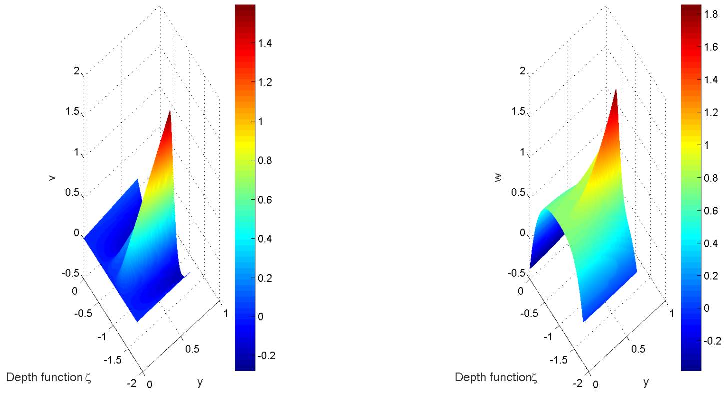

Figure 6: (a) Horizontal velocity v (b) Vertical velocity w, for quadratic-quartic profile of EUC at x = 0.25.

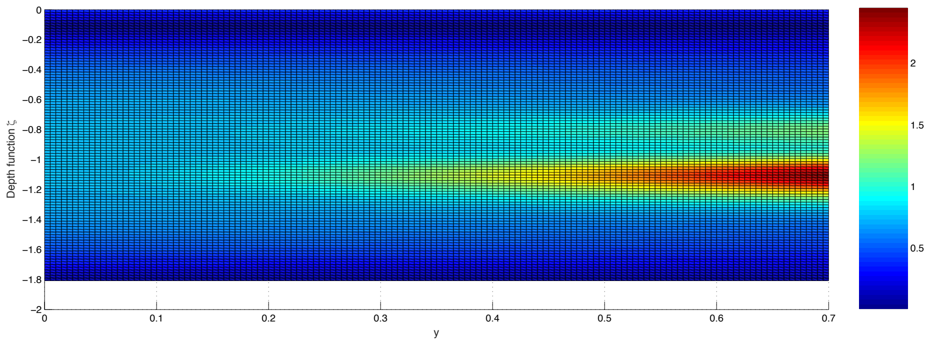

Figure 7: In-plane velocity amplitude u_{in-amp} map for quadratic-quartic profile of EUC for x =0.25.

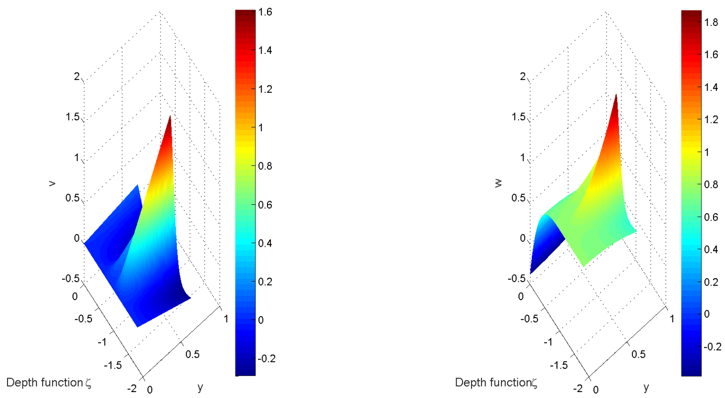

Figure 8: (a) Horizontal velocity v (b) Vertical velocity w, for polynomial profile of EUC at x = 0.25.

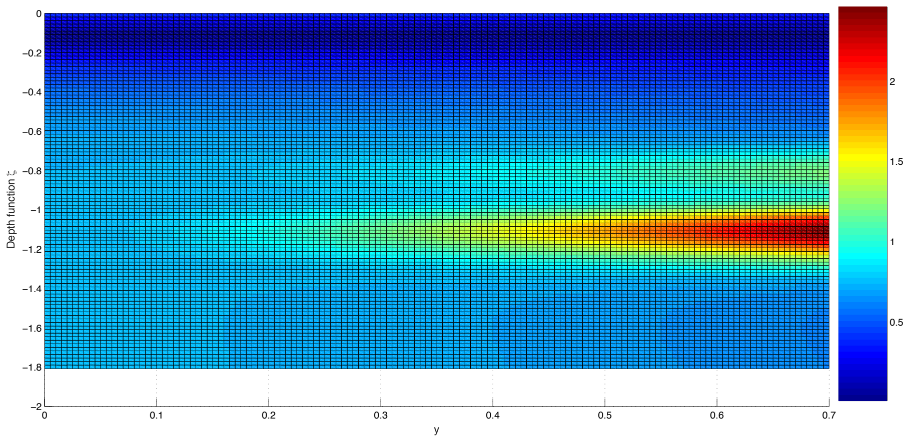

Figure 9: In-plane velocity amplitude u_{in-amp} map for polynomial profile of EUC for x =0.25.

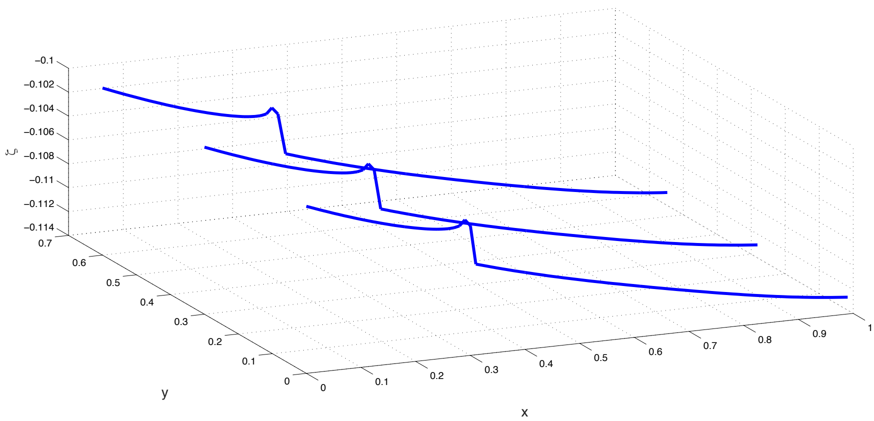

Figure 10: 3D flow paths for quadratic-quartic EUC profile with paths initiating from points near surface.

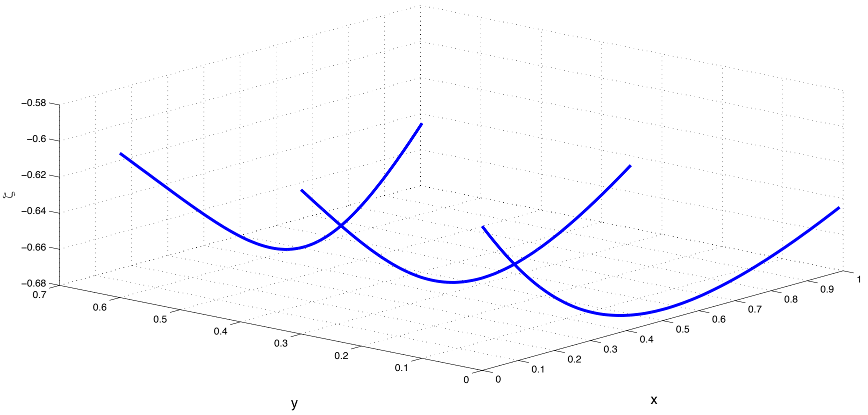

Figure 11: 3D flow paths for quadratic-quartic EUC profile with paths initiating from points at intermediate depths.

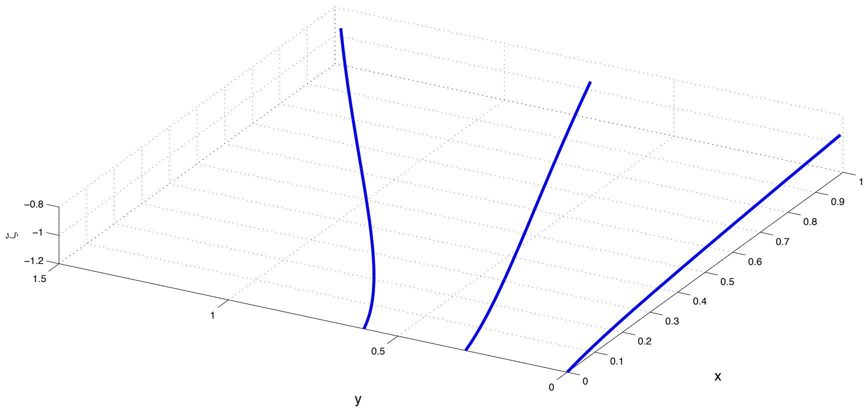

Figure 12: 3D flow paths for quadratic-quartic EUC profile with paths initiating from points at deeper locations.

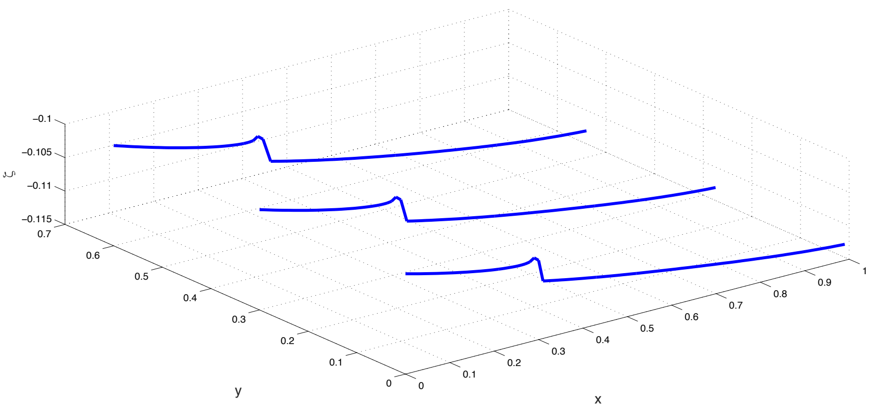

Figure 13: 3D flow paths for polynomial EUC profile with paths initiating from points near surface.

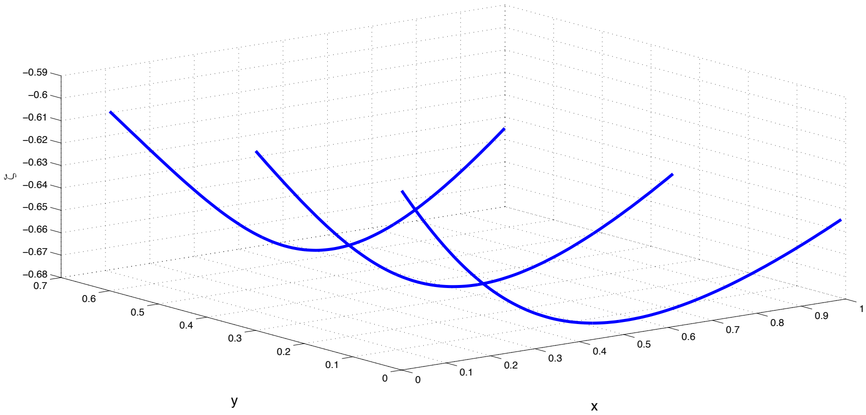

Figure 14: 3D flow paths for polynomial EUC profile with paths initiating from points at intermediate depths.

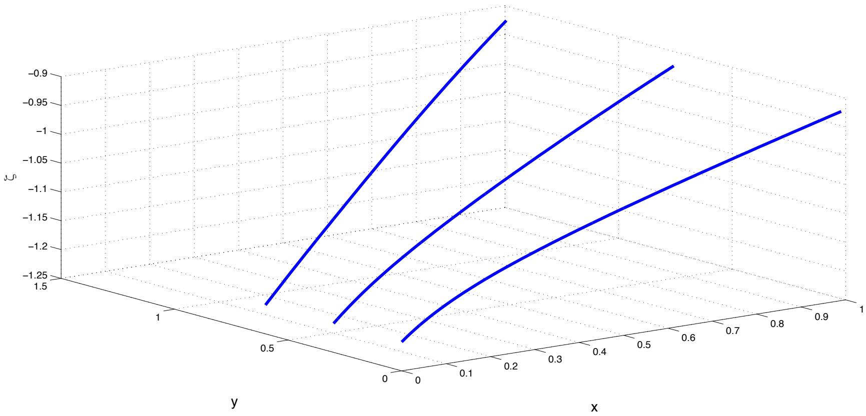

Figure 15: 3D flow paths for polynomial EUC profile with paths initiating from points at deeper locations.

3 Conclusion

The investigation carried out in this paper and the analyses of the velocity field and flow paths have resulted in a number of observations and findings. Strong regions of flow field exist away from the equator at intermediate depths. Variation of the velocity amplitudes with depth or along the meridional direction are more pronounced away from the equator. Results are similar for the two models of EUC considered - though the details of the velocity profle are model sensitive, their broad natures are unaffected by the EUC model used. For example, in the numerical investigation, the vertical velocity attains higher negative values at greater depth for polynomial profile of the EUC, in contrast to the corresponding velocities obtained for the quadratic-quartic model. Analyses of the flow paths shown sharp changes in their gradients. Another remarkable feature observed in this study is the presence of a sub-sea ocean bridge in the west-to-east direction. Extra-equatorial trajectories, forcing both toward the equator and poleward, have also been observed. In particular, poleward extra-equatorial flow paths originating from a deeper initial source at the western end of the equator are spectacular. All the features of the flow path strongly reinforce the three-dimensional nonlinear nature of the flow, demonstrate that the Constantin-Johnson model is capable of modelling these features, some of which are known from observations and some still possibly unknown. From the study we conclude that the Constantin-Johnson model for Pacific equatorial ocean dynamics shows promise, and with some further development, is a potential candidate to become an Ocean General Circulation Model.

Acknowledgements

Discussions with Prof Robin Stanley Johnson, NewCastle University, UK and suggestions given by him are gratefully acknowledged. The useful suggestions by the reviewers are also appreciated.

References

[1] B. Blanke and S. Raynaud. Kinematics of the Pacific equatorial undercurrent: An eulerian and lagrangian approach from gcm results. *J. Phys. Oceanogr.*, 27:1038–1053, 1997.

[2] M. A. Cane. The response of an equatorial ocean to simple wind stress patterns: I. model formulation and analytical results. *J. Mar. Res.*, 37:232–252, 1979.

[3] M. A. Cane. The response of an equatorial ocean to simple wind stress patterns: II. numerical results. *J. Mar. Res.*, 6:355–398, 1979.

[4] J. G. Charney. Non-linear theory of a wind-driven homogeneous layer near the equator. *Deep Sea Res.*, 6:303–310, 1960.

[5] A. Constantin. An exact solution for equatorially trapped waves. *J. Geophys. Res.*, 117:C05029, 2012.

[6] A. Constantin. Some nonlinear, equatorially trapped, nonhydrostatic internal geophysical waves. *J. Phys. Oceanogr.*, 44:781–789, 2014.

[7] A. Constantin and P. Germain. Instability of some equatorially trapped waves. *J. Geophys. Res.*, 118:2802–2810, 2013.

[8] A. Constantin and R. S. Johnson. The dynamics of waves interacting with the equatorial undercurrent. *Geophys. Astrophys. Fluid Dyn.*, 109:311–358, 2015.

[9] A. Constantin and R. S. Johnson. An exact, steady, purely azimuthal equatorial flow with a free surface. *J. Phys. Oceanogr.*, 46:1935–1945, 2016.

[10] A. Constantin and R. S. Johnson. A nonlinear, three-dimensional model for ocean flows, motivated by some observations of the Pacific equatorial undercurrent and thermocline. *Phys. of Fluids*, 29:056604, 2017.

[11] T. Cromwell. Circulation in a meridional plane in the central equatorial Pacific. *J. Mar. Res.*, 12:196–213, 1953.

[12] T. Cromwell, R. B. Montgomery and E. D. Stroup. Equatorial undercurrent in Pacific ocean revealed by new methods. *Science*, 119:648– 649, 1954.

[13] E. J. Drenkard and K. B. Karnaukas. Strengtheing of Pacific equatorial undercurrent in the soda reanalysis: Mechanics, ocean dynamics, and implications. *J. Amer. Meteorol. Soc.*, 27:2, 2405–2415, 2014.

[14] A. V. Fedorov and J. N. Brown. *'Equatorial waves' in Encyclopeida of Ocean Sciences*, edited by Steele, J. Academic Press, San Diego, 2009.

[15] R. A. Feely, T. Takahashi, R. Wanninkhof, M. J. McFadden, C. E. Cosca, S. C. Sutherland and M. E. Carr. Decadal variability of the air-sea CO_2 fluxes in the equatorial Pacific ocean. *J. Geophys. Res.*, 111:C08S90, 2006.

[16] N. P. Fofonoff and R. B. Montgomery. The equatorial undercurrent in the light of the vorticity equation. *Tellus*, 7:518–521, 1955.

[17] A. E. Gill. The equatorial current in a homogeneous ocean. *Deep Sea Res.*, 18:421–431, 1971.

[18] A. E. Gill. Models of equatorial currents. *Proc. Numerical Models of Ocean Circulation*, pp. 181– 203, 1975.

[19] P. J. Goodman, W. Hazeleger, P. de Vries and M. Cane. Pathways into the Pacific equatorial undercurrent: A trajectory analysis. *J. Phys. Oceangr.*, 35:2134–2151, 2005.

[20] M. Grenier, S. Cravatte, B. Blanke, C. Menkes, A. K.-Larrouy, F. Durand, A. Melet and C. Jeandel. From the western boundary currents to the Pacific equatorial undercurrent: Modelled pathways and water mass evolutions. *J. Geophys. Res.*, 116:C12044, 2011.

[21] W. Hazeleger, M. Visbeck, M. Cane, A. Karspeck and N. Naik. Decadal upper ocean temperature variability in the tropical Pacific. *J. Geophys. Res.*, 106:8971–8988, 2001.

[22] D. Henry. An exact solution for equatorial geophysical water waves with an underlying current. *Eur. J. Mech.-B /Fluids*, 38:18–21, 2013.

[23] D. Henry. Equatorially trapped nonlinear water waves in a β-plane approximation with centripetal forces. *J. Fluid Mech.*, 804:R1, 2016.

[24] G. C. Johnson, M. J. McPhaden and E. Firing. Equatorial Pacific ocean horizontal velocity, divergence, and upwelling. *J. Phys. Oceanogr.*, 31:839–849, 2001.

[25] K. B. Karnauskas and A. L. Cohen. Equatorial refuge and amid tropical warming. *Nat. Clim. Change*, 2(7):530–534, 2012.

[26] J. A. Knauss and J. E. King. Observations of the Pacific equatorial undercurrent. *Nature*, 158:601–602, 1958.

[27] P. Lu, J. P. McCreary Jr, and B. A. Klinger. Meridional circulation cells and the source waters of the Pacific equatorial undercurrent. *J. Phys. Oceangr.*, 28:62–84, 1998.

[28] R. Lukas. The termination of the equatorial undercurrent in the eastern Pacific. *Prog. Oceanog.*, 16:63–90, 1986.

[29] J. P. McCreary. A linear stratified ocean model of the equatorial undercurrent. *Phil. Trans. Roy. Soc. London A: Math. Phys. Eng. Sci.*, A298:603– 635, 1981.

[30] J. P. McCreary Jr. Modeling equatorial ocean circulation. *Annu. Rev. Fluid Mech.*, 17(1):359–409, 1985.

[31] J. P. McCreary Jr. and P. Lu. Interaction between the subtropical and equatorial ocean circulations: the subtropical cell. *J. Phys. Oceanogr.*, 24:466– 497, 1994.

[32] W. D. McKee. The wind-driven equatorial circulation in a homogeneous ocean. *Deep Sea Res. Oceanogr. Abs.*, 20:889–899, 1973.

[33] J. Pedlosky. Thermocline theories, in *General Circulation of the Ocean*, pp. 55–101. Springer, 1987.

[34] X. Qin, A. Sengupta and E. V. Sebille. Variability in the origins and pathways of Pacific equatorial undercurrent water. *J. Geophys. Res.*, 120:3113–3128, 2015.

[35] J. P. Ryan, I. Ueki, Y. Chao, H. Zhang, P. S. Polito and F. P. Chavez. Western Pacific modulation of large phytoplankton blooms in the central and eastern equatorial Pacific. *J. Geophys. Res.*, 111:G02013, 2006.

[36] A. R. Robinson. An investigation into the wind as the cause of the equatorial undercurrent. *J. Mar. Res.*, 24:179 − 204, 1966.

[37] N. Schneider, S. Venzke, A. J. Miller, D. W. Pierce, T. Barnett, C. Deser and M. Latif. Pacific thermocline bridge revisited. *Geophys. Res. Lett.*, 26:1329–1332, 1999.

[38] H. Stommel. Wind-drift near the equator. *Deep Sea Res.*, 6:298 − 302, 1960.

[39] L. D. Talley, G. L. Pickard, W.J. Emery and J.H. Swift. *Descriptive physical oceanography: An introduction.* Elsevier, London, 2011.

[40] M. Tsuchiya, R. Lukas and F. A. Fine. Source waters of the Pacific equatorial undercurrent. *Prog. Oceanog.*, 23:101–147, 1989.

[41] G. K. Vallis. *Atmospheric and Oceanic Fluid Dynamics.* Cambridge University Press, 2006.

[42] G. Veronis. An approximate theoretical analysis of the equatorial undercurrent. *Deep Sea Res.*, 6:318– 327, 1960.

[43] K. Wyrtki and B. Kilonsky. Mean water and current structure during the Hawaii-Totahiti shuttle experiment. *J. Phys. Oceanogr.*, 14:242–254, 1984.

[44] R. H. Zhang, L. M. Rothstein and A. J. Busalaccchi. Origin of upper-ocean warming and El Niño change on decadal time scales in the tropical Pacific ocean. *Nature*, 391:879–882, 1998.

On an exact solution of a nonlinear three-dimensional model in ocean flows with Equatorial Undercurrent and linear variation in density

Biswajit Basu

Discrete and Cont. Dyn. Sys. A, 39(8), 4783 - 4796, 2019

Abstract

The aim of the paper is to develop an exact solution relating to a system of model equations representing ocean flows with Equatorial Undercurrent and thermocline in the presence of linear variation of density with depth. The system of equations is generated from the Euler equations represented in a suitable rotating frame by following a careful asymptotic approach.The study in this paper is motivated by the recently developed Constantin-Johnson model [13] for Pacific flows with undercurrent and the exact results provided therein. The model formulated is two-layered, three-dimensional and nonlinear with a symmetric structure about the equator. The equations contain Coriolis effect and is consistent with β - plane approximation. Exact results of the asymptotic system of equations have been derived in a region close to the equator.

1 Introduction

Equatorial Undercurrent plays an important role in ocean dynamics and has a controlling influence on the temperature, salinity, and the nutrient enrichment of equatorial thermocline. It also impacts on biological productivity, atmospheric carbon exchange, and the El-Niño Southern Oscillation.

Since the observation of these undercurrents in 1950s by Cromwell, several investigations have been carried out [29]. Although significant progress has been made to explain features, primarily based on linear theory, which has been successful in modelling a number of observations, there are still some open questions yet to be resolved. In this context, suitable nonlinear theories are expected to provide more insight as the ocean dynamics is essentially three-dimensional and nonlinear [15].

The following three properties of the equatorial dynamics are:

(1) A shallow westward flow of surface current (typically within the top 50m depth). This is confined mainly to a few degrees on either side of the equator.

(2) A strong coherent eastward undercurrent flowing at a speed much faster than the surface current. This is primarily responsible for the vertically-integrated transport. Beneath this undercurrent, a relatively weak flow exists.

(3) Flow in the westward direction on either side of the EUC, with eastward countercurrents poleward of this. This current is strongest in the Northern hemisphere and meets the surface.

The flow structure is nonlinear and complex with regions of upwelling and downwelling superimposed on the EUC. Hence, the flow is essentially three dimensional, though upwelling may be restricted to certain specific zones. While flow at the surface moves predominantly to the west driven by wind, and some flows moving to the north or to the south, further down little is known about flow structures [24, 25, 26]. A schematic shown in Fig.1 describes the basic flow configurations.

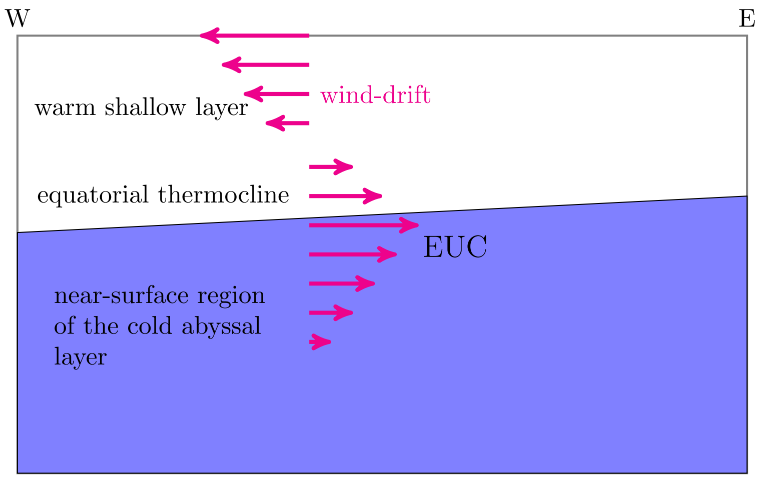

Figure 1: A schematic of the structure of the equatorial ocean flow.

Equatorial ocean dynamics has some striking features. Close to the Equator the meridional component of the Coriolis force is negligible (vanishing at the Equator) leading to the breakdown of geostrophy. Hence, the flow in this region is essentially driven by the easterly trade winds in the Pacific and Atlantic, and by the seasonally reversing monsoonal winds in the Indian Ocean [35]. Equatorial ocean regions also present a pronounced stratification, greater than anywhere else in the ocean [16].

The simplest type of model of the EUC consists of a homogeneous fluid subject to uniform westward stress at the surface. This local model, in a rudimentary form, is unstratified. The model can be further developed to account for the effect of horizontal viscosity and more realistic models can also consider effects of stratification leading to a layered model of undercurrents. Other non-local and physical models involve a pressure head acting on the undercurrent which has an extra-equatorial origin. Observations indicate that some of the water in the EUC flows from sub-tropical gyres as the temperature in the core of the undercurrent ranges between $16 - 22^0$ C. This range of temperature is much lower than the surface equatorial temperatures except at the eastern end of the ocean basins where the undercurrent ends. A two-layer inertial model of undercurrents can account for equatorial and extra-equatorial dynamics.

Local theories of undercurrent were proposed by [14]. These theories were developed further by [34, 36, 33]. Other linear non-dissipative models can be found in [18, 19, 31]. Significant extensions to linear models including effects of continuous stratification are due to [28]. In addition, some nonlinear models have also been developed [5, 3, 4, 31]. Inertial theories began with the work of [17] and were further advanced by [32]. In the investigations by [30], the EUC was considered as a part of a larger and more complex subtropical current system, with both local and inertial effects. However, a complete model of the integrated dynamics requires numerical approaches.

The basic variation with depth of the main azimuthal flow of the EUC can be modelled in the spherical geometry of a rotating Earth [11], to capture the fine structure. Approximations are possible with certain limitations; for an overview of ocean dynamics in the equatorial Pacific in the f-plane setting see [10]. Explicit solutions to the nonlinear governing equations in the equatorial β-plane, were recently obtained in the Lagrangian framework [6, 8, 9, 21, 22]. These solutions represent realistic flow only for the region near the surface or in the neighbourhood of the thermocline.

Constantin and Johnson [13] recently proposed a model based on the classical fluid-dynamics approach. The nonlinear, three-dimensional model, herein called the Constantin-Johnson model, was developed following a systematic approach which is mathematically consistent, capturing the essential properties of the flow observed in the Pacific equatorial undercurrent (EUC), and avoids any oversimplification. The model, for example, accounts for the Coriolis effects due to the rotation of the Earth and retains non-traditional terms arising in the formulation. The model is based on the assumption of slow evolution of a two-layer flow in the equatorial direction and successfully provides asymptotic solutions. Some numerical studies on this model to investigate the properties of velocity field and flow paths have been carried out in [2, 1].

Motivated by the Constantin-Johnson model and the exact results obtained by them, this paper considers the case of linear variation of density along the depth from the surface down to the bottom of the undercurrent which is close to but little below the thermocline, and a constant density below this, which represents a realistic scenario. Exact results have been derived in this paper for the case described with density variation, retaining the nonlinear, three-dimensional structure of the model. This also indicates that the Constantin-Johnson model is indeed versatile enough to cater for several realistic situations.

2 Governing equations for an EUC

We choose a coordinate system that rotates with the Earth, with $\overline{x}$ pointing due east, $\overline{y}$ due north, and $\overline{z}$ vertically upwards (see Fig.2). This chosen coordinate system is

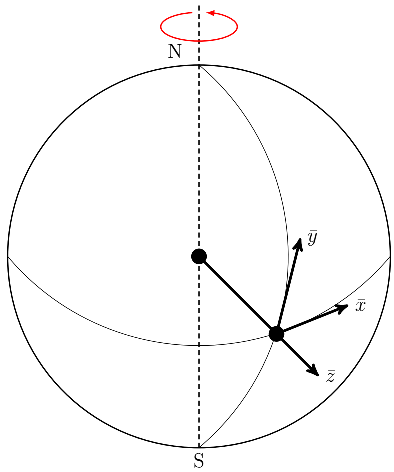

Figure 2: The rotating frame of reference based on tangent plane, with the $\overline{x}$ axis chosen horizontally due east, the $\overline{y}$ axis horozontally due north and the $\overline{\overline{z}}$ axis vertically upward.

the one associated with the tangent plane (and therefore consistent with the β-plane approximation). The β-plane approximation adopts a local "flat" Cartesian coordinate system, while still capturing the effects of the curvature of the Earth's surface. These coordinates are obtained from the original spherical coordinate system by using a two-stage manoeuvre. First, the great circle (the equator) is straightened to become the generator of a cylinder, its circular cross section now representing the interior of the sphere. The coordinate perpendicular to this, on the surface, is then be expressed as the arc length along the circular rim of the cylinder, following the circumference at a mean radius of the Earth. The coordinate $\overline{y}$ in Fig.2 is in the direction of the tangent at a point on the equator. This is, however, not the curvilinear coordinate which we denote by $\overline{\overline{y}}$. In typical Cartesian coordinates, the z-axis points vertically upwards from the centre of the Earth, for all points on the surface; we denote the corresponding cylindrical (radial) coordinate by $\overline{\overline{z}}$. The two governing equations (Euler and mass conservation) with spatially varying density may therefore be written as

$$\frac{D(\rho\overline{\mathbf{u}})}{D\overline{t}} + 2\overline{\mathbf{\Omega}} \times (\rho\overline{\mathbf{u}}) = -\overline{\nabla}\overline{p} + \overline{\mathbf{F}}, \quad \overline{\nabla}.(\rho\overline{\mathbf{u}}) = 0 \tag{2.1}$$

where $\overline{\mathbf{u}} = (\overline{u}, \overline{v}, \overline{w})$ is the velocity of the fluid corresponding to $\overline{\mathbf{x}} = (\overline{x}, \overline{y}, \overline{z})$, $\overline{t}$ is the time (and $D/D\overline{t}$ the associated material derivative), while $\overline{p}$ and ρ are the pressure and the spatially varying density, respectively. The body force is represented by $\overline{\mathbf{F}}$ (which incorporates the effect of constant gravitational acceleration only) and $\overline{\mathbf{\Omega}} = \overline{\Omega}(0, \cos\theta, \sin\theta)$ is the angular-velocity vector describing the rotation of the Earth (with $|\overline{\mathbf{\Omega}}| = \overline{\Omega} \approx 7.29 \times 10^{-5}$ rad s^{-1} and θ the angle of latitude).

We now invoke a suitable approximation of the Coriolis term close to the equator. For small values of $\overline{\overline{y}}/\overline{R}$, where $\overline{R}$ is an average radius of the Earth, we write the term $2\overline{\mathbf{\Omega}} \times \overline{\mathbf{u}}$ as $2\overline{\Omega}(\overline{w} - \overline{\overline{y}}\overline{v}/\overline{R}, \overline{\overline{y}}\overline{u}/\overline{R}, -\overline{u})$, since $\sin\theta \approx \theta$ and $\cos\theta \approx 1$ for $|\theta| \ll 1$. This is in effect the equatorial "β-plane" approximation, which is regarded as acceptable within about 2^0 of the equator [20]. In this context, more recent discussions on equatorial f-plane are available in [7, 27, 12, 23]. We therefore have $\overline{x}$ measured, equivalently, along the curvature of the equator (eastwards) and $\overline{\overline{y}}$ measured along a line of longitude (northwards). It may be noted that, with this same approximation, the curved surface of the Earth drops below the $(\overline{x}, \overline{y})$-tangent-plane by an amount of $\overline{\overline{y}}^2/2\overline{R}$, approximately. This is indeed, consistent with, and a consequence of, the β-plane approximation. We thus have $\overline{\overline{z}} = \overline{z} + \frac{1}{2}\overline{y}^2/\overline{R}$ and $\overline{\overline{y}} = \overline{y}$ (see Fig. 2). With this interpretation of the chosen coordinate system, the distance from the centre of the Earth is $\overline{R} + \overline{\overline{z}}$, so that the gravitational potential is $\rho\overline{\overline{z}}g$ and thus the gravitational field (its negative gradient) becomes $(0, 0, -\rho g)$. The gravity term appears only in the $\overline{\overline{z}}$-component equation. The governing equations for a steady flow therefore become (writing $\overline{y}$ for $\overline{\overline{y}}$)

$$\overline{u}\,(\rho\overline{u})_{\overline{x}} + \overline{v}\,(\rho\overline{u})_{\overline{y}} + \overline{w}\,(\rho\overline{u})_{\overline{\overline{z}}} + 2\overline{\Omega}\rho\left(\overline{w} - \frac{\overline{y}}{\overline{R}}\overline{v}\right) = -\overline{p}_{\overline{x}}, \tag{2.2}$$

$$\overline{u}\,(\rho\overline{v})_{\overline{x}} + \overline{v}\,(\rho\overline{v})_{\overline{y}} + \overline{w}\,(\rho\overline{v})_{\overline{\overline{z}}} + 2\overline{\Omega}\rho\frac{\overline{y}}{\overline{R}}\overline{u} = -\overline{p}_{\overline{y}}, \tag{2.3}$$

$$\overline{u}\,(\rho\overline{w})_{\overline{x}} + \overline{v}\,(\rho\overline{w})_{\overline{y}} + \overline{w}\,(\rho\overline{w})_{\overline{\overline{z}}} + 2\overline{\Omega}\rho\overline{u} = -\overline{p}_{\overline{\overline{z}}} - \rho g, \tag{2.4}$$

$$(\rho\overline{u})_{\overline{x}} + (\rho\overline{v})_{\overline{y}} + (\rho\overline{w})_{\overline{\overline{z}}} = 0, \tag{2.5}$$

with g as the constant acceleration due to gravity.

Let us consider the case of a linear variation of density from the surface down to the bottom of the equatorial undercurrent (EUC) and then constant density below this. If so desired the problem can be reformulated by considering linear variation in density from the surface down to a characteristic depth corresponding to the position of the theromocline. The depth from the surface to the bottom of the EUC is denoted by $\overline{h}$. Let the density at the surface and at the point at the bottom of the EUC be denoted by ρ_s and ρ_0, respectively. Since the warmer water with lower density is at the top of the dense, colder layer, $\rho_s \leq \rho_0$.

Assume the density variation of the form

$\rho(\overline{\overline{z}}) = \rho_s - (\rho_0 - \rho_s)\frac{\overline{\overline{z}}}{\overline{h}}, \quad 0 \leq \overline{\overline{z}} \leq -\overline{h}$

$= \rho_0, \qquad\qquad -\overline{h} \le \overline{\overline{z}} \le -\overline{d}$
where $\bar{d}$ is the depth of the mean ocean surface and we denote $\alpha = \rho_s/\rho_0$.

Equations (2.2)-(2.5) have been expressed within the limitations of the β-plane approximation and, precisely as written, applied to the region above the bottom of the undercurrent. For the region below, the density is assumed to be constant, the equations similar to those given in [13] then follow directly.

The boundary conditions that we require involve the pressure at the surface ($\overline{\overline{z}} = \overline{\eta}(\overline{x}, \overline{y})$) and a kinematic condition that describes the motion of the free surface. These are, respectively, given by the following

$$\left.\begin{array}{l} \overline{p} = \overline{P}_s(\overline{x}, \overline{y}); \\ \overline{w} = \overline{u}\,\overline{\eta}_{\overline{x}} + \overline{v}\,\overline{\eta}_{\overline{y}} \end{array}\right\} \text{ on } \overline{\overline{z}} = \overline{\eta}(\overline{x}, \overline{y}), \tag{2.6}$$

where $\overline{P}_s(\overline{x}, \overline{y})$ is the pressure prescribed at the surface. Further discussions on the pressure will follow later. There is a corresponding kinematic condition at the thermocline ($\overline{\overline{z}} = \overline{T}(\overline{x}, \overline{y})$), which is given by

$$\overline{w} = \overline{u}\,\overline{T}_{\overline{x}} + \overline{v}\,\overline{T}_{\overline{y}} \text{ on } \overline{\overline{z}} = \overline{T}(\overline{x}, \overline{y}). \tag{2.7}$$

However, since there is no pycnocline, the pressure is automatically continuous across the thermocline. Further, the kinematic condition at the impermeable ocean bed $\overline{\overline{z}} = -\overline{d}(\overline{x}, \overline{y})$ is given by

$$\overline{w} + \overline{u}\,\overline{d}_{\overline{x}} + \overline{v}\,\overline{d}_{\overline{y}} = 0 \text{ on } \overline{\overline{z}} = -d(\overline{x}, \overline{y}). \tag{2.8}$$

3 Non-dimensionalization of the equations

The next stage in our analysis is to recast the governing equations in a suitable form by introducing non-dimensionalization of the variables so that we can carry out an asymptotic analysis. To this end, we use the following non-dimensionalization of the variables

$\overline{\mathbf{x}} = (\overline{x}, \overline{y}, \overline{\overline{z}}) = (\overline{L}x, \bar{l}y, \overline{h}z)$,

$\overline{\mathbf{u}} = (\overline{u}, \overline{v}, \overline{w}) = U(u, \frac{\bar{l}}{L}v, \frac{\overline{h}}{L}w)$,

$\overline{p} = \rho\,\overline{U}^2 p$,
where the length scales are $(\overline{L}, \bar{l}, \overline{h})$ and $\overline{U}$ is an appropriate speed scale. The velocity components have been non-dimensionalised in a form that gaurantees the existence of a stream function, via a balance of terms of equal size, irrespective of whether the flow is in the (x, z) or (y, z) frame. Normalizing with respect to ρ_0, (2.2) - (2.5) become

$$[\alpha-(1-\alpha)z]\,(uu_x+vu_y+wu_z)-(1-\alpha)\frac{\bar{l}^2}{\bar{R}\bar{h}}vuy-(1-\alpha)wu$$

$$+\,2\frac{\bar{\Omega}\bar{h}}{\bar{u}}[\alpha-(1-\alpha)z](w-\frac{\bar{l}^2}{\bar{R}\bar{h}}yv)=-p_x\ ; \tag{3.9}$$

$$[\alpha-(1-\alpha)z]\left(\frac{\bar{l}}{\bar{L}}^2\right)(uv_x+vv_y+wv_z)-(1-\alpha)\left(\frac{l}{\bar{L}}^2\right)\frac{\bar{(l)}^2}{\bar{R}\bar{h}}v^2y$$

$$-\,(1-\alpha)\left(\frac{\bar{l}}{\bar{L}}^2\right)vw+2\frac{\bar{\Omega}\bar{h}}{\bar{u}}\,[\alpha-(1-\alpha)z]\left(\frac{\bar{l}^2}{\bar{R}\bar{g}}\right)yu=-p_y\ ; \tag{3.10}$$

$$[\alpha-(1-\alpha)z]\left(\frac{\bar{h}}{\bar{L}}\right)^2(uw_x+vw_y+ww_z)-(1-\alpha)\left(\frac{\bar{h}}{\bar{L}}\right)^2\frac{\bar{h}^2}{\bar{R}\bar{h}}vwy$$

$$-\,(1-\alpha)\left(\frac{\bar{h}}{\bar{L}}\right)^2w^2-2\frac{\bar{\Omega}\bar{h}}{\bar{u}}[\alpha-(1-\alpha)z]u=-p_z-[\alpha-(1-\alpha)z]\frac{g\bar{h}}{\bar{U}^2} \tag{3.11}$$

and

$$[\alpha-(1-\alpha)z](u_x+v_y+w_z)-\left(\frac{\bar{l}^2}{\bar{R}\bar{h}}\right)(1-\alpha)vy-(1-\alpha)w=0\ , \tag{3.12}$$

with the boundary conditions

$$p=\overline{P}_s(\overline{x},\overline{y})/(\rho_0\overline{U}^2)=P_0(x,y);w=u\eta_x+v\eta_y \tag{3.13}$$

on $z=\eta(x,y)$, and

$$w=uT_x+vT_y \tag{3.14}$$

on $z=T(x,y)$, where $\overline{\eta}=\overline{h}\eta$ and $\overline{T}=\overline{h}T$. Here, we do not use the bottom boundary condition since the flow below a certain depth is assumed stagnant and this condition is automatically satisfied by the flow field. It may be noted that if $\alpha=1$, we arrive at exactly the same equations obtained for piece-wise constant density as used in [13].

We further redefine the pressure so that the pressure is expressed relative to the ambient hydrostatic pressure. This gives

$$p(x,\,y,\,z)=[\alpha z-(1-\alpha)\frac{z^2}{2}]\frac{g\bar{h}}{\bar{U}^2}+P(x,\,y,\,z)\ . \tag{3.15}$$

Further, we set $\bar{l}=\sqrt{\bar{R}\bar{h}}$, $\bar{\Omega}\bar{h}/\bar{u}=\omega$. With this choice for $\bar{l}$, we invoke the limiting process described by $(\overline{h}/\overline{L})^2\to 0$ with $(\bar{l}/\overline{L})^2=(\bar{l}/\overline{h})^2(\overline{h}/\overline{L})^2\to 0$ and all other parameters held fixed. For some typical values of length and velocity scales, e.g. for the case of Pacific ocean, see [13]. The governing equations for momentum and mass conservation therefore take the form

$$\begin{aligned}&[\alpha-(1-\alpha)z](uu_x+vu_y+wu_z)-(1-\alpha)vuy-(1-\alpha)wu\\&+2w[\alpha-(1-\alpha)z](w-yv)=-P_x\ ,\end{aligned} \tag{3.16}$$

$$2\omega[\alpha - (1-\alpha)z]yu = -P_y \ , \tag{3.17}$$

$$2\omega[\alpha - (1-\alpha)z]u = P_z \tag{3.18}$$

and

$$[\alpha - (1-\alpha)](u_x + v_y + w_z) - (1-\alpha)vy - (1-\alpha)w = 0 \ , \tag{3.19}$$

with the boundary conditions

$$\left.\begin{array}{l} P(x,y,z) = P_0(x,y) + \kappa\eta(x,y) \\ w = u\eta_x + v\eta_y \end{array}\right\} \text{ on } z = \eta(x,y), \tag{3.20}$$

$$w = uT_x + vT_y \text{ on } z = T(x,y), \tag{3.21}$$

where $\kappa(\eta) = [\alpha - (1-\alpha)\frac{\eta}{2}]g\bar{h}/\overline{U}^2$. The governing equations that correspond to (3.16)-(3.19) and (3.20)-(3.21), but valid below the region with the undercurrent corresponding to constant density, are written as (see [13])

$$\begin{array}{r} uu_x + vu_y + \omega u_z + 2w(w - yv) = -P_x, \\ 2\omega yu = -P_y, \quad 2\omega u = P_z, \end{array} \tag{3.22}$$

$$u_x + v_y + w_z = 0 \ . \tag{3.23}$$

The interpretation of our choice of scales is such that, in the flow direction, we have $0 \le x \le 1$. In the context of the EUC, we could associate the western end, away from any shorelines, by $x = 0$ and correspondingly $x = 1$ at the eastern end. The width must be restricted (by virtue of the β-plane approximation), which we represent by $-y_0 < y < y_0$, for suitable (finite) y_0.

4 Pressure function

We now examine the form taken by the pressure in this asymptotic formulation.

Let us introduce

$$\underbrace{u(x,\, z - \frac{1}{2}y^2)}_{\phi_\zeta(x,\, z - \frac{1}{2}y^2)}[\alpha - (1-\alpha)z] = \bar{\phi}_\zeta(x,\, z - \frac{1}{2}y^2,\, z) \quad \text{with} \quad \zeta = z - \frac{1}{2}y^2$$

leading to

$$P_y = -2\omega\bar{\phi}_\zeta y \ ;$$

$$P_z = 2\omega\bar{\phi}_\zeta \ .$$

It may be noted that $\zeta = \frac{\bar{\bar{z}}}{h}$ is the non-dimensional coordinate measured from the tangent plane. We then have

$$P(x,y,z) = A(x) + 2\omega\bar{\phi}(x,\, z - \frac{1}{2}y^2,\, z) \tag{4.24}$$

where $A(x)$ is an arbitrary function. Once the velocity field u is prescribed, one can then determine ϕ and hence $\bar{\phi}$. For convenience, we define $\phi(x, 0, \frac{1}{2}y^2) = 0$ which implies $\bar{\phi}(x, 0, \frac{1}{2}y^2) = 0$ if $u \neq 0$ at $z = \frac{1}{2}y^2$.

We now investigate the pressure boundary condition in more detail. To do so, we first describe the free surface $z = \eta(x, y)$ relative to the tangent plane by setting

$$\eta(x, y) = \frac{1}{2}y^2 + h(x, y) \tag{4.25}$$

leading to the pressure at the free surface given by

$$P_0(x, y) = A(x) - \left\{\frac{1}{2}y^2 + h(x, y)\right\} \kappa \left(\frac{1}{2}y^2 + h(x, y)\right) + 2\omega\bar{\phi}(x, h(x, y), \eta(x, y)) \tag{4.26}$$

which is the relation between the pressure prescribed at the surface and the surface distortion.

5 Simplifications of the model based on physical considerations

Since the free surface incorporates the curvature in the y direction as measured with respect to the tangent plane, no further dependence on y is assumed in this model, i.e. $h = h(x)$ only. Further, we also prescribe that the free surface is flat in the x direction which is not an unreasonable simplification as the ocean rises from east to west (relative to the curvature of the Earth) by a small amount (e.g. by 0.5 m for the case of the Pacific ocean). Hence, we have $h(x) = 0$. The free surface is therefore the (local) undisturbed surface of the sphere within the β-plane approximation. Pressure at the surface is thus given by

$$P_0(x, y) = A(x) - \left\{\frac{1}{2}y^2\right\} \kappa \left(\frac{1}{2}y^2\right) \ . \tag{5.27}$$

We now invoke the condition of constant pressure along $y = 0$ leading to $A(x) =$ constant.

The thermocline is identified with a plane parallel to the tangent plane (and so follows the curvature in the y-direction), but we allow it to evolve in the x-direction. Thus, we choose to set

$$T(x, y) = -t(x) + \frac{1}{2}y^2. \tag{5.28}$$

Thus the special problem that we discuss here is the one which follows the geometry of the curved surface (in the y-direction, locally) and has a (local) flat free surface associated with a constant atmospheric pressure at the surface along the equator and a thermocline at a level which may evolve in the equatorial direction. This is described by the set of equations

$$\begin{aligned}&[\alpha - (1-\alpha)z](uu_x + vu_y + wu_z) - (1-\alpha)vuy - (1-\alpha)wu \\ &+ 2\omega[\alpha - (1-\alpha)z](w - yv) = -2\omega\bar{\phi}_x,\end{aligned} \tag{5.29}$$

$$[\alpha - (1-\alpha)](u_x + v_y + w_z) - (1-\alpha)vy - (1-\alpha)w = 0 \tag{5.30}$$

with

$$w = yv \text{ on } z = \frac{1}{2}y^2 \text{ and } w = -ut' + yv \text{ on } z = -t(x) + \frac{1}{2}y^2 \tag{5.31}$$

where the prime denotes the derivative with respect to x, and u is assumed given as a function of z on $y = 0$, and therefore it is known across the (z, y) plane (with the x-evolution superimposed on this).

6 Method of solution

We now proceed to solve the problem using some similar concepts used in [13].

At the non-dimensional longitude x, let us denote the depth at which u first vanishes below the surface by $\zeta_0(x) < 0$. Note that field observations indicate that $u(x, 0) < 0$ all along the equator at the surface, while u vanishes in the abyssal layer where there is no motion.

Since $\phi(x, 0, \frac{1}{2}y^2) = 0$, we conclude that

$$\phi(x, \zeta) = -\int_{\zeta}^{0} u(x, \zeta')d\zeta' \quad \text{for } \zeta < 0 \; ; \tag{6.32}$$

now using (3.19) in (3.16) we get

$$[\alpha - (1-\alpha)z](uu_x + vu_y + wu_z) - (1-\alpha)vuy - (1-\alpha)wu \\ + 2\omega[\alpha - (1-\alpha)z](w - yv) = -2\omega\bar{\phi}_x$$

leading to

$$[\alpha - (1-\alpha)z][-u(v_y + w_z) + vu_y + wu_z] + \cancel{(1-\alpha)vuy} + \cancel{(1-\alpha)wu} - \cancel{(1-\alpha)vuy} -$$

$$\cancel{(1-\alpha)wu} + [\alpha - (1-\alpha)z]2\omega(w - yv) = -2\omega\bar{\phi}_x$$

which can be re-expressed as

$$\{\frac{v}{u}E\}_y + \{\frac{w}{u}E\}_z = \frac{2\omega\bar{\phi}_x}{u^2}\frac{E}{[\alpha - (1-\alpha)z]} \quad \text{for } \zeta_0(x) < \zeta < 0 \tag{6.33}$$

where

$$E(x, \zeta) = \exp\Big(2\omega\int_{\zeta}^{0}\frac{d\zeta'}{u(x, \zeta')}\Big) \;\text{ with } \zeta = z - \frac{1}{2}y^2 \tag{6.34}$$

and

$$\bar{\phi}(x, y, \zeta) = -\int_{\zeta}^{0} u(x, \zeta')[\alpha - (1-\alpha)(\zeta' + \frac{1}{2}y^2)]\mathrm{d}\,\zeta', \; \zeta_0 < \zeta < 0 \; .$$

Equation(6.33) gives an equation of similar form as in [13], but with a different expression on the right hand side. To solve (6.33) we follow a similar approach to the one proposed in [13] by introducing a quasi-stream-function and setting

$$\frac{v(x, y, z)}{u(x, y, z)}E\Big(x, z - \frac{1}{2}y^2\Big) = \Psi_z(x, y, z), \tag{6.35}$$

which on integration with respect to the z variable leads to

$$\Psi_y + \frac{w}{u}E = -\hat{I}, \tag{6.36}$$

where

$$\hat{I}(x, y, z) = \int_{z}^{1/2y^2}\frac{2\omega\bar{\phi}_x(x, z' - \frac{1}{2}y^2)}{[u(x, z' - \frac{1}{2}y^2)]^2[\alpha - (1-\alpha)z']}E(x, z' - \frac{1}{2}y^2)\mathrm{d}\,z' \; . \tag{6.37}$$

Expressions for v and w are obtained as

$$v = \frac{u}{E}\Psi_z \quad , \quad w = -\frac{u}{E}(\Psi_y + \hat{I}) \; . \tag{6.38}$$

We can write (6.33) as

$$[\alpha-(1-\alpha)z][u_x - yu_\zeta \tfrac{\Psi_z}{E} - \tfrac{\Psi_y+\hat{I}}{E}u_\zeta] - (1-\alpha)u^2 y\tfrac{\Psi_z}{E} + (1-\alpha)\tfrac{u^2}{E}(\Psi_y+\hat{I})$$
$$-2\omega[\alpha-(1-\alpha)z][y\tfrac{\Psi_z}{E} + \tfrac{(\Psi_y+\hat{I})}{E}] = -\tfrac{2\omega\bar{\phi}_x}{u}, \tag{6.39}$$

and then from (6.39) we obtain

$$\tfrac{-yu_\zeta[\alpha-(1-\alpha)z]-(1-\alpha)u^2y-2\omega[\alpha-(1-\alpha)z]y}{E}\Psi_z - \tfrac{[\alpha-(1-\alpha)z]u_\zeta-(1-\alpha)u^2+2\omega[\alpha-(1-\alpha)z]}{E}\Psi_y$$
$$= -\tfrac{2\omega\bar{\phi}_x}{u} - [\alpha-(1-\alpha)z]u_x + [\alpha-(1-\alpha)]\tfrac{\hat{I}}{E}u_\zeta - (1-\alpha)\tfrac{u^2}{E}\hat{I}$$
$$+2\omega[\alpha-(1-\alpha)z]\tfrac{\hat{I}}{E}\ . \tag{6.40}$$

Let us now define

$$F(x,\,\zeta,z) = \{-u_\zeta[\alpha-(1-\alpha)z] - 2\omega[\alpha-(1-\alpha)z]\}\,/E(x,\zeta)$$

and

$$B(x,\,\zeta) = -(1-\alpha)u^2/E(x,\zeta)\ ,$$

then from (6.40) we have

$$y(F+B)\Psi_z + (F-B)\Psi_y = G(x,\,z,\,\zeta) \tag{6.41}$$

where

$$G(x,\zeta,z) = -\tfrac{2\omega\bar{\phi}_x}{u} - [\alpha-(1-\alpha)z]u_x + [\alpha-(1-\alpha)]\tfrac{I}{E}u_\zeta - (1-\alpha)\tfrac{u^2}{E}I$$
$$+2\omega[\alpha-(1-\alpha)z]\tfrac{I}{E} \tag{6.42}$$

with

$$I(x,\zeta,z) = \int_\zeta^0 \frac{2\omega\phi_x(x,\,\zeta')}{[u(x,\,\zeta')]^2[\alpha-(1-\alpha)(\zeta'+\frac{1}{2}y^2)]}E(x,\,\zeta')\mathrm{d}\,\zeta'\ . \tag{6.43}$$

It may be noted that when $\alpha = 1$, we recover precisely the same equation as obtained in [13] for constant density.

We now proceed to find the characteristic curve for the solutions of (6.41). From (6.41), we have the equations for the characteristics and the compatibility condition as

$$\frac{\mathrm{d}z}{y(F(x,\zeta,z)+B(x,\zeta))} = \frac{\mathrm{d}y}{(F(x,\zeta,z)-B(x,\zeta))} = \frac{\mathrm{d}\Psi}{G(x,\zeta,z)}\ . \tag{6.44}$$

The trajectories of the characteristic curve are given by the differential equation

$$y\frac{\mathrm{d}y}{\mathrm{d}z} = \frac{(F(x,\zeta,z)-B(x,\zeta))}{(F(x,\zeta,z)+B(x,\zeta))}\ . \tag{6.45}$$

Let us now consider a function $H(x,\zeta,z) \in C^1(\bar{D})$ such that

$$H_z(x, \zeta, z) = \frac{F(x, \zeta, z) - B(x, \zeta)}{F(x, \zeta, z) + B(x, \zeta)} \quad . \tag{6.46}$$

By appropriately choosing the vertical length scale and restricting the region of flow of interest to a certain width on either side of the equator, we can limit y to a suitable value y_L, such that $|y| \leq y_L < 1$; and $D = \{(x, \zeta) : 0 < x < 1 \ , \ \zeta_0 < \zeta = z - \frac{1}{2}y^2 < 0$ with $|y| < y_L\}$. Thus, $y^2/2 \ll 1$ and can be assumed to be close to zero within this region for the purpose of evaluating the variation of $H(x, \zeta, z)$ with respect to y in this particular region. Hence, in this domain we may assume

$$H(x, \zeta, z) \approx H(x, \zeta, z)|_{\zeta = z} = \bar{H}(x, z) \tag{6.47}$$

leading to

$$H_y(x, \zeta, z) = 0 \quad . \tag{6.48}$$

In fact, numerical investigations [2] have shown that a number of interesting features are concentrated within a range of $|y| \leq 0.5$, near the equatorial region, which corresponds to a total width of about 35 km (i.e., $\sim$ 20 km on either side of the equator). If the vertical length scale to be used for normalization is chosen to be, e.g. $2\bar{h}$, y would be restricted to values less than 0.35, if we keep the region of interest unchanged (i.e., to a total width of about 35 km); or if we so desire, we can cover a wider region, e.g. with a total width of about 60 km across the equator by allowing $|y|$ to be within a value of about 0.6.

In this region close to the equator, the characteristics curves take the form

$$\bar{H}(x, z) - \frac{1}{2}y^2 = C \tag{6.49}$$

where C is an arbitrary constant.

Notice that in [13], $B(x, \zeta) = 0$, which when used in (6.45) leads to the characteristic curves

$$z - \frac{1}{2}y^2 = K \ , \tag{6.50}$$

with K an arbitrary constant, along which the solutions propagate in [13].

Noting the form of the characteristics of the solution of (6.41) we define a function

$$\xi(x, y, z) = H(x, \zeta, z) - \frac{1}{2}y^2 \quad . \tag{6.51}$$

Let us seek a solution for Ψ in (6.41) of the form

$$\Psi(x, y, z) = y\bar{\psi}(x, \xi(x, y, z)) \ . \tag{6.52}$$

This is consistent with the fact that the velocity v along $y = 0$ should be zero (for symmetry). On using the expressions for H_z and H_y from (6.46) and (6.48) respectively, we then have

$$\Psi_y = \bar{\psi} - \bar{\psi}_\xi y^2 \quad \text{and} \quad \Psi_z = y\bar{\psi}_\xi H_z = y\bar{\psi}_\xi \frac{F - B}{F + B} \ . \tag{6.53}$$

The expressions in (6.53) when substituted in (6.41) gives

$$\bar{\psi} = \frac{G}{F - B} \tag{6.54}$$

leading to

$$\Psi = \frac{Gy}{F-B} \ . \tag{6.55}$$

Using the expression for Ψ; v and w follows. We note that there is a singular term in this solution, (6.55), arising from the zero of $(F-B)$, a problem that we address in the next section.

The expression for v and w are obtained as

$$v = \frac{u}{E}\left[\frac{G_z(F-B)-(F_z-B_z)G}{(F-B)^2}\right] y \tag{6.56}$$

and

$$w = -\frac{u}{E}\left[\frac{G}{(F-B)^3} - y\frac{G_z(F+B)}{(F-B)^2} + y\frac{G(F+B)(F_z-B_z)}{(F-B)^3} + \hat{I}\right] \tag{6.57}$$

respectively, where the subscripts in (6.56) and (6.57) denote partial derivatives. In the region below the bottom of the undercurrent, the solution given in [13] is valid.

With the hypotheses that the singular term $F-B=0$ is avoided, a solution of the velocity field in the fluid region $D = \{(x,\zeta) : 0 < x < 1 \ , \ \zeta_0 < \zeta = z - \frac{1}{2}y^2 < 0$ with $|y| < y_L\}$ is obtained. The solution is also valid for the fluid region $\zeta < \zeta_0$ as it satisfies (22) and (23).

7 Singular term in the solution

For the solution in the previous section to exist, we need $F-B \neq 0$. Consider the following relation

$$F(x,\zeta) - B(x,\zeta) = 0 \tag{7.58}$$

which leads to

$$u_\zeta + \frac{(1-\alpha)}{[\alpha-(1-\alpha)z]}u^2 = -2\omega \tag{7.59}$$

since $E \neq 0$. Since the model is developed based on asymptotic formulation, and the choice of suitable scales and velocity (see [13]) leads to a non-dimensional value of $\omega \approx 0.03$, the consideration of $\omega \to 0$ is relevant and appropriate. When $\omega \to 0$, we need to avoid

$$u_\zeta = -\frac{(1-\alpha)}{[\alpha-(1-\alpha)z]}u^2 \ , \tag{7.60}$$

which on integration yields

$$u(x,z) = -\frac{1}{\ln[\alpha-(1-\alpha)z]} + g(x) \tag{7.61}$$

where $g(x)$ is an arbitrary function. Hence, we need to avoid the profile given by (7.61). However, this is not very restrictive as we can choose various different profiles not of the form in (7.61), e.g., see [13] for some typical profiles. Notice that when $\alpha \to 1$, the profile in (7.61) has a singularity which results in an unbounded and unrealistic profile.

8 Remarks

We notice that for the proposed solution if $u \in C^1(\overline{D})$, then $(v, w, P) \in C^1(\overline{D})$ where $\overline{D}$ is the closure of the fluid domain. If convergence in the sense of distributions is considered then it is convenient to work with the Sobolev space. In particular, if we consider the Hilbert space with $u \in H^1(\overline{D})$, we can relax the regularity requirement and (v, w, P) will belong to the Hilbert space $H^1(\overline{D})$ and will have to satisfy the kinematic and dynamic boundary conditions as previously discussed.

9 Discussions

This paper presents an extension of the original work by Constantin and Johnson, which was for piece-wise constant density, to a linear variation (in depth) of the density. The work carried out in this paper has shown that the Constantin-Johnson model is versatile enough and can be readily developed to include some more realistic flow properties. It may be noticed from (45) that the main contribution to the change in the flow structure due to linear variation (in depth) of density as compared to the one when the density is assumed to be constant, comes from the non-zero $B(x, \zeta)$ term. Since the variation in density is small (less than 1%) over the warm shallow layer, the term $(1 - \alpha) \to 0$ and in turn $B(x, \zeta)$ is close to zero, in general. However, in the presence of strong undercurrents, i.e. large values of u, the term $B(x, \zeta)$ may have non-zero contribution as $B(x, \zeta)$ is proportional to u^2; and the flow structure may be influenced by the linear variation of density in such a situation.

It would be interesting to carry out some numerical investigations, both for the case of solutions close to the equator (for which exact solutions have been developed in this paper) and solutions over a wider range on either side of the equator. In addition, it would also be interesting to observe how the streamlines and flow patterns are for the case with linear variation (in depth) of the density, and compare those with the cellular structures and their evolution along the equator as has been observed in previous studies [13, 2]. Simulations of flow paths to investigate the presence of features such as upwelling, downwelling and extra-equatorial dynamics as observed previously [1] would also be of interest in future studies.

10 Acknowledgements

Discussions with Prof. Adrian Constantin, University of Vienna and Prof. Robin S. Johnson, Newcastle University and the suggestions given by them are gratefully acknowledged. The author is also grateful to the two anonymous reviewers for their helpful suggestions in improving the quality of the manuscript.

References

[1] B. Basu, One a three-dimensional nonlinear model of Pacific equatorial ocean dynamics: Velocities and flow paths *Oceanography*, **31(3)** (2018), 51–58.

[2] B.Basu, Some numerical investigations into a nonlinear three-dimensional model of Pacific equatorial ocean dynamics *Deep-Sea Res. Part II*, **160**, (2019), 7–15.

[3] M.A. Cane, The response of an equatorial ocean to simple wind stress patterns: I. Model formulation and analytical results *J. Mar. Res.*, **37** (1979), 232–252.

[4] M.A. Cane, The response of an equatorial ocean to simple wind stress patterns: II. Numerical results *J. Mar. Res.*, **6** (1979), 335–398.

[5] J.R. Charney, Non-linear theory of a wind-driven homogeneous layer near the equator *Deep Sea Res.*, **6** (1960), 0566041, 303–310.

[6] A. Constantin, An exact solution for equatorially trapped waves *J. Geophys. Res.: Oceans*, **117** (2012), C05029.

[7] A. Constantin, On the modelling of equatorial waves *Geophys. Res. Lett.*, **39** (2012), L05602.

[8] A. Constantin and P.Germain, Instability of some equatorially trapped waves *J. Geophys. Res.: Oceans*, **118** (2013), 2802 – 2810.

[9] A.Constantin, Some nonlinear, equatorially trapped, nonhydrostatic internal geophysical waves *J. Phys. Oceanogr.*, **44** (2014), 781–789.

[10] A. Constantin and R.S.Johnson, The dynamics of waves interacting with the Equatorial Undercurrent *Geophys. Astrophys. Fluid Dyn.*, **109** (2015), 311–358.

[11] A. Constantin and R.S.Johnson, An exact, steady, purely azimuthal equatorial flow with a free surface *J. Phys. Oceanogr.*, **46** (2016), 1935–1945.

[12] A. Constantin, R. I. Ivanov and C. I. Martin, Hamiltonian formulation for wave-current interactions in stratified rotational flows *Arch. Ration. Mech. Anal.*, **221** (2016), 1417–1447.

[13] A. Constantin and R. S.Johnson, A nonlinear three-dimensional model for ocean flows, motivated by some observations of the Pacific Equatorial Undercurrent and thermocline *Phys. Fluids*, **29** (2017), 056604.

[14] T. Cromwell, Circulation in a meridional plane in the central equatorial Pacific *J. Mar. Res.*, **12** (1953), 196–213.

[15] H.A. Dijkstra, *Nonlinear physical oceanography: A dynamical systems approach to the large scale ocean circulation and El Nino*, Springer Science & Business Media, Vol. 28, 2005.

[16] A.V.Fedorov and J. N. Brown, 'Equatorial waves' in *Encyclopeida of Ocean Sciences*, edited by Steele, J, Academic Press, San Diego, (2009), pp. 3679–3695.

[17] N.P. Fofonoff and R.B. Montgomery, The equatorial undercurrent in the light of the vorticity equation *Tellus*, **7** (1955), 518–521.

[18] A.E.Gill, The equatorial current in a homogeneous ocean *Deep Sea Res.*, **81** (1971), 421–431.

[19] A.E.Gill, Models of equatorial currents, *Proc. Numerical Models of Ocean Circulation*, (1975), pp. 181–203.

[20] A.E.Gill, *A*tmosphere-ocean dynamics, Academic Press, New York, 2016.

[21] D.Henry, An exact solution for equatorial geophysical water waves with an underlying current *Eur. J. Mech. -B /Fluids)*, **38** (2013), 18–21.

[22] D. Henry, Equatorially trapped nonlinear water waves in a β -plane approximation with centripetal forces *J. Fluid Mech.*, **804** (2016), R1, 11pp.

[23] D. Ionescu-Kruse and C. I. Martin, Periodic equatorial water flows from a Hamiltonian perspective *J. Differential Equations*, **262** (2017), 4451–4474.

[24] G.C.Johnson, M.J. McPhaden and E.Firing, Equatorial Pacific Ocean horizontal velocity, divergence, and upwelling *J. Phys. Oceanogr.*, **31(3)** (2001), 839–849.

[25] G.C.Johnson, B.M.Sloyan, W.S.Kessler and K. E.McTaggart, Direct measurements of upper ocean currents and water properties across the tropical Pacific during the 1990s *Prog. Oceanogr.*, **52** (2002), 31–61.

[26] W.S.Kessler, The circulation of the eastern tropical Pacific: A review *Prog. Oceanogr.*, **69** (2006), 181–217.

[27] C. I. Martin, Two-dimensionality of gravity water flows governed by the equatorial f-plane approximation *Ann. Mat. Pura Appl.*, **196** (2017), 2253–2260.

[28] J.P.McCreary, A linear stratified ocean model of the equatorial undercurrent *Phil. Trans. Roy. Soc. London A*, **298** (1981), 603–635.

[29] J.P.McCreary Jr, Modeling equatorial ocean circulation *Ann. Rev. Fluid Mech.*, **17(1)** (1985), 359–409.

[30] J.P.McCreary Jr and P. Lu, Interaction between the subtropical and equatorial ocean circulations: The subtropical cell, *J. Phys. Oceanogr.*, **24** (1994), 466–497.

[31] W.D. McKee, The wind-driven equatorial circulation in a homogeneous ocean *Deep Sea Res.*, **20** (1973), 889–899.

[32] J.Pedlosky, Thermocline theories in *General Circulation of the Ocean*, Springer, (1987), pp. 55–101.

[33] A.R. Robinson, An investigation into the wind as the cause of the equatorial undercurrent *J. Mar. Res.*, **24** (1966), 179–204.

[34] H. Stommel, Wind-drift near the equator *Deep Sea Res.*, **6** (1960), 298–302.

[35] L.D. Talley, G. L. Pickard, W.J. Emery and J.H. Swift, *Descriptive physical oceanography: An introduction*, Elsevier, London, 2011.

[36] G.Veronis, An approximate theoretical analysis of the equatorial undercurrent *Deep Sea Res.*, **6** (1960), 318–327.

Abstract

The subject of this thesis is mathematical analysis of non-linear free surface waves interacting with currents. In this context, large amplitude free surface two-dimensional (2D) water waves described by the Euler equations for incompressible and inviscid fluids with a free surface under the influence of gravity over a finite depth are considered.

With regard to the free boundary non-linear problem for large amplitude smooth travelling waves with underlying uniform currents, the qualitative nature of the flow and the pressure fields is investigated. Bounds on the surface profile have been derived. The possible co-existence of propagating surface waves and an underlying current at the wave speed is settled – this can only happen if the surface is flat. The existence of large amplitude 2D water waves with speed c, propagating on the surface of an irrotational flow over a flat bed with uniform underlying current k, is then proved following a bifurcation approach. It has been shown using integral equations and positive operator results that two branches of travelling wave solutions exist for a parameter $\mu = (c^3/q_c^3) < 1$ or > 1 (where q_c is the flow velocity at the wave crest). Out of the two, the existence of the global bifurcating branch of solution for $\mu < 1$ has been unknown so far. The nature of the velocity and pressure fields for large amplitude solitary water waves propagating over a flat bed with uniform underlying currents has also been investigated. Conditions for the existence of solitary waves in 2D with uniform underlying current over a fixed mean depth have been proved. Some bounds on Froude number and on the maximum amplitude of solitary wave height have been derived. Investigations on the properties of the velocity field for steady periodic water waves over a flat bed have further been carried out for a generalized class of C^1 vorticity functions γ. Results are proved by exploiting the maximum principles and are based on a hodograph transformation of the fluid domain. Some properties of the velocities interior to the fluid domain and on the precise locations of the maximum/minimum horizontal fluid velocities are investigated and proved for rotational water waves without any restriction on the amplitude. For $u < c$ and a monotonically varying positive vorticity, the location of the maximal horizontal velocity has been proven to be at the crest, thus generalizing some recently proven results.

As an application of the theoretical results proved on the fluid velocities and the pressure within the fluid domain, the recovery problem of estimating the wave height from pressure and/or velocity data has been considered. Some bounds on estimated wave heights (valid for all ranges of amplitude) from pressure measurements at the flat bed for waves with underlying uniform currents have been derived. Considering the fact that measurements are more convenient at an intermediate depth than at the bed, further bounds on estimates of wave heights have been found. Five different upper bounds based on a combination of velocity and pressure measurements at an intermediate depth have been derived, though there is only one lower bound.

In previous studies related to water waves (rotational or irrotational) mass flux has been assumed to be given, while the flow force (related to the momentum) is the natural driver of flow and can be assumed to be a fixed constant. The monotonicity of 'flow force' lines in the vertical direction allows a transformation of the unknown domain with a free surface to a fixed domain. By virtue of this property, the steady water wave problem has been reformulated in terms of 'flow force' functions. In this framework, the existence of small amplitude irrotational steady periodic water waves propagating over a flat bed and uniform underlying currents, with a given flow force is proved using a variational approach relying on the theory of Crandall-Rabinowitz.

To examine the impact of currents on the geophysical ocean dynamics, some numerical investigations have been carried out on a nonlinear, three-dimensional Pacific Equato-

rial Undercurrent (EUC) model that was recently developed, motivated by observations and capturing some essential properties of the Pacific equatorial region. Streamlines, velocity amplitude maps and flow paths or trajectories have been obtained. Numerical results indicate that the flow configuration evolves along the line of the Equator. Simulations also show evidence of upwelling/downwelling, cellular flow structures, extra-equatorial flows, a subsurface ocean "bridge", and sharp changes in the gradient of the flow path. Further, allowing a linear variation of density in the model, a system of equations is generated by following a careful asymptotic approach. The equations take the Coriolis effect into account and are consistent with β-plane approximation. An exact solution is developed close to the Equator, relating to the system of model equations representing oceans flows with an undercurrent and a thermocline.

Deutsche Zusammenfassung

Diese Arbeit befasst sich mit der mathematischen Analyse der Wechselwirkung von nichtlinearen Oberflächenwellen in Strömungen mit Wirbelstärke. In diesem Zusammenhang betrachten wir zwei dimensionale (2D) Oberflächenwellen mit möglich großer Amplitude, die durch die Euler'sche Gleichungen für nicht komprimierbare und nicht visköse Flüßigkeiten mit einer freien Oberfläche unter den Einfluss von Schwerkraft über eine flachen Boden beschrieben werden.

Nicht-lineare freie Randwertprobleme für die Beschreibung von Wellen mit grossen Amplituden und unterliegene gleichmäßige Strömungen, als auch qualitative Merkmale des Stömungsfeldes und des Druckfeldes wurde untersucht. Abschätzungen für Oberflächenprofile wurde abgeleitet. Die Problematik der möglichen Koexistenz von propagierenden Oberflächenwellen und eine unterliegene Strömung mit der Wellengeschwindigkeit wurde gelöst – es kann nur stattfinden wenn die Oberfläche flach ist. Die Existenz von 2D Wellen mit großen Amplituden mit einer Geschwindigkeit c, an der Oberfläche von einer wirbelfreien gleichmäßigen Strömung über einen flachen Boden wurde anhand von einem Bifurkationsansatz bewiesen. Es wurde mittels Integralgleichungen und der Theorie der positiven Operatoren gezeigt, dass zwei Zweige von propagierenden Wellenlösungen existieren für die Parameter $\mu = (c^3/q_c^3) < 1$ oder > 1 (wo q_c die Flußgeschwindigkeit an der Wellenspitze ist). Die Existenz einer der globalen Bifurkationszweigen von Lösungen war bisher unbekannt. Die Art der Geschwindigkeit- und Druck-feldes für solitäre Wasserwellen, die sich über einen flachen Boden mit einer gleichmäßig unterliegenden Strömung propagieren, wurde auch untersucht. Die Bedingungen für die Existenz von solitäre Wellen in 2D mit einer gleichmäßigen unterliegenden Strömung wurden abgeleitet. Abschätzungen der Froudezahl und der maximale Amplitude von solitäre Wellen als auch Eigenschaften des Geschwindigkeitsfeldes wurden abgeleitet. Zusätzlich wurden Untersuchungen von Eigenschaften des Geschwindigkeitsfeldes von periodische Wasserwellen über ein flaches Boden durchgeführt, für eine allgemeine Klasse von C^1 Wirbelfunktionen γ. Ergebnisse wurden bewiesen mit Hilfe von Maximumprinzipien und basiert auf Hodographtransformationen. Einige Eigenschaften der Geschwindigkeiten unterhalb der Welle und die Lage der maximalen / minimalen horizontale Geschwindgkeit wurden für rotationale Wellen ohne irgendwelche Einschränkungen auf die Amplitude erwiesen. Für $u < c$ und eine monoton variierenden positiven Wirbelstärke wurde nachgewiesen, dass die Lage der maximalen Geschwindigkeit an der Wellenspitze liegt. Dadurch wurden einige neulich bewiesene Ergebnisse verallgemeinert.

Als eine Anwendung von den theoretischen Ergebnissen wurde die Abschätzung von Wellenhöhen aus Druck und / oder Geschwindigkeitsdaten betrachtet. Einige Grenzen für geschätzte Wellenhöhen (gültig für allen Bereichen von Amplituden) aus Druckmessungen am flachen Boden für Wellen mit unterliegende gleichmäßige Strömungen wurden abgeleitet. Mit Rücksicht auf die Tatsache, dass Wellenmessungen an mittleren Tiefen einfacher sind als am Boden, wurden weitere Grenzen betreffend Abschätzungen von Wellenhöhen gefunden. Fünf verschiedene Obergrenzen, basiert auf einer Kombination von Geschwindigkeit- und Druck- Messungen an mittlere Tiefen wurden abgeleitet, obwohl nur eine für die untere Grenze gefunden werden konnte.

In frühere Untersuchungen über Wasserwellen wurde der Massfluss als eine vorgegebene Konstante angenommen, während die Fließtreibkraft (verwandt zum Impuls) die natürliche Triebkraft ist und deswegen als eine logische festgelegte Konstante angenommen werden kann. Die Monotonie der „Fließkraft"-Linien in die vertikale Richtung erlaubt eine Transformation von der freie Oberfläche unbekannten Gebieten zu ein fixiertes Gebiet. In diesem Rahmen wurde die Existenz von kleinen wirbelfreien Wasserwellen, die sich über einen flachen Boden mit einer gleichmäßigen unterliegenden Strömung propagieren, über eine Variations Ansatz bewiesen.

Um den Einfluss von Strömungen auf die geophysikalische Ozeandynamik zu verstehen, wurden einige numerische Untersuchungen durchgeführt, von einem Modell einer nicht-linearen, drei-dimensionalen äquatorialen Unterströmungs (EUC), die von Constantin und Johnson neulich vorgeschlagen wurde. Strömungslinien, Geschwindigkeit- und Fliesspfade oder Richtungen wurden bestimmt. Die numerische Ergebnisse zeigen, wie sich die Fließkonfiguration um den Äquator entwickelt. Simulationen zeigen wieterhin, dass es auftreibende / sinkende Strömungen, zellulare Fliessstrukturen, extra-äquatoriale Flüße, tiefere Ozean „Brücken" und scharfe Änderungen im Gradient des Fliesspfades gibt. Weiterhin wurde eine lineare Variation in der Dichte im Constantin-Johnson-Modell eingebaut, und eine exakte Lösung wurde gefunden. Das System von Gleichungen ist aus den Euler-Gleichungen mit Coriolis-Effekte, dargestellt in einem geeigneten rotierenden Bezugssystem, mit einem vorsichtigen asymptotischen Ansatz, erhalten worden.